E L E C T R O N M I C R O S C O P E S T U D I E S
O F G R A P H I T E O X I D A T I O N

---

by

J. R. Fryer

Department of Chemistry, University of Glasgow.

Thesis submitted for the degree of

Doctor of Philosophy.

June 1969

ProQuest LLC.
789 East Eisenhower Parkway
P.O. Box 1346
Ann Arbor, MI 48106 – 1346

SUMMARY

The research described in this thesis is concerned with the study of a reaction at a gas-solid interface by the technique of electron microscopy. The particular reaction studied was the oxidation of graphite by dry air at 400-800°C carried out inside Siemens Elmiskop I and IA electron microscopes. Two types of graphite were studied, British Nuclear Grade and spectroscopically pure natural graphite. Both of these were microcrystalline, and exhibited similar oxidation characteristics. Only the $\{10\bar{1}0\}$ crystal planes were significantly reactive, and kinetic studies upon rates of erosion of these crystal planes showed that both graphites had an activation energy for reaction of 20 ± 1 k cal/mole.

Catalytic oxidation of these graphites in the presence of small amounts of platinum and palladium evaporated on to their surfaces was also studied, with air as the oxidising agent. Platinum had little effect upon oxidation rates below 800°C, but above this temperature channels were formed running in the $\langle 11\bar{2}0\rangle$ crystallographic directions. Palladium also brought about catalytic oxidation, but did not exhibit any crystallographic preference in the production of channels: oxidation was associated with rapidly moving particles of the metal. A mechanism is suggested to explain this behaviour.

Part of the thesis is devoted to a study of the decoration of graphite with the object of assessing defect concentrations. Thus the effect of ultrasonic disintegration upon the defect concentration of the graphites was carried out. No marked effect was observed; defect concentrations being assessed by the decoration of the graphite surface with silver particles. From these results, and those from other workers, it is suggested that decoration only occurs on chemisorbed species, and not directly on to defect sites.

High resolution electron microscopy on thin graphite flakes revealed an apparent granular structure. The appearance of this structure was ascribed to a phase contrast phenomenon associated with a slight puckering of the graphite lattice. No significant pores in the crystal were seen. This last observation, together with contrast arising from Moiré fringes in the oxidation experiments, led to the conclusion that non-grain boundary pores lie between basal planes. The correlation of Moiré fringes with oxidation morphology showed that graphite cannot be considered as a two dimensional structure, but as stacks of layer planes from 30-200Å in height.

ACKNOWLEDGEMENTS

This work was carried out in the Physical Chemistry Department which is under the direction of Professor J.M. Robertson.

For supervision at the commencement of these studies I would like to thank Dr. I.M. Dawson. To Dr. S.J. Thomson I am indebted for his considerable assistance and guidance during the writing of this thesis, and his continued interest throughout the course of the work.

I would like to express my gratitude to Mrs. F. Earey for her skill and patience in the proof-reading and typing of this thesis. I also thank Mr. T. Baird and the technical staff of the Electron Microscopy group for their help and assistance at all times. In particular Mr. B. McAneney for his assistance during the decoration experiments.

Finally I wish to thank my wife for her unfailing support and encouragement throughout these studies.

G E N E R A L C O N T E N T S

INTRODUCTION

INTRODUCTION

Contents

I N T R O D U C T I O N

The theme of this research can be stated briefly as follows.

The electron microscope is unique in that microcrystalline specimens can be resolved, and their crystal faces indexed whilst retaining an image of the overall morphology of the specimen. Previous studies on graphite had indicated that the different crystal planes had different reaction rates under oxidising conditions; in this thesis there is a description of the first attempt to study the rate of oxidation of graphite wholly within the electron microscope. The techniques involved included high resolution microscopy, decoration, and shadowing.

HISTORY

Graphite has been known from very early times, though its use was probably limited to decorative purposes, for the embellishment of pottery (H.S.Spence 1922). Agricola (1495-1550) describes refractory crucibles made of graphite, but the true identity of the mineral was not established until Scheele (1742-1786) demonstrated the carbon content of graphite by igniting it in a current of oxygen. This distinguished it from molybdenite, but its nature in relationship with diamond and amorphous carbons was not established until Sir Humphrey Davy in 1814 burnt the three minerals in oxygen, showing that carbonic acid gas was produced in each case, and thus concluded that carbon existed in three allotropic forms. These three forms were distinguished chemically by dissolution in a potassium chlorate, nitric acid mixture, when the graphite formed yellow flakes of graphitic acid whilst the amorphous carbon gave a brown substance that was soluble in water. However, this test was not satisfactory in all cases as was shown by Charpy in 1909, but no better method was available until physical techniques, notably X-ray diffraction, were applied to the crystal structure.

The impetus for the study of graphite started with the industrial revolution since it was an important refractory material for the steel and metallurgical

industries. In 1913 the world production was 120,000 tons of which 60% were used in crucible retorts, 15% in furnace and converter linings, 10% in paints, 10% in lubricants and 5% in foundry mouldings. (J.W.Shetley 1918). This demand could be satisfied from natural sources, but as advancing technology required more, both in quality and quantity, than was available from natural sources, synthetic graphites were produced. The iron and steel industries did not require a detailed knowledge of the chemistry of the reaction of carbon. However, the more exotic technologies of the nuclear and aviation industries that arose after the Second World War, made it necessary that the surface reactions of graphite be evaluated in fine detail, even though 50% of the 500,000,000 tons produced in 1966 was still being used by the steel industry. The results presented in this thesis show some of the information about the surface reactions of graphite that can be obtained with the electron microscope.

1. Ideal Structure.

With the development of X-ray diffraction a method now existed for resolving the absolute structures of elemental carbons and Debye and Scherrer in 1917 showed that so called 'amorphous' carbon was composed of small graphite crystallites having an interlayer spacing - ie. c value of 3.41Å. However the stacking sequence of layers they proposed was disproved by Hull in 1922 who showed that graphite is of a hexagonal close packed structure of stacking sequence ABAB.....(Fig.1.) and this work was confirmed by Hassel and Mark, and then by Bernal in 1924. This structure had a c spacing of 6.82Å and a=b=2.45Å. Bernal also found that artificial and natural graphites have similar structures with the atoms arranged at the corners of regular hexagons in parallel planes whose vertical distance apart was half the unit cell. This structure was also shown by electron diffraction (Trendelenburg, Franz and Weland 1933) and the lattice parameters agreed with the X-ray data. These workers also noted that graphite tended to lie on its basal (0002) plane which was parallel to the surface layer. Finch and Wilman (1936) and Trezbiatowski (1937) refined the lattice parameter data on natural graphite giving values of a = 2.456Å and c = 6.695Å, but in 1940 Taylor and

Fig. 1.

Hexagonal layer structure of graphite.

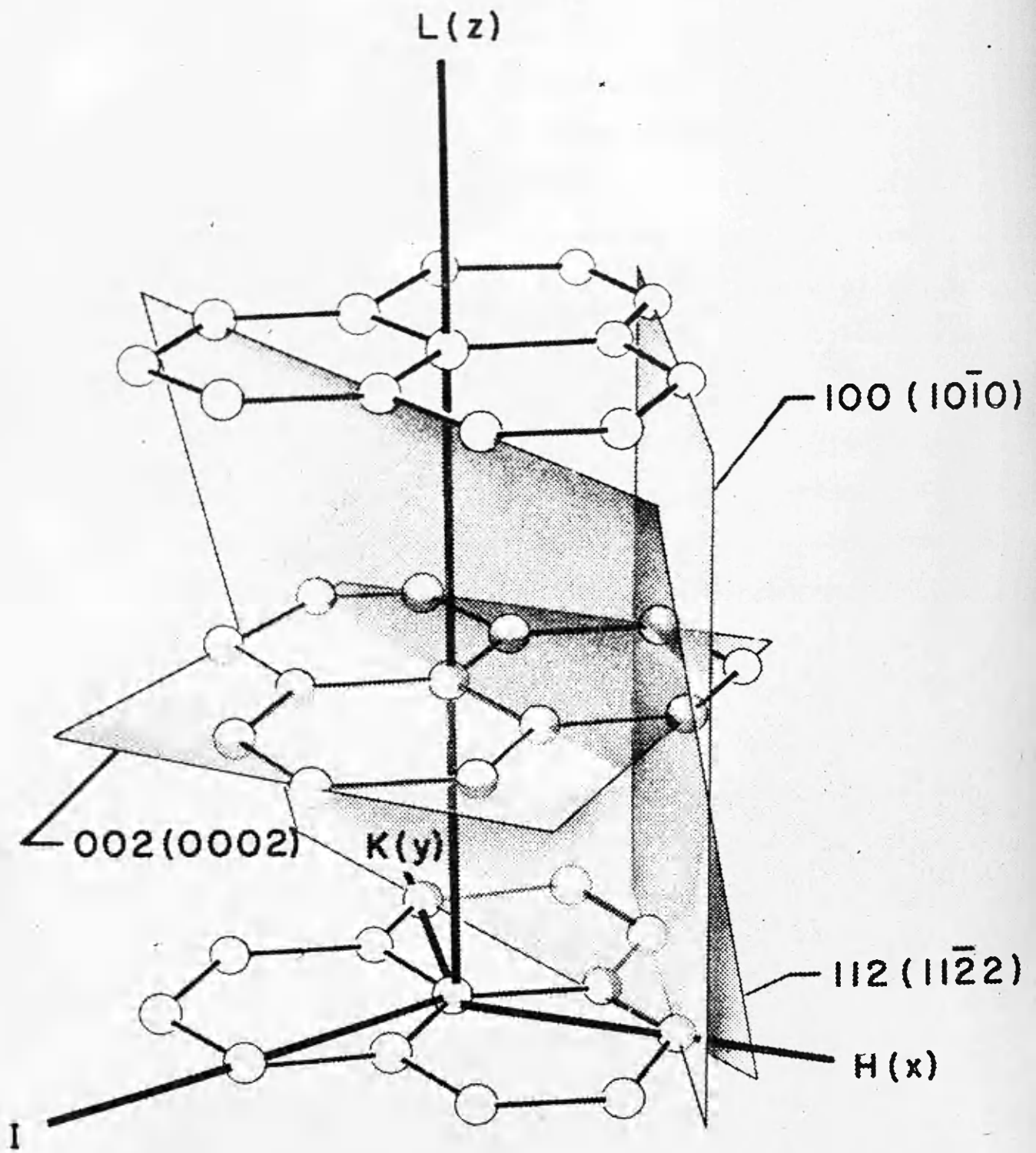
L(z)
100 (10$\bar{1}$0)
002(0002)
K(y)
112 (11$\bar{2}$2)
H(x)
I

Laidler confirmed some work of Mauguin in 1926 who had suggested that other graphite structures may be present from his Laue and rotation X-ray diffractometry measurements. Taylor and Laidler found that extra lines appeared in the X-ray diffraction photograph that indicated small areas of anomalously stacked material within the graphite hexagonal structure. The nature of these anomalous areas was shown by Lipson and Stokes in 1942 to be a rhombohedrally stacked graphite of ABCABC ... stacking sequence (Fig.2). The percentage of rhombohedral structure present was later shown to be variable (Bacon 1950), the amount increasing from 10% in a high quality graphite to 17% for an average graphite, and much higher values being realized after severe mechanical deformation such as grinding. Chemical and thermal treatments also change the proportion of rhombohedral stacked structure present (Taylor and Laidler 1940, Matuyama 1956) showing that the rhombohedral material readily reverts to a hexagonal structure. The energy difference between the two forms is quite small, as has been shown by several workers (Williamson 1960, Baker, Chou and Kelly 1961) their values for stacking fault energy lying between 0.1 and 0.6 ergs cm^{-2}.

Many studies have been made of the transition from microcrystalline 'amorphous' carbon to macrocrystalline graphite (eg. Walker, McKinstry and Wright 1953) and the

Fig. 2.

Hexagonal and rhombohedral stacking sequences of graphite.

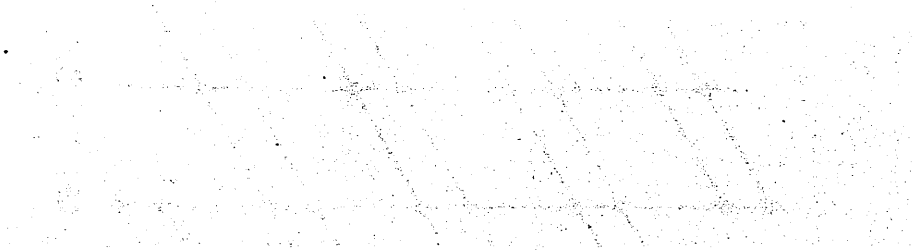

Hexagonal.

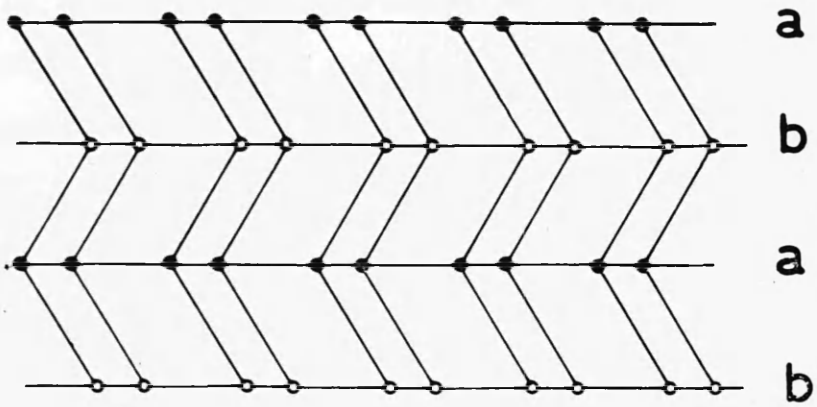

Rhombohedral.

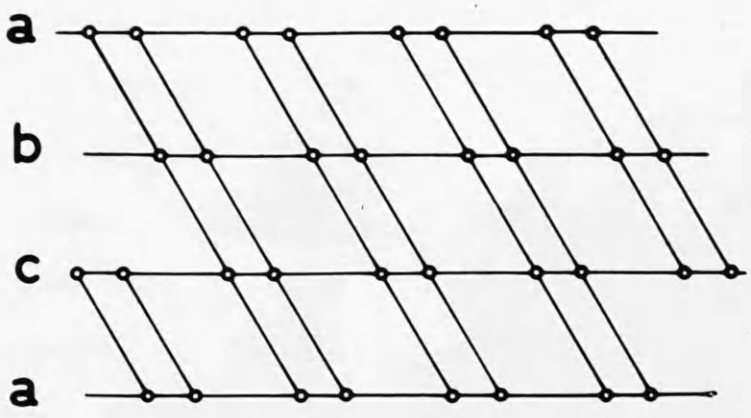

review of knowledge of this transition has been summarised by Ergun (1968). However, synthetic graphites formed by baking 'amorphous' carbons or cokes with a binder - eg. pitch, at temperatures around 3000°C for a few days have lattice parameters that agree with those obtained on natural graphite mentioned above. The major differences between 'amorphous' carbons and graphite lies in their interlayer spacing which is larger than the 3.35Å for graphite and their crystallite size which is less than 30Å. Synthetic graphites tend to be of smaller crystallite size than natural graphites, though this is very dependent upon the method of preparation.

2. Defect Structure.

The layer structure of graphite means that defects within the lattice can be classed as being of basal or non-basal character. In the former, glide normal to the c axis only involves rupture of the weak interlayer bonding forces, and hence stacking faults will readily occur in this plane. The stacking faults of this nature are usually observed in the electron microscope as a network of interacting ribbons of faulted material, the cross section of which is shown in Fig.3. Extensive studies by Amelinckx, Delavignette and Heerschap have been reviewed (1965). Many other workers have studied the formation and removal of rhombohedral stacking structures

Fig. 3.

Basal dislocations in graphite.

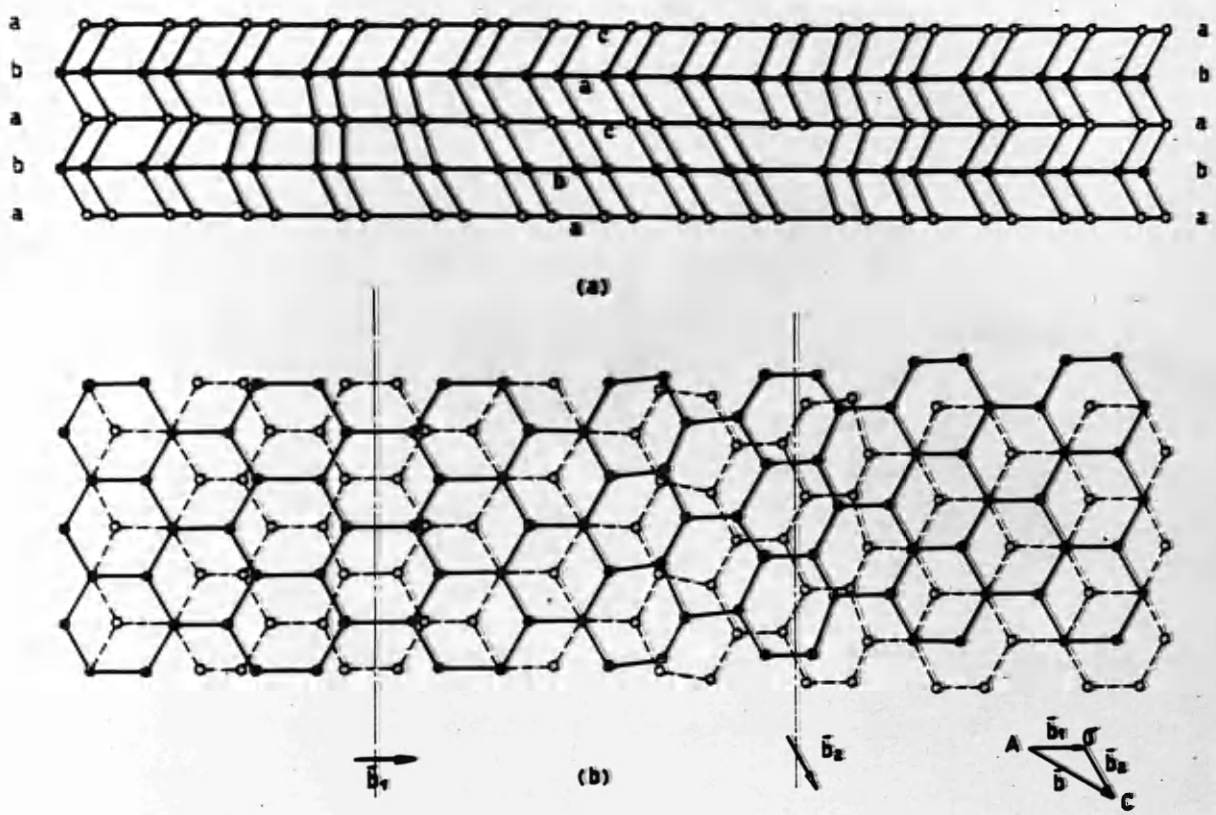

Model of extended 60° basal dislocations in graphite. No C—C bonds are broken. (a) The dislocation has total Burgers vector AC. Notice the lamella of rhombohedrally stacked material between the two partials; (b) projection on the c-plane of one sheet of carbon atoms above and one below the glide plane of the dislocation. The Burgers vectors of the partials are $\bar{b}_1$ and $\bar{b}_2$. The left partial has pure edge character, whereas the right partial is a 30° mixed dislocation.

introduced into graphite by deformation normal to the c axis (Friese and Kelly 1963, Matuyama 1956, 1965, Williamson 1960) Nevertheless, though this type of defect is of considerable importance in consideration of the mechanical properties of graphite, the excess energy available in the defect structure is unlikely to be sufficient to affect chemical reactivity. The non-basal dislocation, however, is generally of much higher energy and thus of more chemical significance.

The two simplest types of dislocation of this nature that could occur are shown in Fig.4. The majority of electron microscope studies have concentrated on basal dislocations and ignored those of non-basal character - ie. where the Burgers vector intersects the basal plane. On occasions the existence of non-basal dislocations has been severely doubted (Williamson 1961) but more recent studies have confirmed their presence in graphite. The first evidence of their existence was provided by Horn (1952) who, by optical microscopy, observed spiral growth patterns on natural graphite crystals with a density of approximately 10^4 dislocations /cm^2 each dislocation having a step height of approximately 500Å. The presence of these large screw dislocations was evidently dependent upon the past history of the graphite since some workers failed to find them (Fujita and Izui 1960, Amelinckx,

Fig. 4.

Non-basal dislocations.

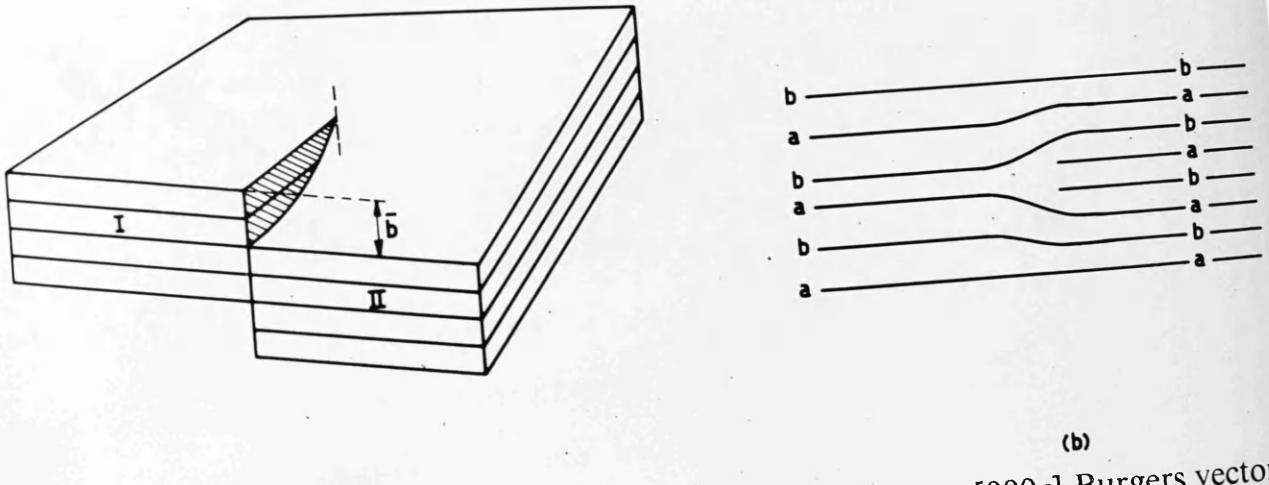

Schematic representation of dislocations having [000c] Burgers vector.
(a) Screw dislocation; (b) edge dislocation.

Delavignette and Heerschap 1965) whilst others found a considerable profusion (Tsuzuku 1957, Austerman Myron and Wagner 1967). The only non-basal dislocations considered in detail by Amelinckx et.al. in their review (1965) were those arising from condensation of vacancies to form loops (Fig. 5), but Thomas in a later review (1968) deals exclusively with non-basal screw and edge dislocation occurring in the lattice and at boundaries of natural graphite crystals. Using catalytic oxidation, Thomas and Roscoe (1966,1967) have shown that non-basal edge and screw dislocations occur extensively in graphite on the electron microscope scale as well as on the large scale that had been observed previously by Horn (1952). The main feature, apart from size, in which the spiral growths of Tsuzuku (1957) differed from those of other workers was the presence of some hollow screw dislocations. This type of dislocation has been observed in other materials when large screw dislocations are present and hence is not unexpected.

The energy of non-basal dislocations is believed to be approximately 10-15 k cal per atom plane for the core of the dislocation (Cotterell 1953, Thomas 1968). The uncertainty about this value arises from the considerable assumptions that have to be made about the environment of the dislocation in the lattice and the allocation of

Fig. 5.

Formation of a loop by condensation of vacancies.

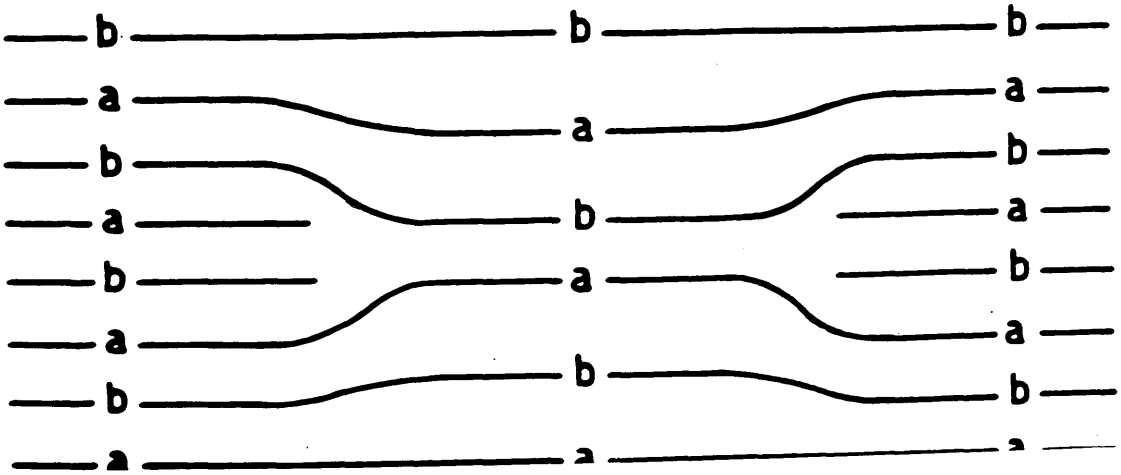
b
b
b
a
a
b
b
a
a
b
b
a
b
a
b
a
b
b
a
a

energy between the core of the dislocation and the surrounding strain field. However, the energy is sufficient to be of considerable importance with regard to chemical reactivity.

Large single crystals of natural graphite are rare, and those coherent crystals that are found are generally faulted and bent, so that perfection within the crystals only extends over a very small area. Bending normal to the c axis will generally take place because the crystal is readily sheared parallel to the c axis and hence is thinner along the c axis than along any other axis. This bending gives rise to extensive twinning and small angle boundaries within the crystal, resulting in a mosaic structure as reported by Dawson and Follet (1959). Their studies employed synthetic nuclear grade graphite and they found mean crystallite dimensions of $0.11 \pm 0.074\ \mu^2$ for the area of individual crystallites which was larger than the values reported by Bacon (1958) for a similar material, but was much smaller than the values obtained for good crystals of natural graphite (Thomas 1965). In the case of natural graphite the most prominent features of the surface were the twin bands that are visible to the naked eye and have been extensively studied (Veselovskii and Vasil'ev 1934, Palache 1941, Kennedy 1960, Thomas Hughes and Williams 1963). For graphite a

Fig. 6.

A twin band in graphite.

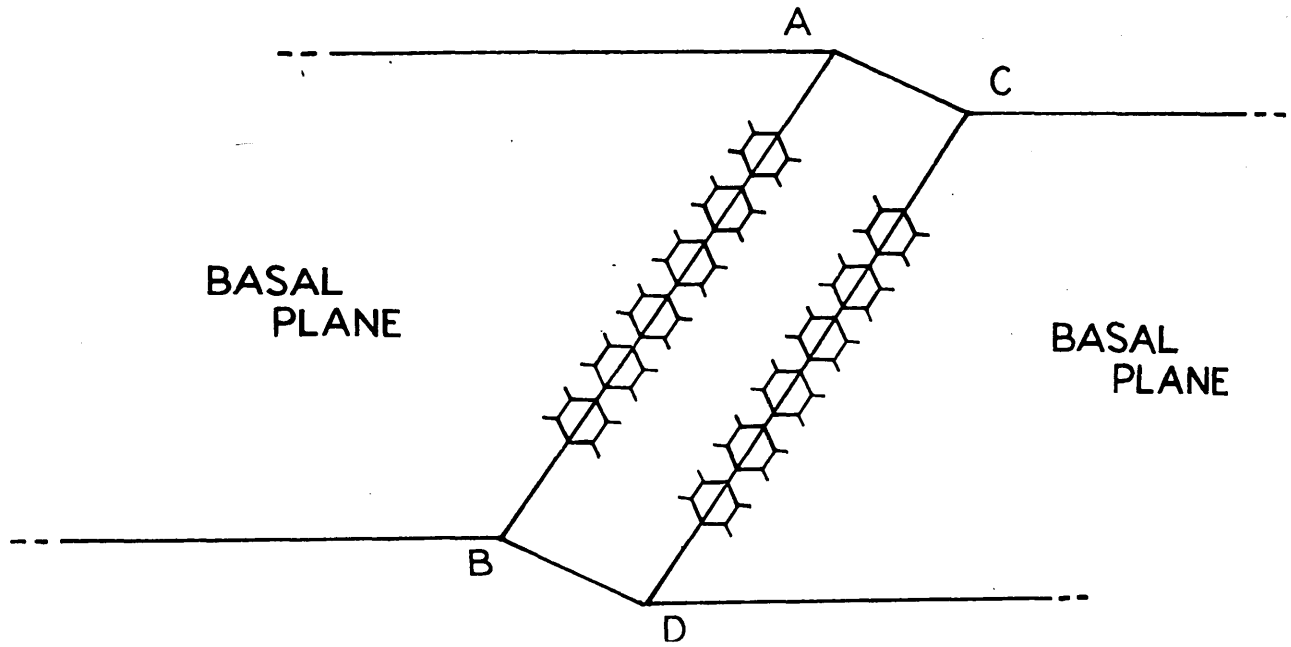
A
C
BASAL
PLANE
BASAL
PLANE
B
D

twin is derived by a rotation of $20^{\circ}48'$ about an axis in the basal plane and along the -C-C- bands as shown in Fig.6. Small angle boundaries are also abundant in graphite and chemical etching by oxygen in the presence of boric oxide has been used to make them visible by optical microscopy (Roscoe and Thomas 1966).

Variations of these grain boundaries producing twist and tilt have been the subject of numerous investigations and are summarized in the reviews by Amelinckx et. al. 1965 and Thomas (1968).

3. Bonding and Electronic Structure of Graphite.

It is most convenient to discuss the bonding of graphite in terms of hybrid orbitals, but these are strictly only approximations of what is known of the electron probability distributions, and thus intermediate states of hybridisation are not only possible but in many cases can be regarded as the most probable situation at a particular point of the lattice.

The C-C bond length in graphite is 1.415Å (Ubbelohde and Lewis 1960) whilst that in benzene is 1.397Å (Stoicheff 1954). A larger aromatic molecule such as ovalene has a bond length of 1.345 - 1.435Å (Donaldson and Robertson 1953). Thus graphite has similar bond lengths to aromatic hydrocarbons and hence falls into the category of sp^2 hybridisation, the delocalised π -orbitals, above and below the plane of the layers, contributing to the

conduction band at all temperatures above $0^{o}K$. The energy of these -C-C- bonds within the layers has been calculated by Feilchenfeld (1957) to be 108 k cal /mole and therefore unlikely to be readily susceptible to chemical attack. From this structure it can be seen that little opportunity exists for covalent bond formation between the layers in an ideal lattice. The interlayer forces are considered to be of van der Waals type but estimates have been made of the interlayer bond energy (Brennan 1952, Feilchenfeld 1957) giving values of 20 k cal/g atom and 7.9 k cal/g atom respectively. A weak covalent bond has been suggested between the layers (Digonskii and Krylov 1960) but the evidence is not conclusive and so the statement made previously about lack of opportunity for covalent bonding is probably correct.

However, even an ideal lattice is of finite size and together with defects that are present in real lattices, there are many exposed edges of carbon hexagons where significant deviations from the sp^2 hybridisation must occur to satisfy free valencies. Coulson (1960) has examined this problem and suggests that three types of carbon atom may exist at the termination of crystal layers:

a) those with free electrons

b) those paired with a neighbouring carbon atom giving a partial triple bond,

c) those that revert to a divalent s^2p^2 state.

With the possible exception of the first, all of these alternatives would indicate that a terminating carbon atom was in a totally different environment from carbon atoms enclosed in the ideal lattice. This is borne out by the work of de Boer (1940) who found that the -C-C bond length was only 1.38Å in very small particles of graphite compared with 1.415Å in large crystals of graphite. Clinton and Kaye (1965) found that in thin sections of graphites the edges tended to pucker and roll up. They suggest that this was due to abrasion of the graphite during sectioning, but the strain energy associated with the terminating carbon atoms is a possible contributory cause. The exfoliation of the edges of graphite layers has been observed by other workers (Feates 1967) which would indicate that the strain is relieved by movement of the individual layer planes and that bonding does not occur between the layer planes. A similar effect would occur at defects where carbon atoms are exposed, and Ubbelohde (1957) has shown that a defect in a layer plane must either result in a buckling of the layer planes, when a chemical compound is formed by a carbon atom with a foreign atom at the defect, or result in trapped unpaired electrons. From data on similar defects in large aromatic structures the buckling of the layer planes in the vicinity of the defect would appear the most likely occurrence.

4. Pore Structure of Graphite.

For a perfect graphite of complete hexagonal stacking the density should be 2.265 g/ml (Hofmann, Wilm and Csalan 1936) however this value is rarely achieved in practice and synthetic graphites often have densities below 2 g/ml.(Ubbelohde 1960). This indicates that there are considerable voids in the structure, and it has been shown by Dawson and Follett (1959) that British nuclear grade graphite contained pores 400 - 800Å wide at junctions of three or more crystallites.

In a layer lattice such as graphite the interlayer spacing could in theory constitute a pore. However the helium density agrees reasonably well with that obtained using hexane and methanol (Ubbelohde 1960) and thus it can be taken that for the definition of pore structure the interlayer spacing is inaccessible. It has been shown, however, by Roberts, Harper and Small (1958) that 40% of the pores that are accessible are less than 20Å in diameter. Access to these pores is improved by oxidation (Butcher and Grove 1961) or grinding (Loch, Austin, Harrison and Duckworth 1958) which suggests that the entrance to the pore is narrow and easily blocked, a 12 - 22% increase in accessible pore volume being achieved after a 6% oxidation (Roberts, Harper and Small 1958). This also indicates that the entrances to pores are preferentially reactive, but this enhanced

reactivity is not shared by the rest of the pore since after the initial rapid change the increase in pore volume becomes more gradual. Butcher and Grove (1961) suggested for synthetic graphite that the part of the graphite derived from the binder during manufacture is more reactive than that derived from the filler but there appears to be very little evidence to support this theory for a good synthetic graphite.

Reactivity of Graphite.

Until modern times the mode of energy production from carbon combustion was not investigated, though one of the products of combustion - namely carbonic acid gas - has been known since the 18th century. Davy (1814) showed that CO_2 was a product of carbon combustion, and his work was later repeated by Copisarow (1919) who found that CO was also produced together with amorphous carbon, the amount of the latter being dependent upon the temperature, and oxygen pressure.

In modern technology graphite enjoys a wide range of applications as a structural material, rather than as a source of energy, hence methods of suppressing its reactivity are of considerable importance. This inhibition was not possible until a more detailed knowledge of its reactions were available, and a vast amount of work has been performed to unravel some of the complexities of the graphite/O_2, graphite/CO_2, graphite/H_2O and graphite/H_2 reactions in particular. In this introduction the properties of the graphite/O_2 reaction are dealt with in some detail since it is of relevance to the results presented later. Reference is made to other reactions though the features that the differing reaction mechanisms have in common are often of an extremely tenuous nature, and hence direct comparisons of different reactant gases are not always valid.

1. Reactions of Bulk Graphite with Oxygen.

Since CO and CO_2 were found to be present in the effluent gas after reaction, the major problem was whether they were both primary products. If not, then the equation $C + O_2 \rightarrow CO_2$ might be valid, the reaction occurring in a single step. The work of Lebeau and Picon (1924) suggested that graphite readily absorbed a variety of gases, since on degassing up to 2000°C in vacuo it gave CO_2, CO, H_2, CH_4 and other hydrocarbons. Meyer (1932) reacted graphite at 1200°C in such a way that reaction products could neither react with each other in the gas phase nor return to the graphite surface. Under these conditions CO and CO_2 were formed in a 1:1 ratio and gave an overall equation of

$$4C + 3O_2 \rightarrow 2CO_2 + 2CO$$

He suggested that the oxygen penetrated the graphite lattice where a reactive transition state was formed. Sihvonen (1932, 1934, 1935) agreed that the chemisorption of oxygen was the first step in the reaction and he postulated a profusion of intermediates that would give rise to CO and CO_2 products and explained the mechanism in terms of activation energy, quoting an overall value for CO formation of 90 k cal /mole, the CO being formed by dissolution of keto surface groups formed with the reactant oxygen.

From results quoted by Meyer (1938), Strickland-

Constable (1944), Audubert and Racz (1945), Duval (1947) and Arthur (1951) it became clear that the mode of oxygen attack on graphite depended upon temperature, and pressure, as well as a large number of subsidiary experimental precautions, and that no one reaction mechanism was valid over a wide range of experimental conditions. However, it was now clear that a multistage reaction was taking place with CO and CO_2 as primary reaction products, though there was considerable disagreement as to the CO/CO_2 ratio under any given set of conditions. Subsequent to 1950 a considerable amount of detailed work on the kinetics of the carbon-oxygen reaction was taking place. The main features that were being sought were the activation energy, the order of reaction, and the rates of production of CO and CO_2.

A large number of activation energy determinations were made giving values from 17 k cal /mole (Lewis, Gilliland and Paxton 1954) to 80 k cal / mole (Blyholder and Eyring 1957). The work of the latter together with that of Hedden and Wicke (1958) showed that one cause of this discrepancy in values was the effect of in-pore diffusion upon the course of reaction. This diffusion is part of a phenomenon known as mass transport and is important when solid/gas reactions are being evaluated. The surface of a porous solid can be considered to be surrounded by a stagnant layer of gas and transport across this layer can

affect the reaction rate. Furthermore transport from a reactive site within the solid to the surface can also be a limiting factor. Neither of these effects, however, are important provided the rate of chemical reaction is not faster than the rate of mass transport. Hence gas/solid reaction may be defined as being either chemically or diffusion controlled.

Hedden and Wicke (1958) divided the reactions of carbon into three zones. In zone 1 the reaction occurring was only limited by the chemical properties of the reactants and the reactant concentration in all of the available pores was similar to that outside the particle. This occurred at low temperatures with high gas flow rates and the measured activation energy was representative of the chemical reaction taking place. At higher temperatures the rate of access of reactants to the pores became significant with respect to the rate of chemical reaction. Over a wide temperature range the reaction within the pores gradually becomes controlled by the rate of arrival of reactant species. This controlling factor defines zone II. Earp and Hill (1957) showed that the reaction of graphite with air became diffusion controlled above 700^{o}C. When the flow rate of air passing over the specimen was increased this threshold temperature rose. Zone III was reached when the temperature had increased to such a level that not only was the rate of chemical

reaction much faster than the diffusion of reactant species within the pores, but also faster than diffusion of reactant species across the boundary layer to the external surface of the graphite. In these latter two zones the measured activation is much lower than the true chemical activation energy for reaction. The conditions under which reaction changes from chemically controlled to diffusion controlled has been shown mathematically by Thiele (1939) and the implications of this, together with experimental verifications, are reviewed by Walker et.al. (1959) and Lowry (1963).

This classification of reaction conditions explained many of the anomalous values of activation energies obtained previously, but several were still outstanding, notably those of Blyholder and Eyring (1957) and Meyer (1938). Their results, however, were obtained using very low oxygen pressures, which would appear to favour a more complex reaction mechanism (Walker et al 1959). Org (1964) showed theoretically that the activation energy depends upon pressure as well as temperature and the zero order reaction observed by Blyholder and Eyring supports this theory.

The values for activation energy have been determined by measuring the loss of carbon from the graphite either by analysis of the effluent gas, or by weight loss of the sample. The accepted value now for the activation energy

in the 500 - 800°C range by these techniques is approximately 49 k cal /mole (Heintz and Parker 1966, Hawtin and Gibson 1966) though abnormal conditions such as low pressure or gas impurities greatly affect this value. To determine the activation energy the rate of reaction at various temperatures must be measured to fulfil the conditions of the Arrhenius equation. The rates of reaction have been found to change during the course of reaction by alteration of various parameters because the topography of the graphite is changed by the reaction.

The major change is the increase in number of accessible pores as oxidation proceeds. The increase in surface area caused by less than 10% burn-off of carbon is a factor of 8-10 in some cases, (Walker et. al. 1959), and in all cases a significant increase in surface area is found (Long and Magnier 1962, 1964). This increased surface area does not necessarily result in a proportionate increase in reactivity but reliable rates on bulk graphites cannot be measured until equilibrium reaction has been established.

In zone I the order of reaction has been found to be between zero and 1 with a large number of values being reported (Armington 1960, Blyholder and Eyring 1957, Thomas 1965, Hennig 1962), but the order is obviously as susceptible to experimental conditions as the activation energy, being dependent upon the type of surface oxide formed under a particular environment.

2. Surface Species on Graphite.

The work of Smith (1863), Baker (1887), and Lebeau and Picon (1924) showed that graphite readily adsorbed foreign molecules, with hydrogen and oxygen being the principal precursors of the adsorbed species. Sihvonen (1932) postulated various carbon-oxygen adsorbed compounds but there was considerable controversy as to whether adsorbed species were stable on the surface or only present as a transition state during reaction (Riley 1937). Graphite exhibits the whole spectrum of gas adsorption with heats of adsorption varying between 1 and 100 k cal/mole, and these can be divided into two classes:-

1. Adsorption with an enthalpy of less than 10 k cal /mole
2. Covalent bonded surface compounds with enthalpies up to 100 k cal /mole

Adsorption in the first class is reversible and comes into the category of physical adsorption (Donnet 1968), except that physisorption is normally regarded as non specific, but Morrison and Lander (1966) have shown that ordered monolayer structures are obtained when certain gases are contacted with graphite under physisorption conditions. Such gases as symmetrical tribromo benzene, ferric chloride and zinc iodide showed this ordering which was reminiscent of an epitaxial film. These particular gases were chosen to suit the experimental conditions for low

energy electron diffraction, but it would not be unlikely for a similar effect to occur with simpler gas molecules. Furthermore the restriction of physisorption to non specific adsorption may not be valid, but until recently experimental methods have not been available to detect any ordering of the adsorbed molecules.

The second class of adsorption is often described as chemisorption and involves the formation of covalent bonds between specific surface atoms and atoms of the adsorbate. In general only monolayer coverage is produced, though polymeric surface species are not unknown, and the nature of the monolayer is dependent solely upon the chemical properties of the atoms involved in its formation. Thus a carbon atom in a particular environment on the surface may form a different compound to one elsewhere, and therefore several types of surface compound may be involved in the course of a reaction. By chemical analysis several types of functional group have been found to be present on a graphite surface exposed to oxygen. These include carboxyl groups (Boehm 1966), quinonoid oxygen (Donnet and Henrich 1960), carbonyl groups (Boehm, Diehl and Heck 1964) and lactones (Rivin 1963). Infra red and low energy electron diffraction studies have confirmed these results, but no general distribution can be deduced (Boehm Diehl and Heck 1964), the quantity and nature of surface oxide being dependent upon the past history of that particular graphite

Boehm (1968) has shown recently that the formation of surface oxides is dependent upon the source of oxygen, with acidic surface oxides being formed after treatment with nitric oxides and ozone, and basic surface oxides being formed after treatment with oxygen. The formation of surface oxide was catalysed by protons.

These oxides and other surface compounds are often unique to carbon atoms in a particular environment. NH_3 does not chemisorb onto the same sites as $-CH_3$, and the (0002) plane is believed to be free of chemisorbed oxygen (Laine, Vastola and Walker 1963, Hennig 1962), furthermore atomic oxygen does not attack the same sites as molecular oxygen (Hennig, Dienes, Kosiba 1958): the atomic oxygen attacking the cleavage surface normal to the c axis, and molecular oxygen attacking the prismatic planes. Hennig postulates three possible surface oxide configurations (Fig.7) for the oxidation of natural graphite by molecular oxygen below 700°C after degassing the material at 900°C. The configuration C. he assumes does not form to any extent since the majority of his results reveal only attack on $\{11\bar{2}0\}$ edge atoms - ie. parallel to the C-C bonds. Of the three configurations Hennig favours B since removal of this oxide by degassing would leave reactive carbon atoms exposed on the surface, and it has been found (Bonnetain Duval and Letart 1959) that this excess temporary reactivity does occur when a carbon surface is

exposed to oxygen after degassing. There is some evidence though (Zarifyanz et al 1967) that oxide B is unstable even at room temperature and thus this configuration should be regarded as an approximation rather than as a molecular structure. Water vapour appears to behave in a similar manner to molecular oxygen, there being very little adsorption on the basal plane (Montet 1961). Heating the graphite in vacuum does not remove the adsorbed water layer quickly, but after 35 minutes heating at 600°C only 83.3% of the adsorbed water layer had been removed whilst there was still a little water remaining at 1200°C (Hennig 1962). These experiments were performed using tritiated water and it is of course the tritium that is being monitored and not the water molecules.

This reluctance of graphite to release adsorbed species leads to question of impurity removal. Lang (1961) has shown that even heating the graphite to 3500°C does not remove completely all impurities and thus all reports on graphite reactivity must bear some measure of doubt until the exact role of impurities in oxidation and surface oxide formation is elucidated.

Fig. 7.

Surface oxide configurations postulated by Hennig.

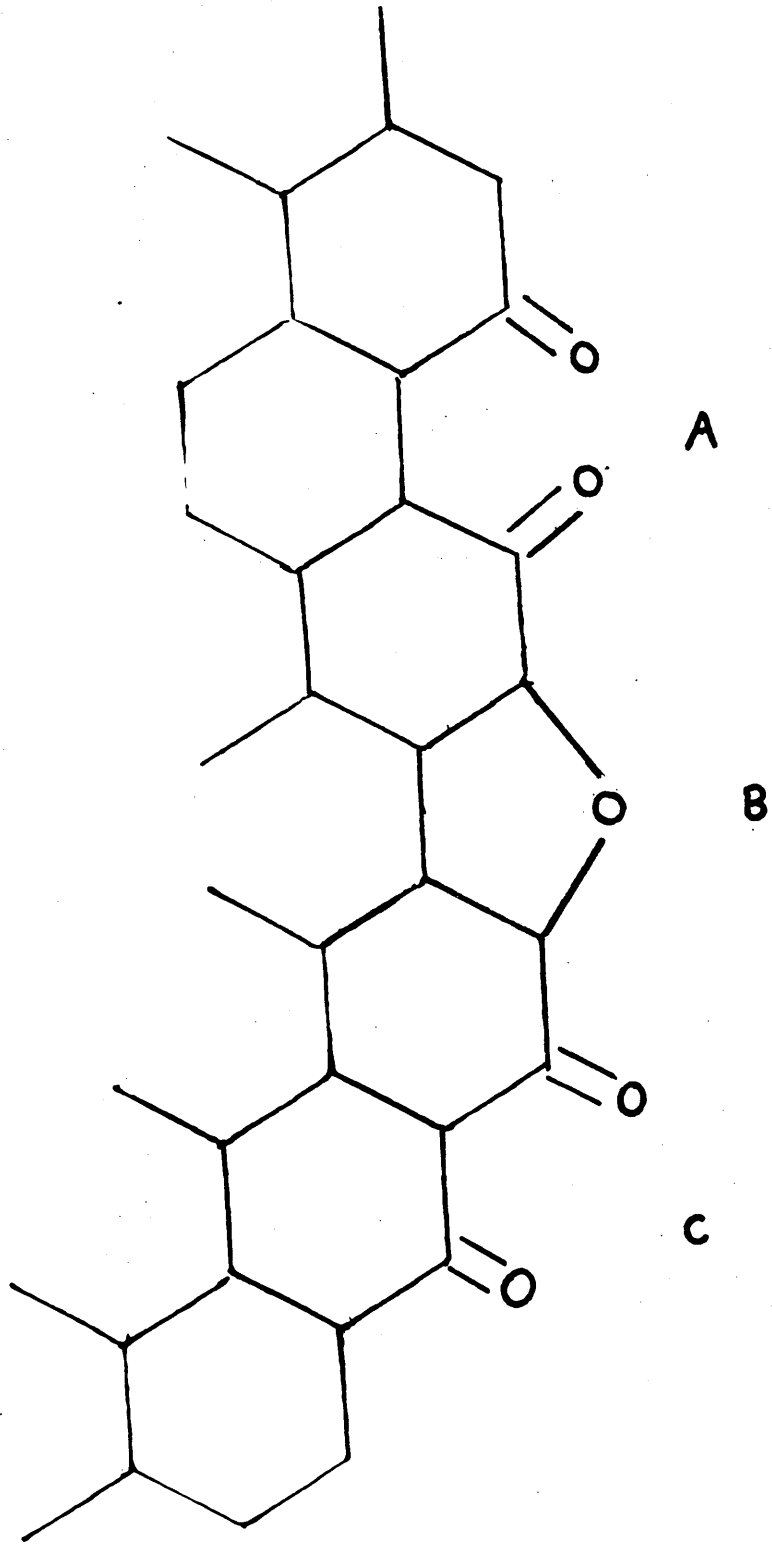
O
O
O
O
O
A
B
C

3. Anisotropy of Reaction.

Structurally graphite is a highly anisotropic material, behaving in one direction as a covalent solid with a high resonance energy, and in the other direction as a weakly bound, porous layer solid. Therefore it is not surprising that graphite should also be anisotropic with regard to its chemical reactivity. Initial experiments were performed using natural graphite crystals which were large enough to be studied individually under the optical microscope. Greer and Topley (1932) observed hexagonal holes produced by treating natural Ceylon graphite with oxygen at 1 torr at 900°C. They suggested that these holes were initiated by trace amounts of iron that were present in their graphite. In the same year Meyer (1932) reported a similar effect when oxidising graphite at 1200°C but concluded that there was preferential oxidation on the basal plane. The mechanism he suggested was that oxygen penetrated between the lattice layers and then formed a reactive entity. In 1935 Boersch and Meyer published electron diffraction data which showed that there was expansion of the lattice in the c direction when graphite was exposed to oxygen between 700°C and 950°C. Riley (1937) agreed with Meyer about the penetration of oxygen and suggested a graphitic oxide type structure formation, however, more recent studies (Walker, McKinstry and Wright 1953) have shown that the expansion of the graphite

lattice is independent of the atmosphere present up to 1118°C and the penetration theory is not widely supported at the present time.

Following the original work of Greer and Topley and Meyer, Bakh and Levitin (1934) found that purified Ceylon graphite produced round holes in the basal plane on combustion in air or carbon dioxide, whilst unpurified material gave hexagonal holes. At this time the sensitivity of graphite to small amounts of impurities was not fully appreciated, but nevertheless, these strong indications that the reactivity of graphite may be governed by crystalline orientation, were not appreciated until Hennig published the results of his studies in 1956 and 1959. Hennig's original studies utilised the optical microscope for studies of natural graphite crystals at various stages of oxidation. He found that the profile of a crystal edge after oxidation was dependent upon the crystalline orientation of that particular edge, and that basal plane pitting appeared to take place only when some catalytic impurity was present. In natural graphite a particular feature is the well developed twin lines that are parallel to the $\{11\bar{2}0\}$ planes. From the twin lines he was able to determine the orientation of the pits that were formed in the graphite during oxidation (Fig. 8). He found from his studies that below 900°C the edges of his pits were perpendicular to the twin lines and concluded that the

$\{10\bar{1}0\}$ planes were most stable to oxidation. There is, however, some doubt about these results, which was shared by Hennig, since he describes these conclusions as incomplete and emphasises the need for further studies. In contrast the anisotropy between the prismatic and basal plane is quite conclusive. Hennig (1961) finds a value for the ratio of the rates of oxidation along and perpendicular to the basal plane ($R_{a/c}$) of 20 below 800°C, and later Hennig (1962) states that $R_{a/c}$ is at least 100 at 800°C. Horton (1961) obtained values for $R_{a/c}$ from 1.51 at 614°C to 7.45 at 1432°C, but in this case bulk graphite in the form of a disc was used and it was assumed that the circular faces of the disc were basal planes - which was reasonable since the disc was cleaved - and the edges would be composed of a mixture of prismatic and basal planes. Thus this ratio has no absolute significance but it shows a variation with temperature which agrees with Hennig, though the change is less dramatic. The comparison between these two worker's results shows that extrapolation from a single crystal to bulk graphite, is a very doubtful exercise, and agreement between the two materials is an exception rather than the rule.

Hennig's studies involved both optical and electron microscopy, but in both cases the crystal was allowed to react only once, viewed in the microscope, and then discarded, so that rates of reaction were computed from a

Fig. 8.

Orientation of etch pits with respect to twin lines (heavy black lines in diagram)

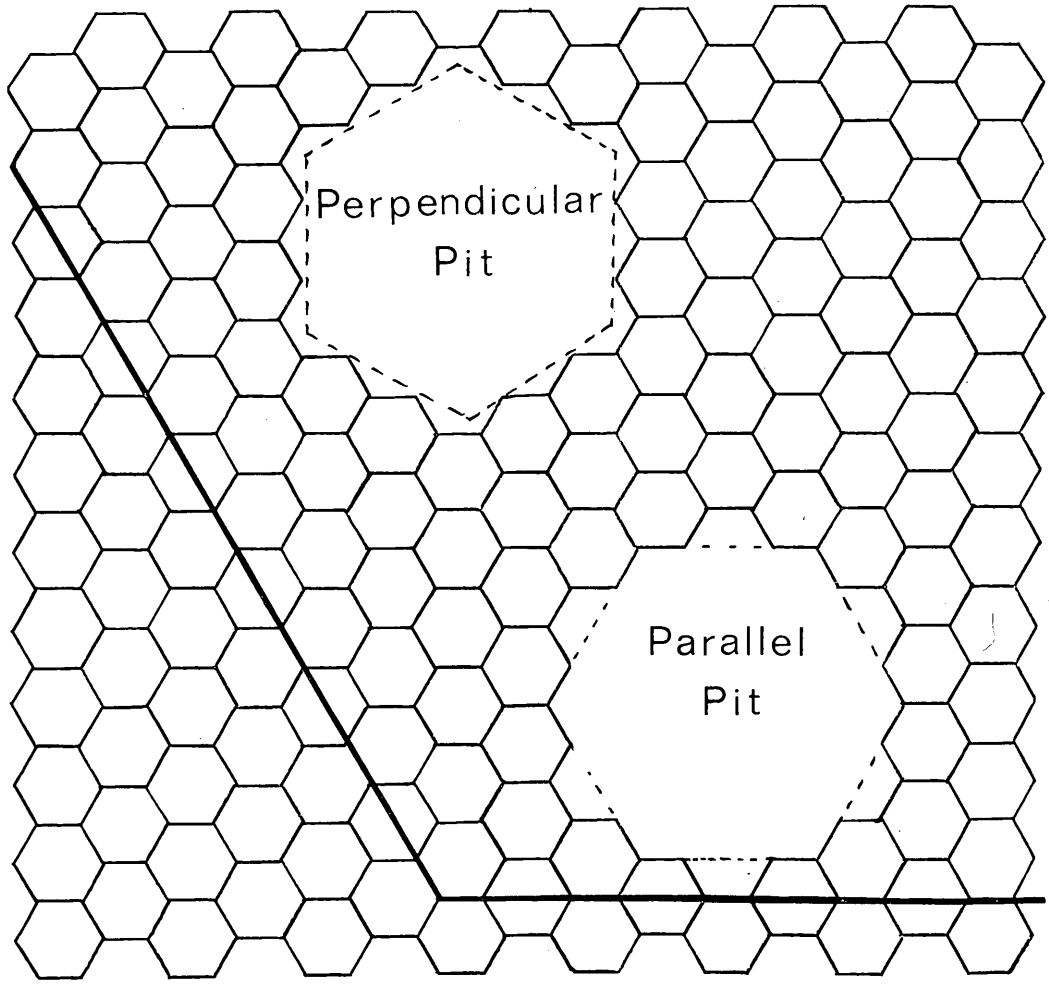
Perpendicular
Pit
Parallel
Pit

large number of different crystals. This profusion of data undoubtedly explains his difficulty in assigning specific values to $R_{a/c}$ measurements. Further studies on natural graphite crystals were made by Thomas and Hughes (1962a,1962b,1963,1964c,1964b) utilising optical microscopy, and this work is reviewed by Thomas (1965). In this case the orientation of etch pits in crystals of natural graphite was determined by establishing the alignment of the etch pit in respect of the twin lines in a manner similar to Hennig, and it was established that $R_{a/c}$ had a value of 26 at 800°C whilst oxidation proceeded most favourably on the $\{10\bar{1}0\}$ planes. Whilst it is clear that the $R_{a/c}$ anisotropy is well established, the variation between rates of reaction on other crystal planes is far less clear. The results of studies upon anisotropy for non-catalysed reactions are summarized in Table I. This work was all performed on high quality natural graphite crystals. The Ticonderoga graphite used by the majority of these workers has a large crystal size, and hence edge attack is usually only manifest in pits or similar breaks in the crystal. Thus when a pit grows laterally by edge attack the planes bordering the pit will be those most resistant to attack, whilst the regression of a straight edge will have exposed the most reactive planes. Therefore it is consistent that Thomas (1962b) should observe pits parallel to the twin lines with edges

Table I

Type of study	Oxidising agent	Temperature °C	Catalyst	Result	Reference
Optical Microscopy	CO_2	Not stated	None. Present but not identified	Round etch pits	Bakh & Levitin 1934
	CO_2/HCl	" "		Hexagonal pits	
Optical Microscopy	CO_2	" "	None	Pits perpendicular to twin lines	
	CO_2/Cl_2	" "	None	Pits parallel to twin lines	Hennig 1956
Optical Microscopy	CO_2	800-900	None	No effect	Thomas 1962a
Optical Microscopy	Air	Not stated	None	No pitting observed	Hennig 1956
Optical Microscopy	Oxygen 1 torr	900	None	" " "	" "
Optical Microscopy	Oxygen 10 torr	760-830	None	Pits parallel to twin lines surface steps $\{10\bar{1}0\}$	Thomas 1962b
Optical Microscopy	Oxygen 10 torr	900	None	Pits perpendicular to twin lines also dodecagnal pits	Thomas 1963
Optical Microscopy	Oxygen 100-200 psi	550	None	Pits perpendicular to twin lines	Patel and Bahl 1965
Optical Microscopy	Oxygen 200-800 psi	550	None	Pits parallel to twin lines	Patel and Bahl 1965
Optical Microscopy	Oxygen 10-100 torr	830	None	Pits-energy of activation(Ea) for parallel pits 62±2kcals Ea perpendicular pits = 66 ± 5kcals	Thomas 1964a

Table I cont.

Type of study	Oxidising agent	Temperature °C	Catalyst	Result	Reference
Electron Microscopy	Atomic Oxygen	200	None	Equal rates of reaction on both prismatic planes	Thomas 1964b
Electron Microscopy	Atomic Oxygen	Not stated	None	Preferential attack on basal plane	Hennig 1959
Electron Microscopy	Atomic Oxygen	200	None	Similar rates parallel and perpendicular to basal plane	Marsh, O'Hair and Reed 1965
Electron Microscopy	Wet Oxygen	550-640	None	$\{10\bar{1}0\}$ surface steps	Hennig 1961
Electron Microscopy	Air	600	None	Pits with edges parallel to $\{10\bar{1}0\}$ planes	Sella and Trillat 1963

of $\{11\bar{2}0\}$ planes whilst the surface steps assume a $\{10\bar{1}0\}$ character. Hennig's results differ from those of Thomas particularly in his definition of the most reactive plane as stated previously, but the variety of data shows that the reactivity difference between the two prismatic planes is very small for this type of graphite and only a slight change in conditions is necessary to change the character of oxidation. Therefore it is quite possible that graphite from different sources could have different relative rates of oxidation between the two prismatic planes, though it is unlikely that such a variation could be obtained that would cause the basal plane to become the most reactive to molecular oxygen.

More recent studies by Long, Gilles, Magnier and Maine (1966) and Myers and Gordon (1968) suggest that water is necessary for the formation of hexagonal pits but since stringent precautions had been taken by the previous workers mentioned above, to exclude water from their apparatus, the evidence is not fully conclusive. Nevertheless there is little doubt that the presence of traces of water severely affect the kinetics of oxidation.

4. Microscopic Studies of Graphite Oxidation.

The description of the crystallographic characteristics of oxidation have been related in the previous section, but there is extensive evidence about other features of the oxidation that deserves a separate title. In 1951 Mitsuishi, Nagasaki and Uyeda observed in the electron microscope moiré patterns on thin sheets of graphite, and more extensive studies on these electron optical interference patterns were carried out by Dawson and Follett (1959) in an attempt to reveal the dislocation content of the graphite, and later work by them (1960) describes the oxidation of graphite. The majority of the oxidation took place along the edges of each crystallite. The graphite was of very small crystallite size, being a nuclear grade synthetic material, and the boundaries in the mosaic structure were etched rapidly by air at 500°C. In a few instances pits formed in the centre of the crystallites but there was no evidence that the terminating half line in the moiré pattern revealed a defect that was conducive to oxidation. Williamson and Baker (1960) concluded that the terminating half line in the moiré pattern was an electron optical artefact and not representative of a dislocation. They also concluded that only basal dislocations form in graphite, which is now not believed to be the case, and therefore some doubt remains. Nevertheless it would appear unlikely that the terminating

moire line represents an emergent dislocation in all cases, and it certainly does not represent a perfect edge dislocation as may be thought at first sight. It does, however, represent some discontinuity in the crystal the nature of which is uncertain at the present time.

Non-basal dislocations have only been revealed by addition of foreign materials to the graphite such as the decoration techniques of Hennig (1965), and this precluded their study as sites of reactivity because of catalytic side effects. Apart from the etch decoration by Hennig (1965), the oxidation of graphite by oxygen or air is revealed as taking place at grain boundaries or pores in the graphite matrix. Pits are occasionally formed but it is not clear whether this is due to catalysis by foreign material or by emergent dislocations or vacancies. Feates (1968) has shown that once a pit is started then it will develop in either a hexagonal or triangular manner according to the exposure of free valencies at the periphery of the pit. It does appear that good hexagonal pits are more common in natural graphites than synthetic graphites, and thus the nature of the pit is probably a function of the crystalline perfection.

At the edges of crystallites the eroded edge is generally perpendicular when oxidation is carried out in air or oxygen, but traces of halogens cause the face to become rounded (Hennig 1957). Oxidation occurring at

vacancies on the basal surface of the crystal has been carried out using O_2/Cl_2 mixtures and subsequent decoration by gold has shown that only single atomic layers are involved and oxidation is quite rapid. (Hennig 1966, Bahl, Thomas and Evans 1967). Oxidation and subsequent decoration using other oxidising gases has been carried out (Feates 1968) and it is significant that usually round holes are formed, whereas in other oxidations mentioned previously, hexagonal holes are formed. This may indicate that round holes are produced by vacancies and angular holes by catalytic oxidation, but reliable evidence is not available to support this idea at present.

Catalytic Oxidation of Graphite.

1. Studies on Bulk Graphite.

In general it has been found that most metals are catalysts for the oxidation of graphite whilst known inhibitors are either non-metals or non-metallic in character. Parker in collaboration with Rakszawski (1964) and Heintz (1966) has investigated both catalysts and inhibitors, determining their effect upon reaction rates and activation energies. For groups III - VIA elements and oxides they found that the kinetic order of the inhibited reaction was the same as that of the uninhibited reaction - ie. first order - and at 700-800^{o}C with 1 atmosphere air pressure the degrees of inhibition or catalysis vary widely. For Si and SiO_2 inhibition appears to occur by the formation of a protective coating, whilst for other additives the mechanism is probably the removal of free electrons from reactive sites. The inhibitors have very little effect on activation energy, and the catalysts decrease the activation energy. The later paper by Heintz and Parker is concerned with the effect of transition metals and inner transition oxides in the temperature range 600-700^{o}C. With the exception of Fe, Ni and Ta all the metals had a positive catalytic effect at 600^{o}C, and with the exception of Ta, all were catalysts at 700^{o}C. A significant feature was that the activation energies were often much higher for the catalytic reaction than

for the pure graphite. For example the measured activation energy of the pure graphite was 48 k cal / mole - in reasonable agreement with other workers - whilst that for the Pd catalysed reaction was 124.5 k cal/mole, but the catalysed reaction rate was higher by a factor of 5.5 at 700°C. This effect was also marked in Au and Pt. Conversely for Ag the activation energy dropped to 11.3 and it inhibited the reaction rate by 14%. Therefore the variation in pre-exponential terms in the Arrhenius equation is considerable and this is the most noticeable feature of catalysis by metallic impurities.

The results from the graphite-air/oxygen reactions cannot be generalised to other oxidising gases. Gallagher and Harker (1964) found cobalt compounds to be excellent catalysts in the presence of oxygen, but indifferent catalysts in the presence of CO_2.

From these various results it is clear that catalysis takes place by a variety of mechanisms and no single hypothesis to explain their actions is valid. Long and Sykes (1952) postulated an electronic mechanism in which the carbon bond is weakened by electron transfer to the impurity atom, and this explains many results - particularly those of Rakszawski and Parker (1964), but the behaviour of Pd and some of the other noble metals obviously does not fall into this category and Hennig (1962) has described how an intermediate metal - oxygen-

carbon bridge structure would explain the catalytic activity of noble metal particles.

2. Microscopic Observations.

A major problem is to distinguish catalytic oxidation from non catalytic oxidation, and it is probable that pit formation is a feature of catalytic oxidation; in pure graphite no pits are formed. Not all impurities in the graphite, however, cause pitting since channelling or even protection of the graphite surface occurs with various catalysts. Thomas (1965) has described the effect of Fe, Ni, Co, Mn, Ta, Ti, Ag, Mo and B on the oxidation of natural graphite, whilst Hennig has used Au, Fe, Ni, Pt, Al and V. Their results are summarised in Table II. Kanter and Hennig (1959) suggest that pitting is not a normal mode of attack by catalysts but can only occur at lattice vacancies, the particular catalyst used in this case being iron. Roscoe (1967) has shown that lattice imperfections are associated with the formation of etch pits, but it is also true that impurities will concentrate at lattice defects as shown by the phenomenon of decoration both internally and on the crystal surface (Bethge 1964, Levinstein and Capio 1967), therefore it is likely that both the impurity and the defect contribute to the energy necessary for pit formation at that particular point.

Previously two theories of catalytic mechanism were mentioned, one involving an electronic rearrangement of

the carbon and the other the formation of an intermediate compound. The evidence for either is not conclusive for all catalytic effects, but a further factor to be considered is that separate phases and eutectic mixtures can also be formed between the catalyst and support (Raub and Falkenburg 1964) which may well influence the immediate environment and structure of the catalytic impurity.

Table II

Gas	Temperature °C	Catalyst	Result	Reference
O_2	900	Au	Channels in $\langle 1\bar{2}10\rangle$ directions	Hennig 1959
		Ag	Channels in $\langle 10\bar{1}0\rangle$ directions	
O_2	500	Fe	Curved channels	
Wet O_2	550-650	Au	$\langle 2\bar{1}\bar{1}0\rangle$ channels	Hennig 1962
Dry O_2	550-650	Au	$\langle 10\bar{1}0\rangle$ channels. Also serration of edges.	"
Wet O_2	550-650	Fe or Au	Pits perpendicular to twin lines Fe has similar activity to Au	"
Dry O_2	550-650	Fe or Au	Pits formed as above Fe more active than Au	"
Wet O_2	550-650	Ni,Pt,Ag,Al,V.	Of similar activity to Fe and Au when V 'wets' surface then it has much higher activity. Catalysis occurs in vicinity of particle.	"
O_2/He	650	Fe	Pits parallel to twin lines	Hennig 1957
O_2	720	Mn	$\langle 11\bar{2}0\rangle$ channels formed preferentially to $\langle 10\bar{1}0\rangle$ channels (ie. $\langle 11\bar{2}0\rangle > \langle 10\bar{1}0\rangle$)	Thomas 1965
	720	Ag	Channels $\langle 11\bar{2}0\rangle = \langle 10\bar{1}0\rangle$	

Table II cont

Gas	Temperature °C	Catalyst	Result	Reference
	720	MoO_3 is reactive species	Varied channels	
	720	$B(B_2O_3$ is reactive species)	$\langle 10\bar{1}0\rangle \rangle \langle 11\bar{2}0\rangle$ channels	
Wet O_2	720	$B(B_2O_3$ is reactive species)	$\langle 11\bar{2}0\rangle \rangle \langle 10\bar{1}0\rangle$ channels	
Dry O_2	720	Fe	Pitting (hexagonal pits)	
		Fe_2O_3 or Fe_3O_4	No activity	
	720	Ni	Pitting - angular	
	720	Co	Channelling	
	720	Ti	Cylindrical pits	
O_2(at 2×10^{-4}torr)	900-1200	Pt	$\langle 11\bar{2}0\rangle$ channels, some pitting	Presland and Hedley 1963.
Air	530	$Fe(OH)_3$colloid	No catalytic attack	Follett 1964
Atomic O	200	Fe	Surface attack inhibited by Fe producing hillocks around particle with $\{10\bar{1}0\}$ faces	Marsh, O'Hair and Reed 1965

Decoration

When a crystal is covered by a thin evaporated layer of gold and heated to 100°C the metal atoms coalesce to small nuclei which preferentially arrange themselves along the discontinuities on the crystal surface, such as surface steps (Bassett 1958 Bethge 1964). This phenomenon was initially investigated on rock salt crystals using Au,Ag,Pt and Pd metals as decoration and it was concluded that the metal particles stopped at monatomic and higher steps on the crystal surface (Bassett 1960, Sella, Conjeaud, and Trillat 1959, Hucher and Oberlin 1961). In 1963 Sears and Hudson proposed that the metal moved on a layer of adsorbed gas, the crystals studied being graphite and molybdenite with silver as a decorating agent. Their suggestion was that the movement was of a Brownian nature and the cessation of movement represented the formation of a true crystallite - substrate contact or interface. The silver particles had a crystalline character even when mobile, since they displayed moiré patterns and were 20-100Å in diameter. This theory of particle movement was shown to be incomplete by Thomas and Walker 1964 who showed that mobility was influenced by the atmosphere surrounding the crystal, and chemisorbed layers could not be involved since graphite does not exhibit chemisorption appreciably on its basal plane. At present the explanation of the

particle movement remains an enigma but two more recent investigations have shown that the problem is more complex than envisaged by Sears and Hudson in the first instance. The first was by Sumner (1966) who decorated rock salt with platinum and observed the usual result of isolated particles 200-300Å apart distributed at surface imperfections. However on dissolving away the rock salt it was found that a coherent film was obtained indicating that the platinum particles were islands on a continuous structureless film, that had evenly covered the rock salt surface. Strenuous efforts were made to ensure that this film did not consist of hydrocarbons, but the film was obtained even in an ion-pumped system, and no film was obtained without the evaporated platinum present. This work agrees with the proposal by Nifontoff (1954) that conduction in thin granular films is via a thin semiconducting layer of metal containing oxygen and other impurity atoms. A phenomenon of this nature would explain the effect on metal of mobility of different gases shown by Thomas and Walker. The other recent work referred to was that of Leviston and Capio (1967) who were able to decorate $LiNbO_3$ and $Li\ Ta\ O_3$ internally with platinum at 600°C with an applied D.C. field of 250-1000 v/cm. The metal diffused into the crystal and collected at dislocation sites. The mechanism was obviously not movement on an adsorbed layer, but since the conditions are

different from normal decoration then possibly an anology is not possible. The decoration of surface steps on the crystals was clear from the initial work of Bassett but whether the steps are monatomic was still in doubt even after Bethge had shown the decoration of evaporation spirals in rock salt. Bahl, Evans and Thomas (1967) resolved the problem beyond doubt by studying the decoration of molybdenite where the alternative layers of molybdenum atoms are at 60^{o} to each other. Successive etching and decoration of molybdenite surfaces showed that at vacancies, pits were decorated whose sides were aligned at 60^{o}, therefore illuminating the layer planes 6.15Å apart.

In addition to the decoration of surface steps Hennig (1964) extended the technique to include dislocations and point defects. Particles of gold aggregated at apparently perfect regions of the crystal surface and the concentration of aggregates was the same order of magnitude as the defect concentration. At higher temperatures the decoration count decreased, and after irradiation it increased, again in a manner typical of defects. Surface impurities such as adsorbed water or acetone also affected the decoration, in some cases preventing decoration completely, and various reactive gases produced patterns unique to that particular gas. Adamson used silver decoration to estimate the defect

concentration of natural and synthetic graphites obtaining values of 0.95×10^{11} particles/cm^2 and 1.68×10^{11} particles/cm^2 respectively, but he stressed that these cannot be taken as absolute figures since the quantity of silver evaporated, and other factors could influence the values. Hence decoration counts should be regarded as relative measures of defect concentration rather than absolute values.

Etch decoration.

This particular technique was pioneered by Hennig (1964) and involved the etching of vacancies on a crystal and subsequently decorating the monatomic edges to the pit thus formed, usually with gold. Extensive work using this technique has been done by Hennig 1964,1965a,1965b, Montet and Myers 1968, Myers and Gordon 1968, Feates 1968, but in general it has been applied only to high quality natural crystals since more defective synthetic graphites would render interpretation difficult. Measurement of pit expansion has given some kinetic values of the reactivity of edge atoms compared to basal plane and this technique has proved particularly useful for radiolytic reactions where vacancy production is a property of high energy radiation.

OBJECT OF PRESENT STUDY

The work of Thomas and Hennig had shown a definite chemical anisotropy in large natural graphite crystals, but it was not possible to study the synthetic or microcrystalline graphites by their methods. The value inherent in a study of synthetic graphites is that they are of considerable commercial importance, and are also reproduceable in character and impurity content, making results obtained with them of much wider interest. However the vast amount of study on graphite that has preceded this present work meant that there was available a reasonable knowledge of how graphite should behave when oxidised with air inside the electron microscope, and yet there was an opportunity to elucidate finer points of the behaviour, and possibly gain a greater understanding of the chemical reactions taking place at the graphite surface.

Therefore subsequent to the experimental problem of designing a suitable apparatus in which the reactions could be conducted, three further problems could be defined:-

1. To correlate types of reaction observed inside the electron microscope, with those observed by other methods.
2. To follow a kinetic study inside the electron

microscope, to obtain details of anistropy of reaction, not only between the basal plane and prismatic planes, but also between individual prismatic planes.

3. To correlate features of the graphite structure with varying degrees of chemical reactivity.

In view of the close affinity this work has with catalytic reactions, the behaviour of palladium as an oxidation catalyst for graphite was also studied. This work was in parallel with that being done also at this university on the behaviour of palladium supported on graphite as a catalyst for the hydrogenation of olefins (Brownlee, Fryer and Webb 1969).

E X P E R I M E N T A L

EXPERIMENTAL

Contents. Page.

Materials

1. Graphite

Two types of graphite were studied, one a poly-crystalline synthetic graphite that had been made to the British Nuclear grade A specification (P.G.A.) and the other a spectroscopically pure natural graphite (S.P.1.) The latter is a purified graphite from Ceylon or Madagascar and has a greater crystallite size and is of lower defect content than the synthetic graphite. The impurity contents of the two graphites are shown in Table III (Labaton 1965). The S.P.1. graphite is of lower overall impurity content, whereas the nuclear graphite is only of comparable purity in elements of high neutron capture cross-section. However the S.P.1. graphite resembles the synthetic graphite much more closely than it did the natural graphites used by Thomas and Hennig in their studies, its crystallite size being of the same order of magnitude as that of the nuclear graphite.

2. Reactant gas

Atmospheric air was used throughout as an oxidising agent and was purified by being passed slowly through a liquid-nitrogen cooled trap, and collected in a 5 litre bulb.

3. Metals

The silver used for decoration was in the form of

Fig. 9.

Gas purification equipment.

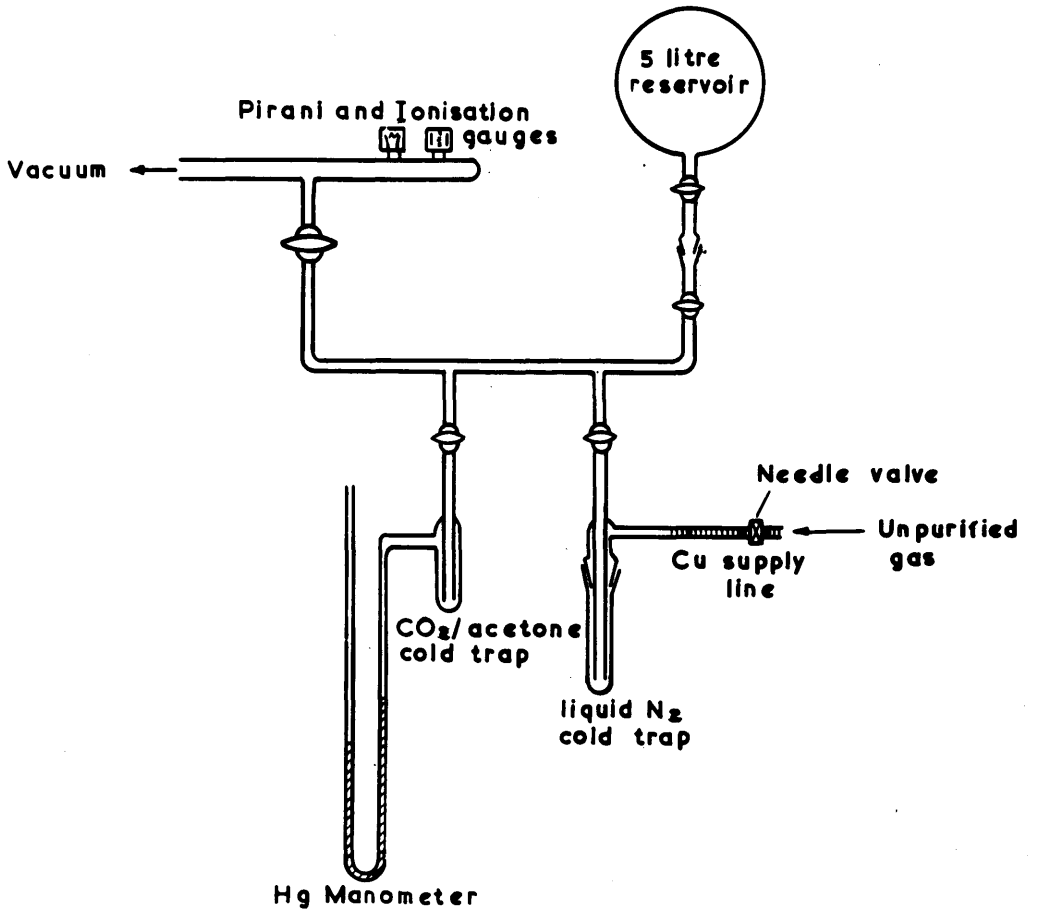
5 litre reservoir
Pirani and Ionisation gauges
Vacuum
Needle valve
Unpurified gas
Cu supply line
CO_2/acetone cold trap
liquid N_2 cold trap
Hg Manometer

Table III

Typical Analysis for Impurity (p.p.m.)

	S.P.I. Maximum	P.G.A.Range
Ash	-	.005 - .025
Aluminium	.015	.25 - 2.5
Barium	.015	.3 - 15
Beryllium	.015	.02 - .03
Bismuth	.06	.06 - .15
Boron	.02	.03 - .16
Calcium	.15	7 - 60
Chromium	.015	.1 - .7
Cobalt	.015	.01 - .03
Copper	.04	.01 - .5
Iron	.05	2 - 16
Lead	.025	.04 - 2.5
Lithium	.005	.04 - .15
Magnesium	.025	.03 - 1.5
Manganese	.015	.01 - .06
Nickel	.025	.03 - 8
Phosphorus	-	.1 - .2
Silicon	.15	15 - 60
Sodium	.1	1 - 2
Tungsten	.08	.08 - 2
Vanadium	.02	.4 - 30
Zinc	.08	.08 - .2
Others	.045	.1 - 1.64

99.9% pure wire. The palladium was also as wire and obtained from Johnson Matthey the quoted purity being 99.99%

Specimen Preparation.

1. Specimen support films.

For the kinetic studies that required the supports to be inert and stable up to 900°C the most suitable were found to be seven holed platinum-iridium mounts covered by silicon monoxide/dioxide films. Thin formvar plastic films were first put on the mount by drying an ethylene dichloride solution of formvar on to a glass slide and the resultant film was then floated off on water. The mounts were raised underneath the film so that the film was removed from the water surface, and dried on the mounts. A silicon monoxide/dioxide mixture was then evaporated on to the formvar by the method of Heidenreich and Peck (1943). The powdered mixture of silicon oxides was placed in a molybdenum boat and evaporated under a vacuum of 10^{-5} torr using a 10v 60amp transformer. The formvar was then removed by heating to a dull red heat in a silica crucible.

One difficulty with the kinetic studies was that the thermal cycling necessary for degassing, and then reaction, resulted in rupture of the films at some point during the course of the experiment. It was found that if the formvar was not removed by the conventional method

described, but left on the mount, then it was completely removed during the degassing period. This meant that in the initial stages of heating the film was separated from the platinum-iridium mount by the formvar layer, and thus was not subject to the mechanical stresses caused by thermal expansion of the mount. Once the temperature had risen about 200-300°C all the formvar had disappeared but the film was less inclined to rupture above these temperatures, and this method of formvar removal was used in the majority of experiments. Prior to this only about 10% of the experiments could be concluded because of rupture of the support film.

For high resolution studies perforated carbon films on platinum-iridium mounts were used since the structure of carbon films is finer than that of silica (ie. silicon monoxide/dioxide) films. These were prepared by floating off wet formvar films (ie. they were sprayed with water from an atomizer before the ethylene dichloride had all evaporated) and then evaporating carbon by the method of Bradley (1954). Holes were obtained of sizes ranging from 100-5000Å in diameter, over which graphite flakes could be supported.

2. Graphite

The purified natural graphite S.P.1. was obtained as a powder and by placing a small amount in a test tube with distilled water and repeatedly centrifuging and

withdrawing the supernatent liquid, a clean sample was obtained. This material was suspended in distilled water and subjected to ultrasonic disintegration (80kc/sec) for 30 seconds, the suspension was then allowed to stand to allow the large particles to settle. A drop of the fine supernatant suspension was put on to a mounted support film and dried in an oven at 50°C. The specimen was then ready for experimental treatment.

The nuclear grade graphite was in block form and thus powder was pared off the block with a razor blade to be disintegrated and mounted in the same way as the S.P.1.

Some doubts have been cast upon the ultrasonic preparation of graphite (K.Carr 1965) and therefore several graphite samples were decorated after being subjected to ultrasonic disintegration for varying lengths of time, as well as being prepared by dusting the dry graphite on to a support film. From the information obtained it appeared that a 30 second period of disintegration in water would not give rise to any abnormal effects in the graphite, and thus this procedure was followed throughout.

3. Decoration.

A known weight of silver was evaporated from a clean tungsten filament which was a known distance above the specimens to be decorated. This operation was carried under a vacuum of better than 10^{-4} torr in an Edwards

12 E6 coating unit. Assuming that the bead of silver on the tungsten film can be regarded as a point source - which is reasonable provided the specimens are more than 10cm from the bead - then a spherical distribution of evaporated metal from the bead can also be assumed. Thus an expression for the thickness of metal on the specimen can be derived:-

$$t = \frac{m \times 10^8}{4 . \pi . r^2 . d}$$

where t is thickness of metal deposited ($\mathring{A}$)
r is distance of specimen from source (cm)
d is density (g/cm^2)

Since the film is of granular structure this is only an approximation, but normally the amount of silver employed was such as to give a 50$\mathring{A}$ film by this formula. Whilst still under vacuum in the coating unit the specimens were then heated to 300-320^{o}C to cause the metal to become mobile and migrate over the graphite and decorate the surface. Below 290^{o}C decoration did not occur and above 350^{o}C the metal nucleated into larger drops. The time of heating was approximately 2 min and the procedure was carried out on a carbon rod with an embedded platinum/rhodium thermocouple.

Initially experiments were carried out as described above, but the decoration counts - ie. ratio of particles on graphite to those on background support film - were not reproducible. This scatter in data was eliminated by preheating the graphite to 900^{o}C in a vacuum of 10^{-5}torr,

immediately prior to decoration. This temperature had been found sufficient to remove the majority of impurities from the graphite surface (Montet 1962). Much better data was then obtained.

4. Shadowing.

This technique highlights the three dimensional structure of the specimen. Several unreacted specimens were shadowed to show the angular configuration of some of the layer planes and also some specimens after reaction. Not all the specimens after reaction were shadowed successfully, because the films - already weak after the thermal cycling they had undergone - ruptured so that the specimen was lost.

The technique was basically as follows. A metal was evaporated from a tungsten filament on to a specimen inclined at an angle to the line between the source and the specimen, so that metal fell on the specimen obliquely, causing a build up of material on one side of an object and leaving a shadow on the opposite side. Since the oblique angle is preset, the height of objects can be calculated from the length of the shadow.

Two materials were used for shadowing, one a nickel-palladium alloy and the other a platinum-carbon mixture. The details of shadowing with these particular materials are described by Bradley in a book edited by Kay (1965.)

The angle generally employed was 15^{o} and the vacuum

was maintained at better than 5×10^{-5} torr. It was found that finer detail was obtained with the pressure in this range, rather than 10^{-4} torr used for decoration. A layer of metal approximately 100Å thick was deposited.

In the catalytic oxidation experiments when palladium was employed, the metal was evaporated on to the specimen by a similar technique, except that the plane of the specimen was set normal to the line between the source and the specimen and not at an angle to it.

Specimen Treatment

1. Reactions outside the electron microscope.

Although extensive studies have been made employing these techniques by other workers, it was felt necessary to perform a few experiments to check that the mode of reaction observed in the microscope was representative and not a function of the specimen environment. The apparatus is shown in Fig.10, and Fig.11 shows details of the reaction furnace. The vacuum was maintained via a conventional glass high vacuum line with pressures of 5×10^{-6} torr being usually obtained. The gas was supplied from a 5 litre reservoir that was filled by the gas purification line shown in Fig. 9. As the gas purification line was part of this same apparatus, gases could be transferred with no danger of contamination. Gas pressures above 0.1 torr were measured on a mercury manometer, the mercury vapour being trapped by the CO_2/acetone cold trap

Fig. 10.

Apparatus constructed to study graphite oxidation outside the electron microscope.

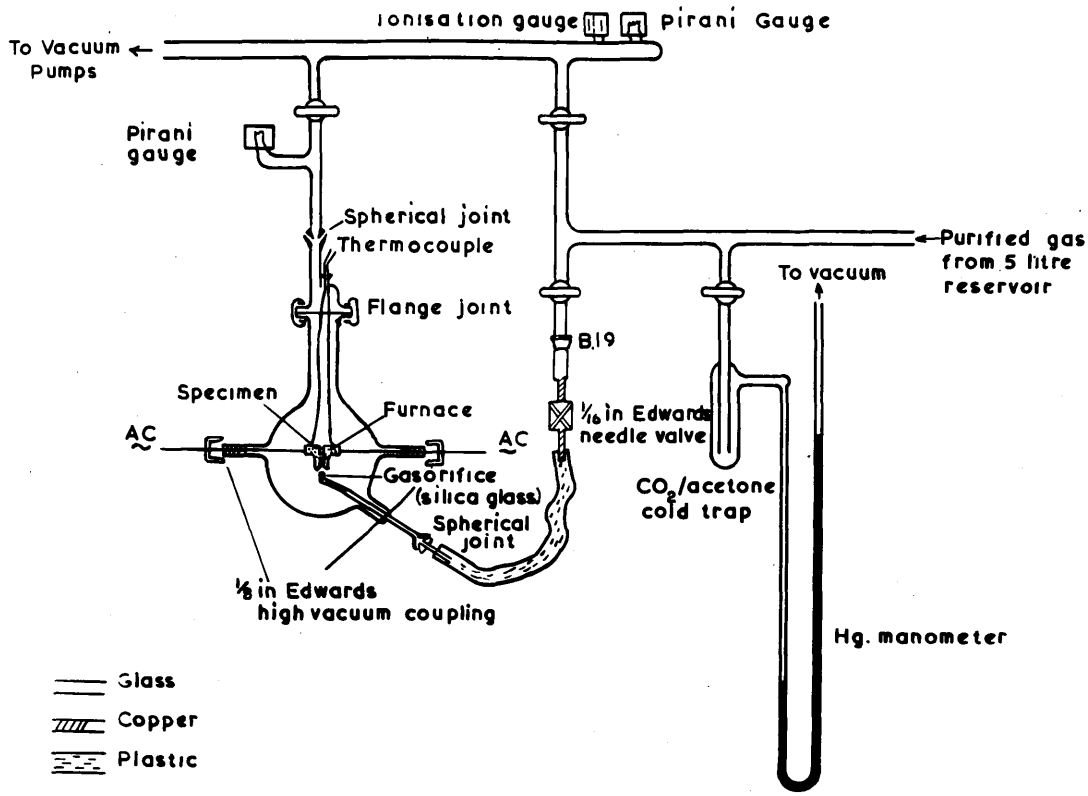
Ionisation gauge
Pirani Gauge
To Vacuum Pumps
Pirani gauge
Spherical joint
Thermocouple
Flange joint
Purified gas from 5 litre reservoir
To vacuum
B19
Specimen
Furnace
AC
AC
1/16 in Edwards needle valve
Gasorifice (silica glass)
CO2/acetone cold trap
Spherical joint
1/8 in Edwards high vacuum coupling
Hg. manometer
Glass
Copper
Plastic

Fig.11.

Enlarged view of furnace used for graphite reaction studies outside the electron microscope.

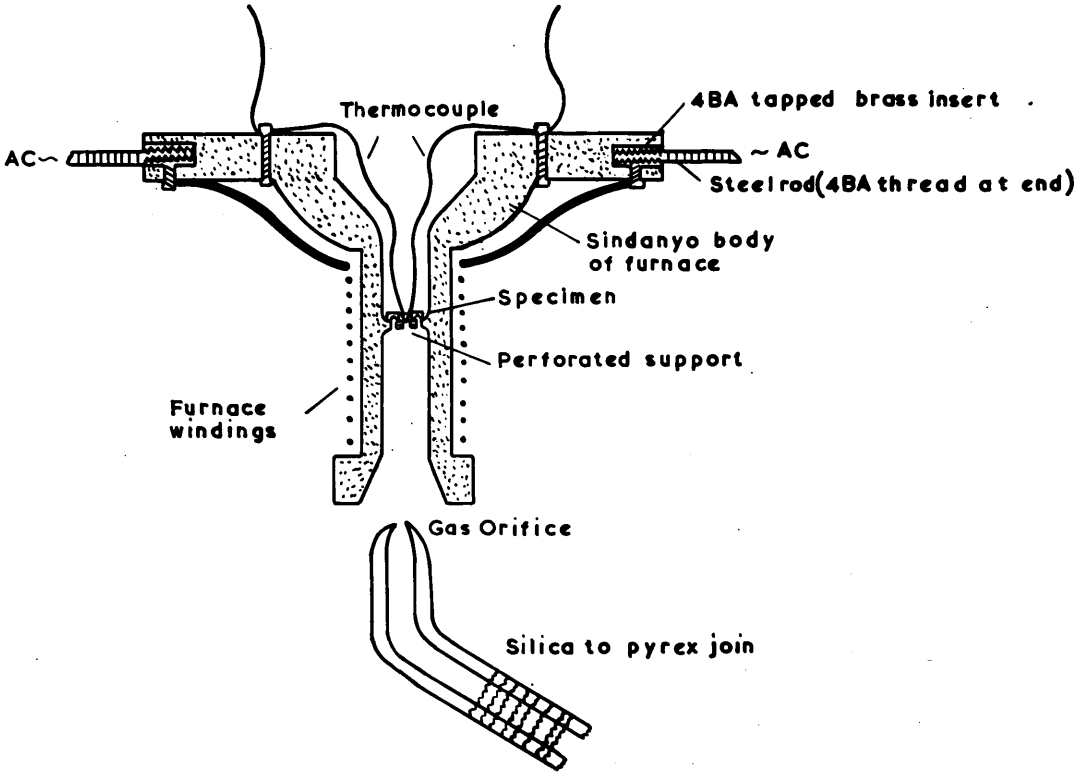
Thermocouple
4BA tapped brass insert
AC~
~ AC
Steel rod(4BA thread at end)
Sindanyo body of furnace
Specimen
Perforated support
Furnace windings
Gas Orifice
Silica to pyrex join

interposed between the manometer and the vacuum line. Care was taken to ensure that gas movements were slow to prevent mercury vapour being carried over. The reactant gas (air) flow was controlled by a needle valve which supplied the gas to the orifice in the reaction chamber. This chamber was a 1 litre bulb which had been extensively adapted as shown in the diagram. Because of high temperatures the end of the orifice was constructed of silica glass and the gas flowed upwards, through the furnace, after which it was pumped away through a cold trap and rotary pump. Fig.10. is diagrammatic, but for removal of the reaction chamber, the waxed spherical joints could be released and the chamber taken away.

After viewing specimens in the electron microscope at the commencement of each experiment, the specimens were placed in the furnace which had been removed from the chamber, and the thermocouple position adjusted so that the junction was adjacent to the specimens. Using the long thermocouple leads that passed through a B10 cone in the top of the greased flanged joint, the furnace was lowered into the chamber where it was held in position by screwing the steel rods into the threaded brass inserts on either side of the furnace. The $\frac{1}{8}$ inch Edwards couplings on the other ends of the steel rods were then tightened on "O" rings to give vacuum seals. The chamber was clamped into position and the spherical joints waxed

together, the free rotation inherent in a spherical joint ensuring that the apparatus was not under strain.

After pumping out the chamber the furnace was heated by passing an alternating current through the nichrome windings via the steel rods. The current was controlled by a variable transformer. After degassing the specimen for one hour - generally at 50°C above the reaction temperature - the gas was admitted via the needle valve. Both static and flow experiments could be performed in this apparatus and a temperature of 850°C could be sustained without the glass walls of the chamber exceeding 70°C.

Whilst this apparatus performed satisfactorily for the experiments required, the Sindanyo asbestos of which the furnace was constructed was not an ideal material for prolonged studies. Asbestos fibres tended to migrate on to the specimen and for future studies a stainless steel or platinum liner to the furnace would be more suitable.

This particular design was made to simulate the conditions within the electron microscope as closely as possible. Other more conventional furnaces generally have disadvantages that outweigh the extra complexity involved in this design.

The majority of the experiments involved reaction of the graphite at 400-500°C with dry air for 15 min and then viewing in the electron microscope to observe the

morphology of the oxidation. Replacement of the sample in the furnace and performing subsequent reactions upon it were not very successful because of increased contamination, and high liability of rupture of the support film.

2. Reaction inside the electron microscope - Gas reaction stages.

The electron microscope was not envisaged as a tool for chemistry, and even today the microscope is commercially designed for the metallurgist or biologist. Therefore it is necessary for the chemist to adapt the electron microscope to his own particular needs, and for this particular work the laboratory could be regarded as the specimen chamber of the electron microscope.

Previous workers had introduced gas into the electron microscope with one of three aims in view.

I. To reduce specimen contamination

II. To observe crystal growth - particularly for oxides.

III. To observe biological systems in their natural state.

Those with the first aim include earlier workers such as Von Ardenne (1948), Heide (1958) and Pashley and Presland (1962) the principle employed being to enclose the specimen in an oxygen or air environment at approximately 10 torr, and this would oxidise any contamination on the specimen. The atmosphere was generally sealed from

the microscope vacuum by thin films placed across apertures above and below the specimen.

This method of enclosing the atmosphere has been widely employed by workers in the other two fields of study. Abrams and McBain (1944) waxed two apertures together, using the enclosed space to support their specimen, whilst Stoyanova (1959) used collodion films to enclose the whole specimen chamber. The latter studied the reaction of silver and hydrogen sulphide in the presence of oxygen inside the specimen chamber.

This approach had a severe disadvantage in that the specimen could not be altered far from room temperature. The reason for this is that plastic films will not withstand heat without melting, and the stresses induced in silica and carbon films lead to their rupture, the films having to cover a large aperture so that the electron beam can scan the specimen. Carbon films are also unsuitable in an oxidising atmosphere because of their reactivity. Another method of treating the problem has been to admit gas adjacent to the specimen through a small orifice whilst pumping through a much larger orifice on the other side of the specimen which is mounted on a grid heater (Hashimoto et al 1966). The difficulties with this technique are that it requires a large specimen chamber for the various gas and electrical services and it also requires that the grid heater be chemically inert to both

the specimen and reactant gas. As has been described, metals are often mobile at temperatures considerably below their bulk melting points and this specification for the grid heater has not been fully realised (Feates 1967). The large specimen chamber has been a feature of Japanese commercial microscopes, and this has permitted several variations on the window and gas flow techniques described (Ho and Hiziya 1958, Hiziya, Hashimoto, Watanabe, and Mihama 1958). In the Siemens Elmiskop 1 and 1A microscopes used in the present work, the space around the specimen is very limited and thus a different approach had to be made, though towards the end of the studies a large object chamber attachment did become available.

The apparatus to be designed and constructed had to fulfil various requirements:-

1. To operate at temperatures up to 1000^{o}C
2. To maintain this temperature in the presence of reactant gas, whilst viewing was in progress.
3. Not to be a permanent attachment to the electron microscope so that the microscope could easily be returned to its usual state for normal use.
4. Not to cause any damage to the microscope.

First Gas Reaction Stage

Because of difficulties encountered with grid heaters these were not considered suitable and a furnace of tubular design was preferred. A furnace of this nature was commercially available from Siemens and it had the added

advantage that the heating element was shielded from the reactant gas. Also the platinum parts in contact with the specimen were sufficiently massive to prevent local heating and migration of metal on to the specimen. However this furnace could not be adapted to take a gas supply through it, and since it was in a very restricted environment, it was decided to introduce the gas supply through the objective aperture drive which was only 4mm away from the specime The positions of the furnace and objective aperture drive are shown in Fig.12 and details of the aperture drive shown in Fig.13. The gas was admitted through a hole 0.2mm diameter made at the end of the aperture drive and then the ga flowed past the variable objective aperture, up through the objective pole piece - the 300 μ decontamination aperture having been removed - over the specimen and out through the specimen chamber vacuum port.

1. Constructional details of apparatus

The reactant gas supply (Fig.14) was from a 5 litre glass bulb connected to a small mobile high vacuum apparatus. This high vacuum attachment was necessary to prevent any unwanted gas entering the bleed line to the objective aperture drive, and would have permitted a changing of gas supplies without admission of air had this been necessary. The vacuum apparatus is of a mixed glass/metal construction, it being preferred to have most of the gas passage through glass tubing since it is easier

Fig. 12.

Position of hollow objective aperture drive in microscope column.

A. Electron beam.

B. Vacuum port.

C. Specimen stage.

D. Heating cartridge.

E. Specimen.

F. Hole for admission of gas.

G. Variable objective aperture.

H. Objective aperture holder.

I. Objective pole piece.

J.K. Electrical connections for heating cartridge.

L. Standard vacuum union.

M. Pirani gauge for gas pressure measurement in bleed line.

N. Gas supply.

O. Needle valve for flow control.

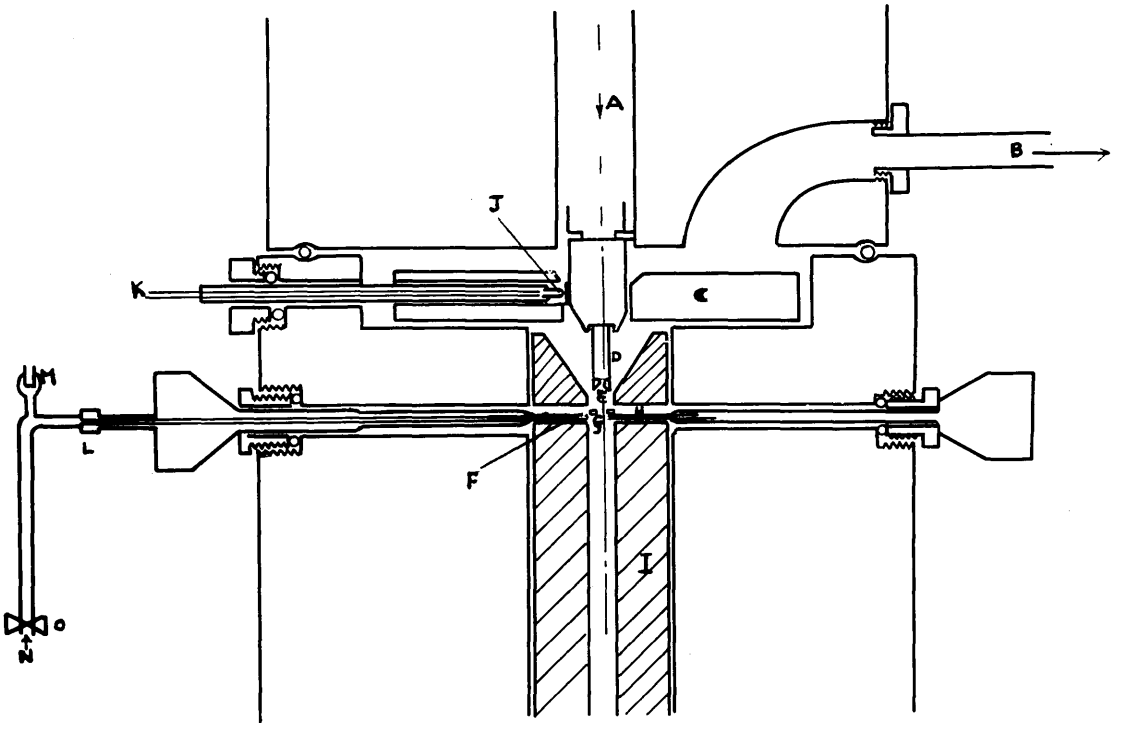
A
B
J
K
C
D
E
F
G
H
L
I
O
N

Fig. 13.

Hollow objective aperture drive.

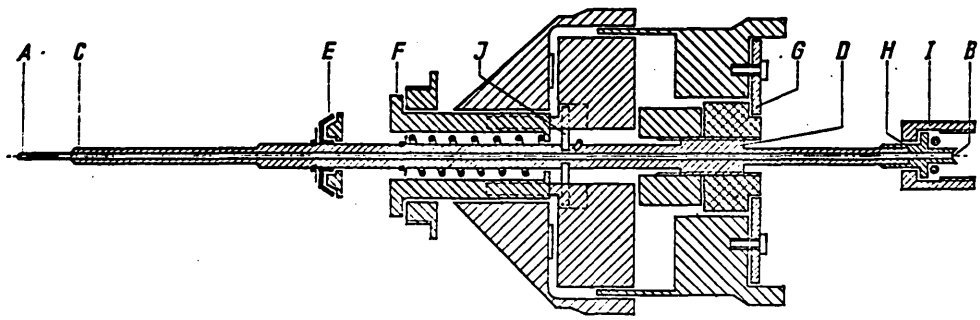

A–B	1/16″ O.D. brass tubing
C–B	Larger tubing fitted outside *A–B*
C–D	1/16″ I.D. brass tube
E	Sealing gasket
F–G	Siemens objective aperture drive mechanism
D–H	1/8″ O.D. copper tubing
I	High vacuum union
J	Locating pins
C, D, H	Vacuum tight joints

Fig. 14.

Reactant gas supply.

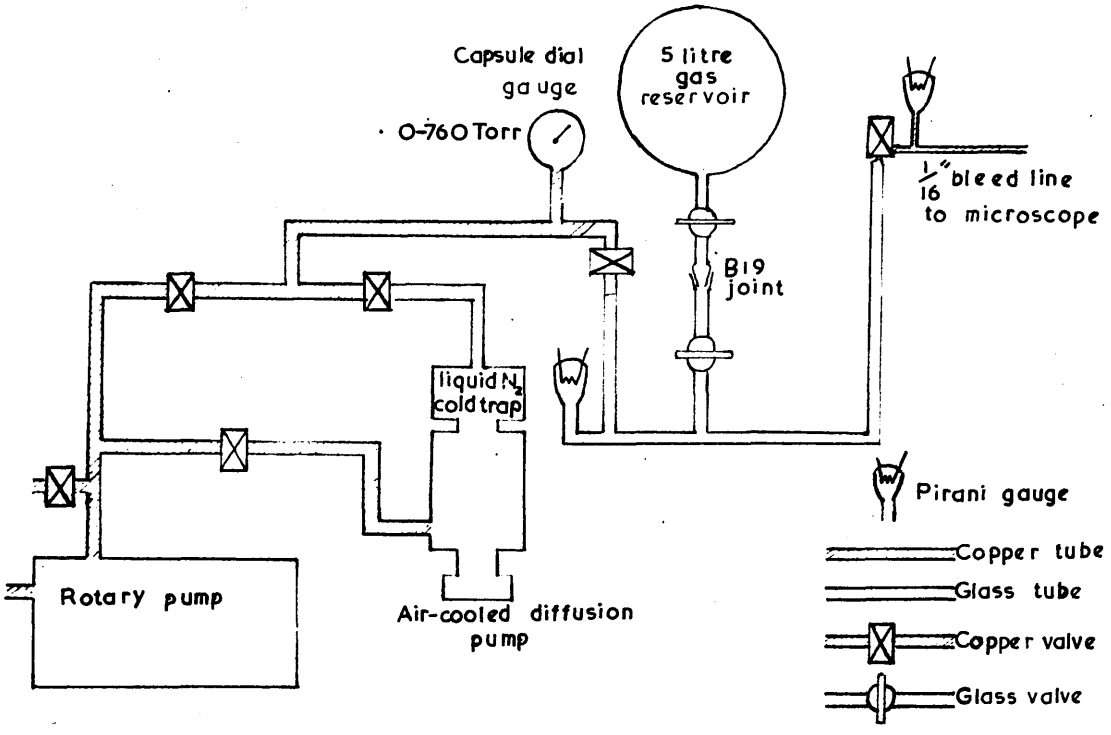
Capsule dial
gauge
0-760 Torr
5 litre
gas
reservoir
1/16" bleed line
to microscope
B19
joint
liquid N2
cold trap
Pirani gauge
Rotary pump
Air-cooled diffusion
pump
Copper tube
Glass tube
Copper valve
Glass valve

to degas and any large contamination is visible. The bleed line, however, had to be of metal and was of $^{1}/16$ in. I.D ($\frac{1}{8}$in.O.D.) copper tubing with hard soldered unions for the various connections. The small diameter results in a very slow evacuation of the tube at the commencement of each experiment, and thus the vacuum system of the gas supply apparatus was used to help evacuate this line which was heated with a flame to remove adsorbed gases from its walls. As shown in Fig.12 this line was connected directly to the objective aperture drive, but for particular experiments, drying tubes etc. were inserted between the line and the drive.

In the aperture drive shown in Fig.13 A-B is $^{1}/16$ in. O.D. brass tubing fitted inside larger tubing C-B. A-C represents the inner brass tube that had been flattened and shaped to resemble a normal objective aperture drive. The end of A was sealed with hard solder and the upper side pierced near A to give a gas exit hole of 0.2 mm diameter. C-D is a brass tube $^{1}/16$ in.I.D. and externally it is similar to a normal objective shaft except that the threaded portion near D is constructed from a standard drive thread that had been drilled to take the $^{1}/16$ in. O.D. tube. This threaded portion was fastened to the end of the shaft with epoxy resin adhesive. The movable link on a standard drive was omitted and the brass tube extended so that the length A-D is the same as a standard

drive. E is a standard sealing gasket held in place by a circlip, and F-G the standard Siemens objective aperture drive mechanism. The $^{1}/16$ in O.D. brass tubing was very liable to fracture if bent, and so for the section D-H some $\frac{1}{8}$in O.D. copper tubing was slid over the brass tubing to give added mechanical strength, and facilitate the attachment of a $^{1}/16$ in. bore Edwards high vacuum union at I. 'Araldite' epoxy resin adhesive was used to fix the copper tube on to the inner brass one, and the same adhesive held the locating pins in position at J. The original pin in the drive was fitted through the shaft and made of case hardened steel. The two pins replacing it were made of stainless steel and were screwed into small tapped recesses in the shaft before fixing with adhesive. All the vacuum joints were made with hard (silver) solder and minor adjustments to the length of the shaft were made by altering the position of the threaded portion in the drive mechanism.

Whilst in position the microscope could be used for bright field, dark field, and diffraction in the normal way

2. Calibration of apparatus.

a. Gas flow rate.

A vessel of known volume with a capsule dial gauge (0-760 torr) attached was substituted for the 5 litre gas reservoir. Initially the vacuum line volume was determined by expanding a known pressure of gas into it from

the calibrated vessel, and then the decrease in pressure during a fixed length of time was determined with the needle valve at a known setting. For gas reaction experiments with the microscope operating the determining value for gas flow depended upon the maximum pressure that could be tolerated within the whole microscope and this was 5 x 10^{-4} torr before the high tension automatically switched off. The variation of flow rate with microscope pressure was surprisingly small, for with a pressure of approximately 300 torr of air in the gas reservoir the flow rate varied between 0.72 - 1.16 ccs (NTP)/min for a microscope pressure variation of 1-4 x 10^{-4} torr.

The microscope pressure represented the gas that passed through the apparatus together with any leaks in the microscope, and was measured above the diffusion pump of the microscope vacuum system. It is therefore unrepresentative of any gas pressure in the vicinity of the specimen and thus has no significance with respect to the reaction; experimentally it was a critical parameter for microscope operation. The pressure of gas in the bleed line was approximately 300 torr and it vented only 4 mm away from the specimen. In the vacuum to which it was admitted the mean free path of air molecules is considerably greater than 4 mm, and it can be assumed that the specimen was exposed to air molecules in a very much greater concentration than was the rest of the microscope. Thus the

Fig. 15.

Siemens heating cartridge.

Heating cartridge

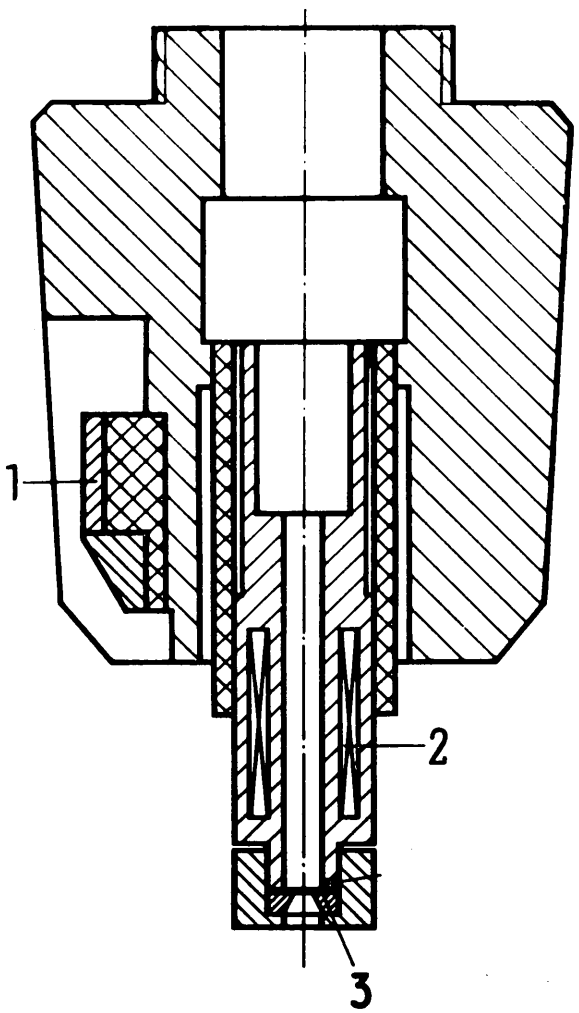

1 Heating contact
2 Heating coil
3 Specimen

reactant gas pressure was probably between 150 and 300 torr in the vicinity of the specimen, but there was no way of checking this assumption.

b. Specimen temperature.

The furnace supplied by Siemens was calibrated by a graph of temperature dependence upon power input. This graph was not precise and also it was dependent upon the furnace being used in normal electron microscope conditions. In this particular case, the furnace was in a relatively high gas pressure, the platinum-iridium seven hole mount was facing down the microscope instead of the reverse way as the makers intended, and the hole in the platinum cap on the end of the furnace (Fig.15) was enlarged to permit better gas admittance to the specimen. The most important factor of all is that the thermal effects of the electron beam can cause temperature rises in the specimen between zero and 2000^{o}C in certain cases,(Hirsch et al 1965) so the calibration graph supplied by Siemens could not be regarded as reliable.

The furnace was calibrated by operating it inside the electron microscope under preset conditions of electron beam intensity and accelerating voltage, and the melting point of specific solids determined by observation. This method has been used previously (Yamaguchi 1956) and a summary of the methods available for temperature measurement are shown in Table IV. In fact the calibration

Fig.16.

Calibration graph of temperature dependence upon power input to the heating cartridge.

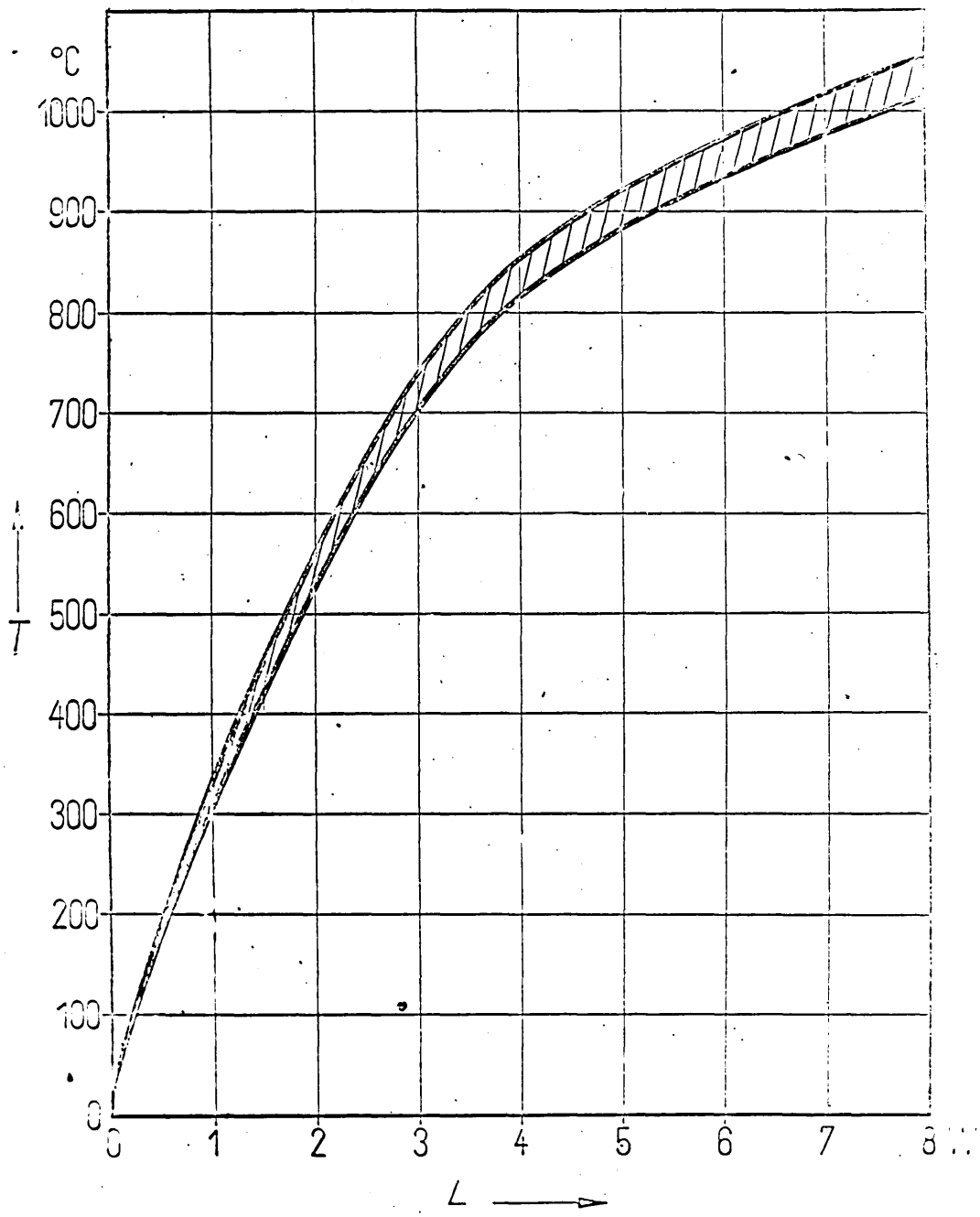
°C
1000
900
800
700
600
500
400
300
200
100
0
T
0
1
2
3
4
5
6
7
8
L

Table IV. Methods for measuring the specimen temperature.

Specimen	Temp. °C.	Observable change	Observation method	Reference
I. Continuous methods Cu-Constanton	600	Thin film thermocouple	Thermocouple voltage	Stoyanova and Belautseva (1958)
Ag-Pd	"	" " "	" "	Watanabe (1961)
Pb	300	Thermal expansion	Electron diffraction	Reimer (1960)
Ni	700	" "	" "	"
Pt-Pt.Rh	900	Thermocouple	Thermocouple voltage	Hashimoto et al (1966)
II. Determination by transformation points.				
(a) Reversible indicators.				
$AuCu_3$ film	388	Lattice change	Electron diffraction	Winkelmann (1956)
Ice	-70	Transition to cubic ice	" "	Honjo et al (1956)
Thin In film	156	Melting and solidification	Bragg diffraction in	Reimer and
Thin Pb film	327	" " "	dark field	Christenhusz (1961,
Thin Ge film	958	" " "	" "	1962)
Paraffin	70	Melting before radiation damage	Electron diffraction	Yamaguchi (1956)
(b) Irreversible indicators				
Pb film	327	Dispersion of Pb from melting cone	Direct imaging	Siemens (1967)
Al_2O_3 film	600	Transition amorphous crystal	" "	"
Sn film	232	Melting		"
Fe film	920	Transition b.c.c.cubic f.c.c.cubic	" "	"
PbO Needles	890	Melting	" "	"
Nacl - crystals	700	Sublimation of small crystals	" "	Balk and Colvin (1961)
other alkali halides	800	Melting of large crystals	" "	Reimer (1959)
$NaHCO_3$, $KHCO_3$	30-60	Decomposition	Electron diffraction	Yamaguchi (1953)

Fig. 17.

Second gas reaction stage.

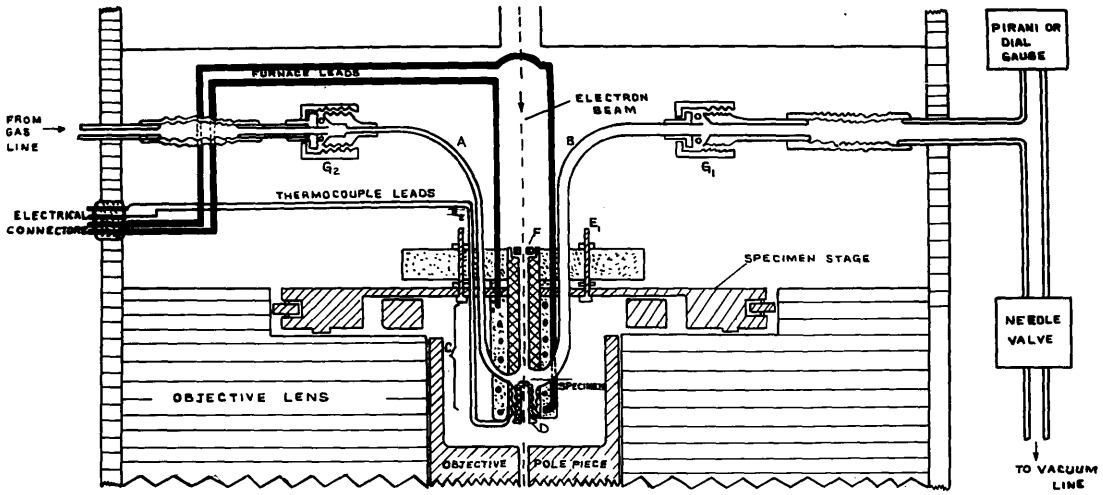

BRASS

PLATINUM

CERAMIC

RUBBER

COPPER

curve obtained was virtually identical to that made by Siemens so presumably the various adverse factors cancelled each other out. The difference was of the order of 10-15°C at 400°C which is within the range of error shown by the Siemens graph in Fig.16.

Second Gas Reaction Stage.

Towards the termination of this study a large object chamber became commercially available for the Elmiskop 1A microscope, together with a long focal length, wide bore objective pole piece. With the extra space available above and around the specimen, it was now possible to design and build a gas reaction stage, which would operate at higher, and more accurately known, gas pressures. Several attempts were made and the final model is shown diagrammatically in Fig.17. This was not perfect and is capable of being improved: it did, however, demonstrate the viability of the design.

1. Constructional details of design.

The body of the furnace was made of platinum and was a tube 1 inch long and $\frac{1}{4}$ inch diameter, with a recess in the top to fit a 300 μ aperture (F). The other end of the tube was drilled and tapped for $\frac{1}{8}$ inch of its length and into this fitted a threaded platinum tube (D) with a recess in the top to fit a 2.3mm platinum-iridium specimen mount. The thread was a coarse B.S.F. so that welding did not take place between the threads as would

have occurred if fine metric threads had been used. The specimen mount was then face upwards and approximately 7 mm from the top of the objective pole piece. Through the walls of the platinum tube adjacent to the specimen, were inserted two tubes of stainless non magnetic steel (A and B). The inlet gas tube was a fine hypodermic needle of $^{1}/_{64}$ inch I.D. and the outlet tube was $^{1}/_{16}$ inch I.D. These tubes were welded in place using platinum wire. At the bottom of the furnace tube a Pt-Pt13%Rh thermocouple was welded on. This position was chosen to avoid close proximity of the thermocouple to the furnace windings.

The furnace windings consisted of two 60w 240v annealed electric light bulb tungsten filament. These were connected in parallel and wound around the furnace in opposing sense helices. This method of winding gave the minimum field distortion to the electron beam. Tests with known masses of stainless steel were made to check the magnetic effect of the gas tubes, but they too had no significant effect on the electron beam. The furnace windings were insulated from each other and the furnace with 'Tiluma' cement, and this also served to bond the furnace to the ceramic plate. Sindanyo asbestos $\frac{1}{4}$ inch thick was used for the ceramic, and the upper surface of it was coated, first with silica, and then with silver, by vacuum evaporation. The silica sealed the asbestos surface, and the silver prevented electro static charging.

This Sindanyo plate was held proud of the surface of the specimen stage by three (only two shown in diagram E_1 and E_2) 6.B.A. brass screws, and washers could be inserted between the plate and the top of the stage so that the specimen height could be adjusted relative to the objective pole piece. Approximately $^5/16$ inch of the furnace tube were above the level of the specimen stage, and the furnace windings were concentrated in the area marked C which was thus approximately $^{11}/16$ inches long. The brass specimen stage was similar to the standard Siemens model as regards drive mechanism and mounting points, but the centre portion had been removed to permit the furnace tube, thermocouple and furnace leads, and gas pipes to pass through without touching any metal parts. The reason for this is that any large thermal contact - eg. a pipe touching the specimen stage - will cause a correspondingly large thermal gradient. This gives rise to specimen movement since the furnace will not reach equilibrium, and whilst 20Å/sec is not large for thermal expansion or contraction, this amount of drift renders focussing of the microscope impossible. The pipes A and B had $^1/16$ inch Edwards couplings on their other ends (G_1 and G_2) and were connected via rubber tubing to copper tubes which passed through the walls of the specimen chamber. The rubber tubing was used for two reasons; the first being to minimise thermal contact as described above, and the

second to reduce vibration from the gas supply apparatus, which was found to transmit along the gas feed and removal pipes. Thick walled rubber tubing, thoroughly cleaned with a variety of solvents, was found to be satisfactory. The copper tubing passing through the walls of the chamber was $^{1}/_{16}$ inch I.D. and vacuum joints were made using hard solder. The electrical connectors through the wall of the chamber were standard features of this chamber as supplied by Siemens.

One item not marked in the diagram is an earth connection from one of the gas pipes to the body of the microscope. This was found to be necessary otherwise an electrostatic charge built up on the furnace and caused vibration of the image.

2. Operation of the second gas reaction stage.

The gas supply apparatus in Fig.14 was modified so that the diffusion pump would operate without the rotary pump for limited periods of time. This was done by insertion of a 10 litre copper tank and pressure gauge between the diffusion and rotary pumps. This provided a suitable backing vacuum and thus the vibration associated with the rotary pump was avoided. The gauge gave indication of when this tank needed evacuation by the rotary pump. A further modification was a tube inserted in the high vacuum line just before the last copper valve. This tube was connected to the outlet side of the gas reaction stage

and with the copper valve closed, gas could be fed into the stage from the glass portion of the gas supply apparatus and pumped out through the diffusion pump by this new tube. Control of the gas flow was initially made by the needle valve on the gas supply apparatus, but fine control and pressure determination was performed by the needle valve on the outlet side of the gas reaction stage. According to the setting of this needle valve the pressure varied on the pirani gauge and since the only other loss of gas occurred through the 300 μ aperture in the furnace, a calibration could be made of the gas pressure existing in the furnace.

The electrical supplies for this furnace came from mains supplies which were fully rectified to provide a good D.C. supply and were variable between 0 and 300 volts. The thermocouple voltage was connected to a Cambridge internally compensated meter so that the temperature value was immediately accessible. The external view of the apparatus is shown in Fig.18.

Thus for installation of this gas reaction stage the normal stage was removed from the microscope, as was the objective pole piece, and the wide bore long focal length pole piece inserted. It was also necessary to take the filament power supply safety switch out of circuit. The gas reaction stage was inserted with the specimen already in position and the various gas and electrical connections

Fig. 18.

External view of Siemens Elmiskop 1A electron microscope fitted with second gas reaction stage.

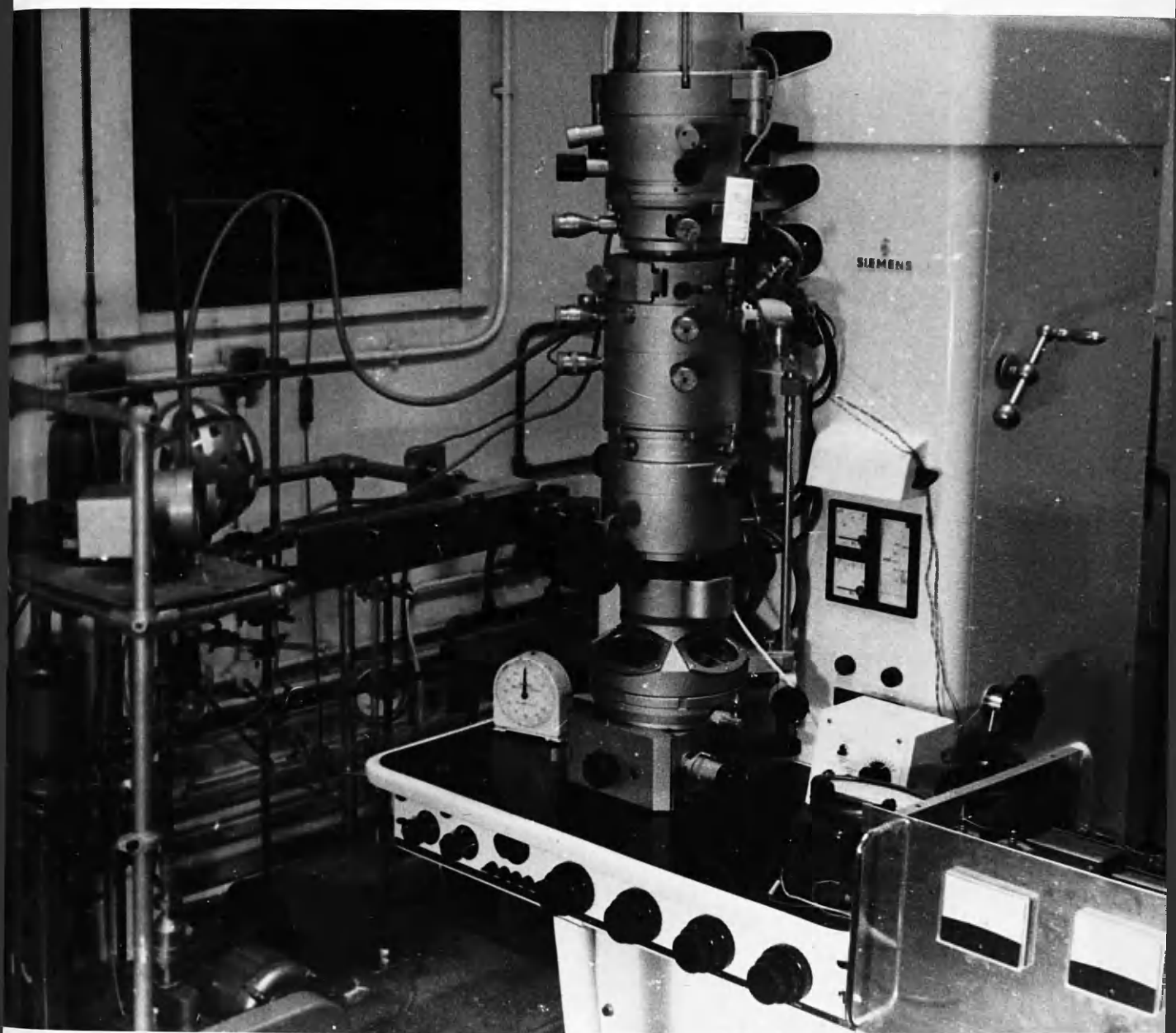
SIEMENS

fitted. The microscope was then evacuated, the stage also being pumped out by the gas supply vacuum system, until a suitable pressure was obtained (10^{-4} - 10^{5} torr) and then the temperature of the furnace slowly raised until the required temperature of oxidation had been reached. The specimen was then left at this temperature for 1 hour, the vacuum still being maintained. It was found that 10 min were sufficient for thermal equilibrium to be established at 800°C from room temperature. When the degassing period of 1 hour had elapsed, the glass portion of the gas supply apparatus was isolated and filled with air from the 5 litre reservoir, and the gas was then slowly bled into the gas supply line to the stage. The rotary pump was also turned off. During this period the outlet gas line had had all valves fully open so that under these conditions the limiting pressure over the specimen was determined by the leakage of gas through the 300μ aperture to the microscope. The supply needle valve was then partially closed so that a sub limiting pressure obtained over the specimen and in the microscope, and the outlet needle valve closed so that the gas pressure over the specimen increased. Again the limiting pressure was that set by leakage to the microscope, but in this case the approximate value of the pressure could be measured from the pirani or dial gauge.

From the commencement of gas admittance the time was

recorded, thus micrographs could be taken at known reaction times. In fact this pressure equilibrium occupied less than 30 sec so the variable pressure at the start of the experiment was not of great significance.

At the termination of the experiment the reverse procedure was followed.

Electron Microscopy.

1. Introduction.

The basic design of the transmission electron microscope has altered very little since the inaugeration of the first commercial instrument by Siemens in 1938; the electrons being emitted from a heated filament, collimated by one or more condenser lenses, passing through the specimen, and the image produced is magnified by several lenses - a three stage magnification system being the most common (Fig.19). The theory of electron scattering and lens design has been extensively reviewed (Zworykin, Morton, Ramberg, Hillier and Vance 1945; Cosslett 1951; Hall 1953, and Hirsch, Howie, Nicholson, Pashley and Whelan 1965), and the different aspects of various commercial instruments have been described. All the high resolution electron microscopes being produced at the present time have magnetic lenses for condenser and magnification systems, though electrostatic lenses have been used on smaller instruments. More recent innovations in lens construction are the permanent magnet condenser lens systems as used in the Hitachi 8 S instrument which has a quoted resolving power of 8Å, and superconducting lenses as have been constructed by Fernandez-Moran (1966) which together with other improvements in filament and pole piece design have consistently produced point to point resolutions of 2.8-3Å. However,

Fig. 19.

Ray diagram of electron microscope utilising all lenses.

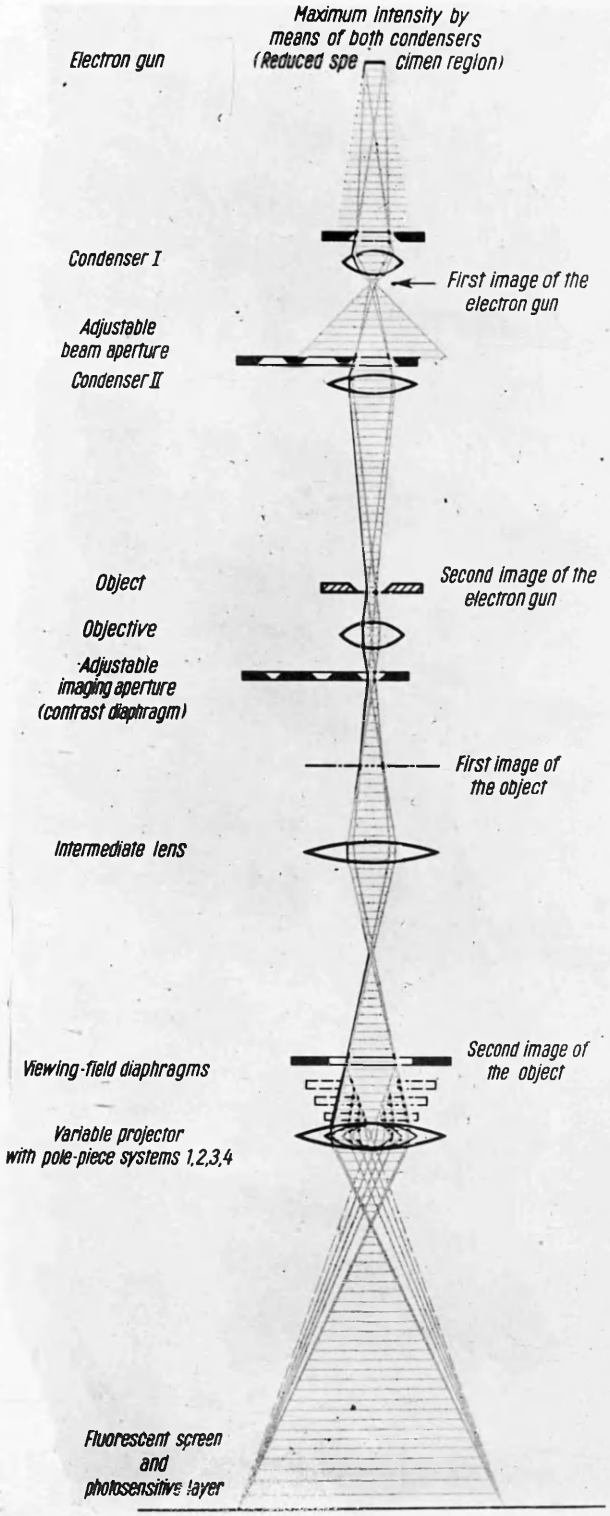
Maximum intensity by
means of both condensers
(Reduced spe cimen region)
Electron gun
Condenser I
First image of the
electron gun
Adjustable
beam aperture
Condenser II
Object
Second image of the
electron gun
Objective
Adjustable
imaging aperture
(contrast diaphragm)
First image of
the object
Intermediate lens
Viewing-field diaphragms
Second image of
the object
Variable projector
with pole-piece systems 1,2,3,4
Fluorescent screen
and
photosensitive layer

the majority of the major microscope manufacturers are now producing instruments capable of resolving point objects 3-6Å apart (GEC-AEI Ltd, Siemens Ltd, Hitachi, J.E.O.L. R.C.A, and Phillips 1968)

In this study Siemens Elmiskop 1 and 1A instruments were used, the dimensions and arrangement of these two machines were virtually identical, but the 1A microscope had more sophisticated electronics for lens and high tension stabilization, thus permitting a quoted resolution limit of 8Å. Normally both condenser lenses were used to focus the electron beam on the specimen since this gave optimum resolution and minimum contamination over the whole specimen. These instruments could however operate satisfactorily with only one condenser lens energised, and for decoration studies this latter method was employed.

2. Image formation.

Accelerating voltages for the electrons vary between 40 and 100 kv in normal electron microscopes and in this work an accelerating voltage of 80 kv was most commonly used. An electron travelling in this potential gradient has a wavelength of approximately 0.04Å and thus will be scattered appreciably by objects of greater size than 0.04Å. The confusion between corpuscular and wave terminology is rather marked for a discussion of electron scattering, but since electron emission is not being reviewed, and at these accelerating voltages less than 5%

of the characteristics of the electron beam are due to relativistic mass increase, then for a qualitative discussion the electron can be regarded as having only wave properties.

Since all the structure relevant from a chemical point of view in a specimen is larger than the beam wavelength, then the beam contains the total information about the specimen after passing through it. The information will be carried in the scattered portion of the electron beam and not in the undeviated transmitted beam. The beam can be scattered for a variety of reasons. The main effect is that of diffraction when a crystalline specimen is being examined, and the electrons scattered by the crystal lattice obey the Bragg relationship with regard to angular scatter and lattice dimensions. Thus these diffracted beams can be interrupted in a similar manner to X-rays and form an image of the reciprocal lattice at the objective lens focal plane. Electrons will also be scattered when they encounter an atom, the extent of deviation being dependent upon the atomic number of the atom in question and therefore the more atoms - ie. the thicker the specimen - then the greater the scattering that occurs. The total effect of this scattering is that at the objective lens image plane is formed an image constructed of all these scattered electron beams, overlaid with the transmitted beam which contains no information

but is of high intensity.

This image would be complex enough to interpret but various other factors make the task even more involved. The first of these is the coherence of the electron beam illuminating the specimen. It is necessary that this beam is parallel and coherent otherwise the corresponding lack of uniformity appears in the image. The use of both condenser lenses enables fairly high coherence to be obtained but small deviations do occur because of faults in cathode and condenser lens construction. The major aberrations, however, are present in the objective lens, the most severe being that of spherical aberration, so that the widely scattered electrons are brought to a focus before the more axial beams. This can be overcome by inserting small apertures in the focal plane of the objective lens to remove these widely scattered beams, but this results in a corresponding loss of information and a compromise must be reached: it is expressed in the equation.

$$\delta \text{ min} = B\lambda^{\frac{3}{4}}Cs^{\frac{1}{4}}$$

where δ min is the minimum size of point object that can be resolved

λ is the electron beam wavelength
Cs the spherical aberration constant
B a constant (approximately unity)

and an optimum objective aperture size $\propto$ opt:-

$$\propto \text{opt} = A\lambda^{\frac{1}{4}}C_s^{-\frac{1}{4}}$$

where A is a constant (again approximately unity)

In practice $\propto$ opt - the angle subtended at the

specimen by the objective aperture - is about 6×10^{-3} radians, ie. approximately 40μ diameter. Therefore an image is obtained where contrast occurs in the transmitted beam by removal of the diffracted component by means of an objective aperture. For a particular area of a crystal the intensity of the undeviated transmitted electron beam emergent from the lower side of the crystal depends upon the proportion that has been scattered or diffracted by inhomogeneities present in that particular area. If these diffracted beams are not permitted to reach the image plane of the objective lens because of an inserted aperture, then the transmitted beam for that particular area of the crystal suffers a net loss in intensity. This contrast is termed diffraction contrast and it is the most important for thin crystalline specimens where resolution of objects greater than 10Å in size are being determined. It is not valid for periodic images, thick specimens, or objects less than 10Å in size as will be described later.

The relative intensities of contrast in the image produced by this method can be calculated if the relative intensities of the diffracted and transmitted beams can be determined. This quantitative approach has been described by Whelan (1959) and Hirsch et.al.(1965) and is termed the kinematical theory of electron diffraction but these authors stress that since other factors have such

a large influence upon the diffracted beam intensities, the ideal situation is never realised and thus it cannot be regarded as a quantitive theory in practice.

3. High resolution microscopy.

Studies at very high resolution were performed to give detailed information of the morphology of the graphite, and to determine whether there was any significant structure that was not resolvable during the dynamic experiments. The graphite was mounted on a perforated film, and only very thin flakes were chosen for study, the areas protruding over the holes being most useful, since the image was not confused by the structure of the carbon support film.

Two aberrations present in the microscope were not mentioned in the previous section, but are extremely important when high resolution studies are being undertaken. The first of these is astigmatism inherent in the lenses, and induced astigmatism in the electron beam. Both the condenser and objective lenses have astigmatism compensation devices, which can correct for faults in lens construction provided extreme care is taken during compensation, and it is done under the highest possible magnification conditions. The induced astigmatism is more difficult since it arises from contamination which builds up an electrostatic charge, thus distorting the electron beam. The majority of contaminants can be removed

by thoroughly cleaning the microscope and specimen stage, and using clean apertures, but contamination does build upon the objective apertures where it has a very serious effect upon astigmatism. The most satisfactory method of overcoming this was to use thin film apertures which were not found to accumulate contamination. 50 μ apertures of this nature are commercially available but other sizes were made by the method of Stabenow (1968). With these apertures no astigmatism aberration was observable, and thus stigmator corrections only had to be made for the lenses.

The other aberration is chromatic aberration which relates to the differing wave length of electron beams having different paths down the microscope. With modern microscopes fluctuations in high tension and lens supplies are negligible, but the most serious effect of chromatic aberration arises because of different path lengths taken through the specimen. Dupouy and Perrier (1966) have shown that chromatic aberration will limit the resolution of a point in a graphite lattice to approximately $^{1}/_{10}$ of the sample thickness using 100 kv electrons, and thus it was necessary to produce lamellae of graphite thinner than 80Å even to reach the quoted resolution of the 1A microscope. Prolonged ultrasonic treatment was able to achieve this.

Differing path lengths through the specimen will give rise to phase differences in the various electron

beams and below 10Å it is believed that contrast is produced by this phase contrast mechanism. Extensive studies have been made on this, both theoretically and experimentally by Heidenreich (1967,1968), Fernandez-Moran (1966), Thon (1966), van Dorsten and Premsela (1966), and whilst the evidence is very strong for some of the high resolution claims made in the 2-5Å range, and certainly points are reproducible thus showing their reality, there is some doubt about the interpretations made of the nature of the resolved objects.

Therefore in the high resolution studies made in this work care was taken to overcome all the normal aberrations present in the electron microscope, and a liquid nitrogen anticontamination stage was inserted around the specimen. The apertures chosen for the objective lens were of sizes applicable to diffraction contrast imaging rather than phase contrast.

A separate criterion of resolution is that of resolution of a crystal lattice. A few attempts were made to resolve the 2.18Å lattice spacing in graphite, but no undisputable success was achieved, a possible reason being that it was not possible to tilt the illumination system of the microscope in the manner of Komoda (1964) and Watanabe, Shinagawa and Shirota (1966). Efforts to tilt the electron gun resulted in asymmetric astigmatism being produced thus nullifying any high resolution work.

4. Electron diffraction and orientation.

In the majority of this work, the identity of the specimen was known and thus this technique was not employed for analytical purposes. However it is possible to determine from the diffraction pattern, the orientation of any particular crystal, since the geometric relationship between the specimen and its image can be experimentally determined. Consequently the diffraction pattern can be superimposed upon the bright field image. This relationship had been observed previously (Hirsch et al 1965) but in this particular case it was employed to determine the crystalline habit plane of each edge visible in the bright field micrograph.

For a standard, an MoO_3 specimen was used which had markedly rectangular crystals, and the diffraction pattern from one of these crystals superimposed on the bright field image is shown in Fig.20. From the spread of the diffraction pattern the angular deviation between the bright field and diffraction image could be measured. This deviation being caused by the rotation of the image formed by a magnetic lens. Having superimposed the two images the crystal plane represented by a point on the diffraction pattern would run normal to a line down from that point to the centre of the diffraction pattern, and pass through that point. This construction stems from the derivation of the reciprocal lattice net which is

represented by the diffraction pattern.

Selected area diffraction patterns were also amenable to this treatment, the only criteria necessary was that the microscope operated under exactly the same conditions of magnification and projector lens exitation as were used for the MoO_3 calibration. The angle of rotation when the bright field micrograph was taken at a magnification of 21,000X was 25^{o}.

5. Dark field microscopy.

For a normal bright field image viewed under diffraction contrast conditions, the objective aperture is placed around the central transmitted beam, which when normally aligned passes along the magnetic axis of the microscope. A dark field image is produced when the objective aperture is shifted so as to permit only a diffracted beam to be used for image formation, the transmitted beam being excluded. In this case the image produced only has contrast associated with those parts of the specimen giving rise to the particular diffracted beam chosen for image formation (Hall 1948, Bassett and Pashley 1959, Pashley and Presland 1959, Pashley and Stowell 1963, Bollmann 1966, Rudee 1967). However the image is being produced by an electron beam which is travelling down the periphery of the lens system, far enough away from the lens axis for spherical aberration to be significant, and thus the image is elongated along

Fig. 20.

Diffraction pattern superimposed upon a bright field image of a MoO_3 crystal. The relative rotation between the two images is 25^{o}.


25°

a line towards the lens axis. Hence from basic optics

$$\text{Elongation } R = C_s \alpha^3$$

where C_s is spherical aberration constant

α is angle made by beam with lens axis.

Furthermore the diffracted beam suffers from spherical aberration in cross section since it is conical and not parallel-sided.

If the difference in angle between one side of the beam and the other is $\Delta\alpha$

$$\frac{dR}{d\alpha} \Delta\alpha = 3C_s\alpha^2 \Delta\alpha$$

Thus if $\alpha \approx \frac{\lambda}{d}$ where d is lattice spacing of crystal: elongation $= 3C_s \lambda^2 \frac{\Delta d}{d^2}$

To consider the loss in resolution for 80 kv electron imaging a lattice spacing of 2Å

$$\Delta\alpha = 10^{-3}$$

$$3C_s = 10^{8}\text{Å}$$

Therefore elongation $R = 40\text{Å}$ which is a measure of the loss of resolution.

In this work this elongation of a point was of particular value, since if the transmitted electron beam is aligned on the lens axis the elongation is directed towards the transmitted beam in the diffraction pattern. Thus from the reciprocal lattice construction the lattice planes giving rise to the particular dark field

reflection will lie normal to the elongation direction and the orientation of various parts of the crystal can be determined from this.

Dark field studies were undertaken for this purpose and these were achieved by this displaced aperture technique. It is possible to obtain dark field images without this elongation by tilting the illumination so that the particular diffracted beam under study passes down the lens axis, but this technique was not relevant in this particular case.

6. Contrast stop dark field.

The resolution of a crystal lattice is not a function of diffraction or phase contrast as in point imaging, but is a function of the interference between transmitted and diffracted beams. Therefore a lattice image can be obtained even though the comparable point to point distance of the lattice separation cannot be resolved. Previously when this was mentioned it was stated that because of the spherical aberration affecting the diffracted beams from the $\{10\bar{1}0\}$ reflections in graphite, for example, the lattice could not be resolved, and astigmatism prevented tilting of the illuminating system for high resolution studies. However if an objective aperture is chosen of such a size as to permit two diffracted beams to pass down the lens on either side of the lens axis then these two beams will have equal and

opposite spherical aberration and will give rise to a non aberrated interference image. Unfortunately the transmitted beam is of greater intensity than the diffracted beams and not of the same phase, so three beam constructive interference cannot occur.

This can be overcome if the transmitted beam is cut off as suggested by Dupouy (1967) who laid a 6μ tungsten wire across the centre of an objective aperture and positioned this so that the transmitted beam was cut off, and the diffracted beams allowed to pass. Thus one saw a dark field image made up of all the diffracted beams but the intensity is much higher than a normal dark field image which only utilises one diffracted beam. This method appeared to have considerable advantages over other methods of lattice imaging, the main difficulty being the construction of a suitable aperture. This was done in this study by positioning a 2 mm length of 12μ tungsten wire across a 100μ aperture whilst viewing through an optical microscope. The wire was held in position with 'Araldite' epoxy resin adhesive, first one end of the wire being embedded in a blob of viscous adhesive and then the wire being manouvered so that it lay centrally across the aperture hole, and then the other end fixed. It was then placed in a vacuum coating unit and a 200$\mathring{A}$ layer of palladium evaporated on to it. The aperture was then heated under vacuum to approximately 1300^{o}C to carbonize the adhesive and prevent non-conducting points occurring

which would cause astigmatism in the electron beam. This temperature also served to solder the tungsten to the mount with the palladium. This method proved successful for the construction of apertures with a centrally placed wire, and the wire was firmly held in position.

The apertures were positioned in the microscope by obtaining the image of the diffraction pattern of the specimen under study, and then aligning the aperture so that the wire obscured the transmitted beam. The microscope could then be adjusted to the required magnification.

7. Image recording.

The normal method with the Siemens electron microscope is to expose $3\frac{1}{2}$ x $2\frac{1}{2}$ inch plates carried in a 12 plate camera situated beneath the final fluorescent screen. For the majority of the work this was used, with Ilford Special Contrasty plate proving satisfactory. For the dynamic experiments involving mobility of metal particles the exposure time for these plates was too long for clear imaging of the moving objects, and thus a closed circuit television unit was employed with the results recorded on videotape. The television camera records the image shown on the fluorescent screen by viewing through the windows in a similar manner to the operator. Since a fairly high intensity of illumination was necessary for definition of the image, this method of recording was only suitable for low resolution studies.

Experimental Procedure Carried Out To Study Uncatalysed Oxidation Of Graphite Using First Gas Reaction Stage.

The Siemens heating stage was inserted in the microscope and the 300μ aperture removed from the objective pole piece. The hollow objective aperture drive was also put in at this time and connected to the gas supply apparatus. The microscope was then evacuated using both the normal vacuum system and the gas supply apparatus vacuum system, until an operating vacuum had been reached $< 10^{-4}$ torr. The microscope was then aligned with both condenser lenses in use, and adjusted so that suitable illumination of the image would be obtained in the 20,000-60,000 X magnification range. The heating cartridge was cleaned, the threads on the cap lubricated with 'Hydrokollag' - a colloidal suspension of graphite - and the specimen mount inserted so that when in position it would face down the microscope column. The graphite specimen had been mounted on a silica + formvar film as described previously. When the specimen was in position in the microscope various suitable areas of graphite were briefly studied, and micrographs taken. The brevity of the study was necessary to avoid contamination of the graphite with hydrocarbon impurities which were radiolysed in the electron beam. The use of both condenser lenses meant that the area of illumination could be kept small, thus avoiding general contamination. The electron beam

was turned off and the specimen heated for 1 hour at the predetermined reaction temperature under the microscope vacuum. Ideally a 900°C degassing temperature would have been used, but it was found, as will be described later, that silica migrated into the graphite.

After degassing, a further micrograph was taken of the area of interest, and then the reactant gas admitted through the objective aperture drive, a stopwatch also being started at this time. Micrographs were taken at known intervals of time, though those taken very near to the commencements of reaction tend to be of poorer quality, since the influx of gas altered the thermal equilibrium of the specimen causing some movement. Selected area and superimposed diffraction micrographs were also obtained from single crystal specimens to determine orientation, and dark field micrographs from polycrystalline specimens. It was thought desirable to keep the illumination of the specimen at a minimum to avoid any contamination difficulties, though in practice this contamination was never observed to form after reaction had commenced; nevertheless this mode of operation was followed.

Two main difficulties were encountered. The first was that at preset time intervals the specimen had to be focussed and a micrograph taken whilst making frequent adjustments to the needle valve and the microscope vacuum equipment to ensure a steady flow of gas over the specimen.

For reactions at high temperature this involved very rapid experimental working, and thus micrographs taken under these conditions were not necessarily in perfect focal adjustment. The second difficulty was that only 12 plates were available and though it was found possible to change plates during the course of a reaction, this procedure was fraught with experimental difficulties and was not always accomplished successfully. The hazard was of air admittance to the microscope which would not only react with graphite, but would also oxidise the furnace windings. This would have entailed replacing the furnace (delivery 6 months).

After the reaction had proceeded adequately, the reactant gas was shut off and the furnace allowed to cool in vacuo. The specimen was then removed and in some cases it was then shadowed using Ni/Pd alloy and again viewed in the microscope. It was found that after reaction the specimen support film had become very fragile and very few specimens survived the post reaction shadowing without extensive film rupture.

The micrographs were developed and printed in a conventional manner and quantitative measurements of eroded areas made by tracing the outline of a particular area on tracing paper, cutting around the outline and weighing the piece of tracing paper. Since the weight of the tracing paper per unit area was easily determined, the

area of the eroded sections of graphite could be calculated and for a succession of micrographs the change in eroded area could thus be measured. The edge length of the particular reacting crystal under scrutiny was measured using a conventional wheel type map measurer, and thus the area eroded per unit edge length of crystal could be determined.

RESULTS

Contents

Contents cont. Page.

Behaviour of Gas Reaction Stages.

1. First Gas Reaction Stage.

This proved a reliable piece of equipment. The main faults occurred with the heating cartridge, since the threads of the platinum on the furnace tended to weld together. However adequate lubrication, and abandoning the recommended mounting tools to insert the specimen in favour of manual fitting, cured this problem.

It was feared that when this stage was used some damage might be caused to the objective pole piece of the microscope, but none was observed. A major problem in previous studies on graphite was the contamination that built up upon the specimen with successive viewings in the microscope. With the heating stage at 400^{o}C, but no gas flow, a slight contamination was observed on prolonged viewing, contrary to the evidence of Ennos (1954). However the rate of contamination under these conditions was much less than when the specimen was maintained at room temperature. The presence of an oxidising gas such as air removed this contamination layer, and prevented further deposition, even though specimens were studied for several hours. This gas reaction stage operating at elevated temperatures thus was an efficient method of preventing specimen contamination, and the kinetic data obtained with this apparatus should have been

representative of a clean graphite surface.

Without heating and with gas flow the apparatus did not inhibit contamination. In Fig. 21a a graphite specimen is seen that was illuminated with a high intensity electron beam both to produce contamination in the gas phase, and to elevate the temperature of the graphite. The subsequent micrographs Fig 21b and c after 4 and 7 min respectively show that the contamination was deposited on to the specimen despite the gas flow.

Another fear was that filament life would be excessively shortened because of the reactant air entering the microscope. This proved to be groundless, showing that no significant quantity of air diffused into the electron gun chamber, and that it was removed by the vacuum orifice adjacent to the specimen stage.

2. Second gas reaction stage.

This was built primarily in order to investigate gas reaction systems, and not to facilitate the graphite studies. Therefore its completion was not achieved until after the majority of the graphite studies had been made. Thus the dynamic graphite studies reported were all performed using the first gas reaction stage.

The details of the design have been described previously, and modifications were made as a result of trials. The basic design of the stage appeared to be satisfactory, though the method of insertion of the

specimen from underneath, which necessitated the removal of the stage with each specimen change, was probably not ideal. A top mounted specimen would have several advantages but the design would have to be somewhat more complex so that the electron beam would have a free path through the very narrow cylindrical holes in the specimen mount. In the light of experience this extra complexity would be justified for future studies.

Another difficulty encountered was aligning the electron beam through the aperture at the top of the specimen mount and out of the bottom into the magnification system, since this required perfect vertical alignment of the stage. This was achieved satisfactorily, but a full seven hole mount could not be scanned since cut off of the beam did occur about half way across the outer hexagon of holes in the mount.

The most serious difficulty in operation was that of the furnace filament windings. The type of filament and method of winding solved any problems of field distortion, but crimping the very fine tungsten wires to connectors was not ideal and on several occasions the filaments burnt out at the joint. The thermal flexing of the filament caused the crimped wire to be extremely weak. Once the filament burnt out it could not be stretched since it was no longer in an annealed state, and a new filament had to be wound. The winding was extremely

Fig. 21a

Graphite flake on support film before reaction.

Magnification 120,000X

Fig. 21b

Graphite flake on support film after 4 min exposure to gas and electron beam.

Magnification 120,000X

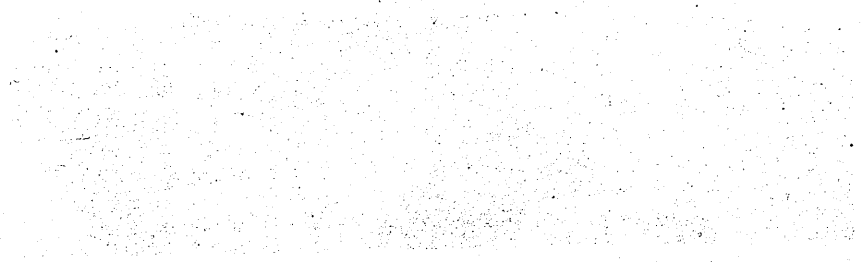

Fig. 21c.

Graphite flake on support film after 7 min exposure to gas and electron beam.

Magnification 120,000X.

tedious and, with the application of fresh insulating cement, took several days to accomplish.

However this stage did show that it would operate without image distortion at 800°C with gas pressures of several torr; as a prototype it had considerable potential.

High Resolution Studies of Graphite Morphology.

These studies were carried out to determine the exact nature of the edges of graphite crystals, and whether micropores of a few angstroms in size became visible under high resolution.

1. Investigations using bright field illumination.

Initial work was performed with S.P.1. graphite supported on a carbon film. This proved unsatisfactory since the structure of the underlying film masked any significant graphite structure (Fig.22) and thus in further studies the S.P.1. graphite flakes were supported across holes in a carbon film. This technique also had the advantage that structure due to 'noise' in the electron beam is visible in the hole in the film, and thus its significance can be taken into account. Fig.23 and 24 show successive micrographs of the same piece of graphite lying across such a hole, the surrounding carbon film being in much greater contrast. A minimum of two micrographs is necessary for assessment since random contrast can be very misleading and it is necessary to identify a feature on both micrographs before its real

existence can be assumed. Quite large features such as at 'A' in Fig.23 are not visible in Fig.24. The resolution in these two micrographs is high, and the Fresnel fringe alone shows that less than 7Å are resolvable. The points arrowed are separated by 4.5Å and are visible on both micrographs and thus in this case it can be taken that the resolution is equal to or better than this value. Nevertheless whilst the edge of the graphite crystal is serrated it is not deeply indented, as the values for surface area would suggest. These micrographs were typical of several graphite crystals studied in this way and in no case were severe indentations visible. The graphite is apparently less rough than the surrounding carbon film, but this is probably an illusion since the crystallites in the carbon film would be arranged so that the C-spacing was at an angle for diffraction in many cases, and this diffracted beam would be very strong, thus enhancing the contrast produced by the carbon film.

The granular appearance of the graphite is rather misleading since in many cases the apparent areas of contrast are not reproducible from one micrograph to the next. They are, however, strongly reminiscent of the work of Heidenreich (1967) but their structural significance is not clear. Also visible are pairs of lines running for short distances over the graphite surface. These may be lattice reflections, though the objective aperture

Fig. 22.

Graphite flake on carbon film.

Magnification 640,000X.

Fig. 23.

Graphite flake lying across a hole in a carbon film.

Magnification 2,400,000X

(1mm = 4Å)

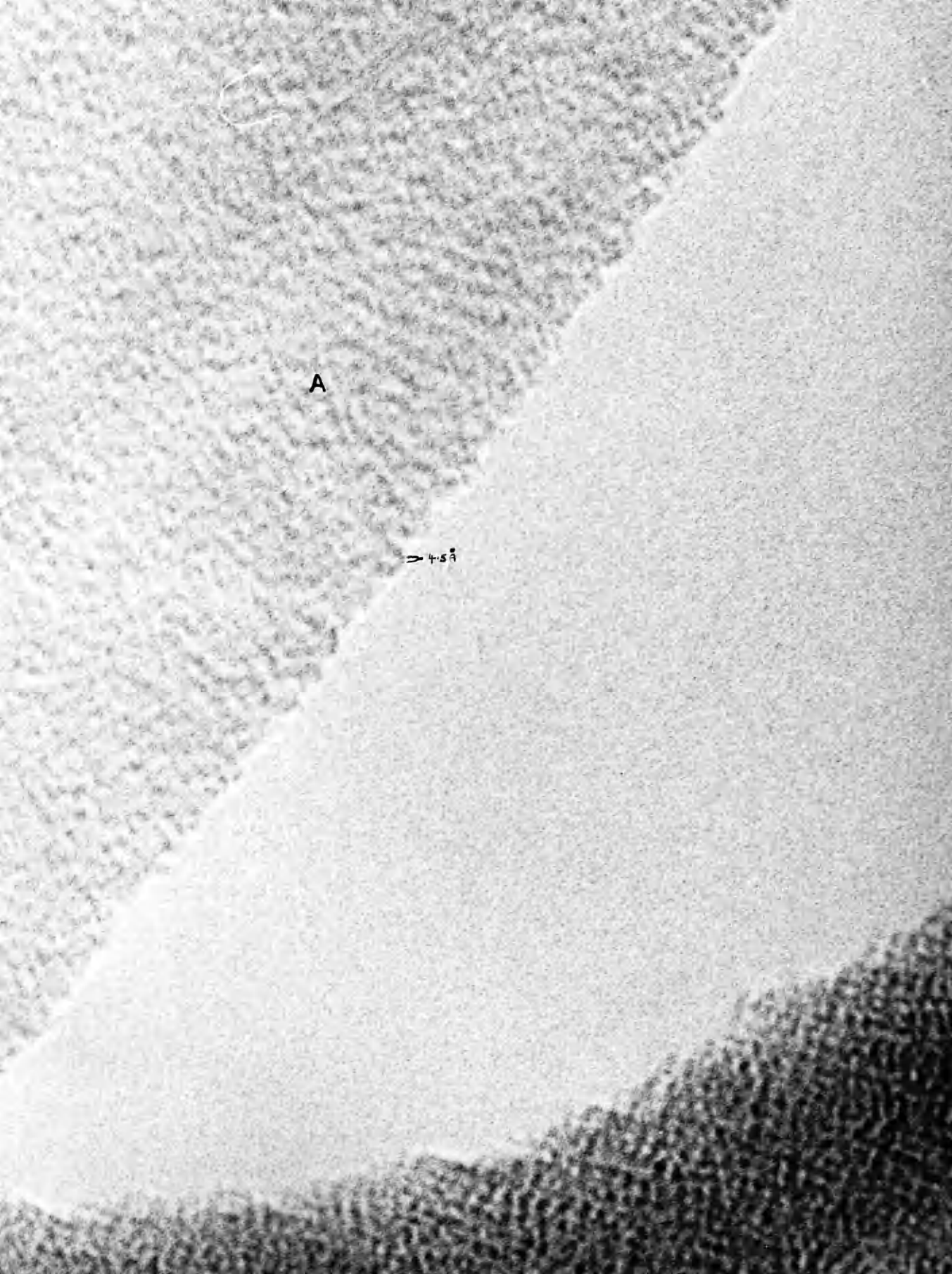
A
> 4.5 Å

Fig. 24.

Graphite flake lying across a hole in a carbon film.
The same area as Fig. 23 in slightly different focus.
Magnification 2,400,000X.
(1mm = 4Å)

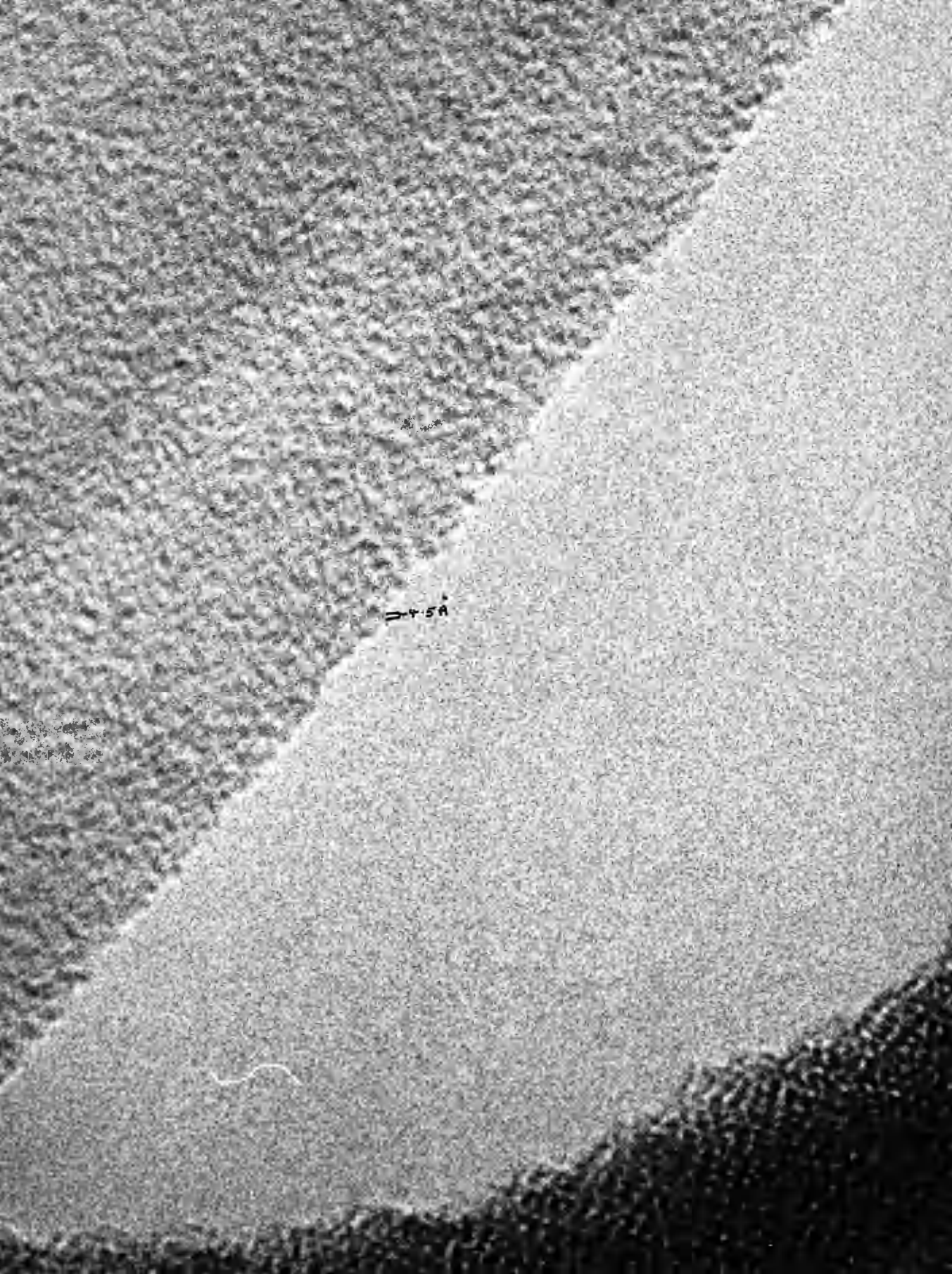
d=4.5Å

was not sufficiently large to permit reflections from the prismatic planes, unless buckling was present. Similar features - albeit less regular - are visible in the hole, caused by electron noise, so no definite conclusion can be drawn as to the identity or reality of these lines.

2. Investigations utilising the contrast-stop method.

(N.B. Reverse contrast applies in dark field so that strong reflecting areas appear white)

Micrographs 25 and 26 were taken under high resolution conditions, but with a tungsten wire across a 100μ objective aperture, which was positioned so as to obscure the transmitted (0000) beam. The band of material lying at the bottom left hand side of the micrographs is a strip of carbon film whilst the graphite flake is lying at just less than 90^{o} to it. The triangular area of low contrast is neither support film nor graphite and development in this area arises from noncoherence in the electron beam (ie.'noise').

The striking feature of these micrographs is the enhanced contrast compared with the bright field method: also the difference in contrast between the carbon film and the graphite is not as vivid. Again the resolution is approximately 5Å and reproducible points are visible in both micrographs - marked A and A'. In this case it can be stated definitely that granularity of approximately 5Å

Fig. 25.

Graphite flake (large dark area) lying over a hole (triangular lighter area) in a carbon film (smaller dark area)

Magnification 2,400,000X

(1mm = 4Å)

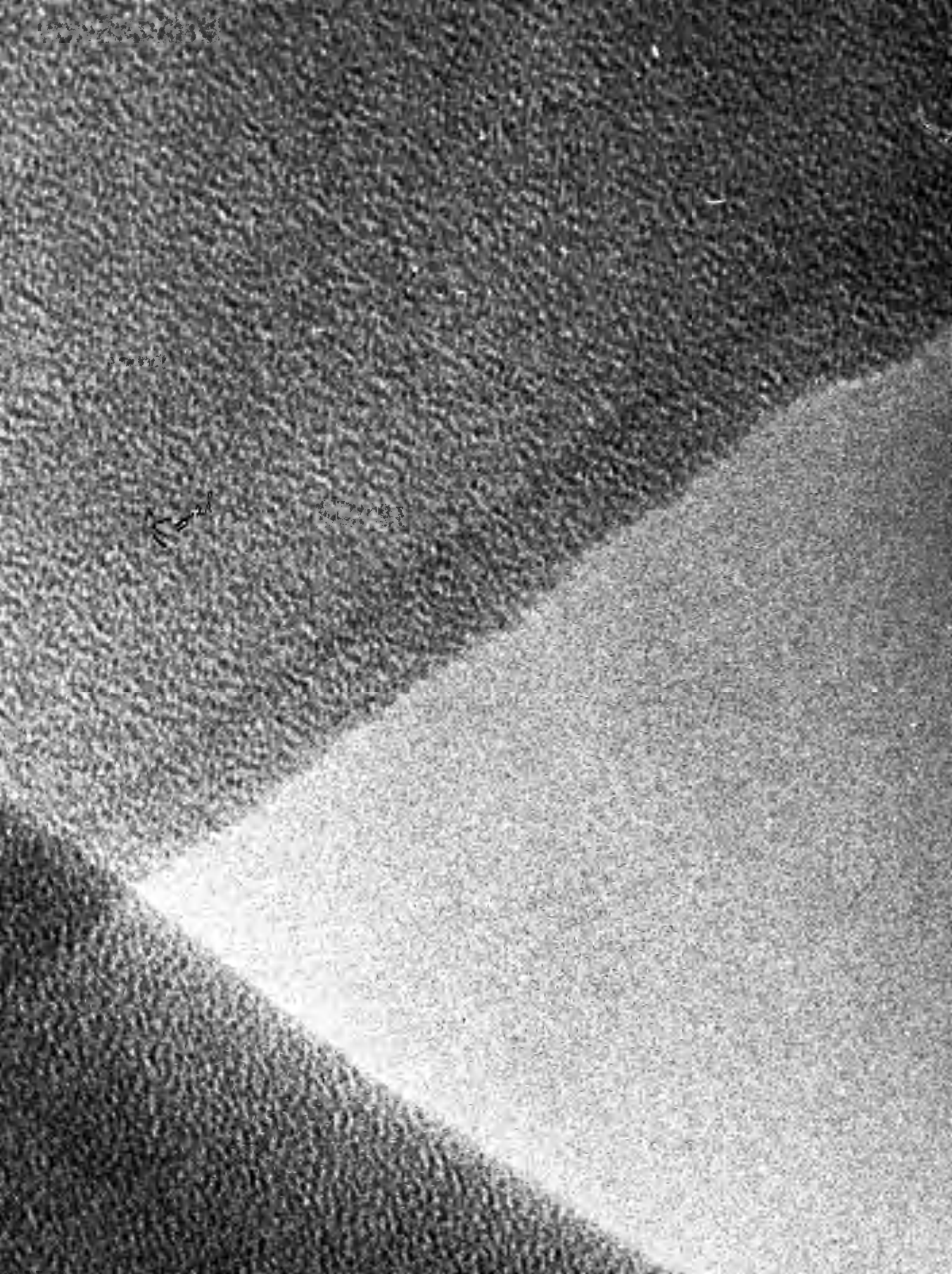

Fig. 26.

Graphite flake lying over a hole in a carbon film.

The same area as in Fig.25 in slightly different focus.

Magnification 2,400,000X

(1mm= 4Å)

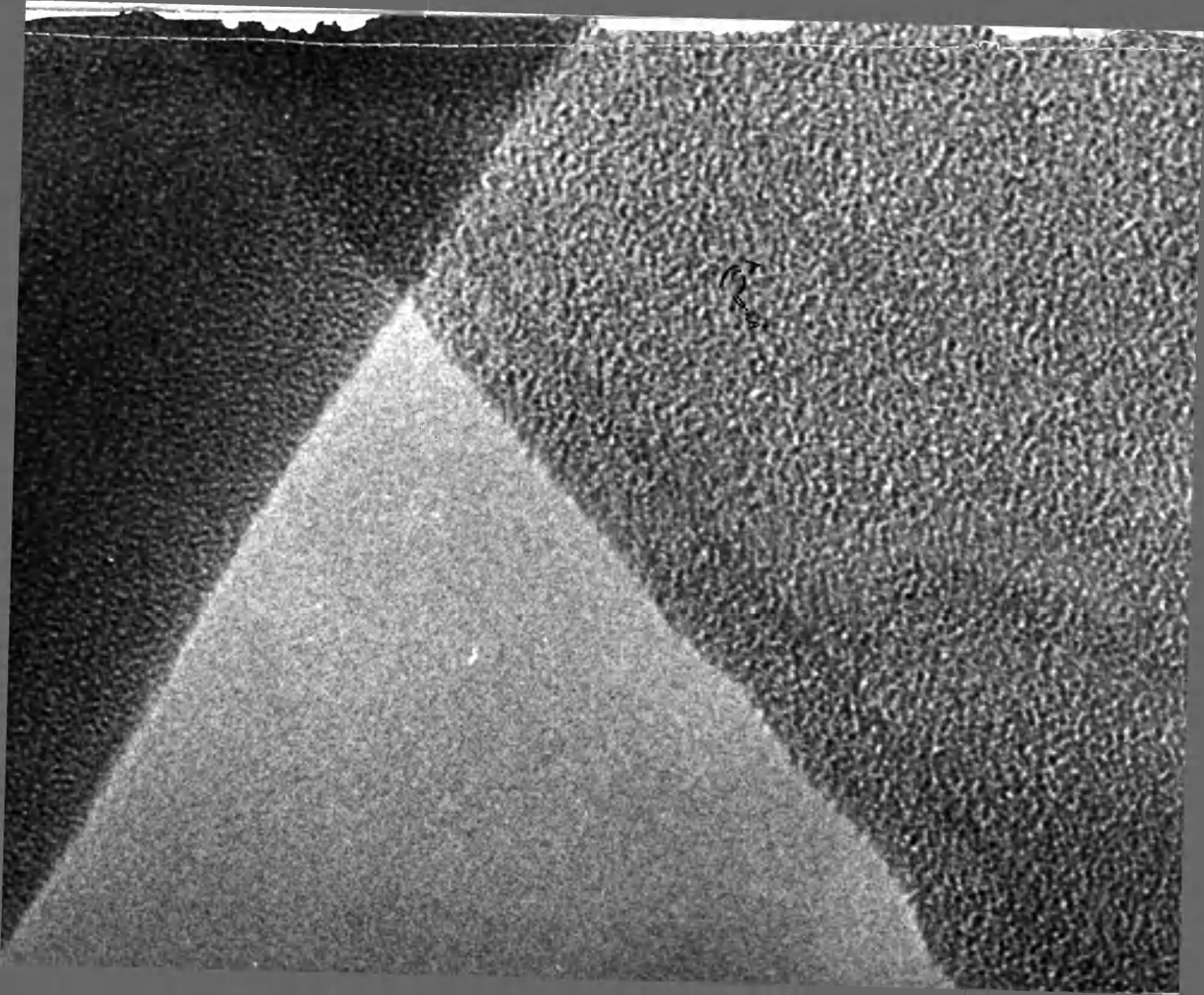

in size is visible in both micrographs in the same region of the graphite, but the structure of the edge of the crystal is similar to that shown in Figs. 23 and 24, and no pores in the form of channels are visible.

No change in contrast is visible at the edge of the crystal which might indicate that exfoliation of the edges was present, nor are any lattice lines visible though in this case the objective aperture would have permitted reflections from the prismatic planes to pass. This exclusion of lattice lines is similar to that in bright field, since similar short lengths of regular striations are visible with approximately 2Å separation, but the evidence is not conclusive.

3. Moiré fringes.

These arise from either lattices of two different spacings overlapping, or two similar lattices rotated relative to each other (Kay 1960). In graphite the latter applies, and provides a method for imaging the crystal lattice. Unfortunately a true correspondence between the image and the lattice is not obtained and terminating lines which were originally thought to be edge dislocations (Dawson and Follett 1959) are now not believed to be so, but must be regarded as discontinuities or buckling within the lattice where a layer plane has moved out of contrast, rather than terminated in the crystal. (Williamson and Baker 1960, 1961). Typical moiré

patterns are shown in Figs. 27 and 28, the micrographs both being of the same area of S.P.1. graphite, but in Fig. 28 $\{10\bar{1}0\}$ dark field illumination has been used so this will only pick up moiré patterns arising from these particular planes. Applying the standard formulae: rotation moiré:-

D - the measured distance between moire bands

$$D = \frac{d}{E}$$

where E is the rotation angle in radians and d is the lattice spacing of the planes giving rise to the moiré bands.

In this particular case E = 44 min

A bright field high resolution micrograph of moiré arising from $\{10\bar{1}0\}$ planes is shown in Fig. 29 which correspond to a rotation of $7^{o}48$ min. In this case the lines are much less regular, though the background carbon film produces a granular image which is of similar size to the line width, and thus may be causing some confusion.

4. Heavy metal shadowing.

This does not strictly come into the category of high resolution microscopy but it reveals much about the three dimensional nature of the specimen that is not possible by any other method.

The major feature of these studies was the high proportion of specimens which had regions twisted out of the plane of the specimen support film. Fig.30 is a

Fig. 27.

Moiré patterns in graphite (S.P.1.) shown by bright field microscopy.

Magnification 200,000X

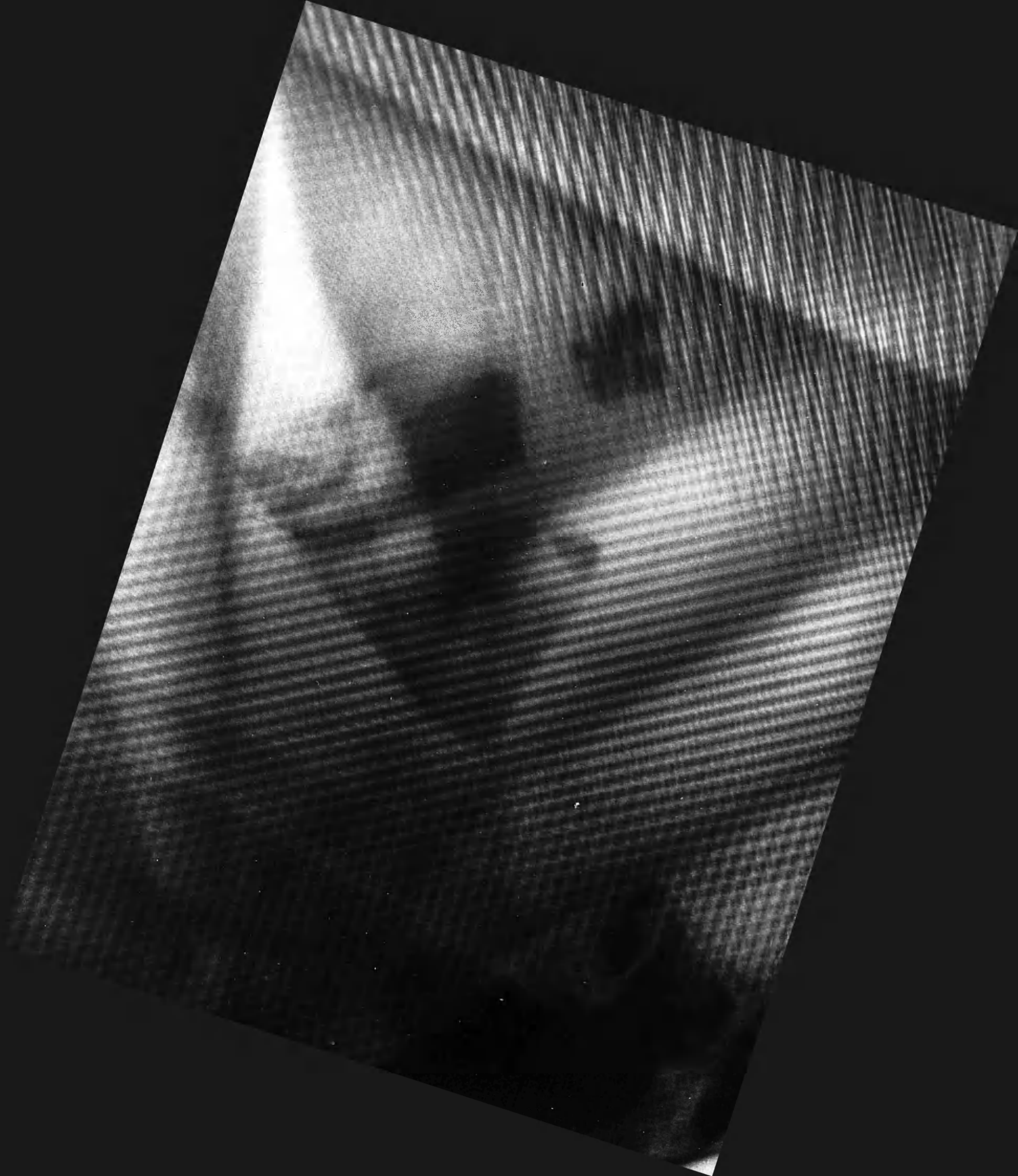

Fig. 28

Moiré pattern in graphite (S.P.1.) shown by dark field microscopy the $(10\bar{1}0)$ reflection being used.

This is the same area as in Fig. 27.

Magnification 200,000X

Fig.29

Moiré pattern shown by high resolution bright field microscopy. This is the same area as in Fig.22 in slightly different focus.

Magnification 640,000X

sample of [illegible] which has been shadowed twice at right angles with Ni/Pd alloy angled at 30° to the specimen surface. Some of the flake is pointing vertically upwards - marked A - and some is bent away from the support film, marked B. It is also clear that a large number of layer planes do not extend to the edge of the main crystal, but finish at steps on the crystal surface. At 'C' these steps are 43Å high. The resolution of structure by this technique is dependent upon the grain size of the shadowing material. Simultaneous evaporation of platinum and carbon give the finest structure, and Fig.31 shows a resolution edge height of 22Å at X. It is of interest in this micrograph that the edge, of which X is a part, has a ragged appearance as shown by the shadowing material. This may be because of the treatment to which the specimen has been subjected since it had to be close to the evaporating source for adequate carbon/platinum deposition. However there is no suggestion of exfoliation of the layer planes at the terminating step so any structure of this nature must be less than 10Å high - if it exists - since this is the resolvable limit in this micrograph.

Fig. 30.

Graphite crystal shadowed at 30^{o} with Ni/Pd alloy. Two depositions were made at right angles to each other. (N.B. the 'shadows' are the lighter areas of the crystal and support which the depositing metal has been unable to reach.

Magnification 80,000X

A
C
B

Fig. 31.

Graphite flake shadowed with carbon/Platinum at 15^{o} to the specimen surface.

Magnification 160,000X.

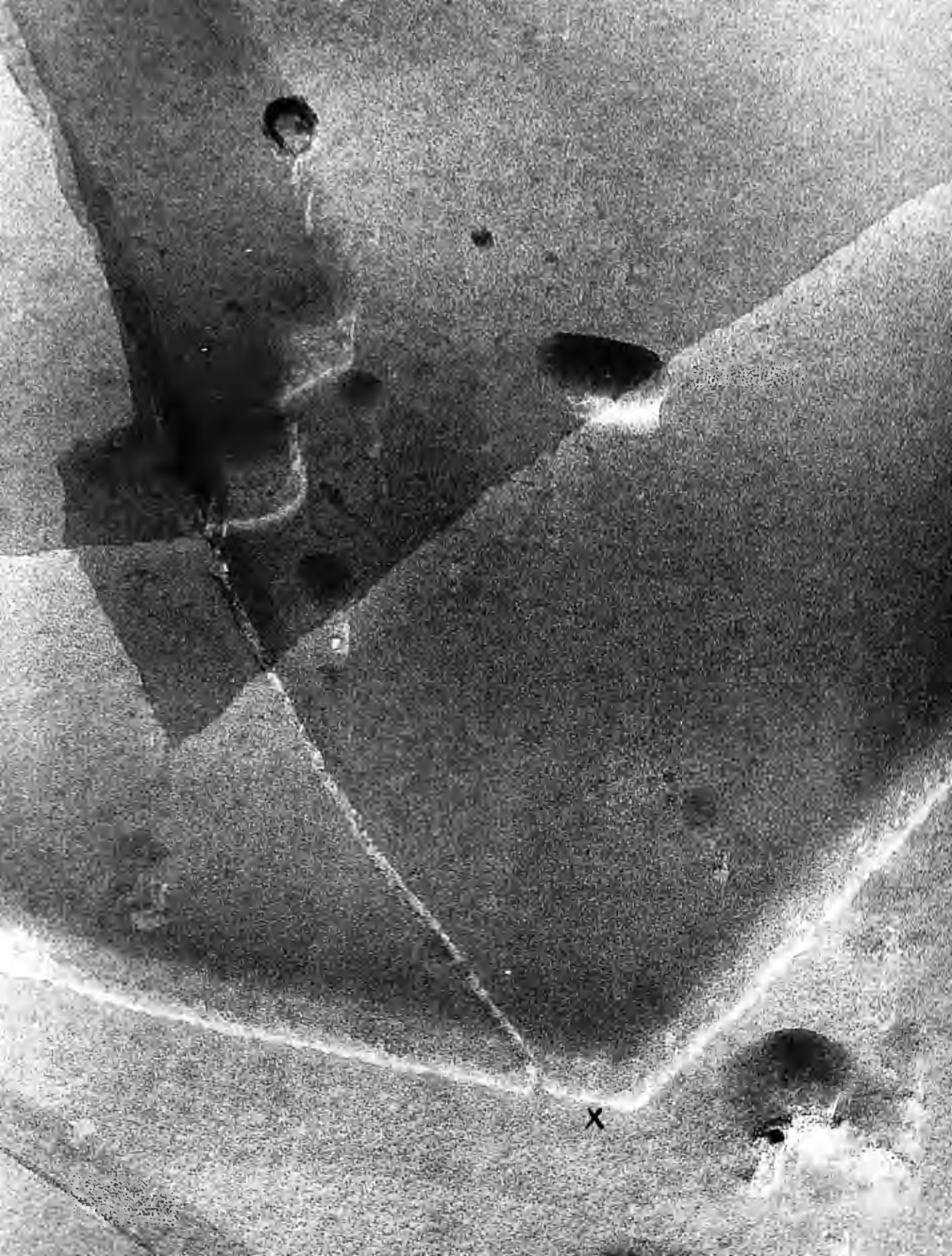

Decoration.

1. Decoration counts.

The purpose of this was primarily to investigate the specimen preparation technique. Therefore samples were decorated that had been subjected to ultrasonic disintegration for varying lengths of time; the effect of different solvents was also investigated.

A typical experimental series was conducted as follows:-

S.P.1. graphite specimens were subjected to ultrasonic disintegration in water for specific lengths of time, and then heated to 600°C, decorated with silver at 300°C and micrographs taken. Areas of a graphite flake where the particle density appeared reasonably typical for that specimen were chosen, the delineated area generally being $10cm^2$. The number of particles in the area were then counted and compared with a count of a similar area on the background film. The ratio was taken as a measure of defect concentration on the specimen.

The series shown in Figs. 32,33,34,35 show S.P.1. graphite that has been disintegrated for 1,3,6 and 10 min respectively. In fact three different specimens at each time interval were studied, and two decoration counts made of each on the graphite, and one on the background film. The average values for decorations counts, and appropriate ratios are shown in table V. This duplication

Fig. 32.

S.P.1. graphite decorated with silver after 1 minute ultrasonic disintegration and 600^{o}C heating.

Magnification 120,000X

Fig. 33.

S.P.l. graphite decorated with silver after 3 minutes ultrasonic disintegration and 600^{o}C heating.

Magnification 120,000X

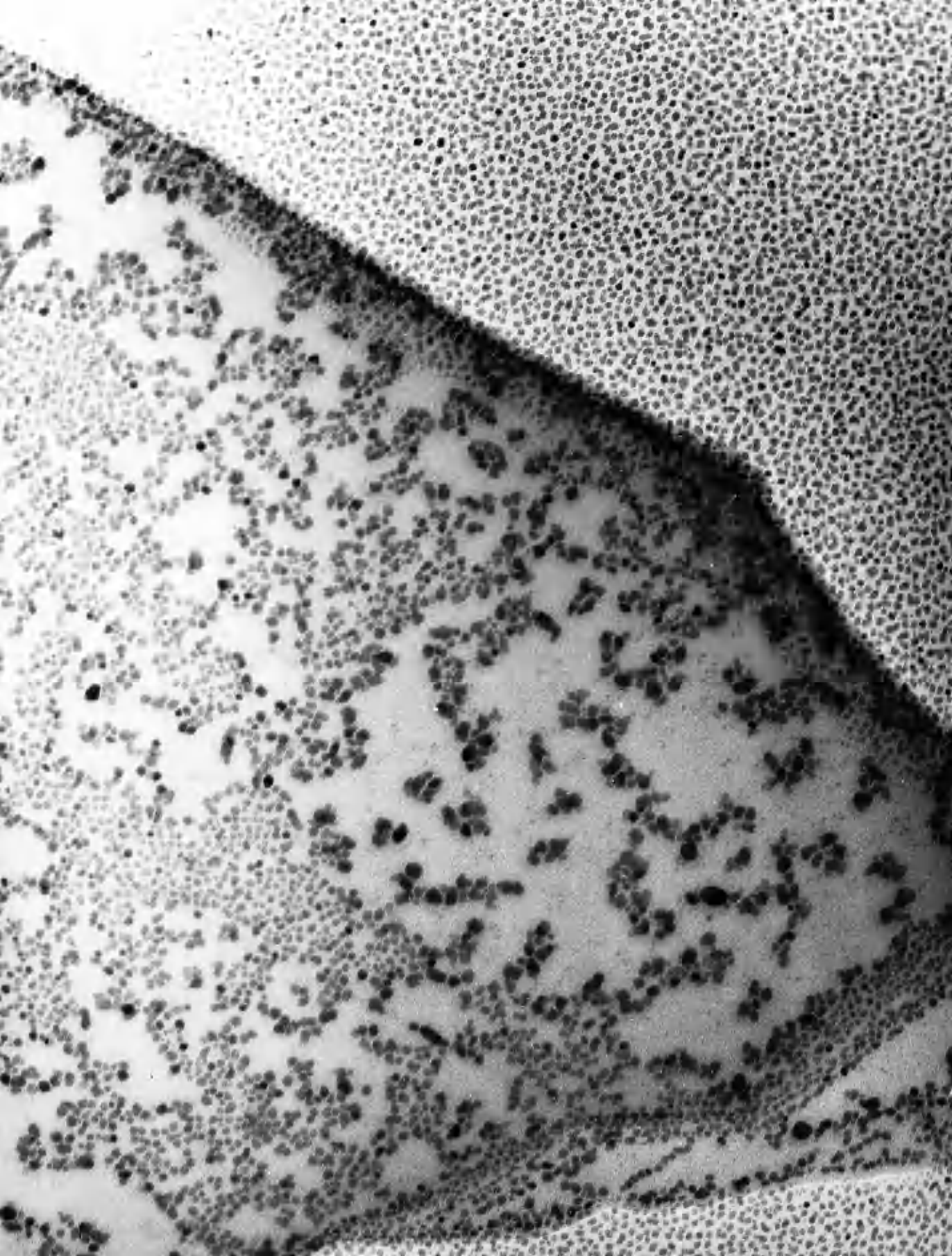

Fig. 34.

S.P.l. graphite decorated with silver after 6 minutes ultrasonic disintegration and 600°C heating.

Magnification 120,000X

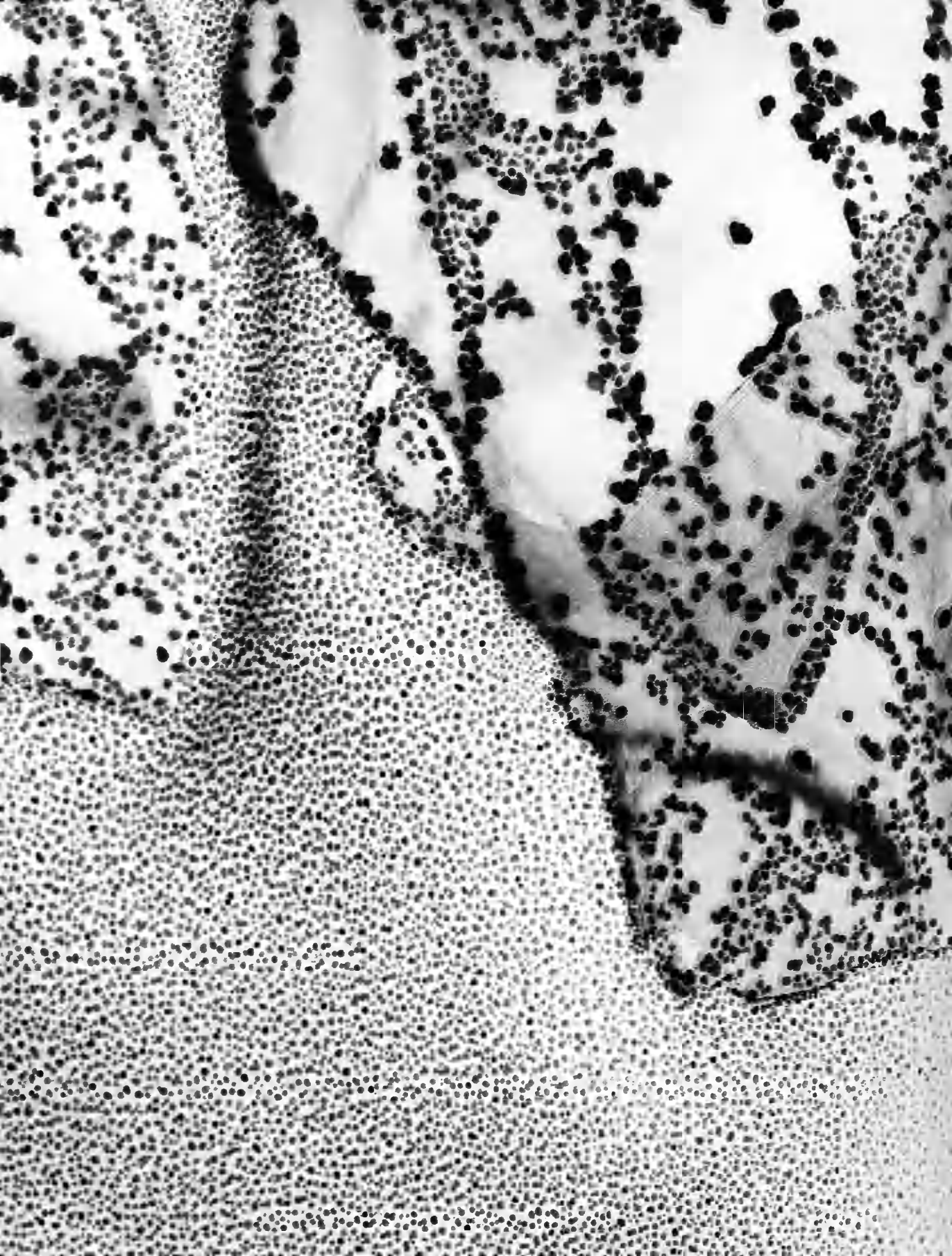

Fig. 35.

S.P.l. graphite decorated with silver after 10 minutes ultrasonic disintegration and 600^{o}C heating.

Magnification 120,000X

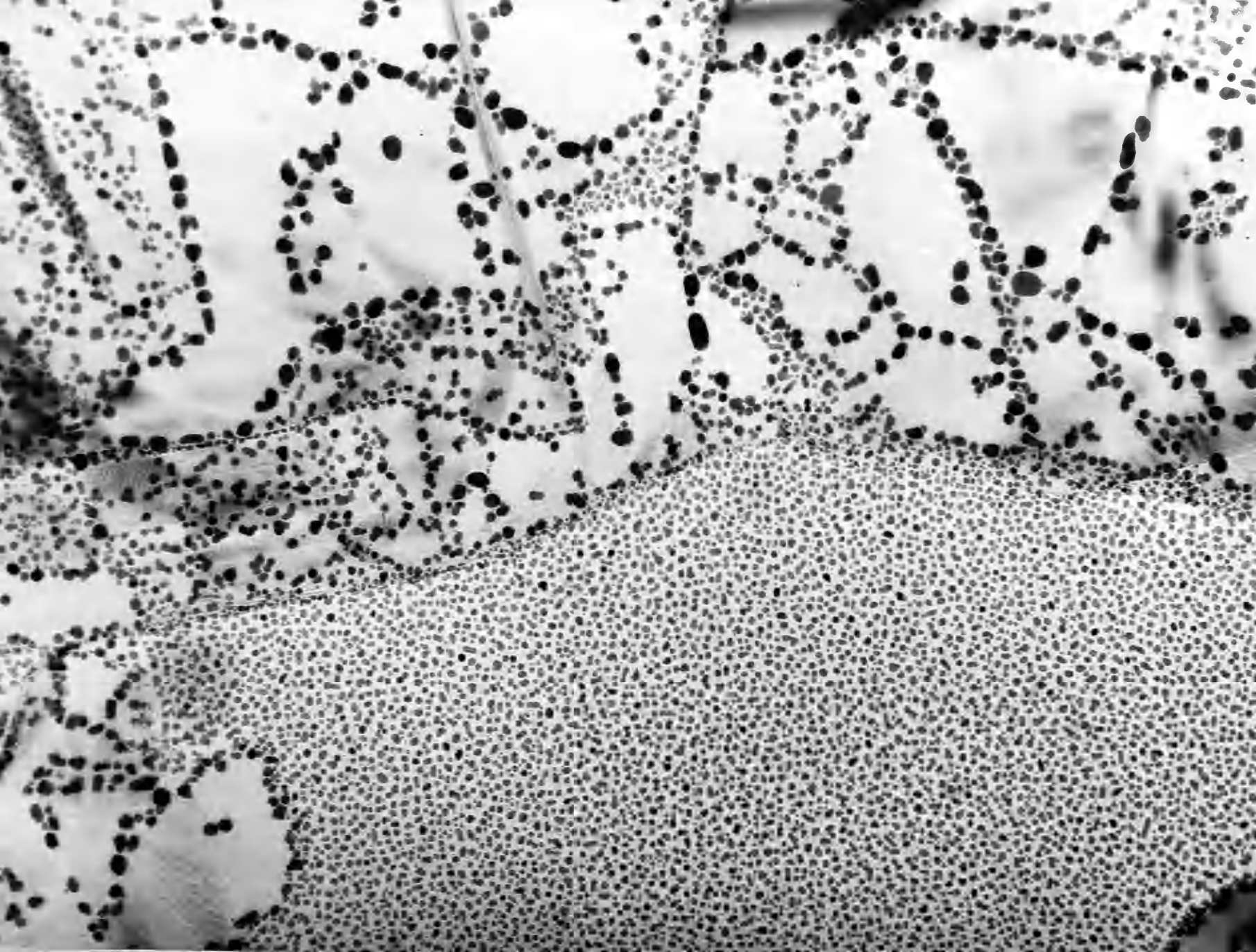

Table V

S.P.1. graphite heated to 600^{0}C after disintegration in water and then decorated.

Time of disintegration. Min	No.of particles/ cm^2 on graphite		No.of particles/ cm^2 on background		Ratio
1.	18.3 19.3 16.6 13.5 22.4 24.9	average 19.2 σ=3·7	26.8 45.3 38.8	average 36.9 σ=7·65	0.52±0.26
3.	15.2 13.4 15.6 16.1 14.3 13.5	average 14.7 σ=1·02	35.6 34.3 34.1	average 34.7σ=0·66	0.42±0.04
6.	14.1 14.5 15.7 15.7 11.6 14.5	average 14.3 σ=1·37	35.4 36.4 34.9	average 35.6 σ=0·63	0.40±0.05
10.	12.0 11.8 15.0 16.1 13.0 13.5	average 13.6 σ=1·55	35.6 34.8 36.4	average 35.6 σ=0·65	0.38±0.05

Table V. cont.

P.G.A. graphite heated to 600°C after disintegration in water and then decorated.

Time of disintegration Min	No.of particles/ cm^2 on graphite		No.of particles/ cm^2 on background		Ratio
1.	21.0 24.6 12.5 12.1 18.4 17.1	average 17.6 $\sigma = 4.4$	39.0 21.8 26.4	average 29.0 $\sigma = 7.3$	0.61 ± 0.39
30.	17.8 17.6 14.8 13.1 27.0 20.3	average 18.4 $\sigma = 4.5$	39.1 28.1 38.1	average 35.1 $\sigma = 5.0$	0.52 ± 0.24

These results are plotted graphically in Fig. 36.

Fig. 36.

Dependence of decoration ratio upon the duration of unltrasonic disintegration. 600°C pretreatment.

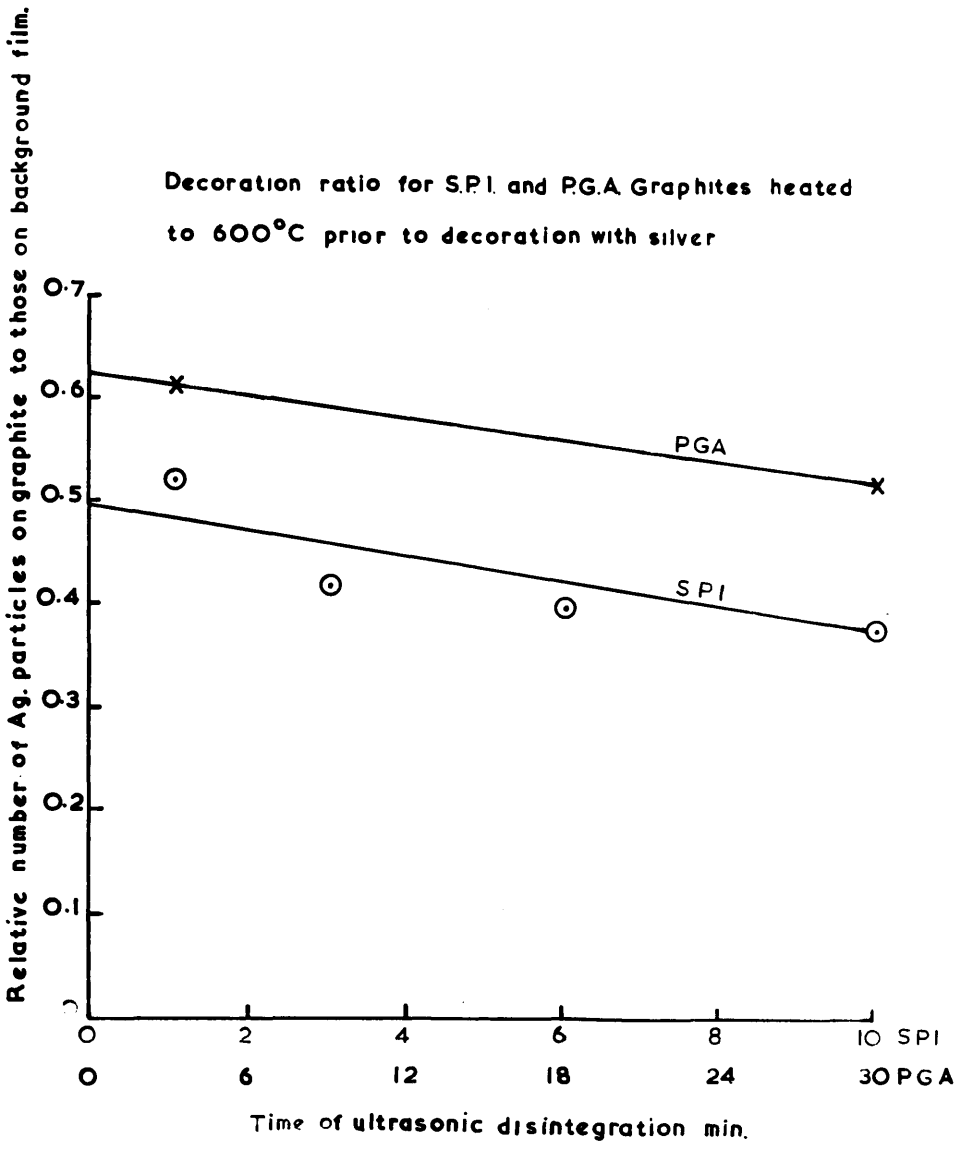
Decoration ratio for S.P.I. and P.G.A. Graphites heated to 600°C prior to decoration with silver
Relative number of Ag. particles on graphite to those on background film.
0·7
0·6
0·5
0·4
0·3
0·2
0·1
0
PGA
SPI
0
2
4
6
8
10 SPI
0
6
12
18
24
30 PGA
Time of ultrasonic disintegration min.

of measurements was used to overcome the subjective element in choice of area in which the count was taken. The appropriate micrographs for the P.G.A. are Figs.37 and 38 showing the effect of 1 and 30 minutes disintegration respectively.

The experimental procedure was now changed so that the specimens were degassed at 900°C after disintegration and prior to decoration, without exposing the specimen to atmosphere during this treatment. Whilst there was not likely to be much defect movement at this temperature since graphite is prepared at 2800-3000°C, the majority of chemisorbed surface species will be removed at 900°C (Montet 1962, Feates and Parry 1964). Thus the previous experiments were repeated with this new procedure. Fig.39 refers to S.P.1. that has been cleaved between glass slides, immersed in water, and then mounted for decoration, and Figs 40-44 refer to S.P.1. that has been subjected to ultrasonic disintegration for 2,4,6,8 and 10 min respectively. Figs.45 -49 refer to a comparable series of experiments (excluding 2 min) using P.G.A. graphite. The decoration count ratios are presented graphically in Fig. 50. Also in this graph are two further points which represent the decoration count ratio when the graphite was not immersed in water after cleaving, and the other shows the value after 6 min ultrasonic treatment in cyclohexane.

Fig. 37.

P.G.A. graphite decorated with silver after 1 minute ultrasonic disintegration and 600°C heating.

Magnification 120,000X

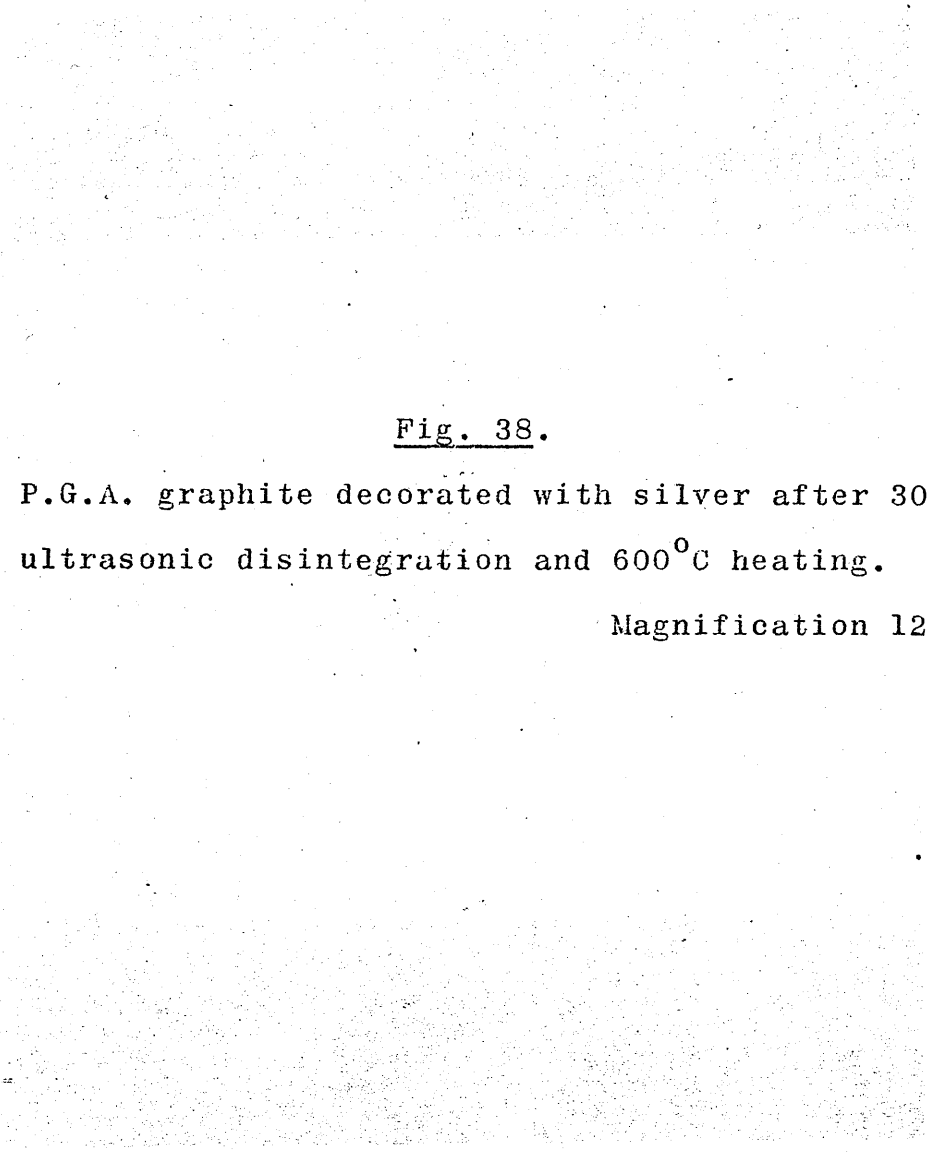

Fig. 38.

P.G.A. graphite decorated with silver after 30 minutes ultrasonic disintegration and 600^{o}C heating.

Magnification 120,000X.

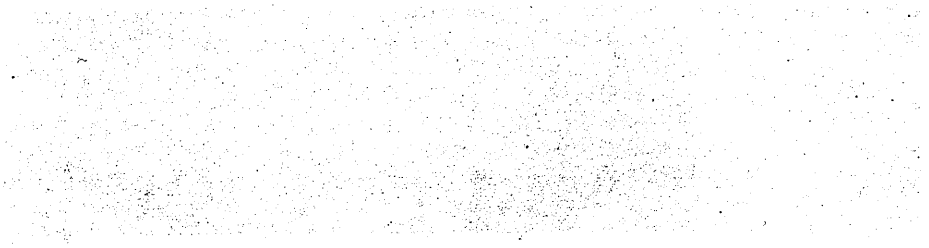

Fig. 39.

S.P.I. graphite decorated with silver after the graphite had been cleaved in water and heated to 900°C.

Magnification 120,000X

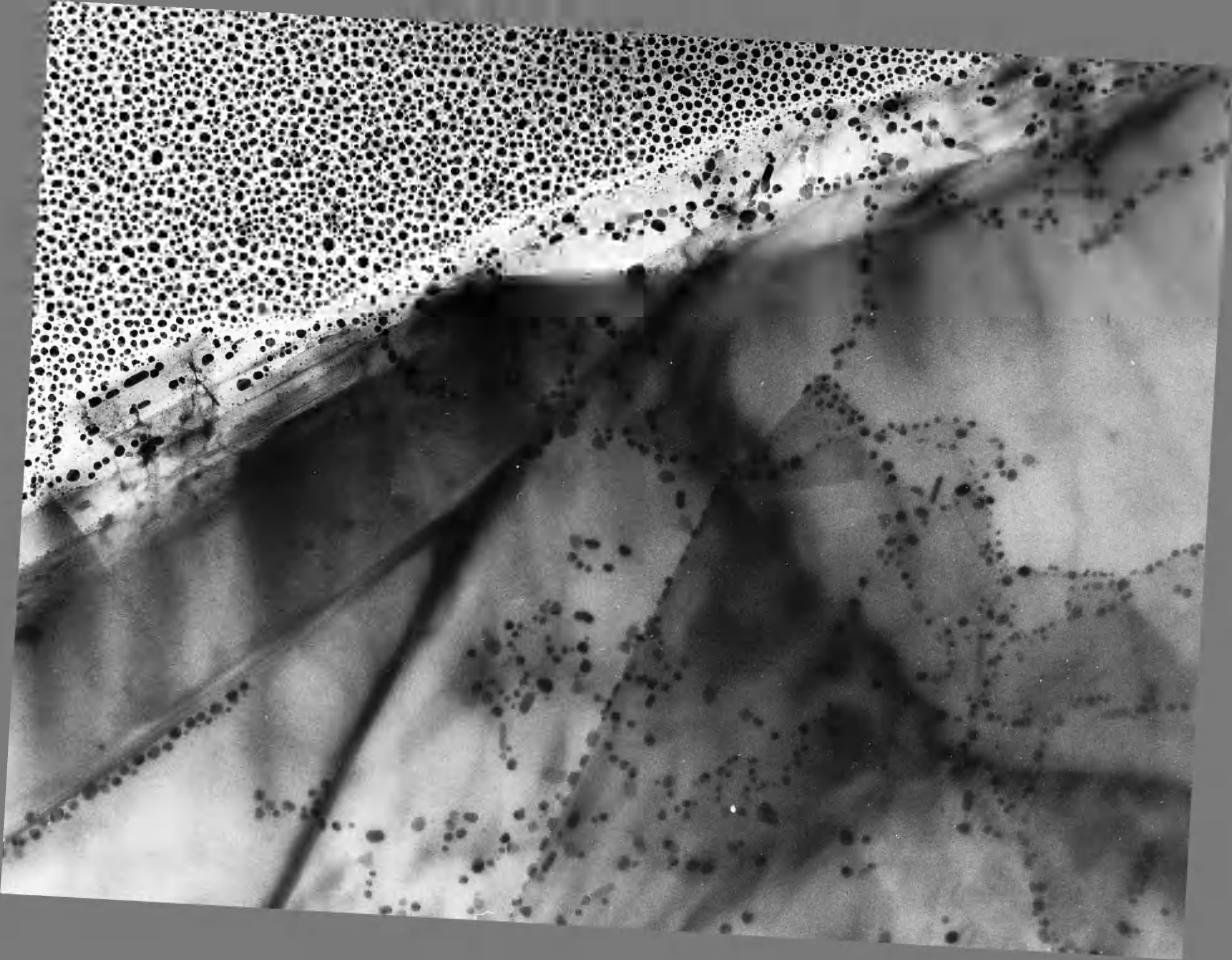

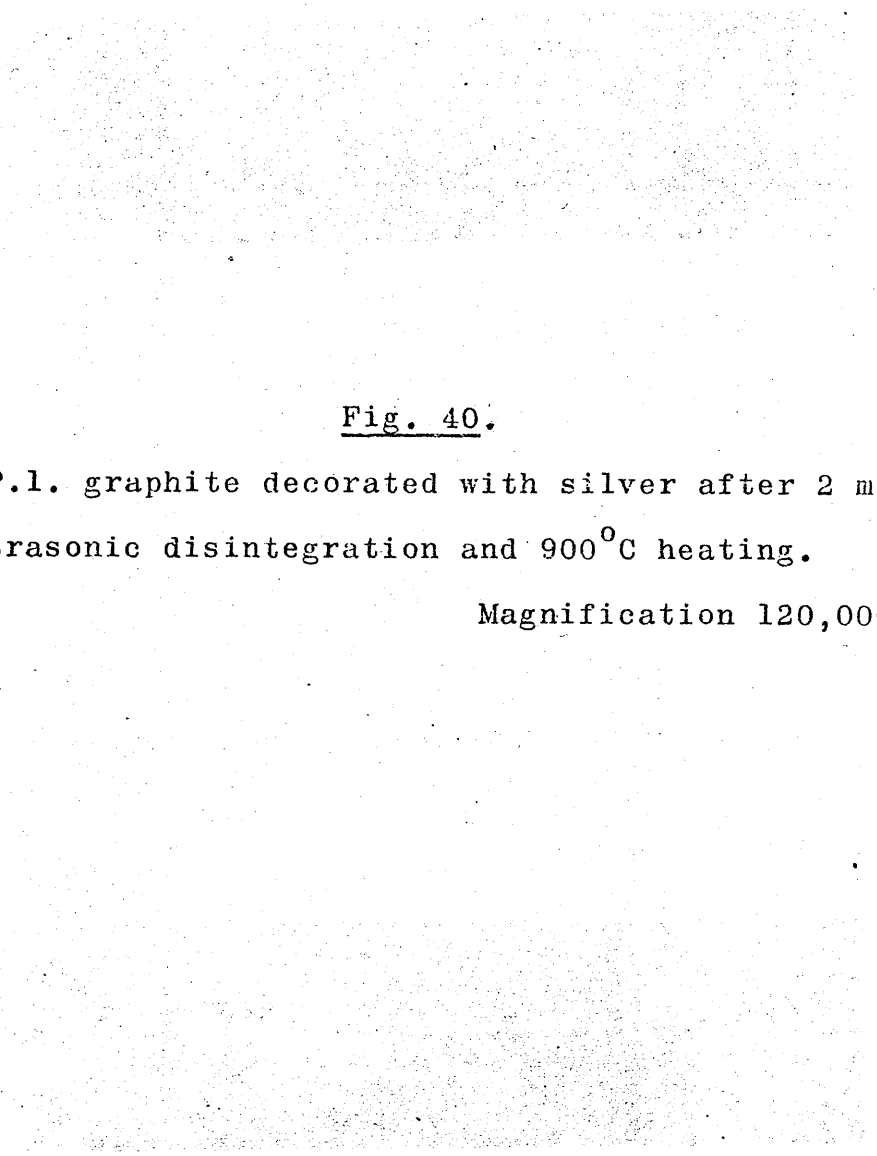

Fig. 40.

S.P.I. graphite decorated with silver after 2 minutes ultrasonic disintegration and 900^{o}C heating.

Magnification 120,000X

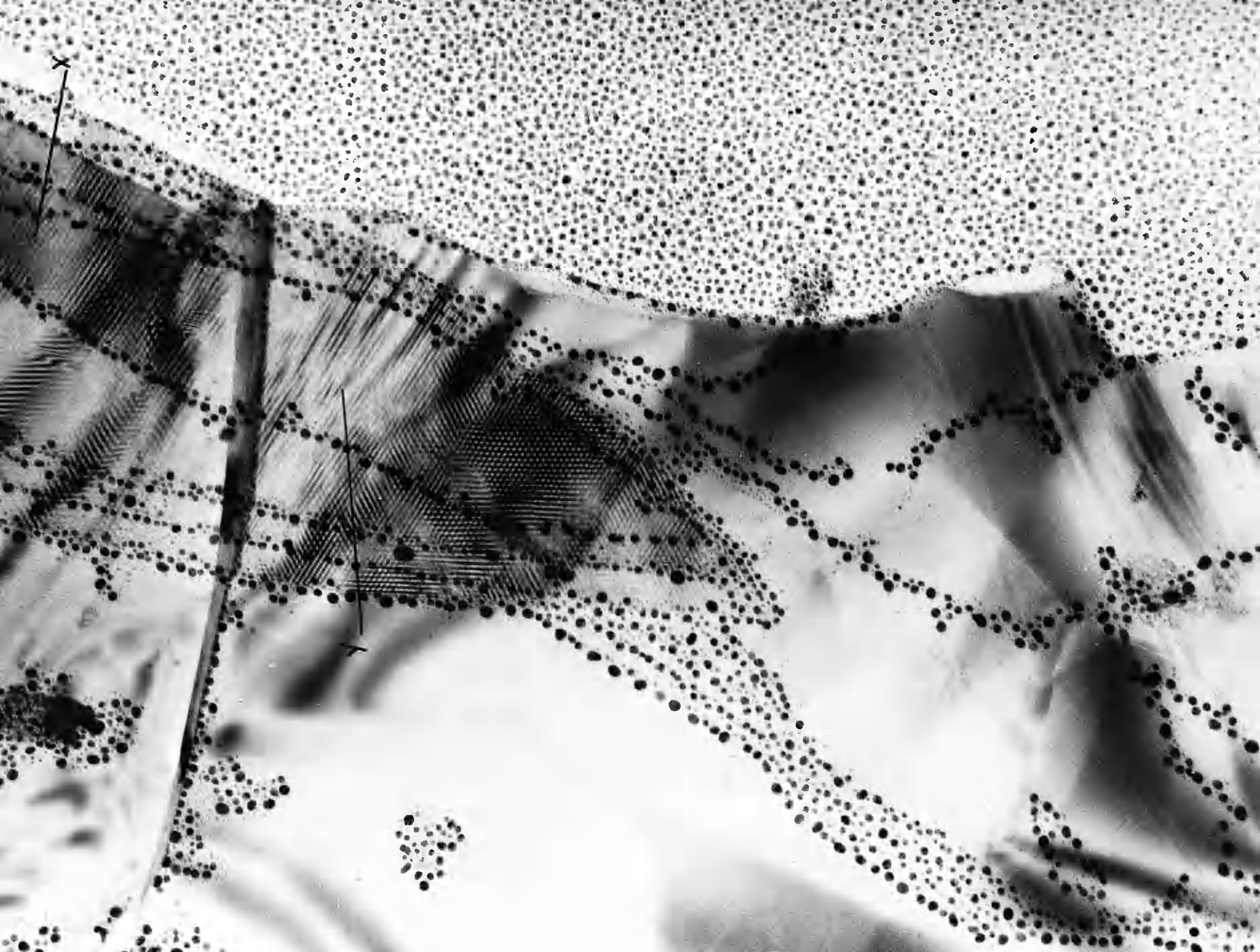

Fig. 41.

S.P.1. graphite decorated with silver after 4 minutes ultrasonic disintegration and 900^{o}C heating.

Magnification 120,000X.

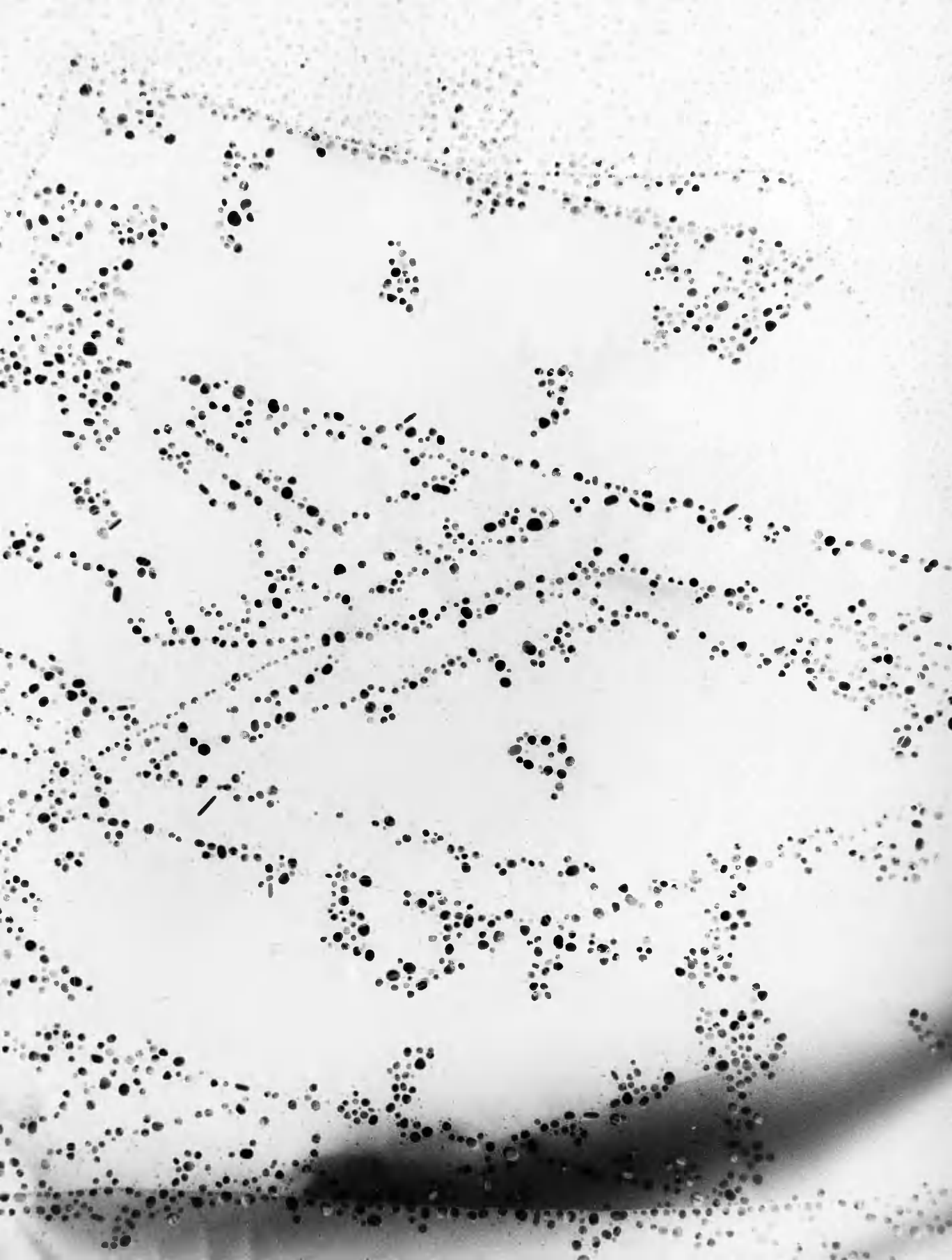

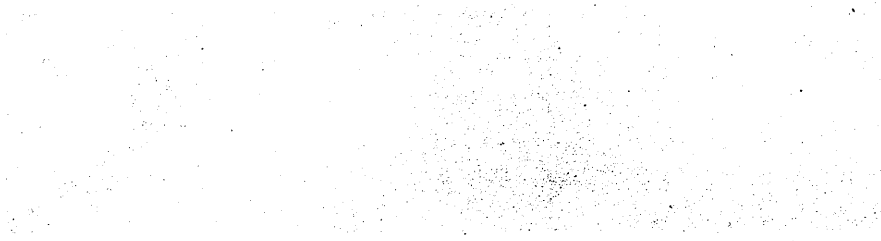

Fig. 42.

S.P.1. graphite decorated with silver after 6 minutes ultrasonic disintegration and 900°C heating.

Magnification 120,000X.

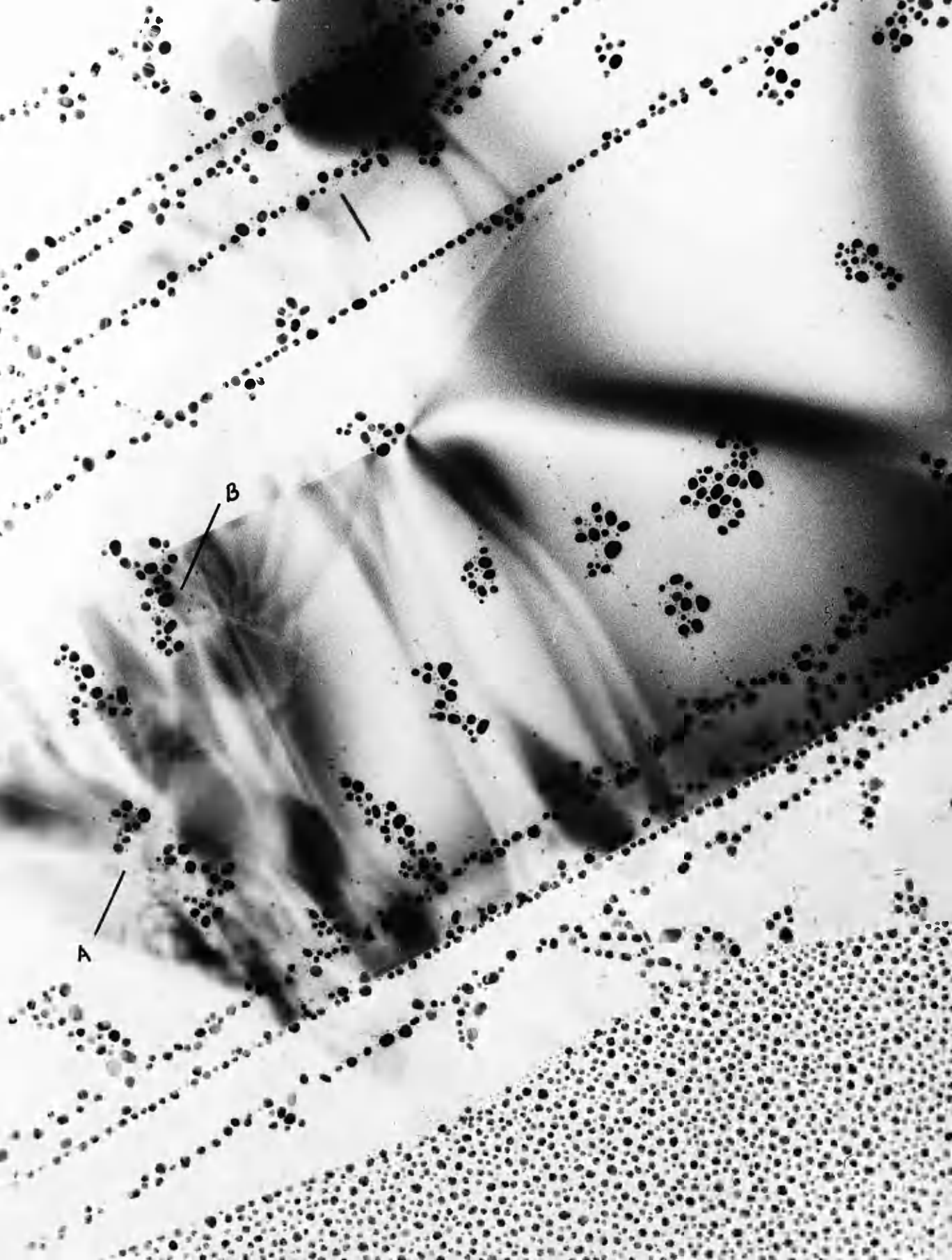
B
A

Fig. 43.

S.P.1. graphite decorated with silver after 8 minutes ultrasonic disintegration and 900^{o}C heating.

Magnification 120,000X

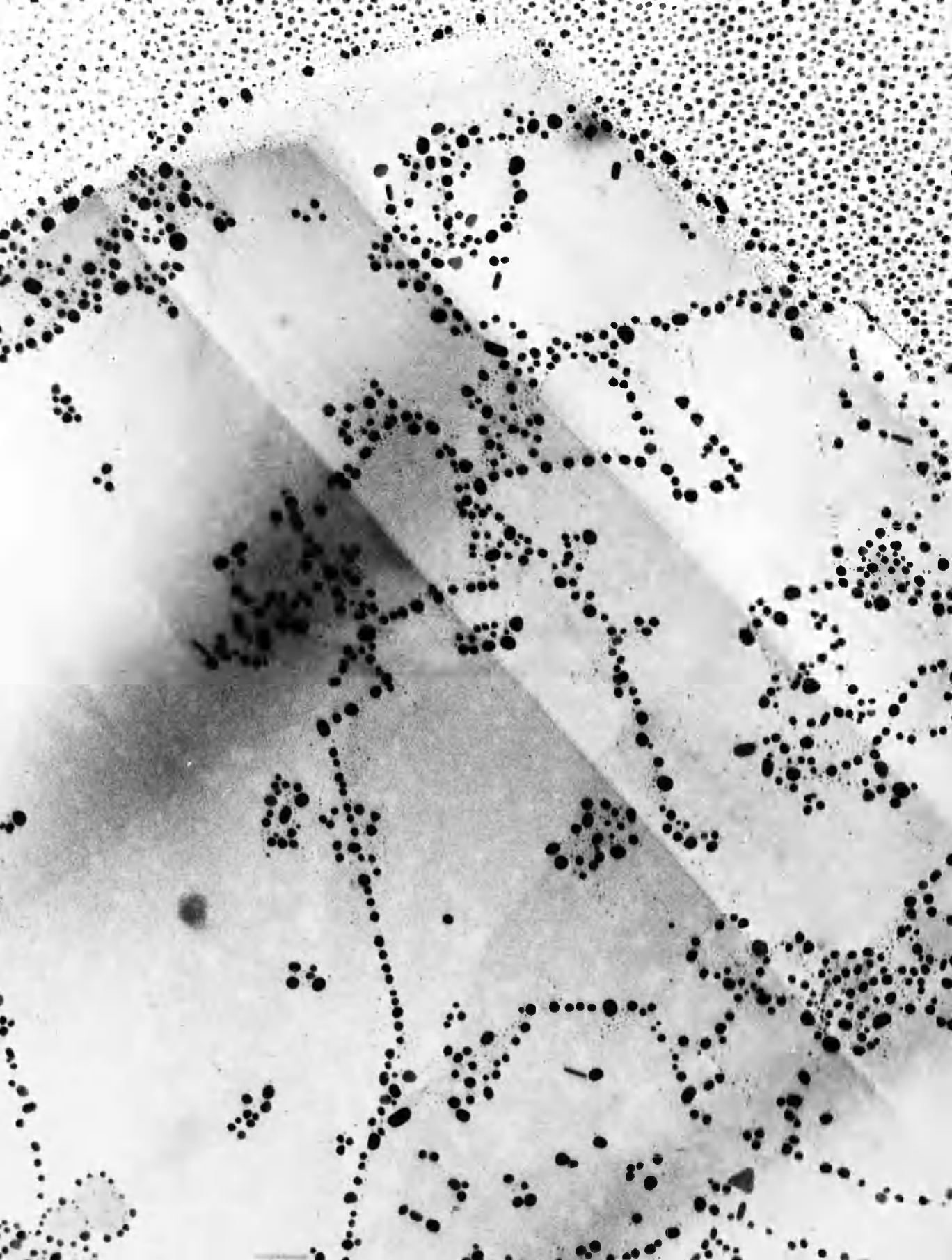

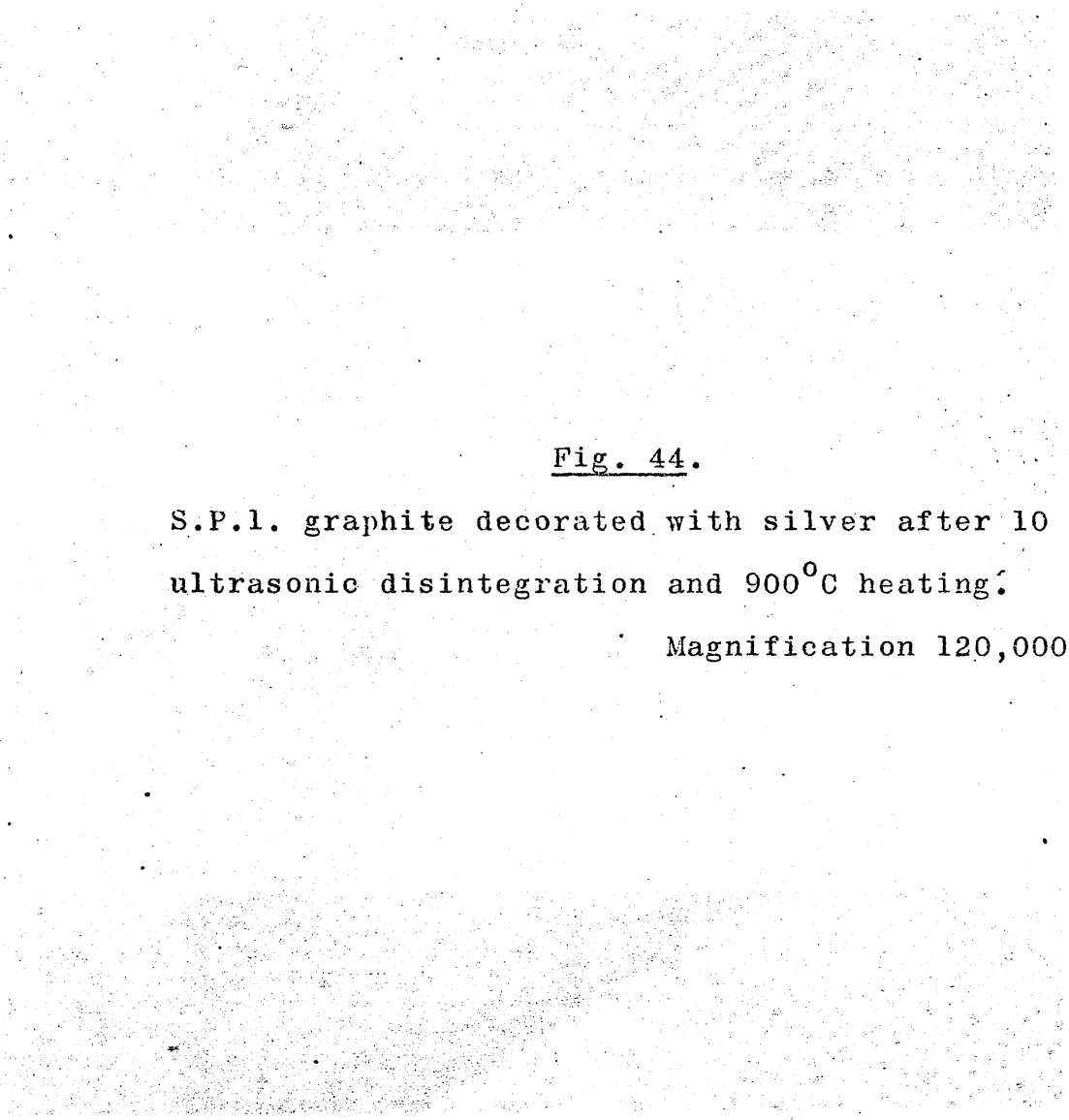

Fig. 44.

S.P.1. graphite decorated with silver after 10 minutes ultrasonic disintegration and 900°C heating.

Magnification 120,000X

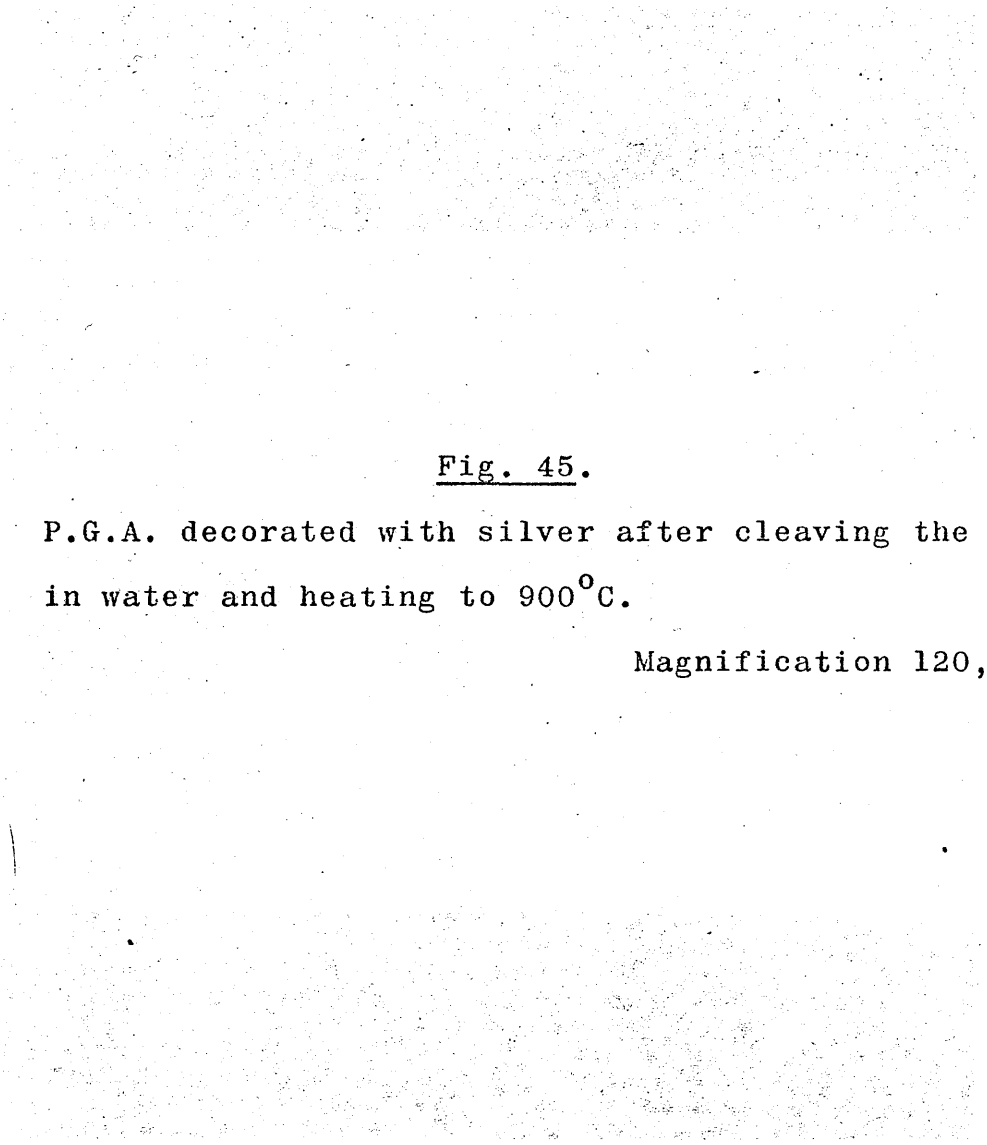

Fig. 45.

P.G.A. decorated with silver after cleaving the graphite in water and heating to 900°C.

Magnification 120,000X

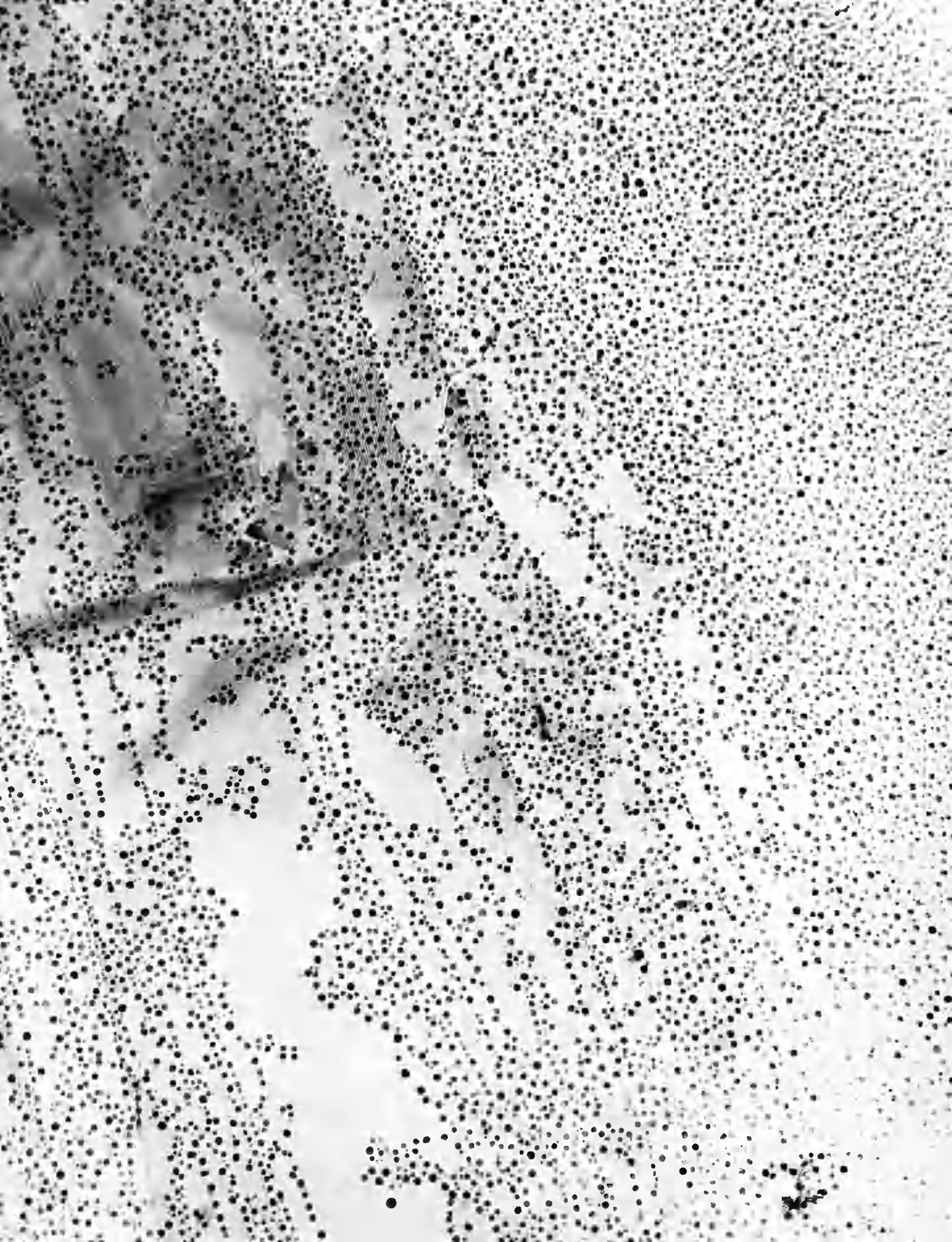

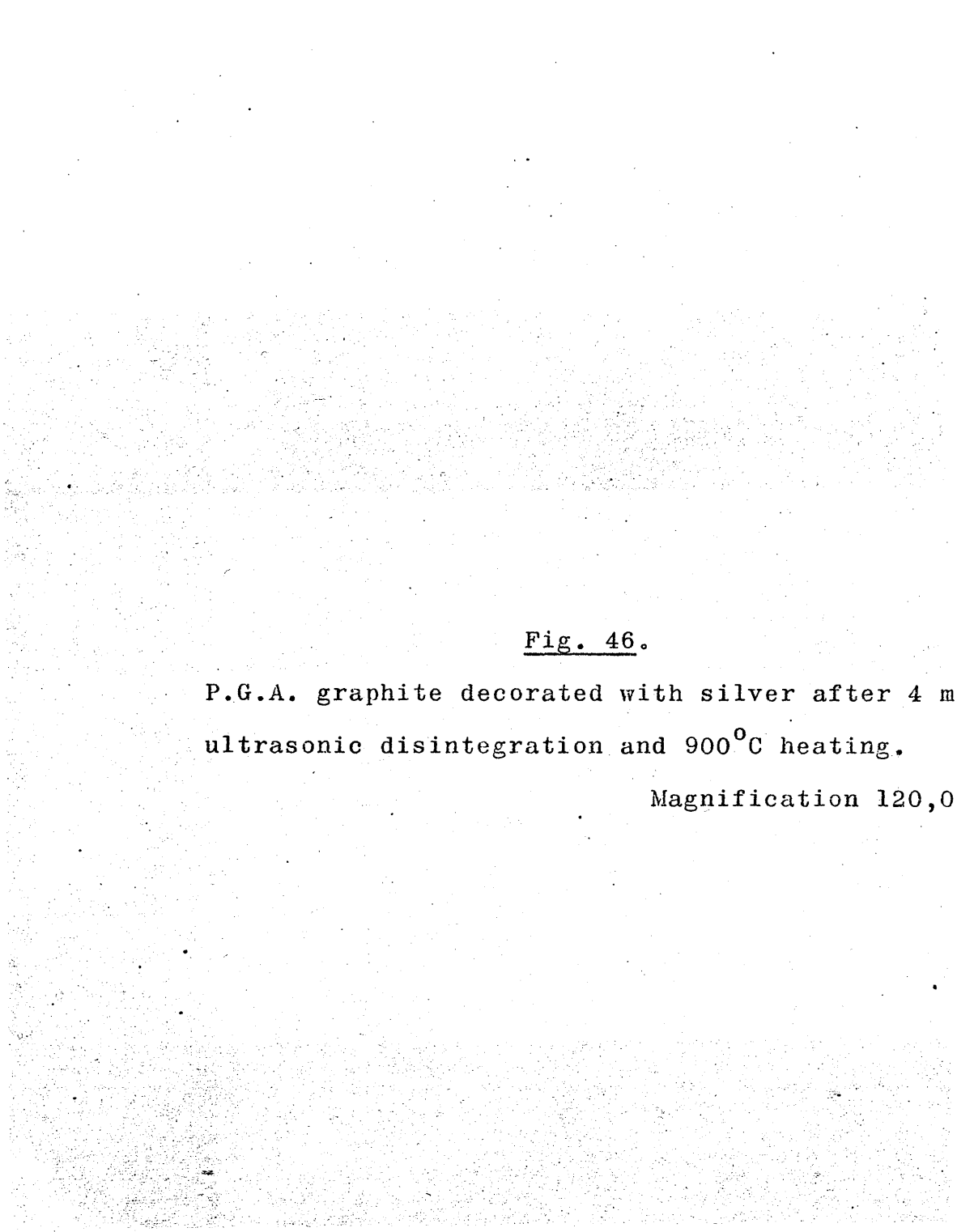

Fig. 46.

P.G.A. graphite decorated with silver after 4 minutes ultrasonic disintegration and 900^{o}C heating.

Magnification 120,000X

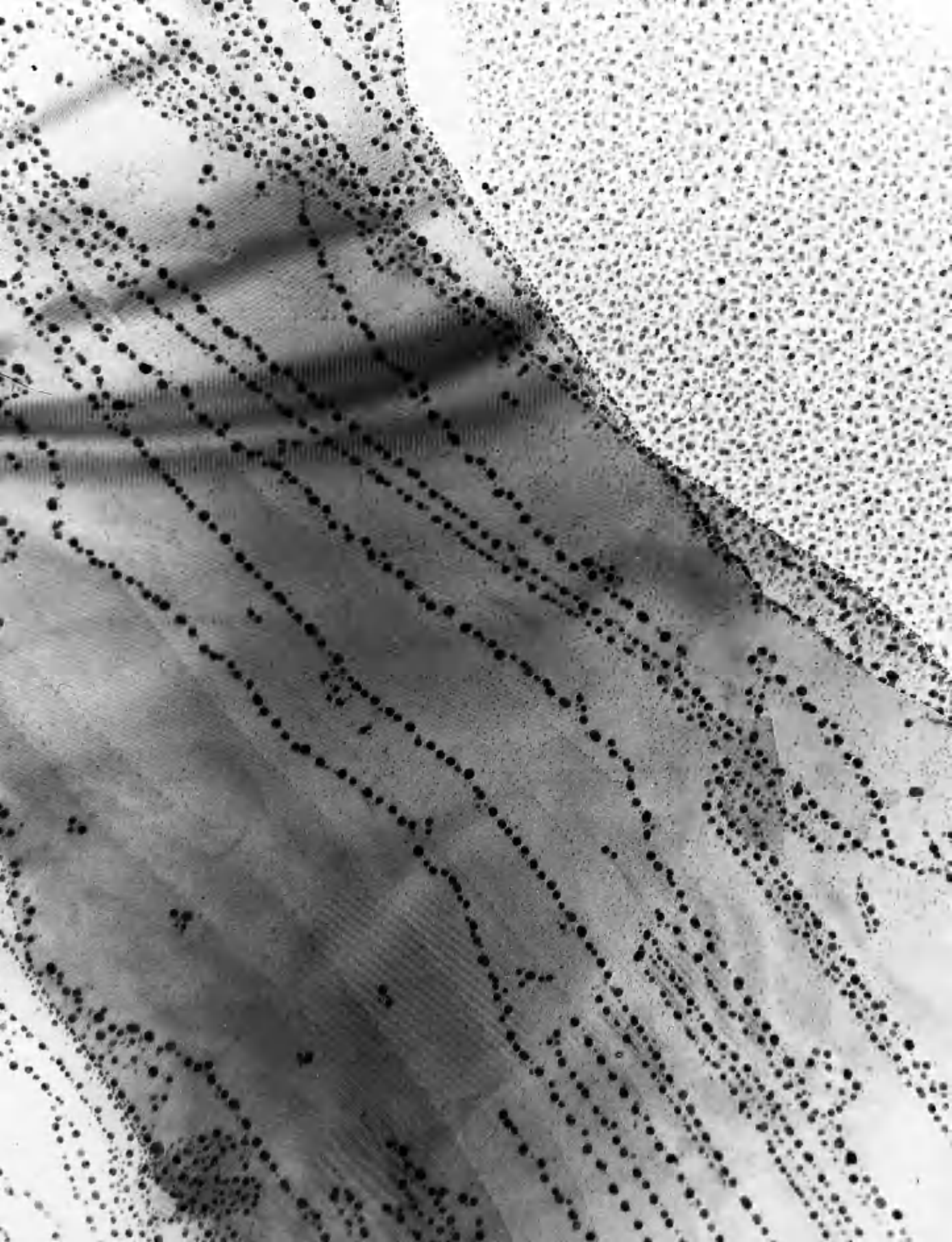

Fig. 47.

P.G.A. graphite decorated with silver after 6 minutes ultrasonic disintegration and 900^{o}C heating.

Magnification 120,000X

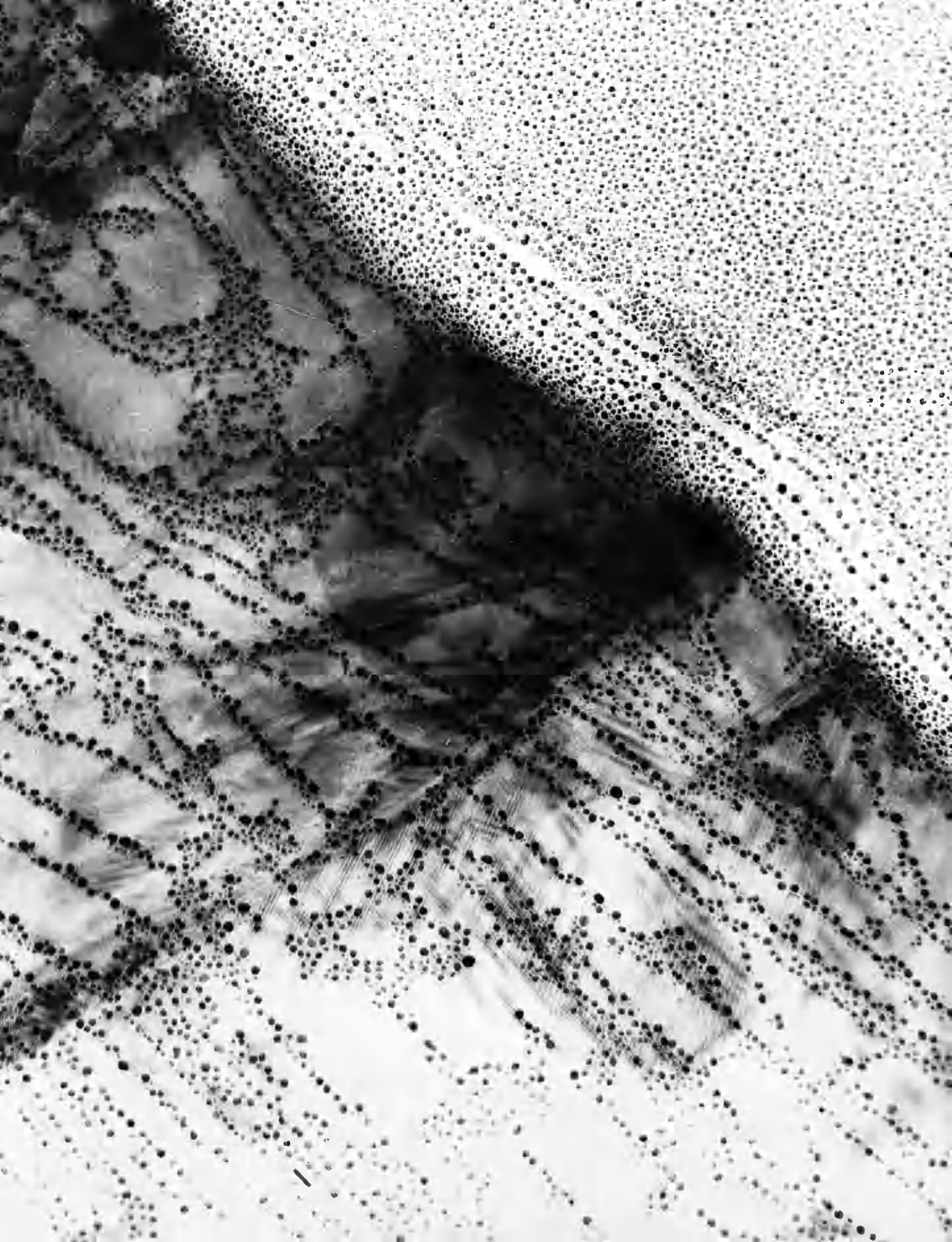

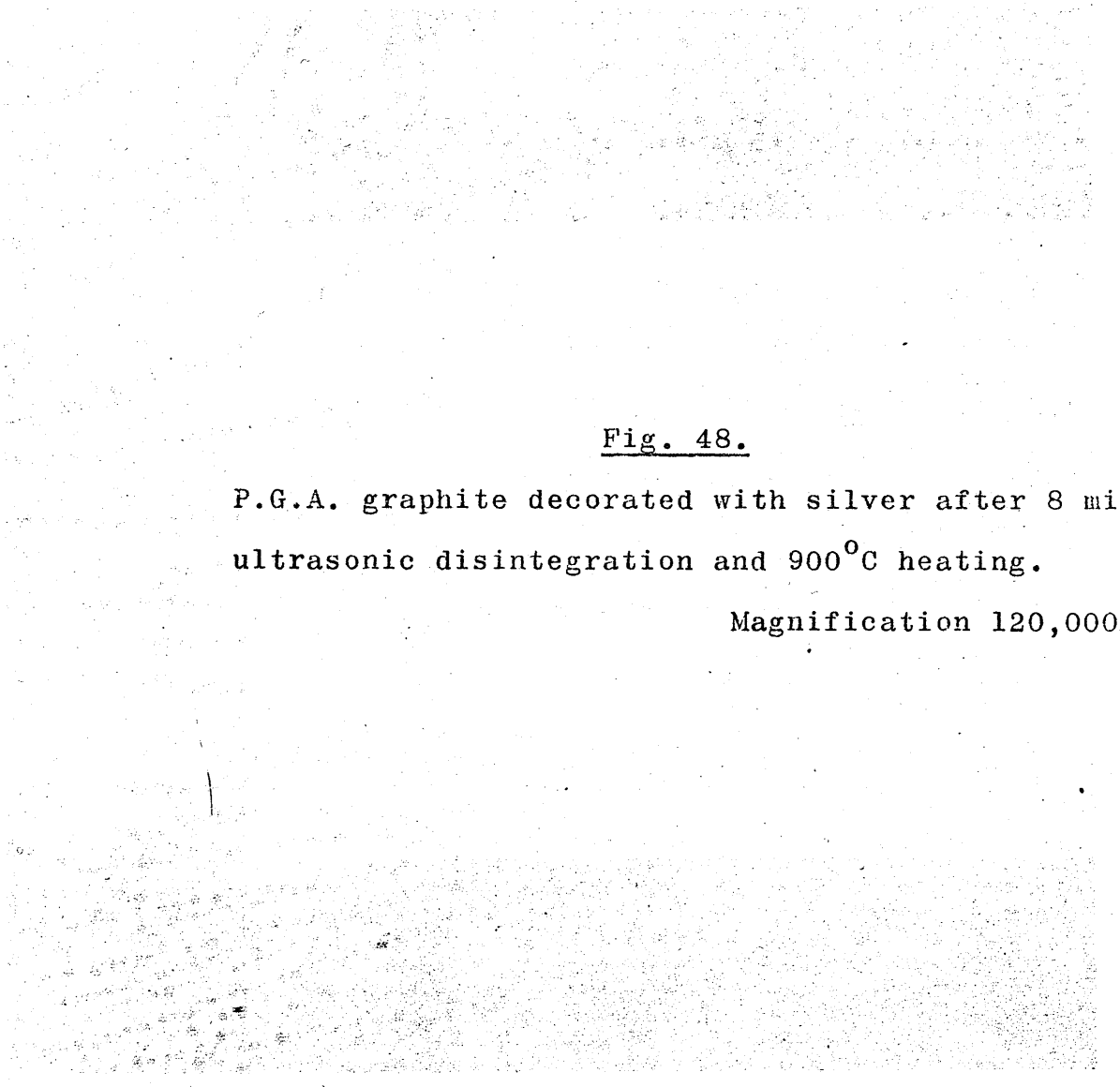

Fig. 48.

P.G.A. graphite decorated with silver after 8 minutes ultrasonic disintegration and 900^{o}C heating.

Magnification 120,000X

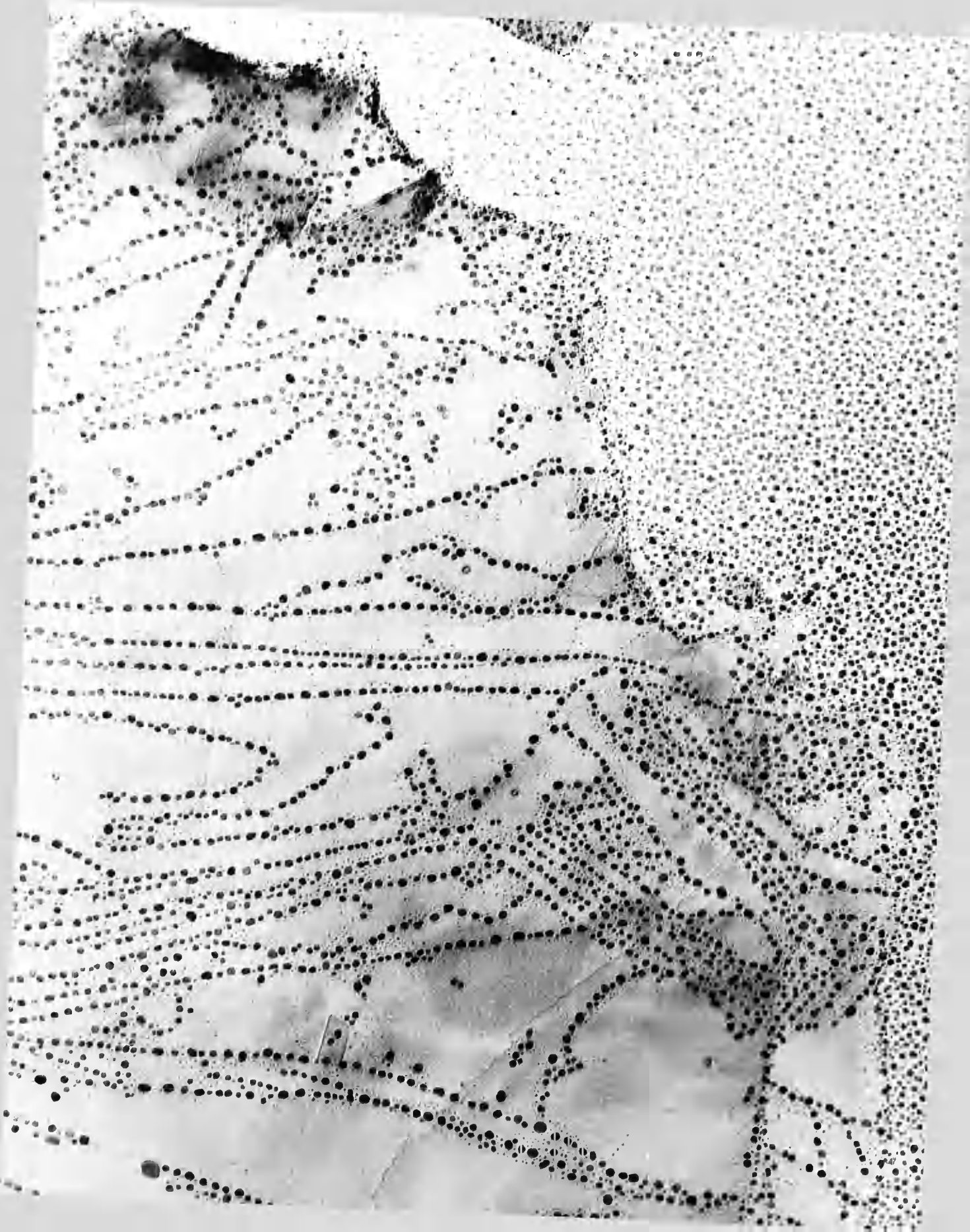

Fig. 49.

P.G.A. graphite decorated with silver after 10 minutes ultrasonic disintegration and 900^{o} heating.

Magnification 120,000X

Fig. 50.

The dependence of decoration ratios upon the duration of ultrasonic disintegration. 900°C pretreatment.

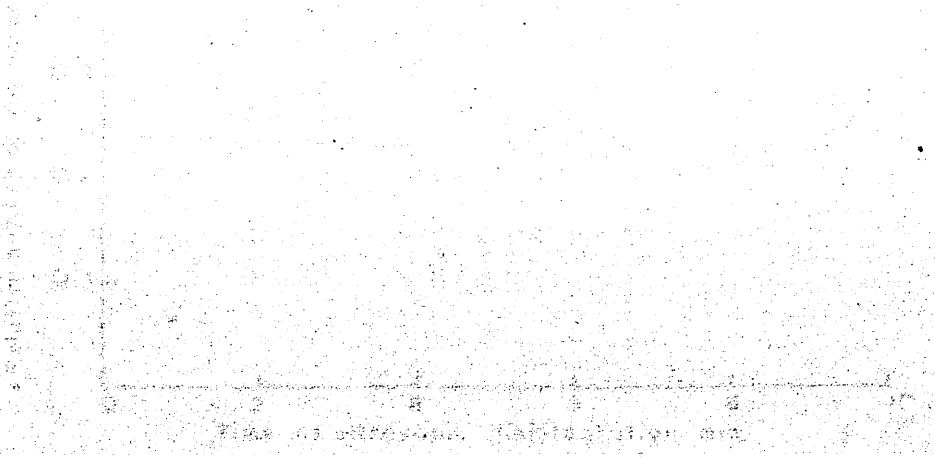

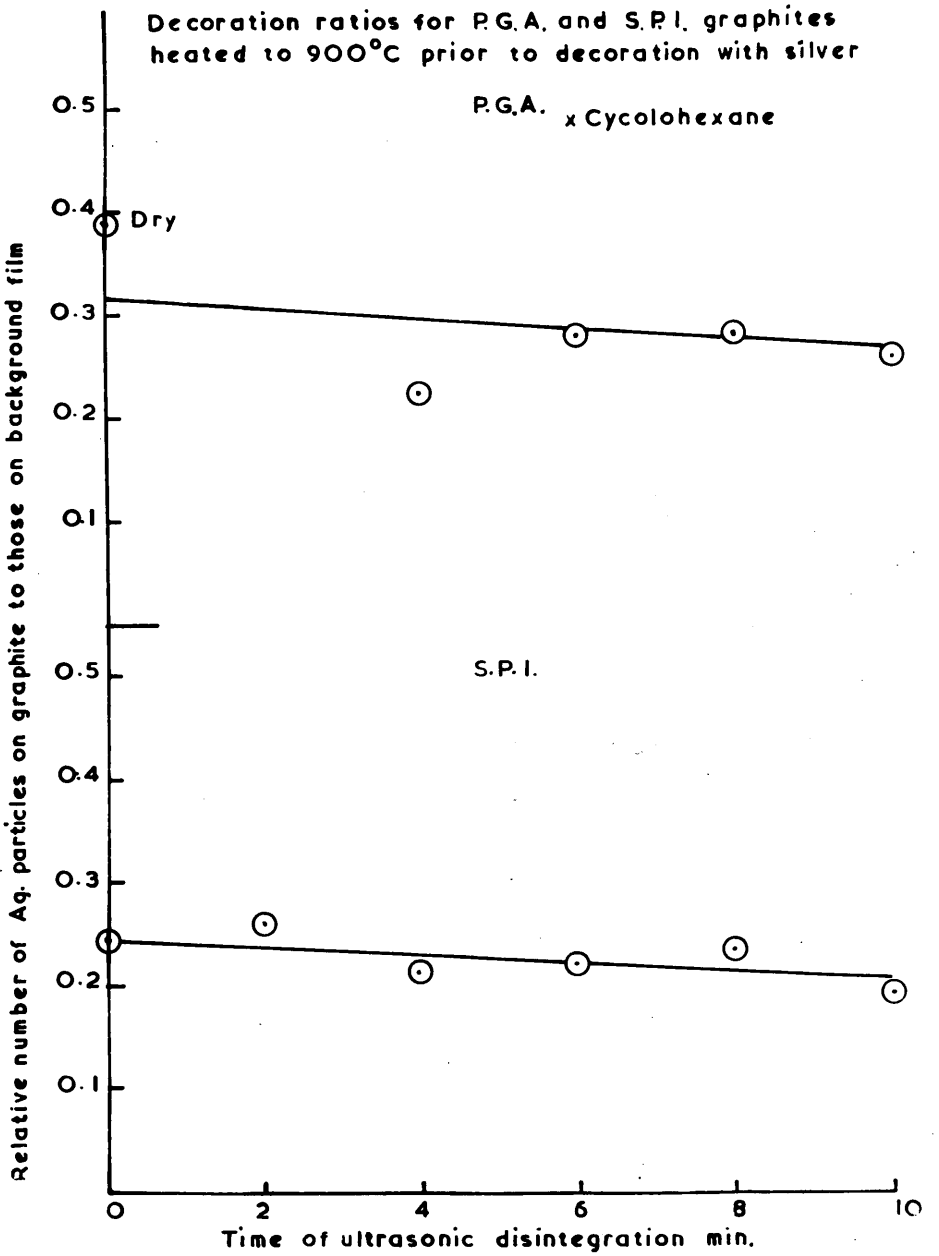
Decoration ratios for P.G.A. and S.P.I. graphites
heated to 900°C prior to decoration with silver
P.G.A.
x Cycolohexane
Dry
S.P.I.
Relative number of Aq. particles on graphite to those on background film
0.5
0.4
0.3
0.2
0.1
0.5
0.4
0.3
0.2
0.1
0
2
4
6
8
10
Time of ultrasonic disintegration min.

It is clear that no radical change was caused by the ultrasonic treatment, and though the 900°C treatment reduced the decoration ratio, it is believed that this is caused more by removal of impurities from the surface than annealing of defects within the crystal. Therefore it does not appear that ultrasonic disintegration in water causes any anomolous effects in the graphite.

2. Nature of decorated sites.

There are apparently three different forms of aggregation of the decorating particles:-

1. 100-200Å particles aligned along terminating edges of basal planes.
2. 100-200Å particles in circular or irregular clusters on the top surface of the crystal.
3. 30Å particles on both edges and clusters.

In case 3 the 30Å diameter is very approximate since there is a wide divergence in size of particles in this range (Fig.40). In many cases these small particles decorate sites which are not decorated by the larger silver particles, the converse also occurring, but since there is no marked divergence between types of site chosen it is not reliable evidence that the mechanism of decoration is different for the different size particles.

The predominating features decorated by the larger particles are the edges of crystal planes. The decoration is regular, with spacings of 12-150Å between the

particles (Fig.42) the particles often being flattened on the side facing the terminating plane. The particles are crystalline as is shown by their surface structure, but the flattening appears to have caused no enforcement of orientation in the case of silver, unlike gold where epitaxy of the decorating particles occurs (Evans, Bahl and Thomas 1967). The clusters mentioned in case 2 show in Fig.42, some indication of decoration at defects. The area marked A shows the decorating particles clustered around a convergence of contrast lines arising from some defect within the graphite. At 'B' the cluster is a little distance from the defect line convergence but this may be because the line of the defect is not in a prismatic plane and so it is emergent some distance away from where contrast occurs, eg. if the crystal is 200Å thick and the image of the defect is apparently in the middle of the crystal, a defect line of 15° to the basal plane will emerge on the upper surface of the crystal 375Å away from the area of maximum contrast.

The majority of defects in a crystal will not be in a reflecting position for contrast to occur, since the graphite is lying normal to the electron beam and thus only those defects of line parallel to the electron beam will be visible. Whilst it can be seen that decoration is associated with defects there is no indication that every silver particle represents an emergent defect.

Therefore decoration counts cannot be taken as an absolute measure of defect density.

Previously it was mentioned that terminating moiré fringes are not indicative of a non-basal dislocation. This is borne out in Fig.40 where at Y several terminating fringes are visible without decoration having occurred, and at X severe distortion of the fringes has occurred, again without corresponding decoration.

The use of cyclohexane as a medium for ultrasonic disintegration prevented subsequent decoration of P.G.A. graphite. Only a poor decoration was obtained after a 900°C preheating to clean the graphite surface, and below this temperature there was an apparently random distribution of particles on the graphite. The particle density on the graphite was similar to that on the background film. This agreed with the findings of Hennig (1964) who had studied the effect of various solvents.

In a few cases the orientation of the crystal steps were determined from diffraction data, but there was no difference in particle count between the $\{10\bar{1}0\}$ and $\{11\bar{2}0\}$ edges.

Catalysed Oxidation of Graphite.

During the oxidation of graphite it was noticed that particles of metal from the mount and furnace migrated on to the specimen. So that confusion between uncatalysed and catalysed oxidation is not made, the mode of action of catalysis by metals is described first.

1. Platinum

It is a characteristic of catalysis by platinum and also by gold, that the particle moves parallel to the basal plane, carving out a channel of its own width. This had been studied by Presland and Hedley (1963) and Hennig (1962) who considered that any excess width of channel beyond the diameter of the catalysing particle must have originated from uncatalysed oxidation.

No channelling of this nature was observed below a reaction temperature of 780°C and Fig. 51 shows that even after 180 min. reaction at 640°C with a profusion of platinum particles, there is no evidence of channelling. At 780°C the first signs of catalytic attack appear and Fig.52 shows a channel at X after 40 min reaction but it is clear that the channel is much wider than the particle and uncatalysed oxidation predominates. At 810°C however, catalytic reaction is rapid and exceeds the uncatalysed oxidation rate producing long parallel sided channels as shown in Fig. 53. Also of interest in this micrograph is the superimposed diffraction pattern which, after allowing

Fig. 51.

S.P.1. graphite flake after 180 minutes reaction with air at 640°C.

Magnification 320,000X.

Fig. 52.

S.P.1. graphite after 40 minutes reaction with dry air at 780°C.

Magnification 120,000X

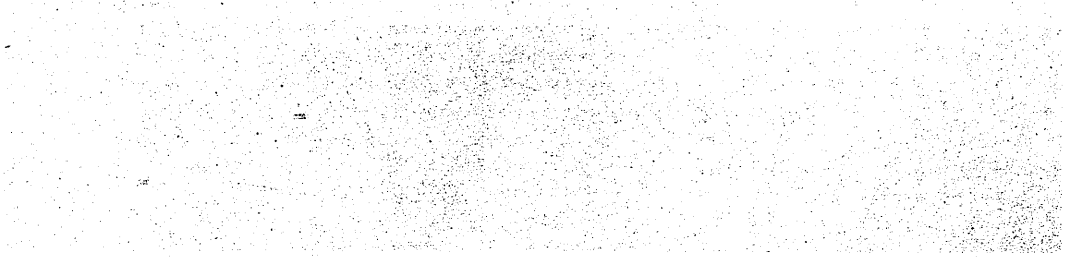

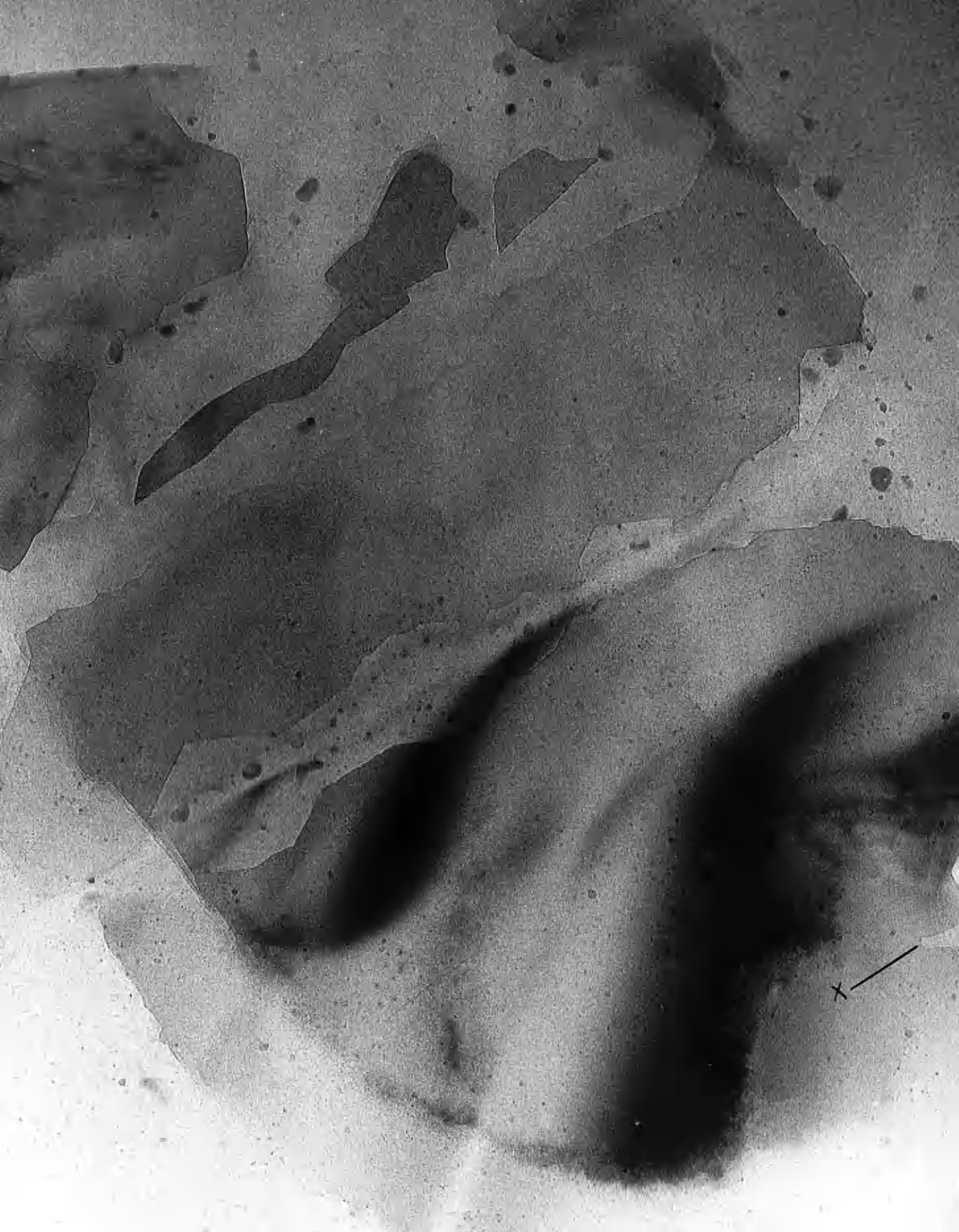

for lens rotation, makes it possible to determine the orientation of the channels. As can be seen the channels are all bounded by $\{10\bar{1}0\}$ planes and it is noticeable at 'A' that the channel changes direction through 60^{o} to retain the $\{10\bar{1}0\}$ boundaries. Uncatalysed oxidation is also taking place at the boundaries of the inlet marked 'B' and the difference between the 120^{o} edge erosion and the channels is very prominent.

The change in catalysed oxidation rate between $780^{o}C$ and $810^{o}C$ is large and obviously is a function of particle mobility. There is no evidence of decoration by the platinum prior to oxidation, nor are all the particles mobile, so that it would appear that decoration is not a precursor to catalytic oxidation.

The channels pass through steps on the crystal and for contrast reasons they must be several atomic layers deep. The regularity of the channels together with these features show that they are not functions of defect concentration, and in fact appear quite unperturbed by variations in thickness or other features of the crystals, but proceed in directions governed by the overall lattice geometry alone. Therefore in the absence of these features it is reasonable to assume that the small particles of platinum have no significant effect upon the mode or rate of oxidation of the graphite.

Fig. 53.

S.P.1. graphite after 27½ minutes reaction with dry air at 810°C

Magnification 84,000X.


B
{11$\bar{2}$0}
{10$\bar{1}$0}
(10$\bar{1}$0)
A

2. Palladium

The motivation for the use of palladium came from an early experiment in which the specimen was supported on a palladium grid and it was found that palladium migrated on to the specimen and catalysed oxidation. Figs 54 a,b,c and d show the results of this early experiment conducted at 900^{o}C with dry air. Fig.55 is the selected area diffraction pattern confirming the presence of palladium and graphite. The graphite protruded into a grid square that had no support film, and even after a degassing period of 1 hour some reaction had occurred with the residual air in the microscope. When air was admitted the reaction was much faster and there was considerable mobility of the palladium particles as they carved out irregular channels in the surface of the graphite. There was no apparent orientation preference to the channels and the palladium seemed to diffuse into the graphite at the metal/graphite interface. After 7 minutes reaction the flake was so eroded that it collapsed, the majority of the graphite having been removed. In several places the particles appeared blurred whilst their surroundings were in focus, showing that the particles were moving rapidly, not only in the direction of the channel, but also changing shape in a random manner.

In addition to this experiment, there was considerable interest in palladium for two other reasons, these

Fig. 54a.

P.G.A. graphite with palladium prior to oxidation.

Magnification 120,000X

Fig. 54b

P.G.A. graphite with palladium after 2 minutes oxidation with dry air at 900°C.

Magnification 120,000X.

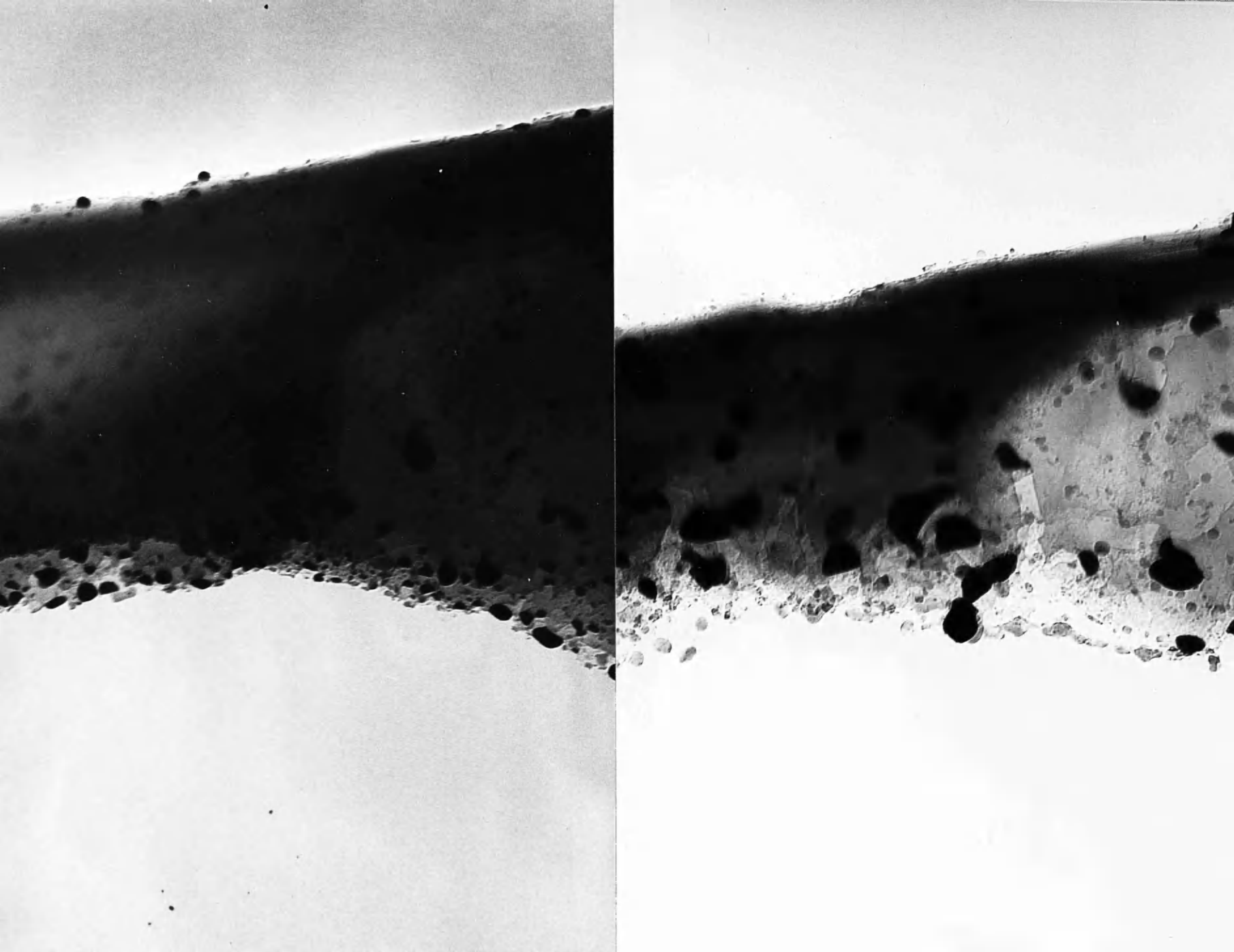

Fig. 54c.

P.G.A. graphite with palladium after 3 minutes reaction with dry air at 900°C.

Magnification 120,000X.

Fig. 54d.

P.G.A. graphite with palladium after 6 minutes reaction with dry air at 900°C.

Magnification 120,000X.

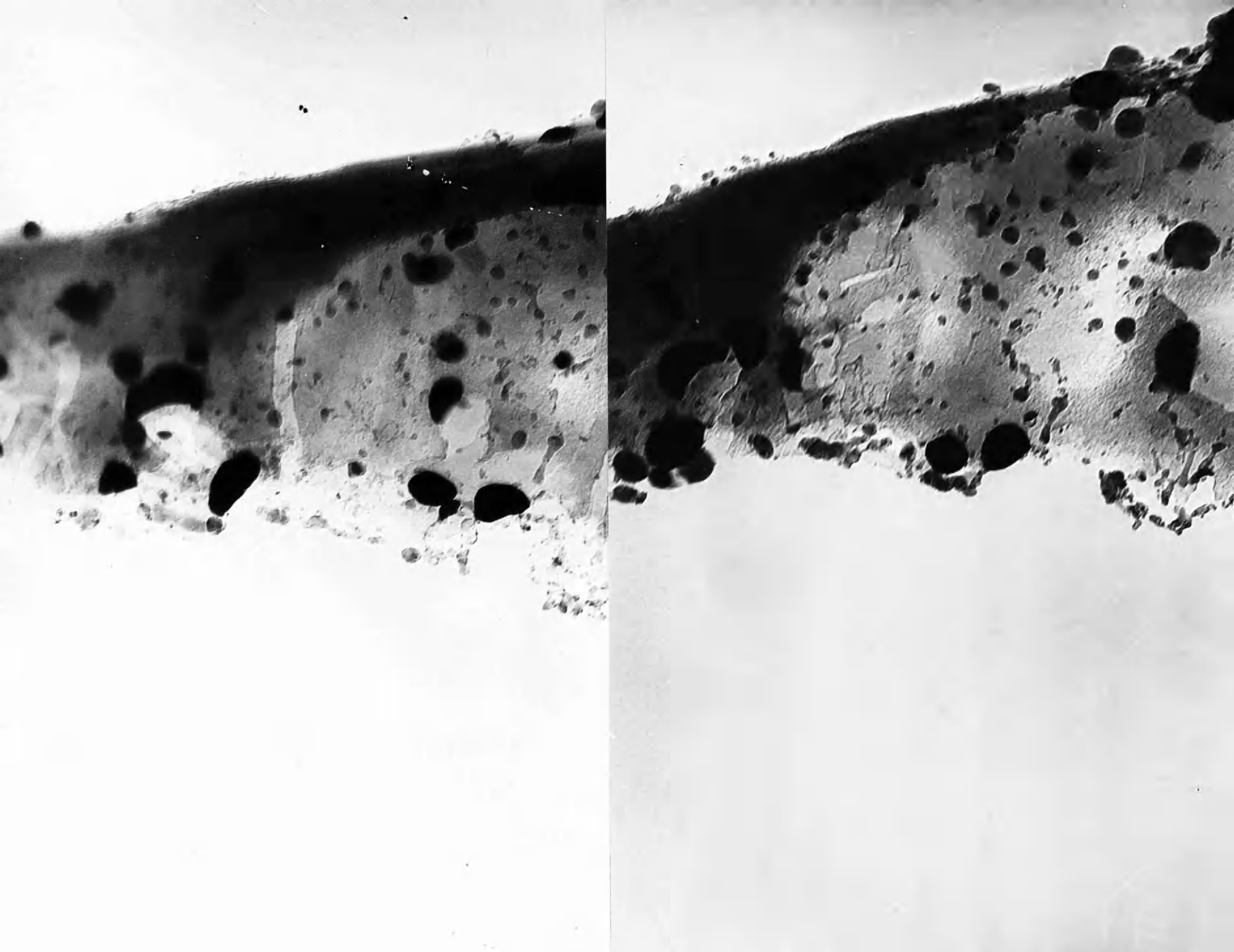

Fig.55.

Selected area diffraction pattern of area in Fig.54a, showing both palladium and graphite reflections.

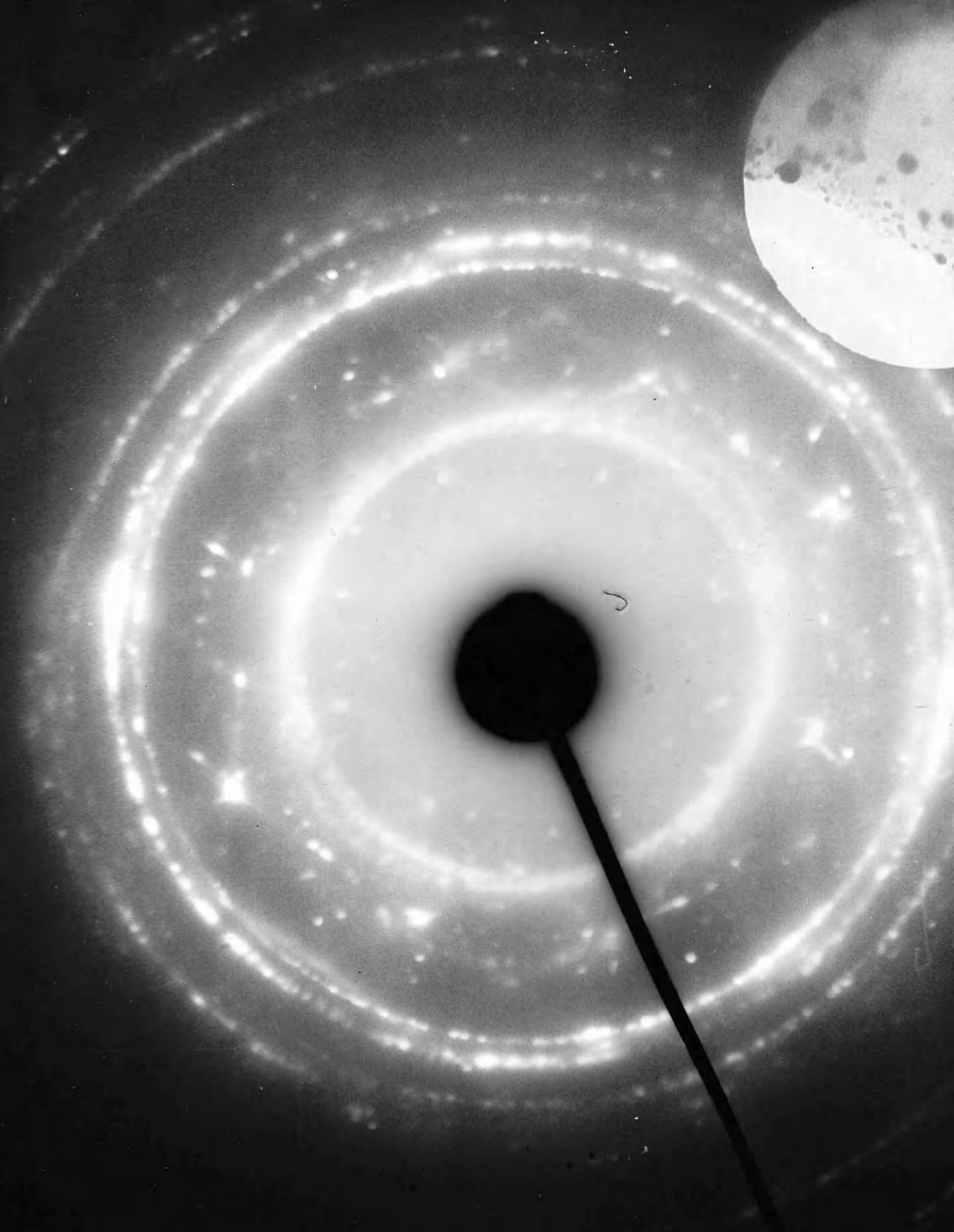

being the high activation energy for reaction found by Heintz and Parker (1966) and some studies on the catalytic effect of palladium for hydrogenation of olefins that was studied in this department (Brownlee, Fryer, and Webb 1969)

Therefore palladium metal was evaporated on to both S.P.l. and P.G.A. graphites and the reaction studied in more detail than in the early experiment.

A 100$\mathring{A}$ layer of palladium on an S.P.l. graphite crystal is shown in Fig.56, with a light shadow (white area) that may have been caused by unevenness of the support film. The temperature was then slowly raised with the specimen under high vacuum environment within the microscope. Figs. 57a,b,c, and d show the specimen at the temperatures of 140^{o}C, 200^{o}C, 315^{o}C and 410^{o}C respectively as annealing and crystal growth of the palladium film took place, and Fig.58 shows the specimen at the reaction temperature of 515^{o}C just before the air was admitted. The total time for this heating procedure was 86 min with at least 10 min at each temperature mentioned, to minimise drift of the specimen caused by thermal movement of the specimen stage. The crystal growth of the palladium was a gradual process up to 350^{o}C when it was seen that a few areas of graphite were decorated with small palladium particles. The majority of the film continued to exhibit the crystal growth

behaviour, especially in areas that had been extensively viewed with the electron beam. At 410°C spontaneous nucleation of limited areas of the palladium film occurred, as seen in Fig.57d with large particles of palladium being formed whilst other areas of the film remained unchanged. This coalescence increased until 515°C was reached when the majority of the palladium was distributed as shown in Fig.58. The coalescence was a very rapid process and individual movements within the film could not be identified. After coalescence there remained traces of palladium on those places where the film had previously been as shown by the fine dark lines in Fig.58, and also some limited decoration of surface steps by 50-200Å particles. The remainder of the palladium was nucleated in particles exceeding 200Å diameter, some being several thousand angstroms in size. Despite the irregular shape of these large particles they were clearly crystalline. The effect of the electron beam was probably the deposition of a layer of contamination that prevents coalescence of the palladium film. Dry air was then admitted and after 8½ minutes reaction a still plate micrograph shows a reacted area as in Fig.59. The large particles of palladium are still crystalline, as shown by the contrast lines visible on some of them, but many of the smaller particles have carved channels in the graphite, and are now stationary and have assumed a faceted shape.

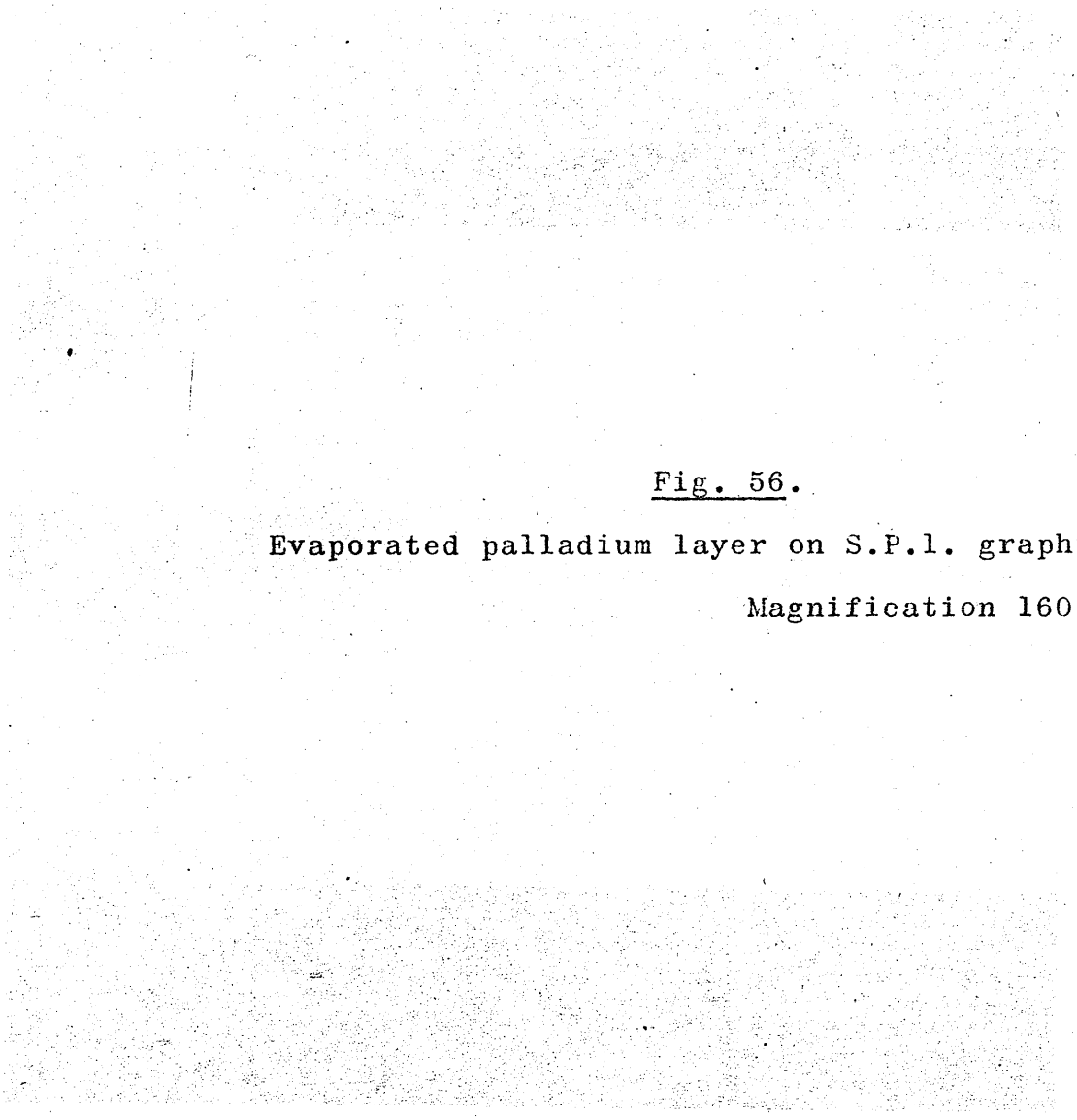

Fig. 56.

Evaporated palladium layer on S.P.l. graphite.

Magnification 160,000X.

Fig. 57a

Annealing of evaporated palladium film on S.P.1. graphite.

140°.

Magnification 120,000X.

Fig. 57b

Annealing of evaporated palladium film on S.P.1. graphite.

200°C.

Magnification 120,000X.

Fig. 57c.

Annealing of evaporated palladium film on S.P.1. graphite.

315°C

Magnification 120,000X.

Fig. 57d.

Annealing of evaporated palladium film on S.P.1. graphite.

410°C.

Magnification 120,000X.

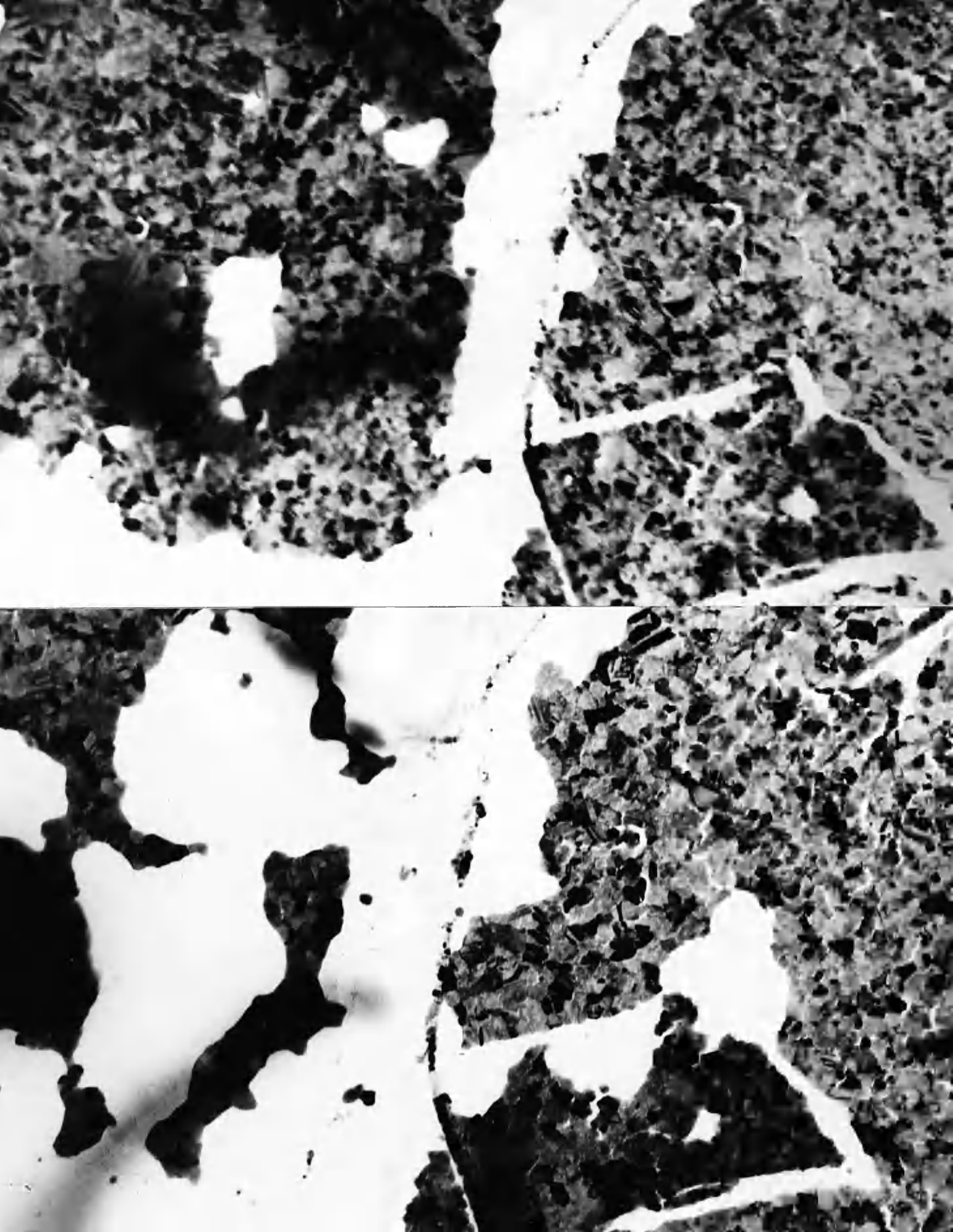

Fig. 58.

S.P.1. graphite with evaporated palladium film at 515°C.

Before air admitted to specimen.

Magnification 160,000X.

Graphite has been extensively removed around many of the particles but it is not clear how this erosion occurred. Figs. 60a and b show an area of graphite adjoining that of Fig. 59 (the two areas overlap top and bottom respectively), Fig.60 a, being taken after 13 min reaction and Fig.60b after 19 min reaction. The particle of palladium at A and A' has changed its shape and eroded more graphite in the 6 minutes reaction between these two micrographs. Also the dark areas of contrast on the graphite have changed during this time. The mode of attack immediately becomes clear when a videotape record of the reaction is studied. Whilst dynamic effects were apparent to the operator, their significance was often lost with the preoccupation in operating the microscope and obtaining a record of the results.

The closed circuit television system with videotape recording enabled dynamic effects to be studied at leisure and in this reaction the attack on the graphite was only associated with mobile palladium particles. Preceding the attack there was severe distortion of the graphite lattice as shown by the black bands and moiré patterns that flashed across the graphite surface and in some cases the graphite flake even lifted completely from the specimen support film. These contrast effects are shown in Fig.61 after 64 min reaction, where at X a moving palladium particle was catalysing attack on part of a graphite flake.

Fig. 59

Palladium on S.P.1. graphite after $8\frac{1}{2}$ minutes reaction with dry air at 515°C.

Magnification 160,000X.

Fig. 60a.

Palladium on S.P.1. graphite after 13 minutes reaction with dry air at 515°C.

Magnification 120,000X

Fig. 60b

Palladium on S.P.1. graphite after 19 minutes reaction with dry air at 515°C.

Magnification 120,000X.

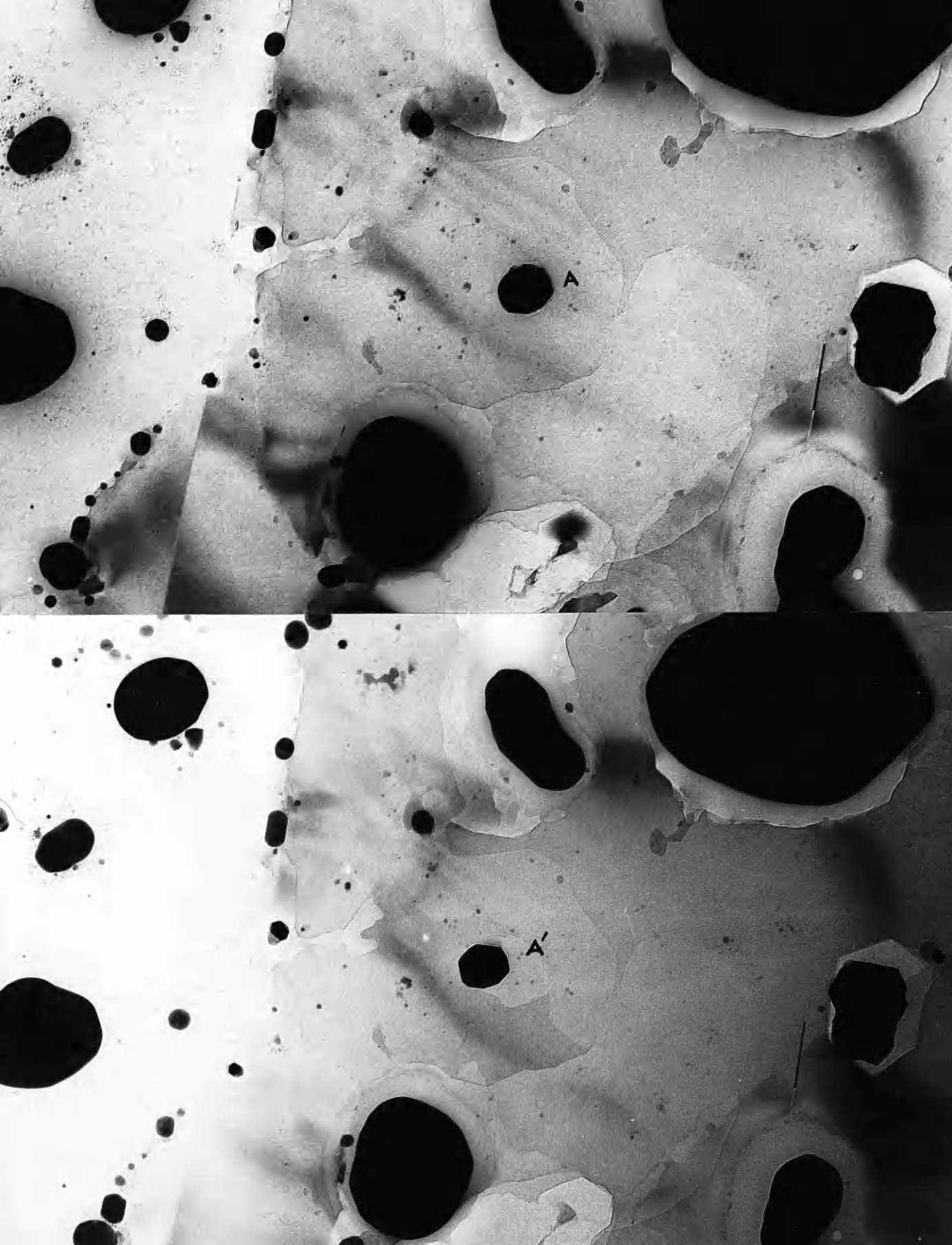
A
A'

Whilst in motion the palladium particle exhibited the characteristics of a strongly agitated liquid droplet with rapid changes of shape, and protuberances rising and falling from the surface. However the particle at X is shown to retain a 120^{o} geometry at its leading edge whilst the rest of the particle is in motion. Other experiments showed that there was no significant difference in reactivity between P.G.A. and S.P.1. graphites and that when a mobile particle reached the edge of a crystallite it reversed direction and catalysed reaction on remaining graphite within the crystallite, and did not cross the grain boundary. Finally the particle came to rest for no apparent reason and assumed a faceted overall shape and other features associated with a crystalline state. There was no apparent diminution of size of the reacting particle during the course of reaction. Overall the channels carved out by the particle were parallel sided showing that uncatalysed oxidation was not significant (as would be expected at this temperature) but the channels had serrated sides reminiscent of 120^{o} geometry. There was, however, no preferential orientation of the channels with either of the prismatic planes.

The rate of reaction was very variable for this catalysed reaction since the mobile particles moved at rates between 50 and 5000$\mathring{A}$/sec whilst the majority of surrounding particles remained stationary. There was no

Fig. 61.

Palladium on S.P.1. graphite after 64 minutes reaction with dry air at 515°C.

Magnification 160,000X.


X

significant effect from electron beam heating since increasing the beam intensity had no visible effect either on the proportion of particles moving at any one time (about 1%) or their velocity. At higher furnace temperatures the number of moving particles did increase. (N.B. The intensity of the electron beam need not increase the temperature of the specimen significantly since it depends upon the thermal contact the specimen has with the support film, which in graphite is generally large).

One further feature of the palladium catalysed attack is shown in Fig. 62 which is of a graphite flake on the silica-support film. At A,B,C and D areas of silica film have been removed. This micrograph was taken after the 75 minute reaction had been terminated and also shows superimposed electron diffraction pattern and a light circle denoting from whence it came. The removal of silica at these temperatures is much more than that which would have been expected from a comparable uncatalysed reaction, and therefore it would appear that the palladium also catalyses the diffusion of silica from the support film. It is significant that the areas of removal were in close proximity to a large particle of palladium.

Fig. 62.

Palladium on S.P.1. graphite after 75 minutes reaction with dry air at 515°C. Loss of silica from the support film is shown by the formation of holes.

Magnification 84,000X.

A
B
C
D

Uncatalysed Oxidation of Graphite.

This refers to oxidation experiments on S.P.1. and P.G.A. graphites with dry air in which the catalysis of the type previously described does not appear to have taken place, and there is no visible interaction between any spurious contaminants and the graphite.

1. Preferred orientation of reacting edges.

a. Reactions conducted outside the microscope.

With dry air around the specimen a series of experiments was conducted employing a pressure range from 92-478 torr at a temperature of approximately 450°C. Attempts were made to perform sequential reactions on the same specimen, but contamination deposited both in the microscope and the furnace, prevented quantitative kinetic data from being obtained. Figs.63a and b show a flake of S.P.1. graphite before and after 15 minutes at 450°C under a pressure of 478 torr of dry air. Fig. 63b has an orientation diagram superimposed on the micrograph, the orientation being determined from a dark field micrograph. Though the eroded edges are very ragged it can be seen that $\{10\bar{1}0\}$ planes are exposed at reacting edges in preference to $\{11\bar{2}0\}$ planes. Similarly this preferred orientation is shown in Fig. 64 which was produced by reaction at 450°C and 376 torr. In Fig.65 which is another area from the experiment performed at 478 torr, two of the edges of the indentation are bounded by $\{10\bar{1}0\}$ planes

Fig. 63a

S.P.1. graphite prior to reaction outside the electron microscope.

Magnification 120,000X.

Fig. 63b

S.P.1. graphite after 15 minutes reaction at 450^{o}C in 478 torr air pressure.

Magnification 120,000X.

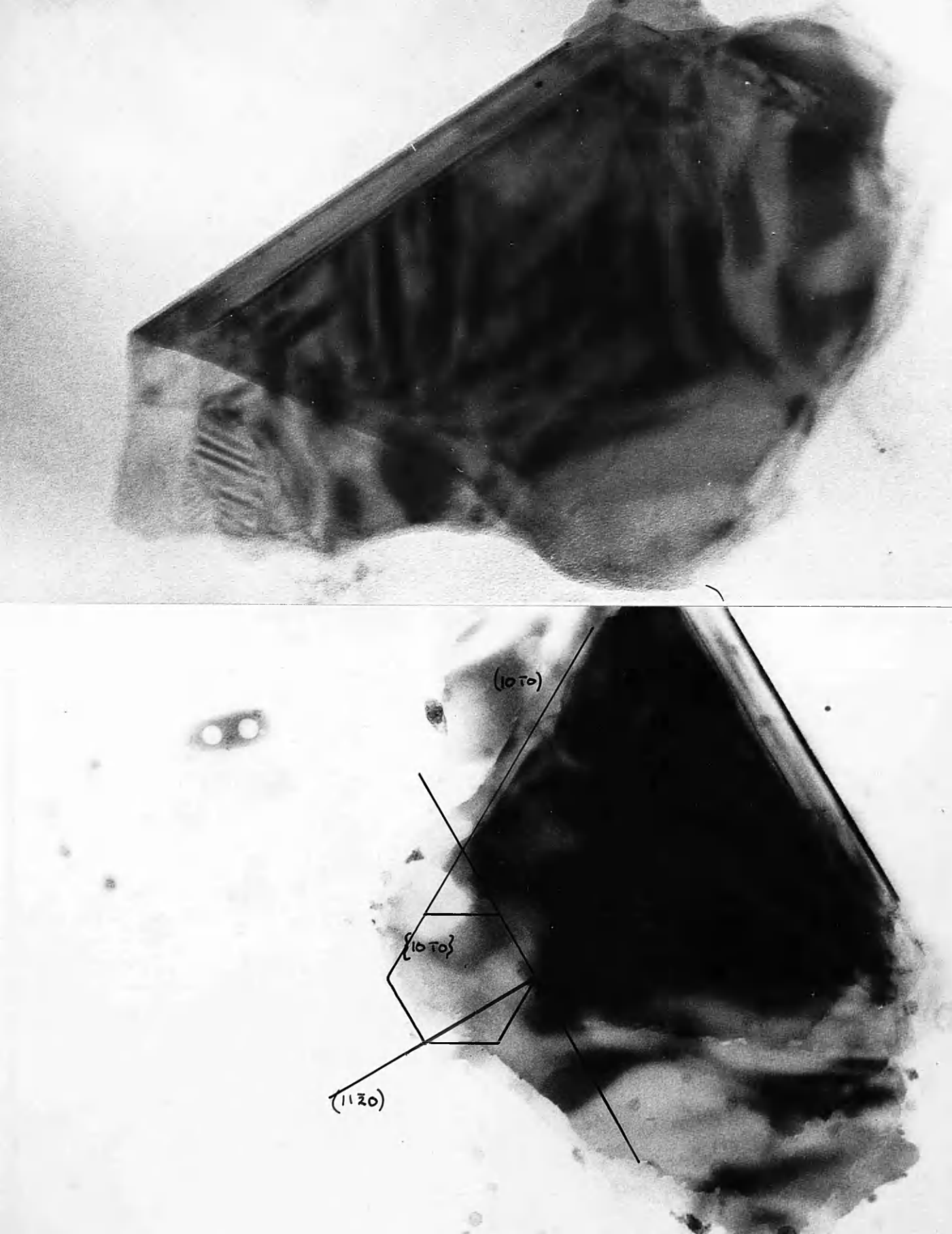
(10$\bar{1}$0)
{10$\bar{1}$0}
(11$\bar{2}$0)

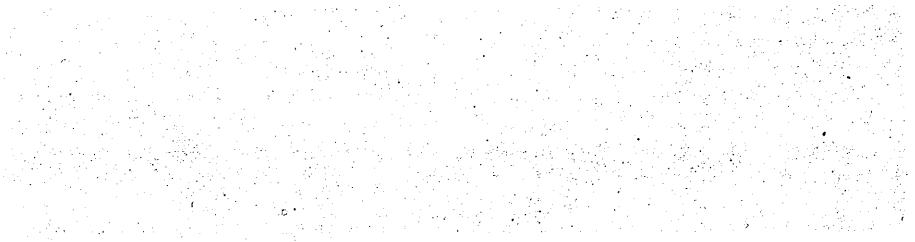

Fig. 64.

S.P.l. graphite after reacting with dry air at 450°C and 376 torr, outside the electron microscope.

Magnification 168,000X.

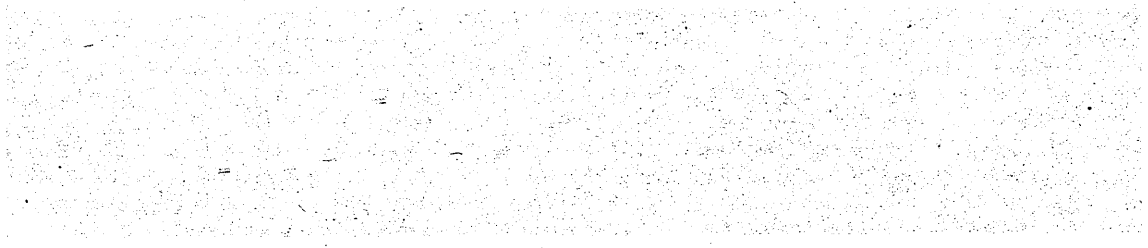

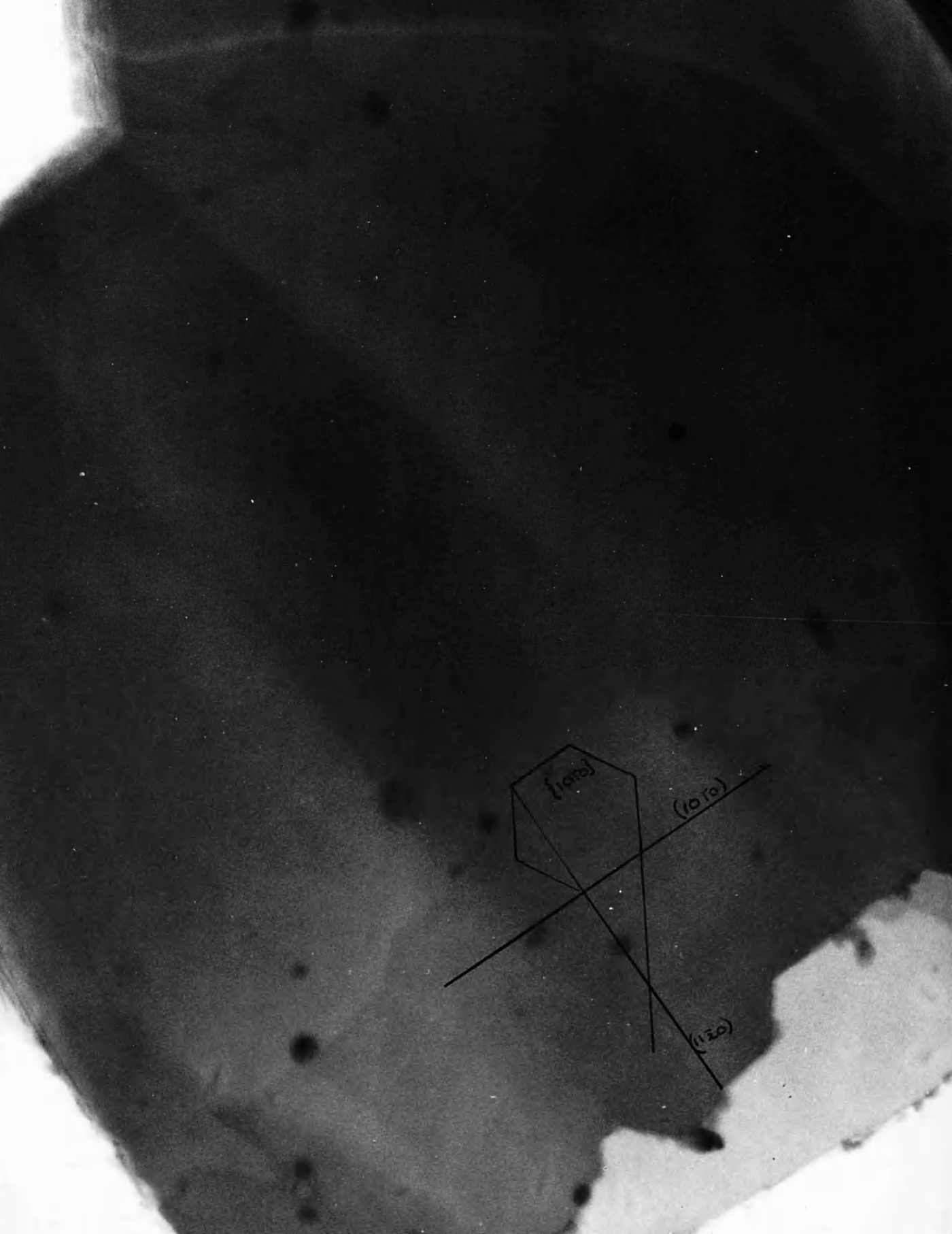
{10$\bar{1}$0}
(10$\bar{1}$0)
(11$\bar{2}$0)

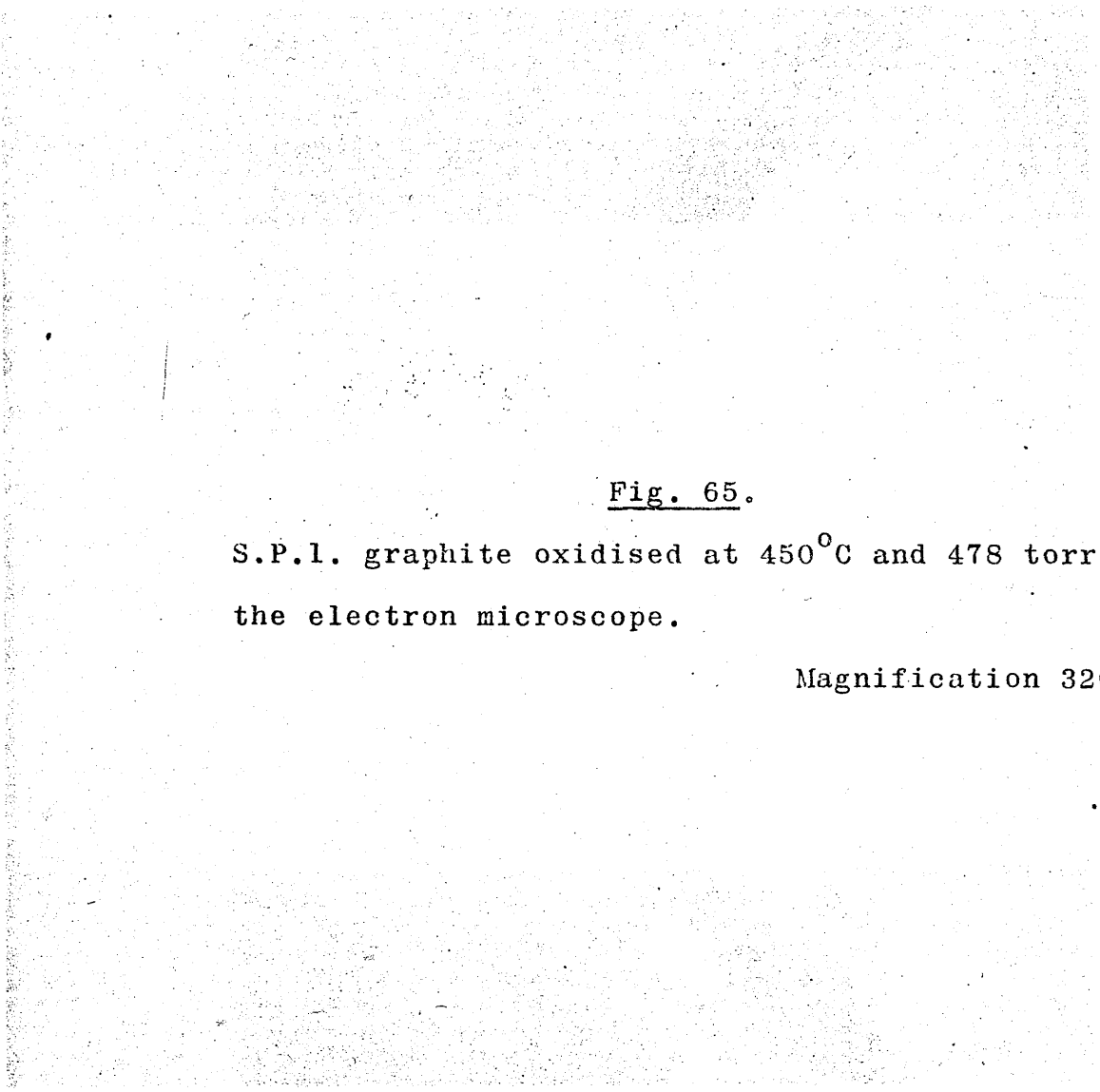

Fig. 65.

S.P.1. graphite oxidised at 450^{o}C and 478 torr outside the electron microscope.

Magnification 320,000X.

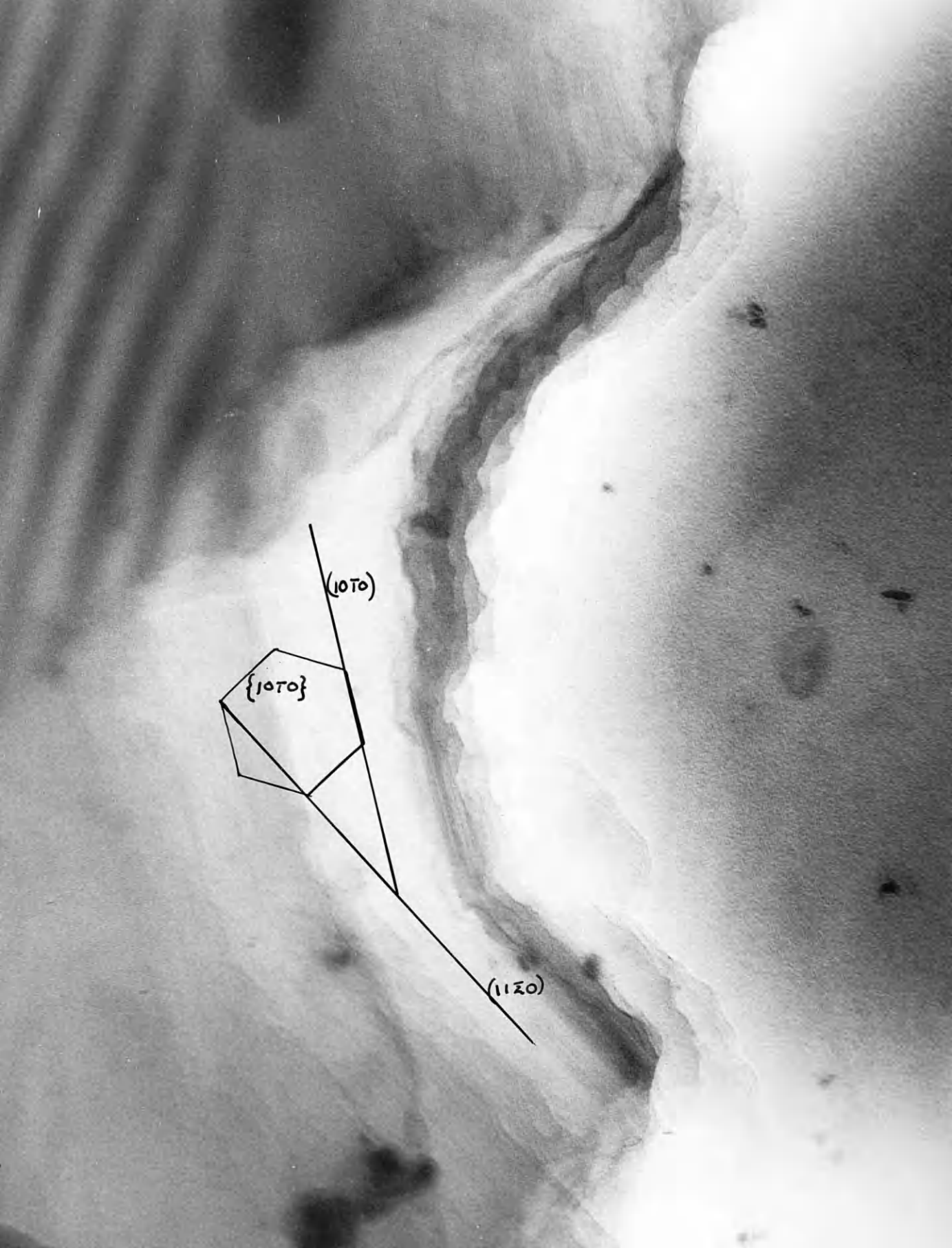
(10$\bar{1}$0)
{10$\bar{1}$0}
(11$\bar{2}$0)

whilst the third is $\{11\bar{2}0\}$. The latter was being oxidised in a manner that changed the orientation, so that in many cases the exposed edge was converted to exposure of $\{10\bar{1}0\}$ planes. Therefore there appeared a definite preference for this orientation.

All the experiments performed in the pressure range 90-500 torr at 450°C showed this orientation effect and it appeared independent of the amount of contamination that was present on the specimen. The majority of the contamination was shown to be Na Al $O_2 \cdot 3H_2O$ by electron diffraction, and it is unlikely that this would have given rise to catalytic activity of this nature.

b. Reactions conducted inside the electron microscope.

Under these reaction conditions using the first gas reaction stage, the pressure of the dry air was not known, but the reaction could be carried out under far cleaner conditions. However, despite these differences the results were the same with the eroded edges of the crystals having $\{10\bar{1}0\}$ planes exposed. Fig. 66 shows a flake of S.P.1. graphite after 8 min reaction at 715°C, and Fig.67 a flake of P.G.A. graphite after 4 min oxidation at 520°C. In both cases $\{10\bar{1}0\}$ orientation was assumed by the reacting edges despite the initial orientation of that edge of the crystal. This is shown vividly in Figs. 68a and b where 'a' represents a flake of S.P.1. graphite prior to reaction at 740°C and 'b' shows the same area after 50 minutes

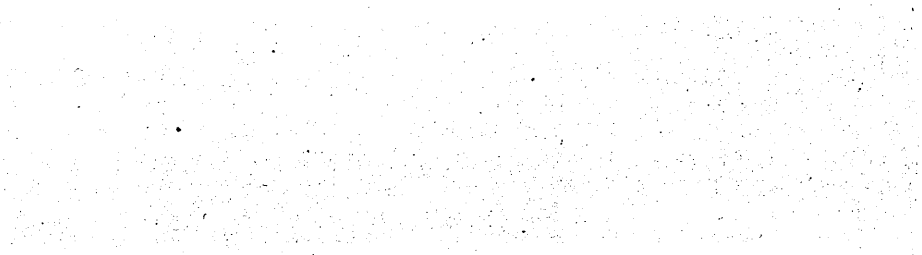

Fig.66.

S.P.1. graphite after 8 minutes oxidation at 715^{o}C with dry air inside the electron microscope.

Magnification 160,000X.

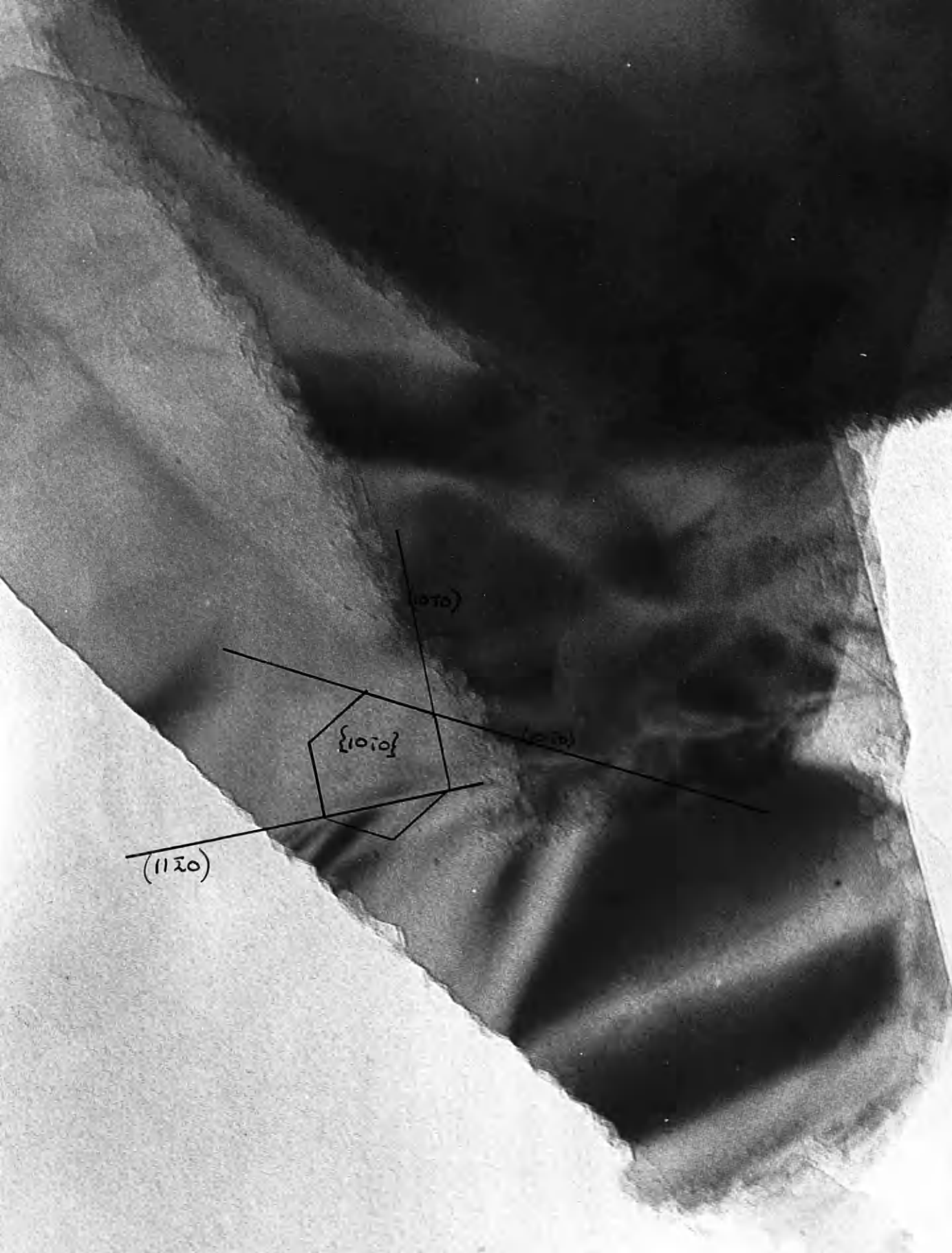
(10$\bar{1}$0)
{10$\bar{1}$0}
(11$\bar{2}$0)

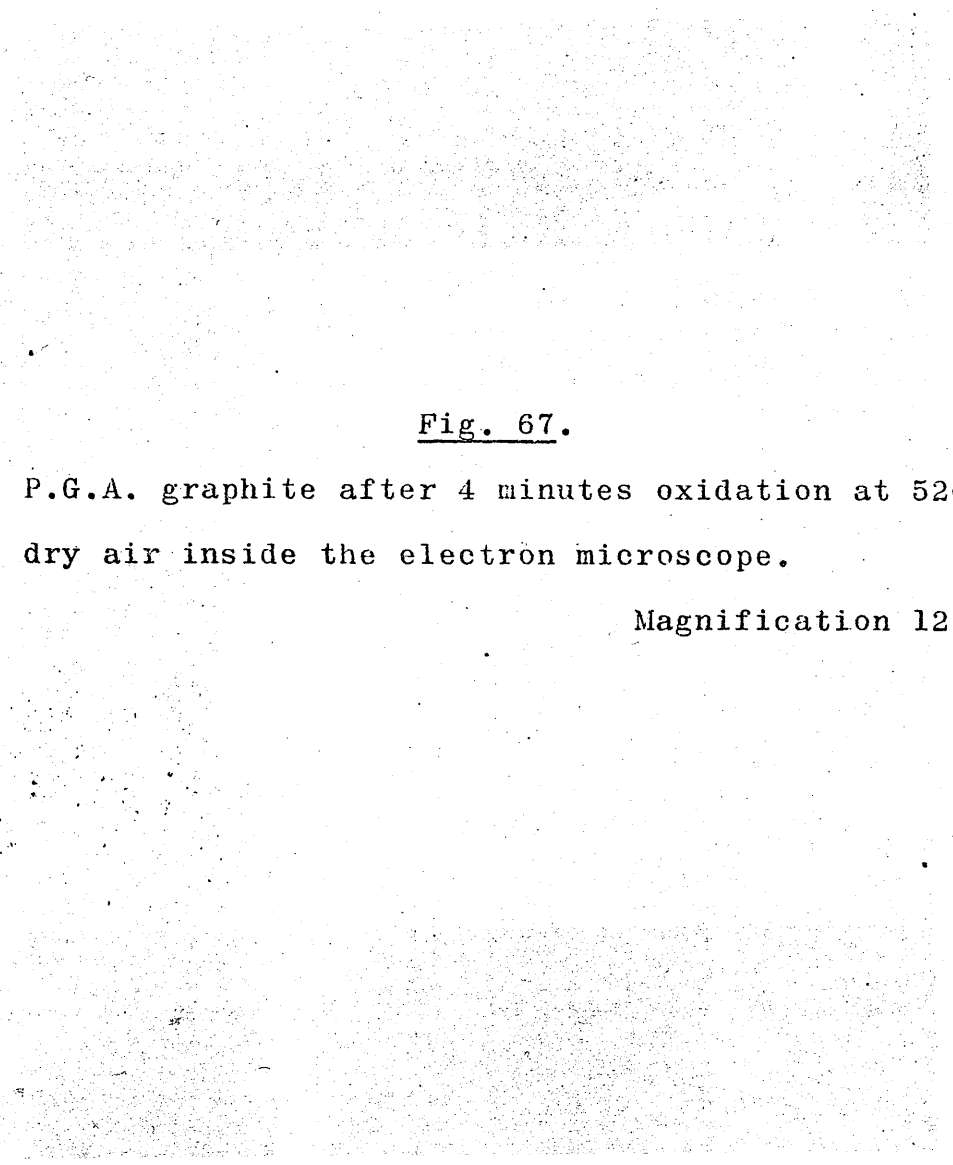

Fig. 67.

P.G.A. graphite after 4 minutes oxidation at 520°C with dry air inside the electron microscope.

Magnification 120,000X.


{10$\bar{1}$0}

Fig. 68a.

S.P.1. graphite prior

to reaction.

Magnification 100,000X.

Fig. 68b

S.P.1. graphite after 50 minutes reaction with dry air at 740°C inside the electron microscope. Diffraction pattern of this area can also be seen.

Magnification 100,000X.

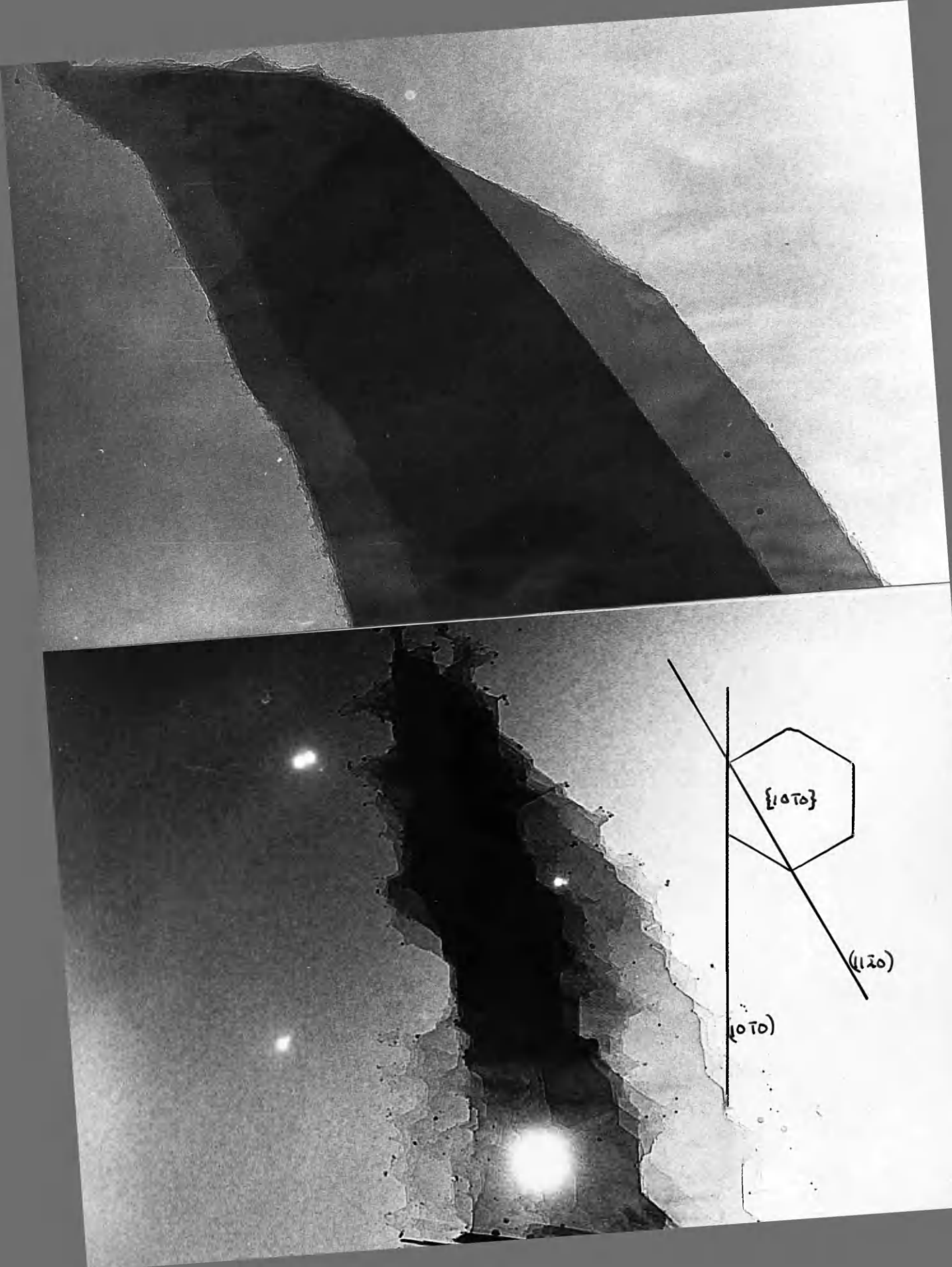
{10$\bar{1}$0}
(11$\bar{2}$0)
(0$\bar{1}$10)

reaction, together with a diffraction pattern. Though the initial orientation of the right hand side of the crystal was largely with $\{11\bar{2}0\}$ exposed planes, after reaction the faceted indentation all had $\{10\bar{1}0\}$ exposed planes. In the last reaction the small particles of metal from the furnace or the mount are visible, but they do not appear to have influenced the orientation, particularly since the same preferred orientation was obtained when the particles did not migrate on to the specimen.

The orientation of a specimen from the dark field micrograph is not as straightforward as the diffraction method, but this was the only possible method in the case of P.G.A. where the crystallites were very small and only a ring diffraction pattern could be obtained. A typical example is shown in Figs 69a and b where apparently the orientation of the erosion changes between A and B, but the dark field ($(10\bar{1}0)$ reflection) shows that there are several crystallites present, and in fact by constructing an orientation diagram from the elongation of image points for these crystallites, it is clear that in fact they all follow the preferred $(10\bar{1}0)$ orientation for eroded edges. This specimen of P.G.A. had been oxidised at 690°C for 7 minutes.

From all the graphite specimens studied and reacted between the temperatures of 430°C and 815°C, the eroded edges were bounded by $\{10\bar{1}0\}$ planes and the progress of

the reaction was by regression of these planes of the specimen, irrespective of the initial orientation of the edges of the specimen. The only difference in appearance between the P.G.A. and S.P.1. graphites was that the areas of hexagonal symmetry comprising two or three sides of a hexagon were smaller for P.G.A. but greater in number than in the S.P.1. This was expected because of the greater crystalline perfection of the S.P.1.

2. Kinetic studies on graphite oxidation.

The experimental procedure for kinetic analysis has been described previously but it did not include the analysis of the results gained from it. Described here is a typical experiment in detail, so that repetition of results in their unprocessed form can be omitted for each experiment.

S.P.1. graphite was mounted on a silica film and treated in the microscope in the usual manner. The degassing time in vacuum at the reaction temperature was 65 minutes with the orientation being determined by electron diffraction prior to degassing. The reaction temperature was 640°C, and Fig.70a shows a graphite flake after degassing. Fig.70b-m refer to reaction times between 3 and 179 minutes respectively, the time each micrograph was taken being shown by the micrograph legend. The two areas selected for measurement are marked P and Q in Fig.70g. A different flake of graphite on the same specimen is shown

Fig. 69a

P.G.A. graphite after 7 minutes reaction with dry air at 690°C, inside the electron microscope.

Magnification 100,000X

Fig. 69b.

Dark field micrograph of area shown in Fig.69a.

A $(10\bar{1}0)$ reflection was used in this micrograph.

Magnification 100,000X.

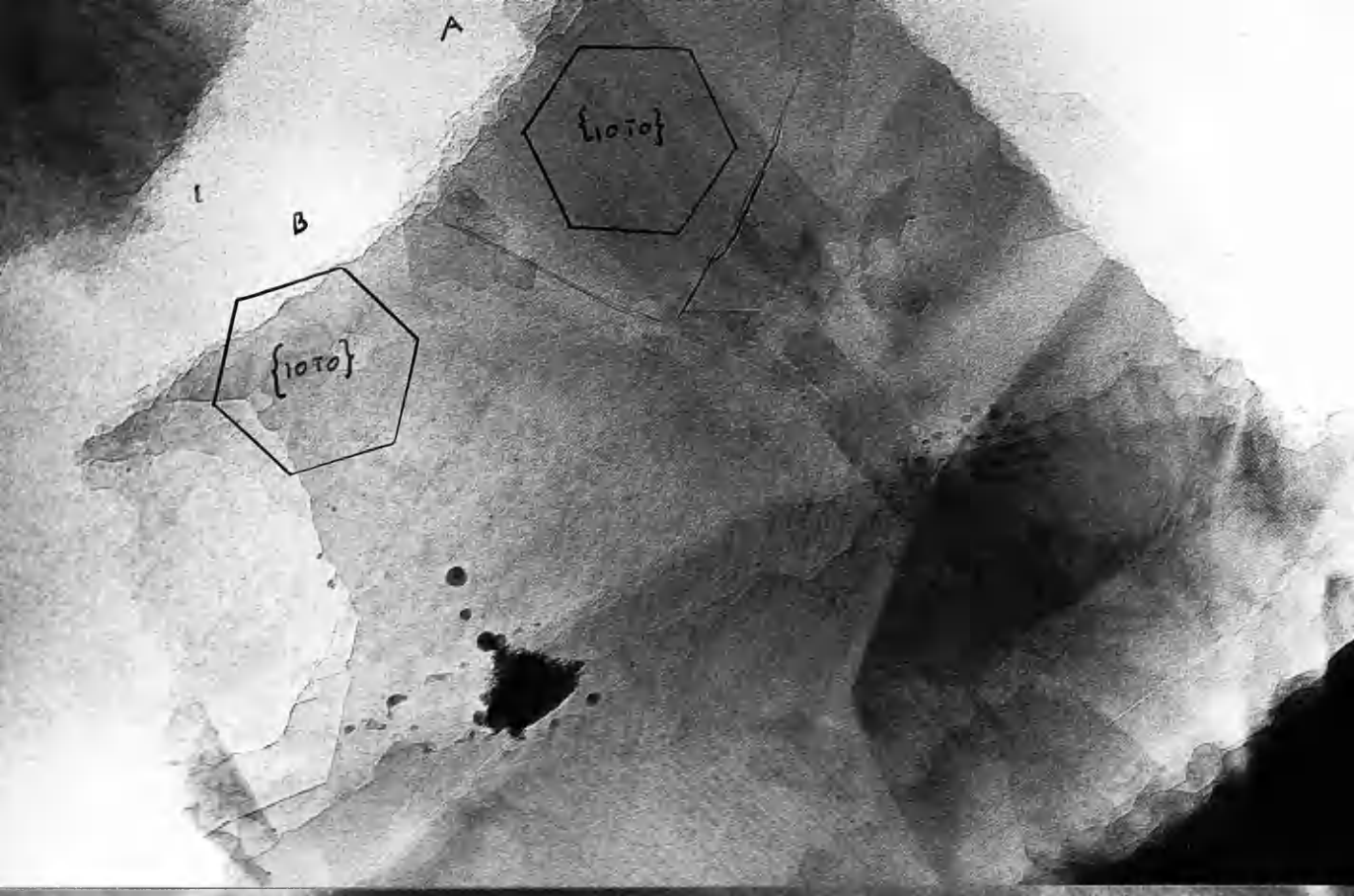
A
{10T0}
B
{10T0}

in Fig.71a-c, the area chosen for measurement being marked R in Fig.71c. In fact two measurements could be made from this area since two overlying flakes are being eroded and it is possible to separate the contribution of each. For each of the areas chosen P, Q, R, (the latter incorporating two areas) the area at different reaction times was measured by the tracing technique and the edge length of the eroded area also measured. Thus values were obtained for areas eroded per unit length of exposed edge, the units being $\text{Å}^2/\text{Å}$. The results for this experiment are shown graphically in Fig.72 for areas P and Q, and Fig.73 for both areas R. Reasonably linear graphs are given, but since the range of values is small, any exponential component would not be particularly outstanding.

The slopes of these graphs are:-

area P = 6.2 Å/min

Q = 4.4 Å/min

R = 5.8 Å/min

R' = 5.5 Å/min

These values represent edge attack on the graphite assuming that basal plane attack is negligible by comparison. The graphs do not necessarily pass through zero since the attack undoubtedly started at some inhomogeneity in the crystal, and thus a finite size of reactive site would be present at the start of reaction.

Fig. 70a

S.P.1. graphite after degassing at 640°C for 1 hour and prior to reaction in the microscope at the same temperature, with dry air.

Magnification 63,000X.

Fig. 70b

After 3 minutes reaction at 640°C.

Magnification 63,000X.

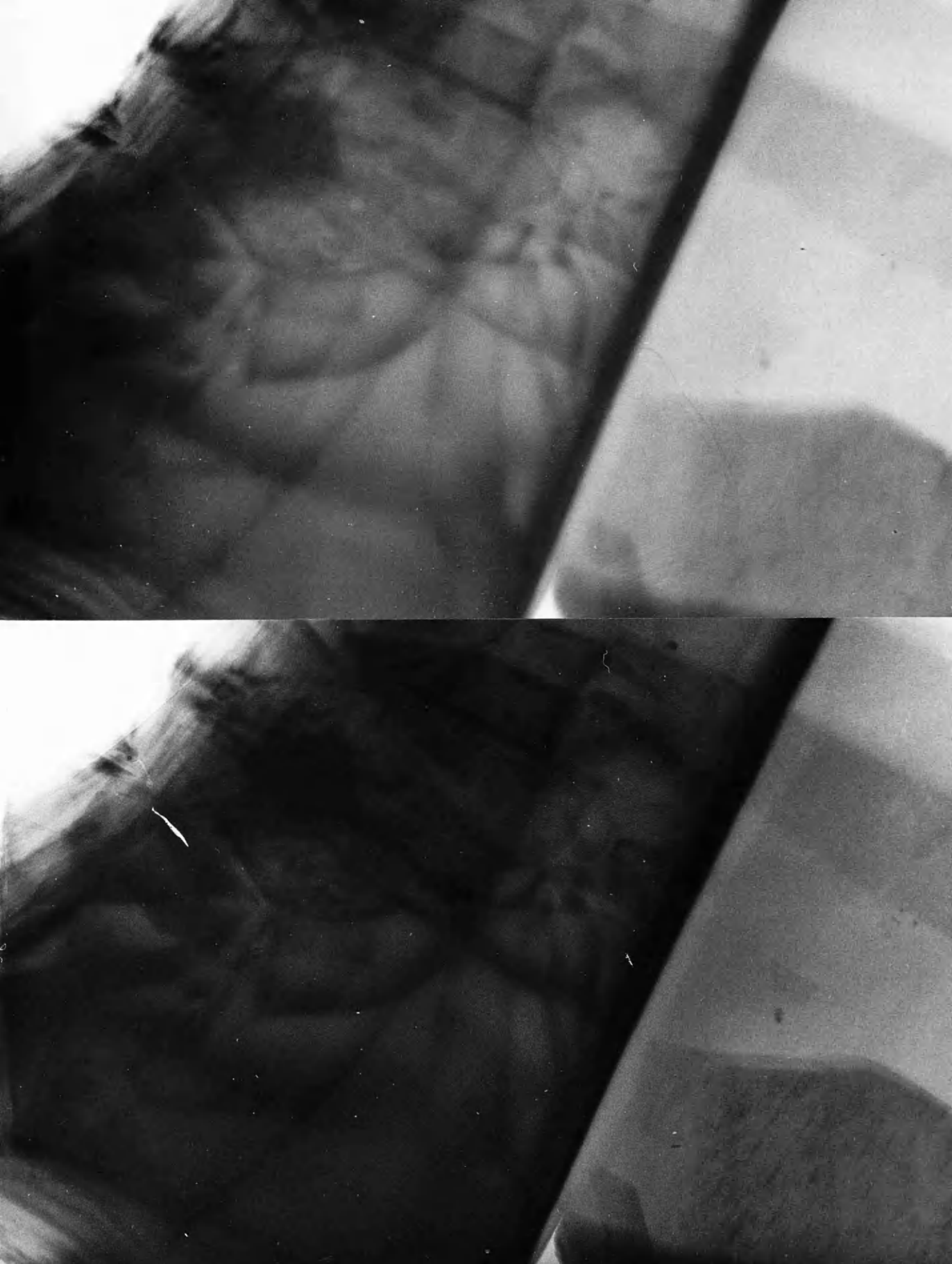

Fig. 70c.

After 8 minutes reaction

at 640°C.

Magnification 63,000X.

Fig. 70d.

After 16 minutes reaction

at 640°C.

Magnification 63,000X.

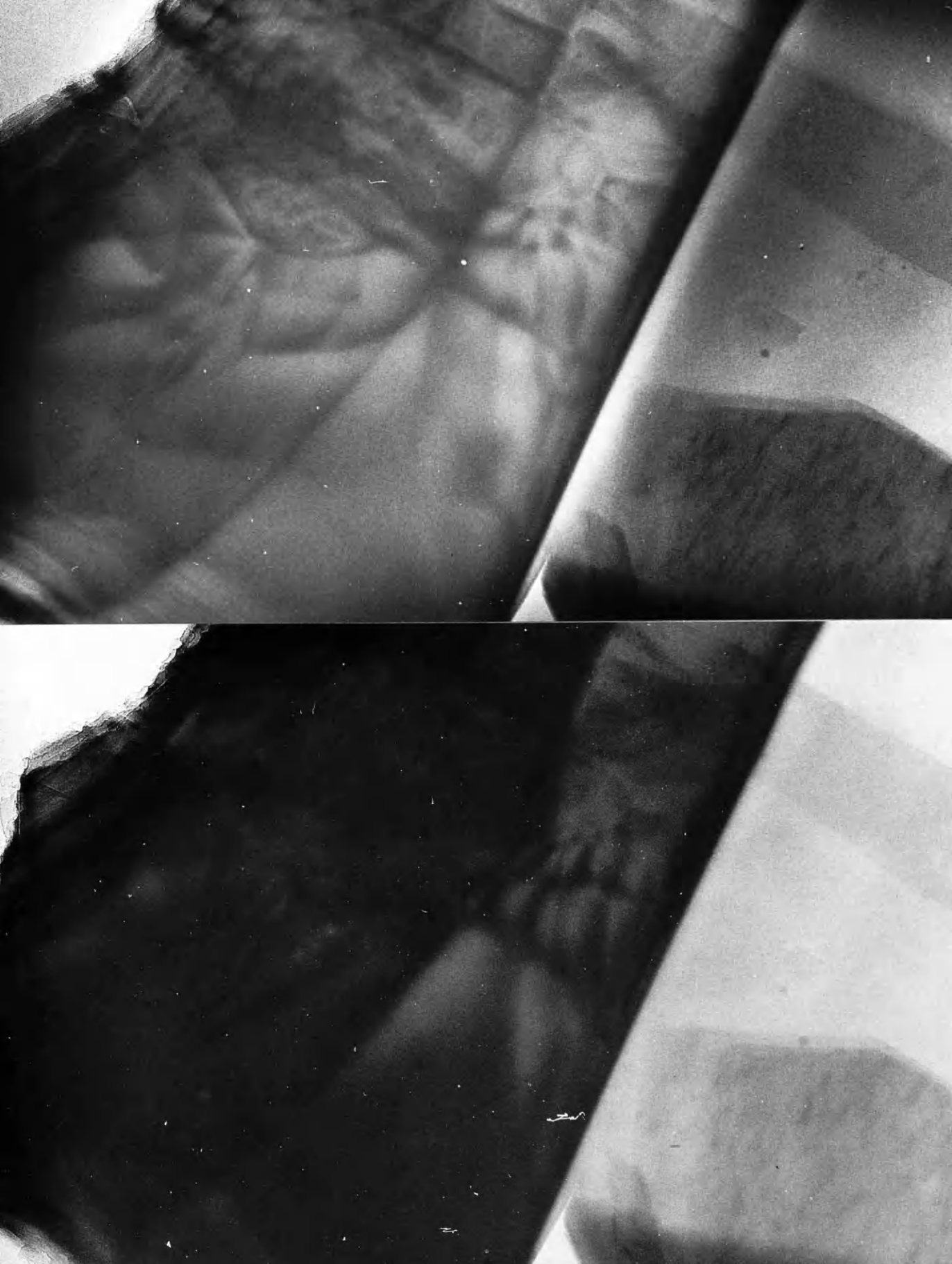

Fig. 70e.

After $21\frac{1}{2}$ minutes reaction at $640^{o}C$.

Magnification 63,000X.

Fig. 70f.

After 46 minutes reaction at $640^{o}C$.

Magnification 63,000X.

Fig. 70g.

After 60 minutes reaction at 640°C

Magnification 63,000X.

Fig. 70h.

After 63 minutes reaction at 640°C

An adjacent area.

Magnification 63,000X.


Q
P

Fig. 70i.

After 89 minutes reaction at 640°C.

Magnification 63,000X.

Fig. 70j.

After 126½ minutes reaction at 640°C

Magnification 63,000X.

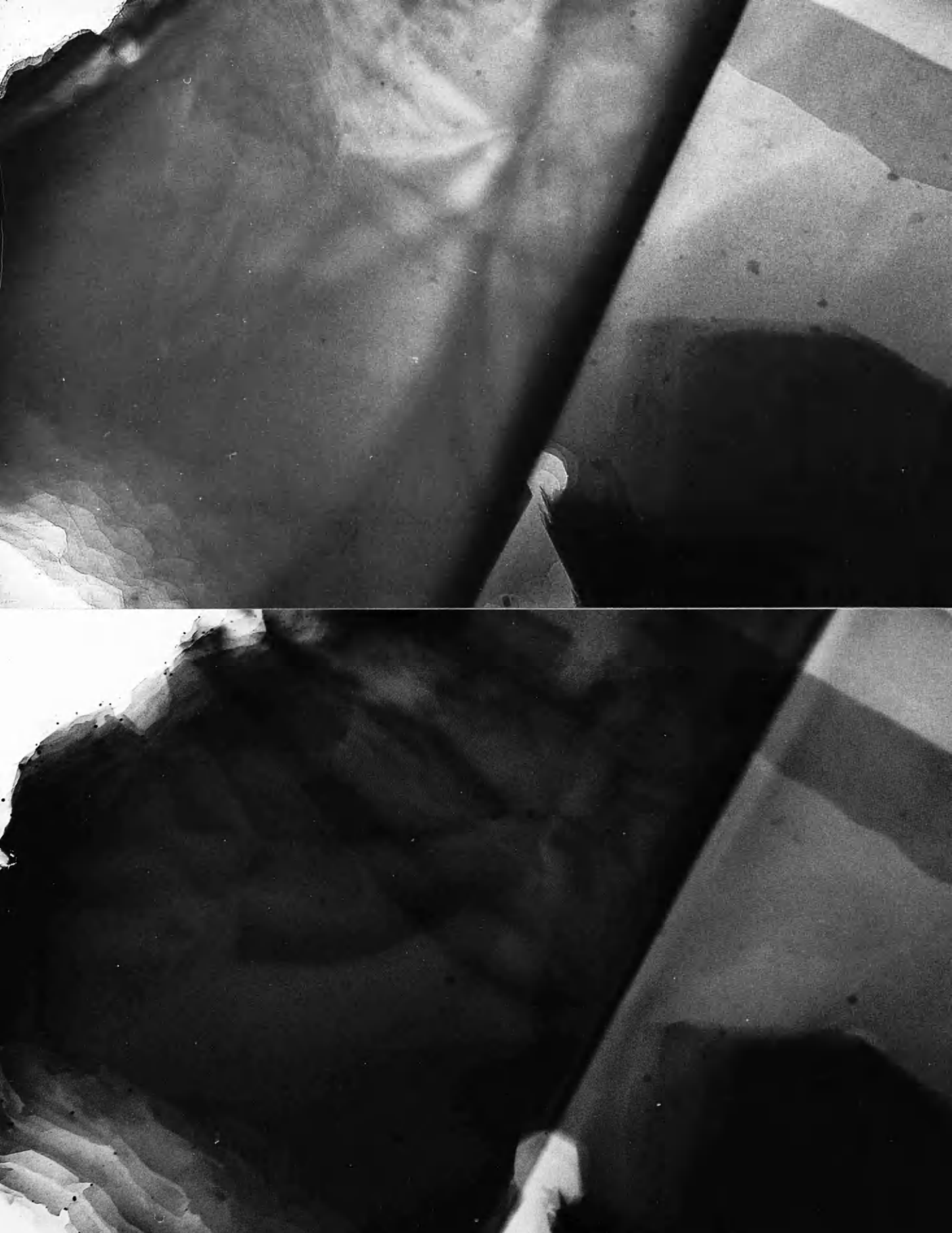

Fig. 70k.

After 143 minutes reaction at 640°C.

Magnification 63,000X.

Fig. 70l.

After 164½ minutes reaction at 640°C.

An adjacent area.

Magnification 63,000X.

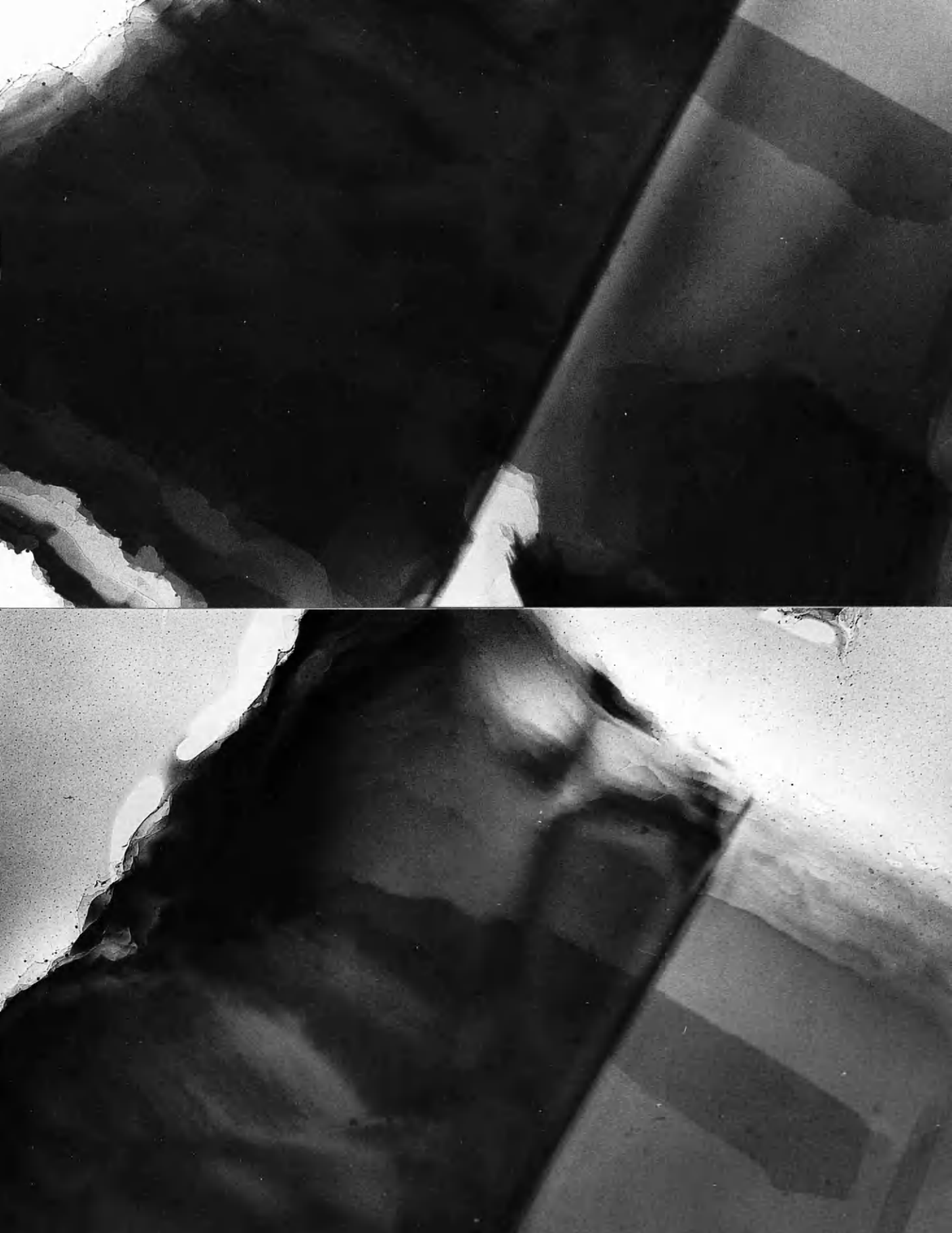

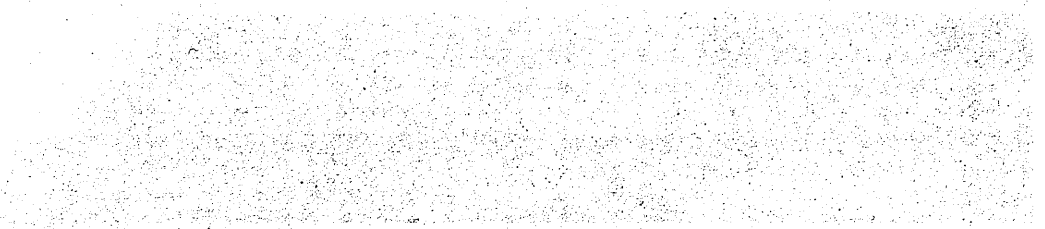

Fig. 70 m.

After 179 minutes reaction at 640°C.

Magnification 63,000X.

Fig. 71a.

S.P.1. graphite after 19 minutes reaction at 640°C with dry air inside the electron microscope.

Magnification 100,000X.

Fig. 71b

After 66 minutes reaction.

Magnification 100,000X.

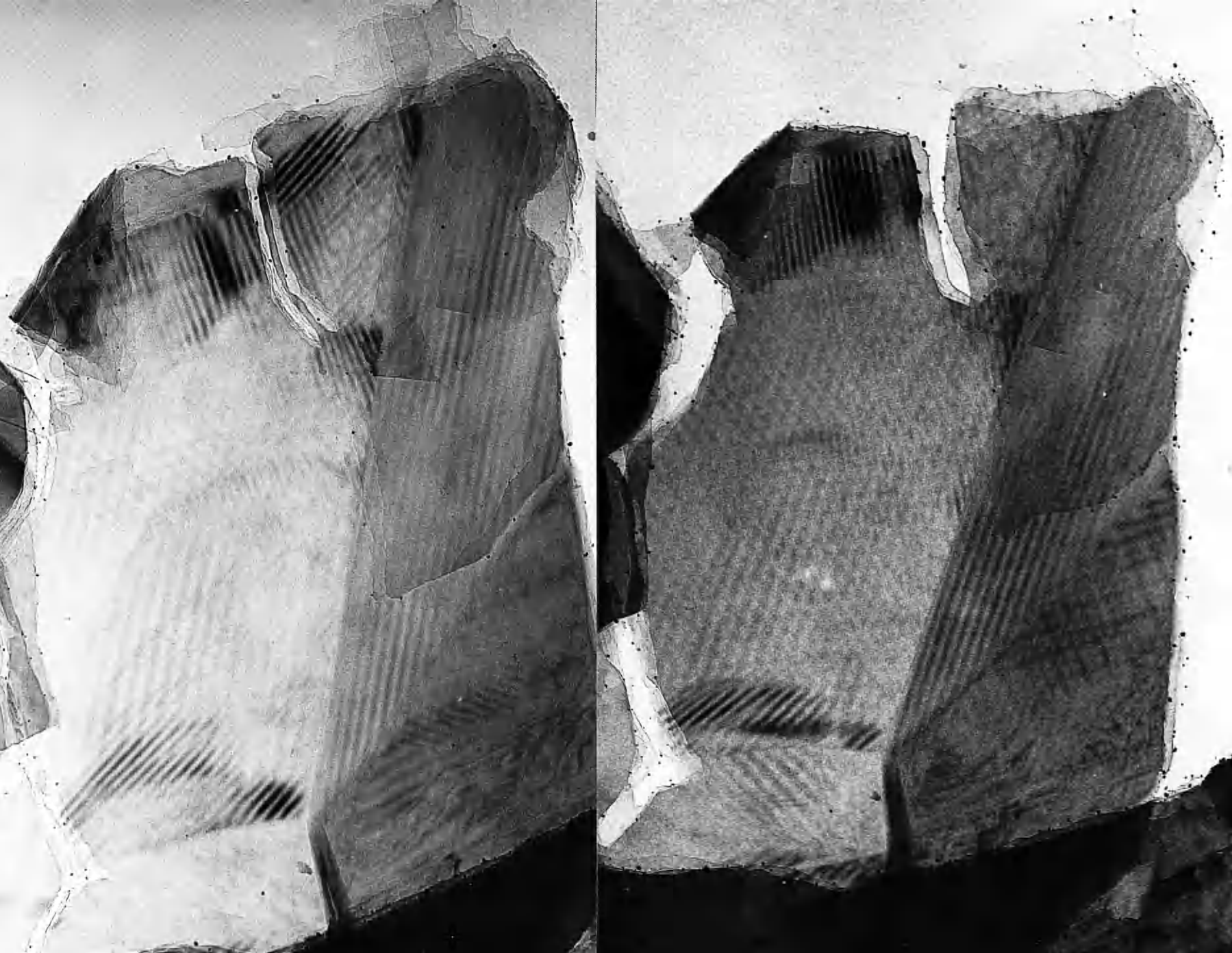

Fig. 71c.

After 130 minutes reaction at 640°C.

Magnification 100,000X.

Fig. 71d.

After 166 minutes reaction at 640°C.

Magnification 100,000X.

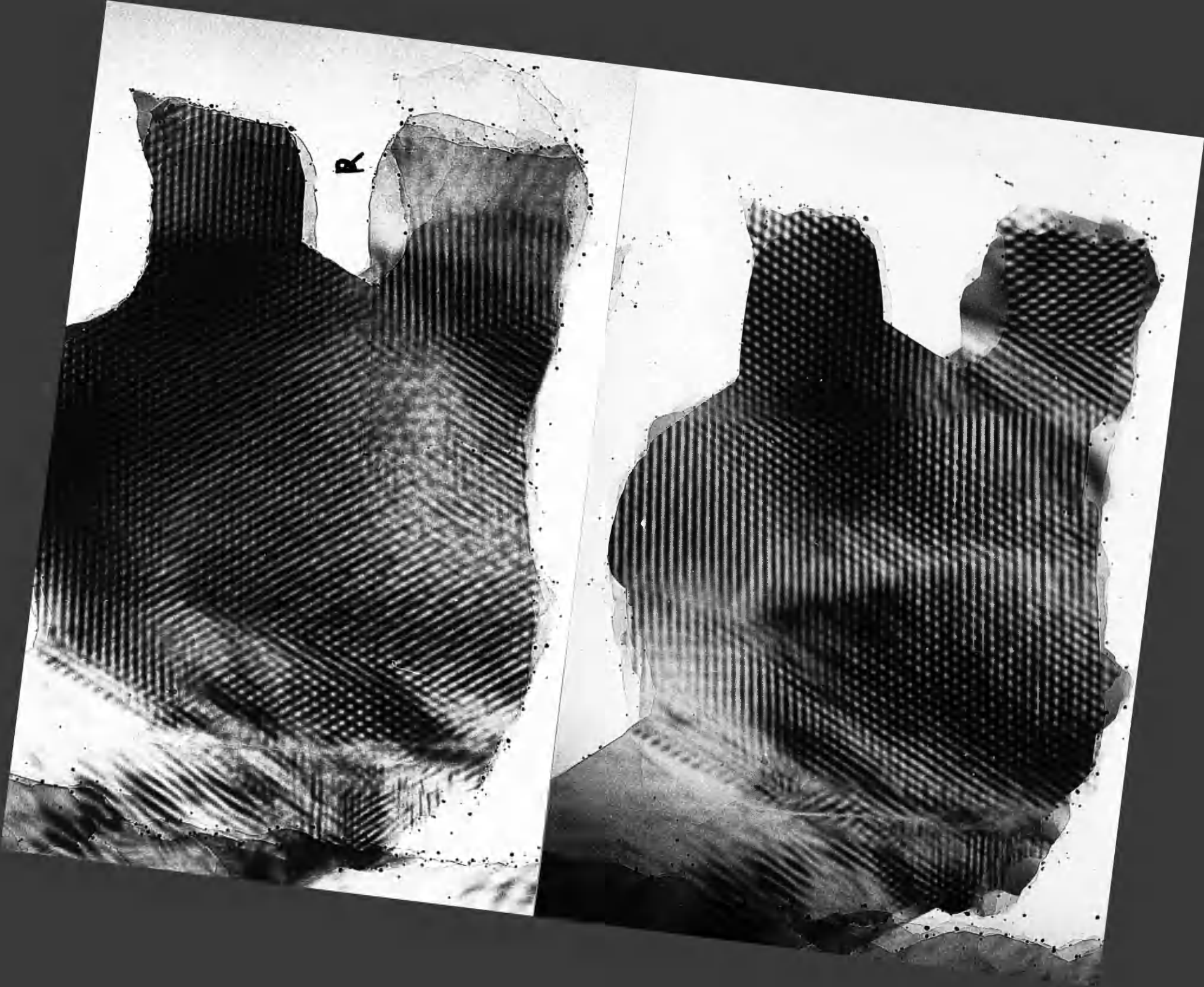
R

Fig. 71 e.

After 180 minutes at 640°C.

Magnification 100,000X.

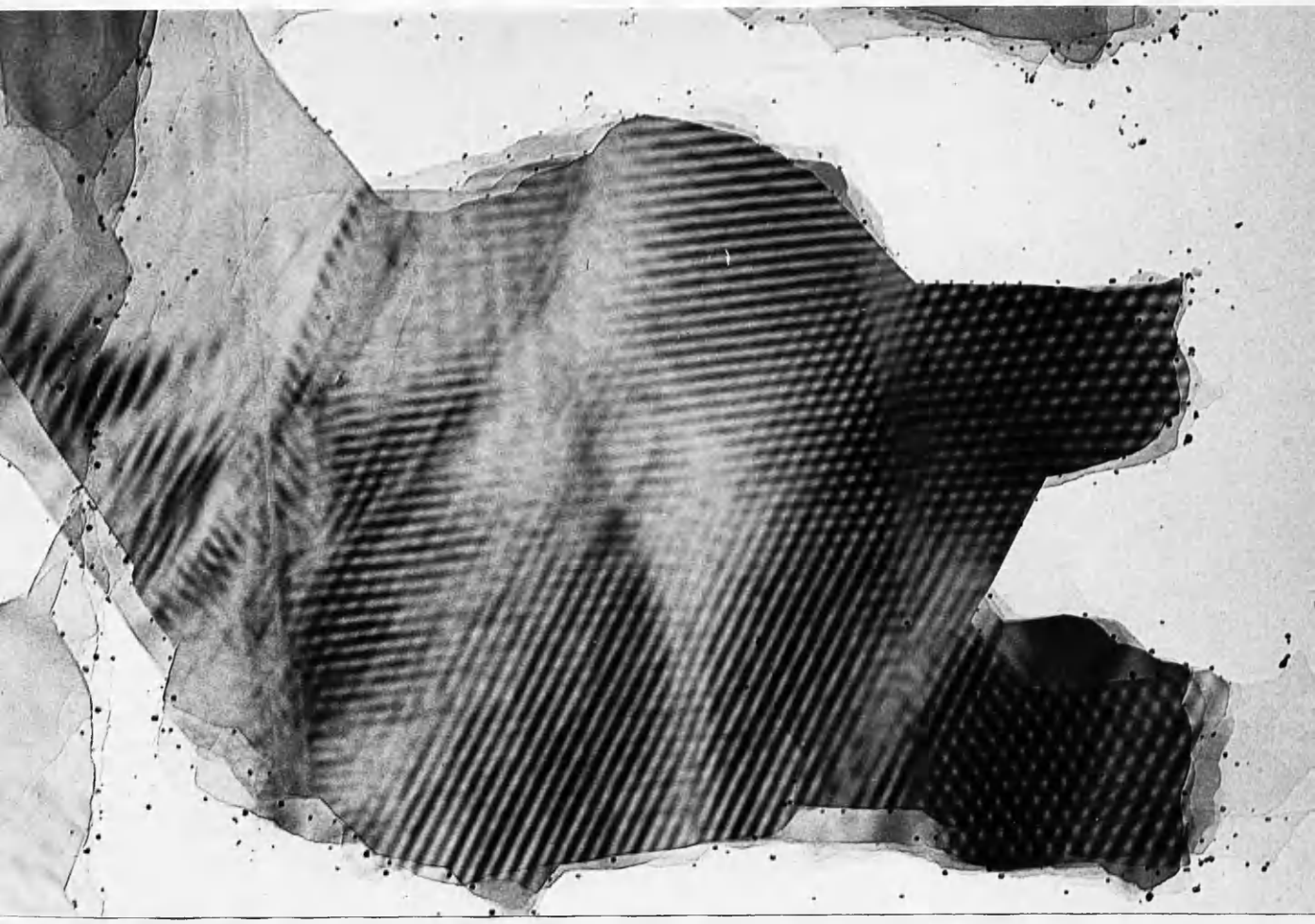

Fig. 72.

Time dependence of rate of removal of carbon from crystallite edges in areas P and Q shown in Fig.70a-m.

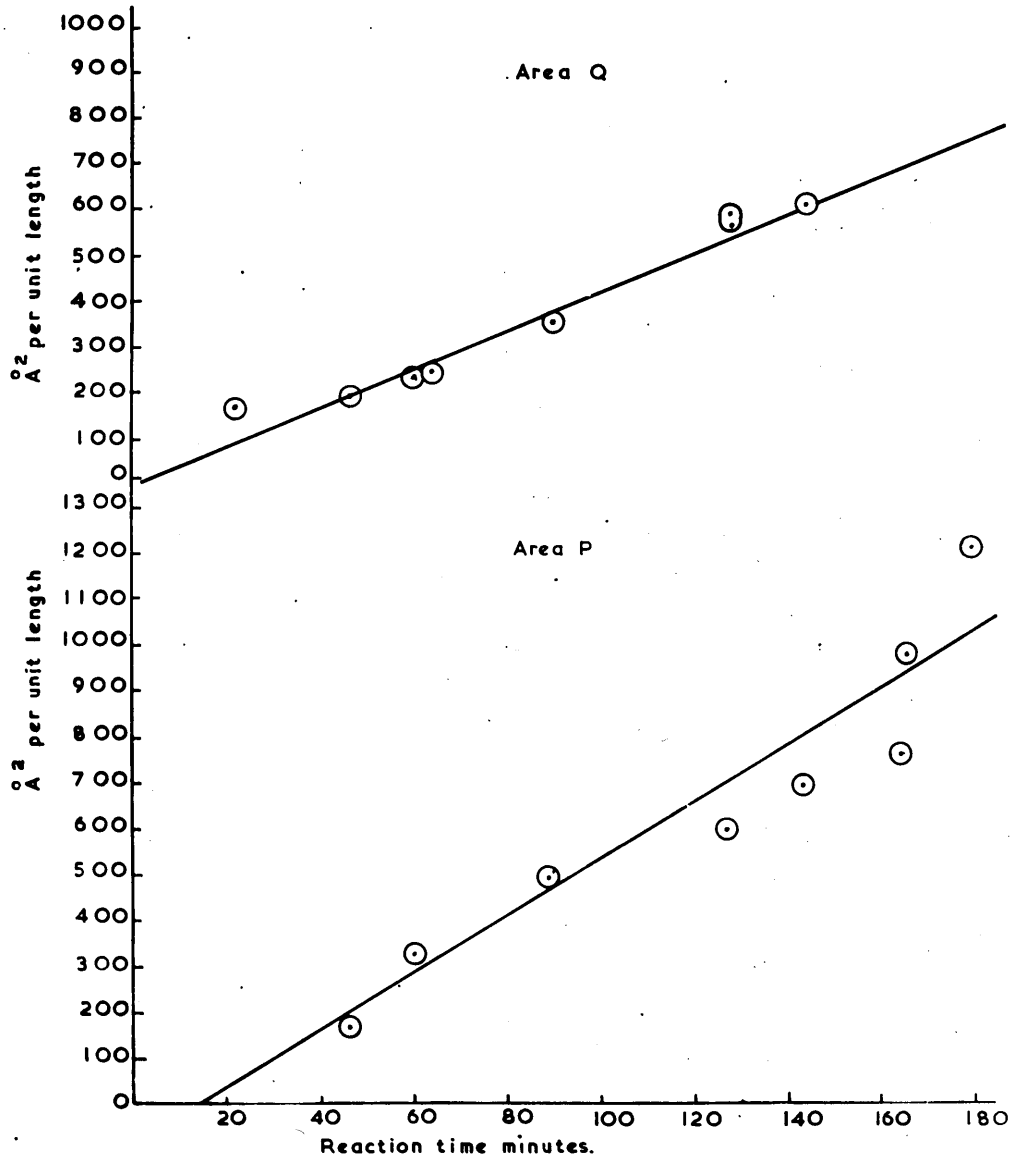
Area Q
Area P
$A^{\circ 2}$ per unit length
$A^{\circ 2}$ per unit length
1000
900
800
700
600
500
400
300
200
100
0
1300
1200
1100
1000
900
800
700
600
500
400
300
200
100
0
20
40
60
80
100
120
140
160
180
Reaction time minutes.

Fig. 73.

Time dependence of rate of removal of carbon from crystallite edges in areas R and R' shown in Fig.71a-e.

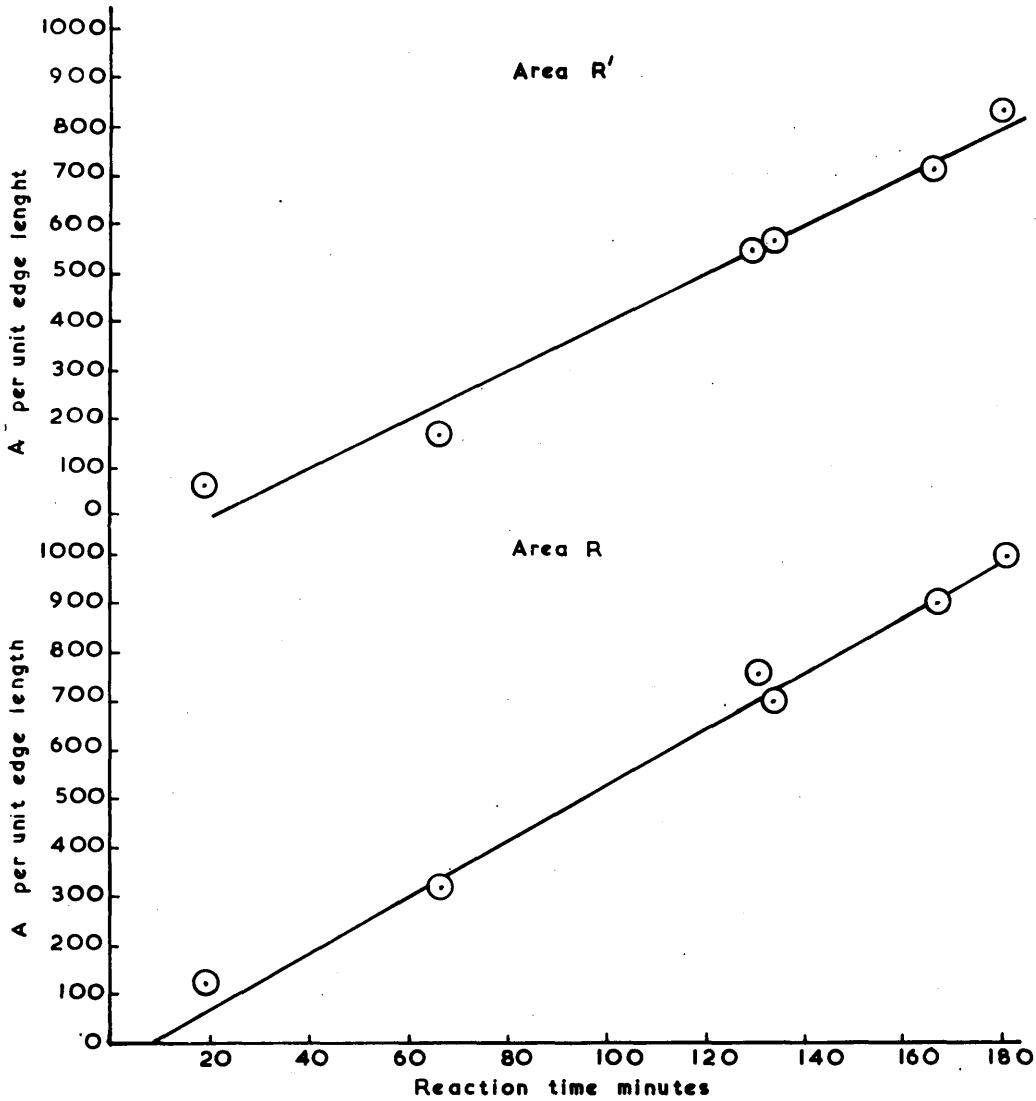
Area R'
A per unit edge lenght
1000
900
800
700
600
500
400
300
200
100
0
Area R
A per unit edge length
1000
900
800
700
600
500
400
300
200
100
0
20
40
60
80
100
120
140
160
180
Reaction time minutes

Three of these values - P, R, and R' - are in reasonable agreement with each other, the rate for area Q being significantly lower. Examination of the micrograph Fig.70m shows areas of loss of silica along the edge of the graphite of which Q is one area. The loss is made manifest by the appearance of holes in the support film, and therefore it is not unexpected that silica inhibition of oxidation occurred. Area P was not resting directly on the graphite and was thus some distance from the silica film and the areas R and R' do not show signs of any adjacent loss of silica. Probably the graphite flake was not in close contact with the support film. The shadowing experiments described previously show that it was common for not all of a graphite flake to be in intimate contact with the support. Therefore the value for rate of oxidation at area Q is suspect and where close proximity of a measured reaction area and loss of silica occurred the result for rate analysis was examined separately from the normal areas, eg. P,R and R'.

In Table VI the values for rates of reaction are tabulated for both P.G.A. and S.P.1. graphites. Micrographs are included to demonstrate the nature of the graphite flakes chosen for study, but the complete series of micrographs for each reaction are not included because of the large number involved, i.e. each experiment comprised a minimum of 12 micrographs and sometimes as many

Table VI

Temperature of reaction °C.	Type of graphite	Rate of reaction Å/min {10$\bar{1}$0}	Remarks
495	P.G.A.	1.05	
520	P.G.A.	0.77	Pitting in other parts of specimen. Fig.67.
535	P.G.A.	2.7	
535	P.G.A.	5.5	Pitting in specimen of irregular shape.Fig.74a,b,c,d
580	P.G.A.	3.9	No pitting.Fig.75.
640	P.G.A.	8.6	
690	P.G.A.	14.0	Fig.69a and b
715	P.G.A.	29.2	Slight pitting
745	P.G.A.	4.82	Extensive pitting Fig.76a,b
535	S.P.1.	1.6	Fig.79a and b.
580	S.P.1.	2.0	
635	S.P.1.	9.6	Fig.77a and b.
640	S.P.1.	5.8	Fig.70a-m,Fig.71a-e
685	S.P.1.	13.5	Slight pitting
715	S.P.1.	11.2	Fig.66
740	S.P.1.	24.9	Fig.68a and b
780	S.P.1.	28.6	Fig.52
810	S.P.1.	35.9	Fig.78

Fig. 74a.

P.G.A. graphite after 1½ minutes reaction with dry air at 535°C inside the electron microscope.

Magnification 120,000X

Fig. 74b.

After 6 minutes reaction at 535°C.

Magnification 120,000X.

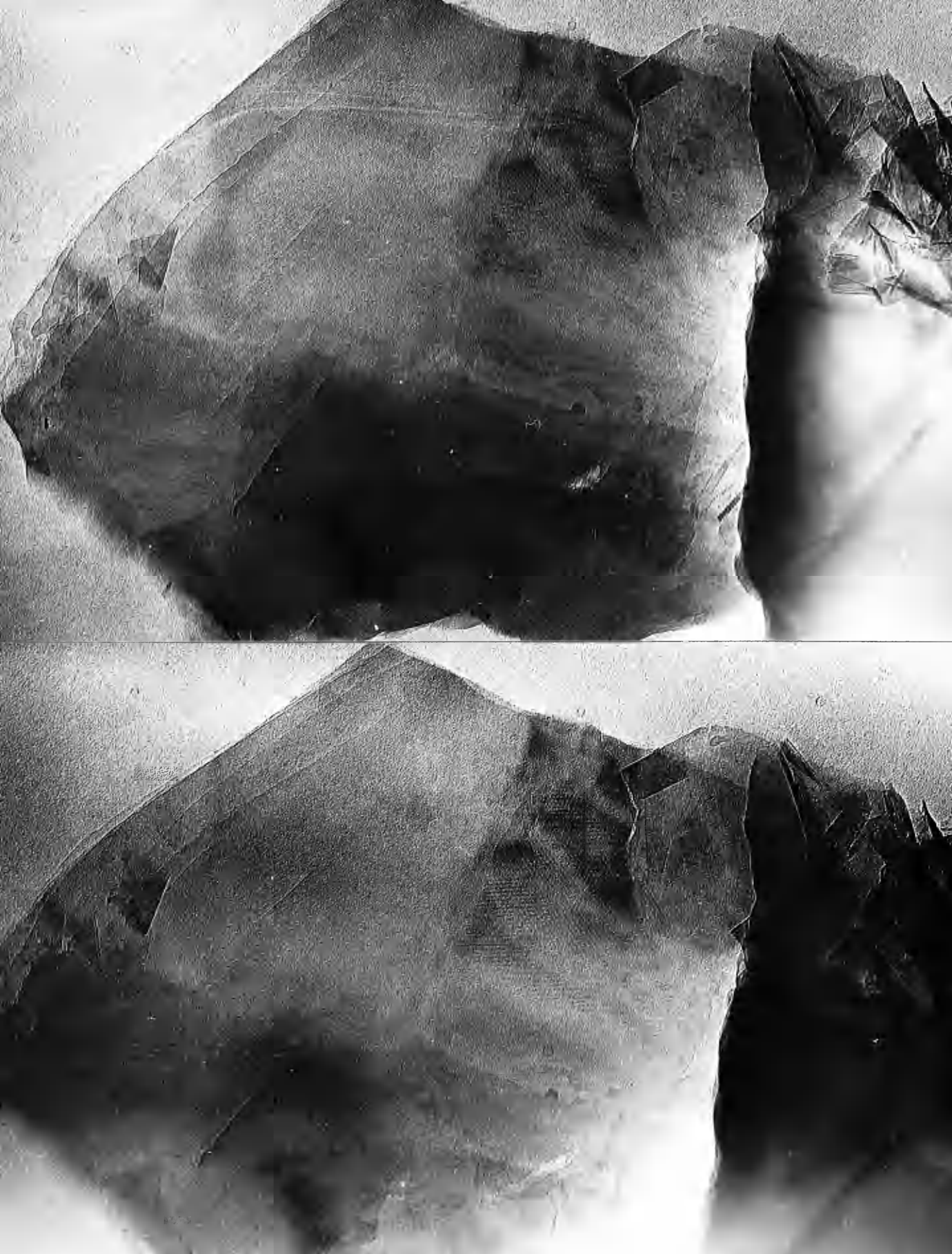

Fig. 74c.

After 10 minutes reaction at 535°C.

Magnification 120,000X.

Fig. 74d.

After 17 minutes reaction at 535°C.

Magnification 120,000X.

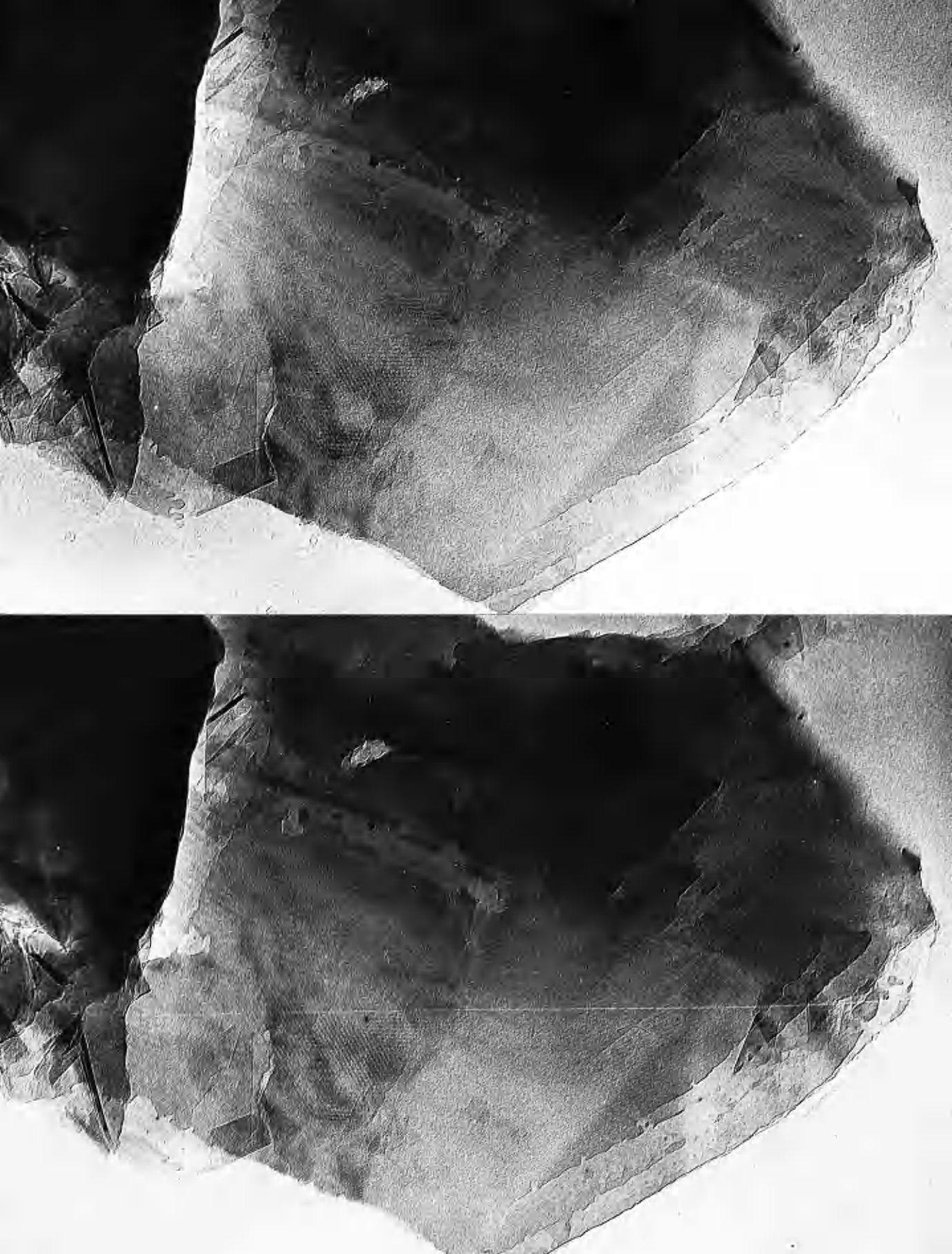

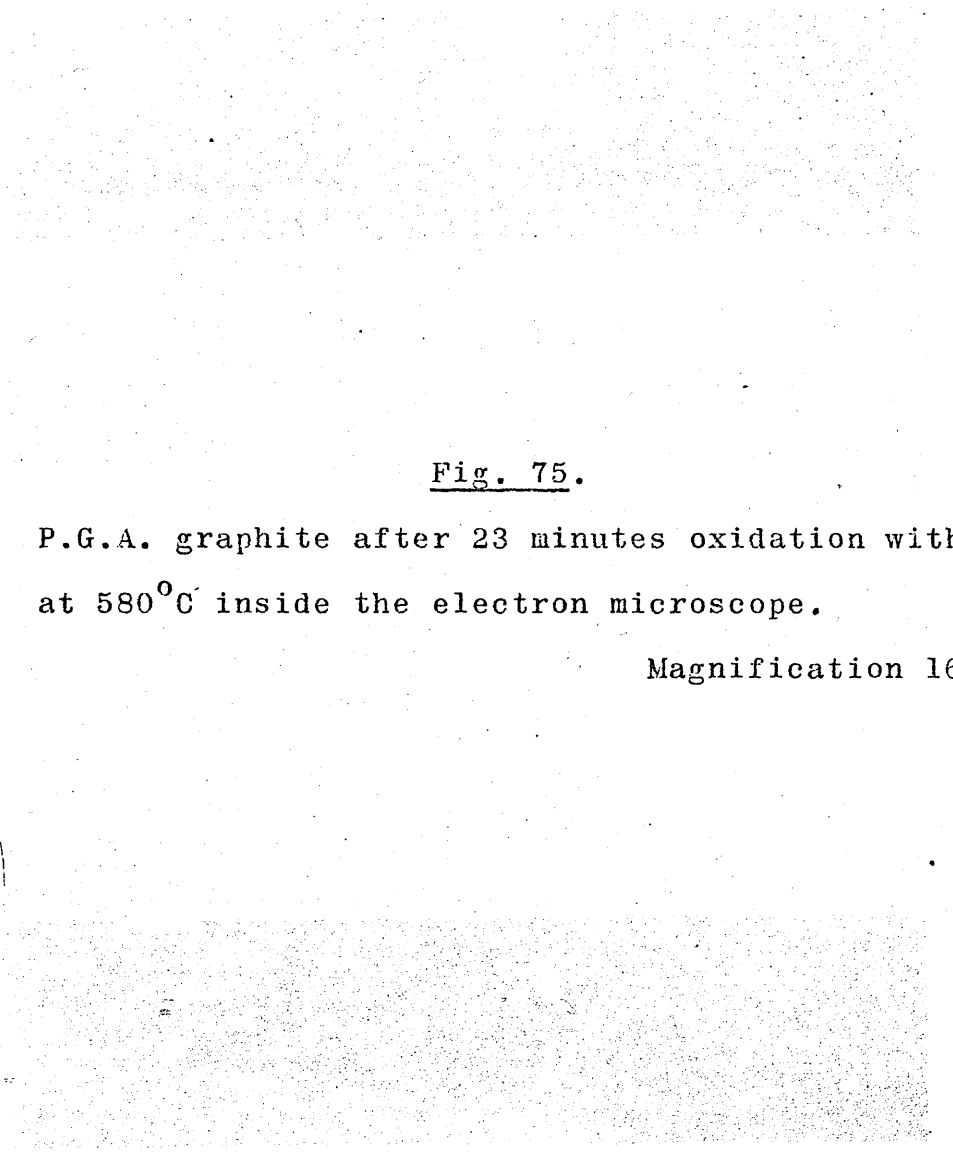

Fig. 75.

P.G.A. graphite after 23 minutes oxidation with dry air at 580°C inside the electron microscope.

Magnification 160,000X.

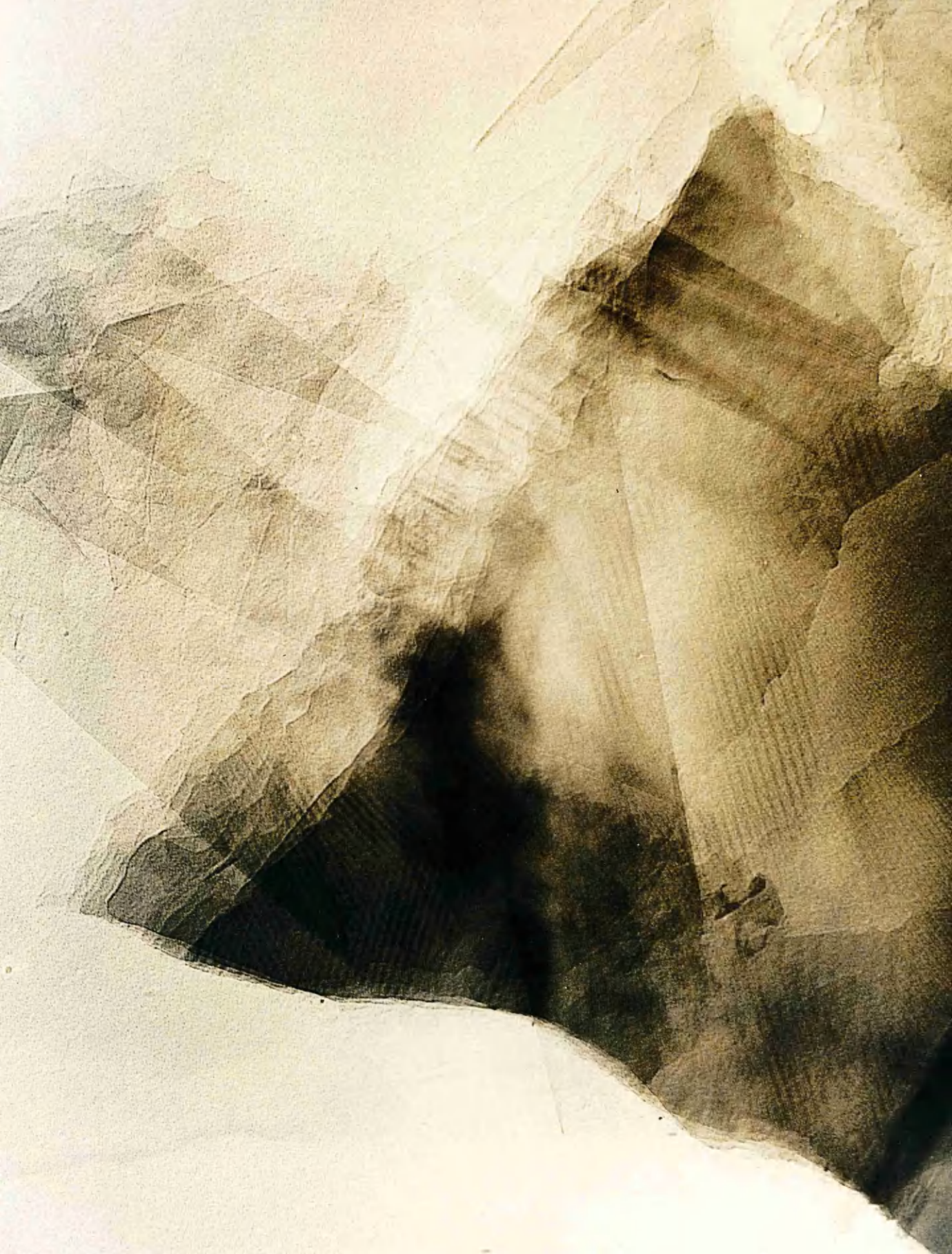

Fig. 76a

P.G.A. graphite after 20 minutes oxidation with dry air at 745°C inside the electron microscope.

Magnification 120,000X

Fig. 76b.

After 32 minutes reaction at 745°C.

Magnification 120,000X.

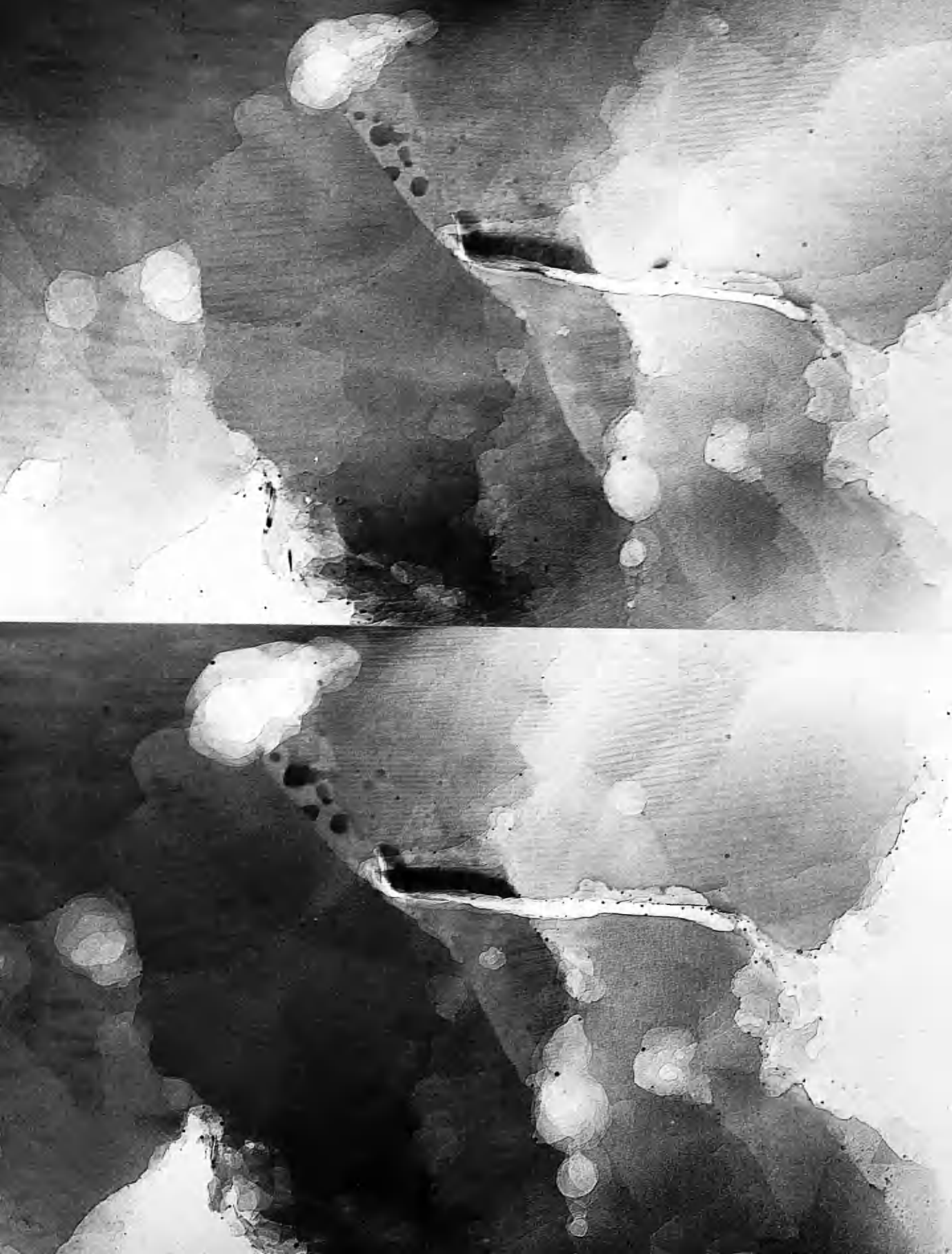

Fig. 77a.

S.P.l. graphite before reaction.

Magnification 120,000X

Fig. 77b.

S.P.l. graphite after 7 minutes reaction with dry air at 635^{o}C inside the electron microscope.

Magnification 120,000X.

Fig. 78.

S.P.1. graphite after 15 minutes reaction with dry air at 810^{o}C inside the electron microscope.

Magnification 160,000X.

Fig. 79a.

S.P.1. graphite prior to reaction.

Magnification 120,000X.

Fig. 79b.

S.P.1. graphite after 9 minutes reaction with dry air at 535^{o}C inside the electron microscope.

Magnification 120,000X.

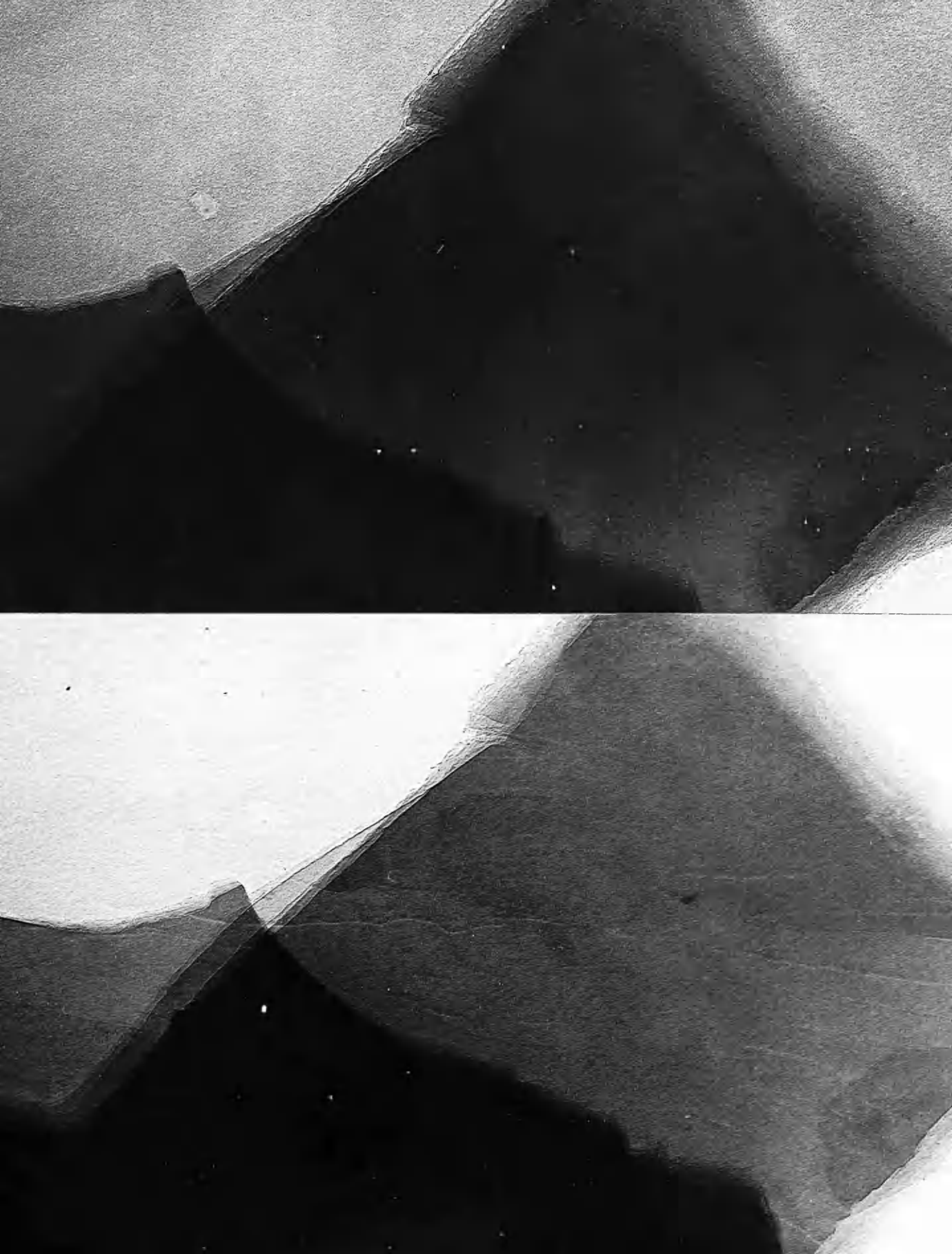

as 50 micrographs for the slower reaction rates. The rates given are the mean values obtained from the various parts of the specimen that were chosen for measurement. Where a value was obviously erroneous because it was taken from an area in close proximity to obvious silica diffusion, or catalytic attack, then this was not included, but in view of the danger in selectivity of these exclusions, then the reasons for exclusion had to be cogent. In some cases several experiments were performed at the same temperature, and where different values were obtained for each experiment then these values are listed separately - eg. P.G.A. at 535°C. However, it was more normal for a reasonable agreement to be obtained. The pits that sometimes occurred gave varying results in that only at 745°C with P.G.A. graphite were they at all typical of the mode of oxidation; this experiment, however, gave anomolous results as the oxidation rate shows, and thus may have been severely contaminated. In other cases the pits appeared to have been formed by the presence of impurities or some non-general defects in the graphite, and the kinetic data measured from pit expansion did not give consistent data. In some cases the kinetic value agreed with the edge regression values, and in some cases not. There was no visible evidence to account for this.

As mentioned earlier, there was no indication whether an exponential or linear relationship existed for the

Fig. 80.

Variation in time dependence of reaction rate for S.P.1. graphite oxidised at 740°C inside the electron microscope with dry air. The specimen from which these kinetics were measured is shown in Fig.68a and b.

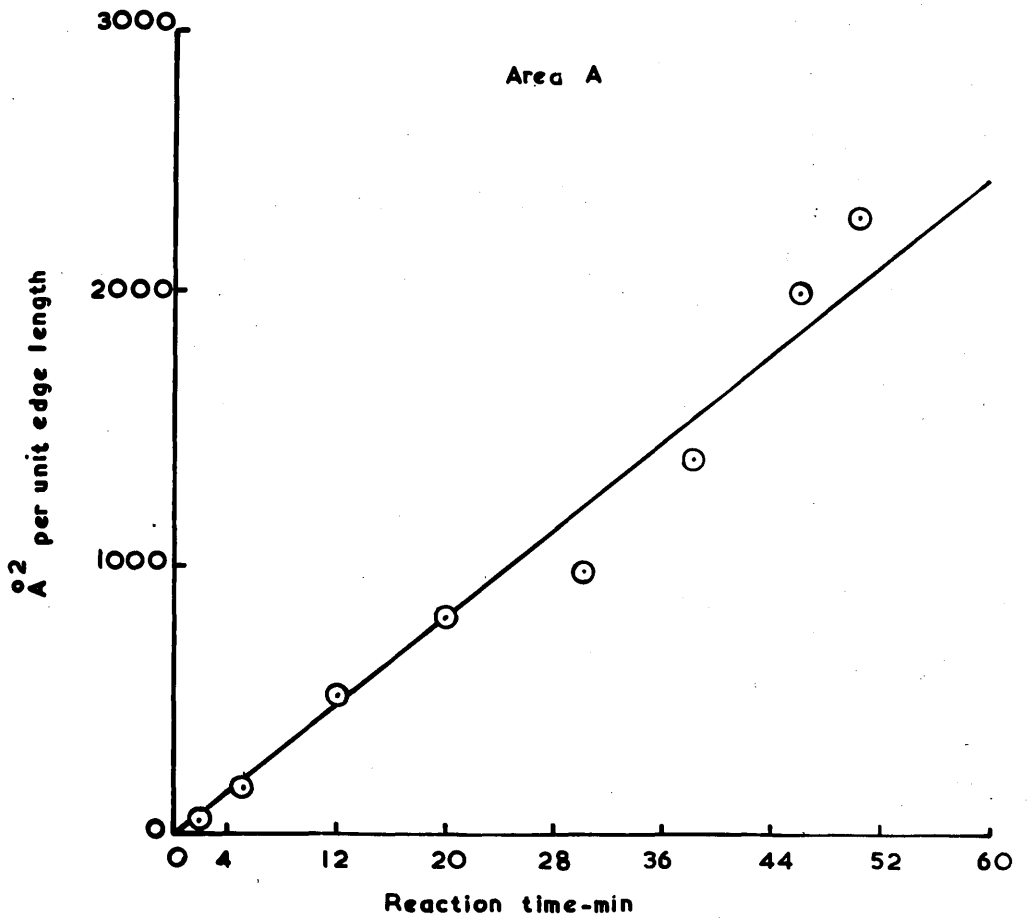
Area A
3000
2000
1000
0
A^{o2} per unit edge length
0
4
12
20
28
36
44
52
60
Reaction time-min

Fig. 81

Activation energy determination for P.G.A. graphite.

P. G. A. graphite
Arrhenius plot.

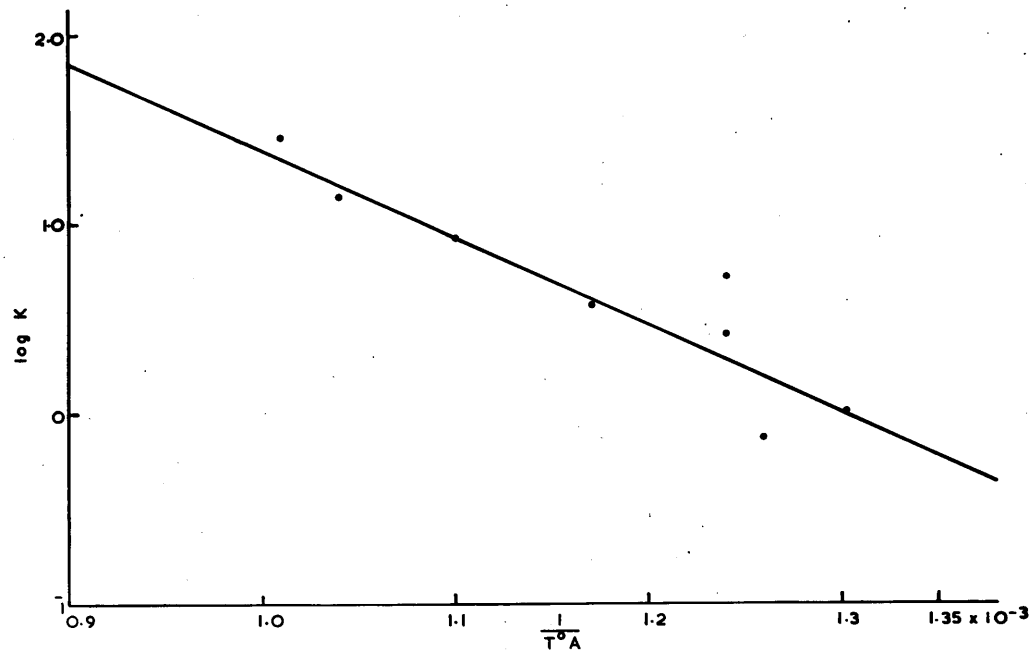

Fig. 82.

Activation energy determination for S.P.1. graphite.

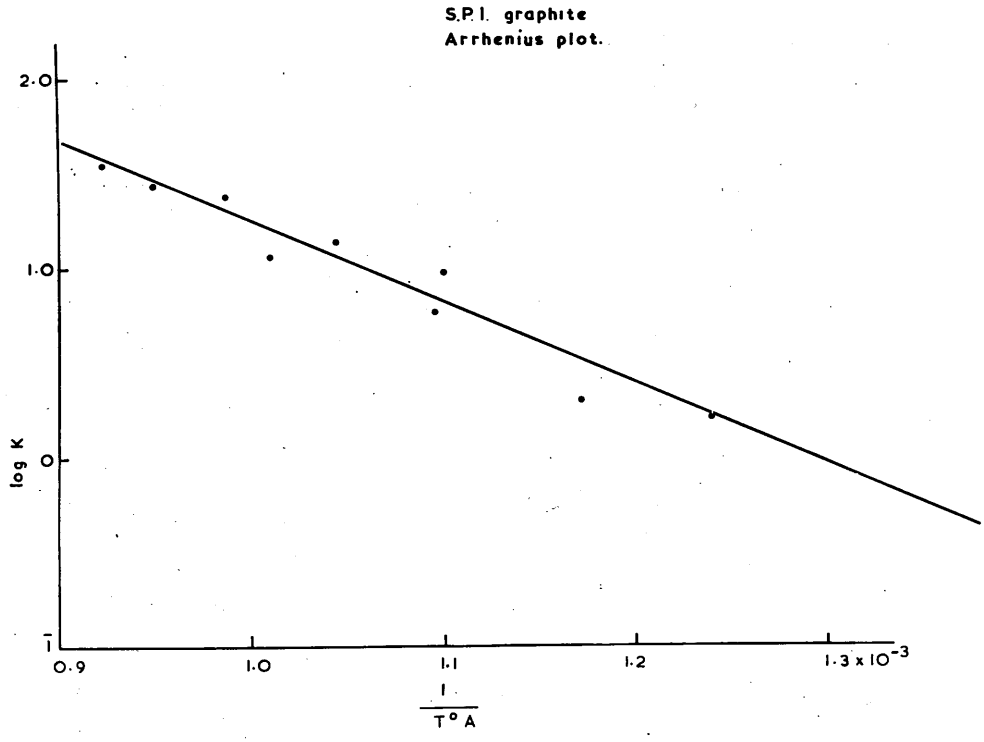
S.P.1. graphite
Arrhenius plot.
2.0
1.0
0
log K
0.9
1.0
1.1
1.2
1.3 x 10⁻³
1/T°A

kinetic graphs, and thus a linear relationship was arbitrarily chosen. No general deviation from linearity was observed as reaction time increased, and the only feature that did reappear from experiment to experiment was an undulation in the graph soon after the reaction had commenced. This did not occur in all cases, and in several it was not significant. It was observed on several occasions and Fig.80 shows an example. This inflexion generally occurred after approximately 16 minutes reaction time, and the phenomenon was independent of temperature. However if the effect was real - which is far from certain- it was probably a function of the apparatus rather than being of any chemical significance.

The rates show that S.P.1. was more resistant to oxidation than P.G.A. on the $\{1010\}$ planes, and it can be seen that the eroded edges of the S.P.1. were usually more symmetrical and bounded by 120^{o} angles than in the case of P.G.A. The latter was also much more susceptible to pitting.

3. Activation energies.

The graphical descriptions of these reactions are linear and thus are typical of a zero order reaction. This is not unexpected from previous results reported. Furthermore since a single reactant plane of the graphite is involved, it is probable that there is a strong adsorbtion of gas on to this plane, making the reaction

independent of pressure, and thus zero order. The reaction rate constants k at various temperatures can be used to determine the activation energy from the Arrhenius equation.

$$k = Ae^{\frac{-E}{RT}}$$

A is a constant

E - the activation energy

R - the gas constant

T - absolute temperature.

Plotting log k against T^{-1} the graph has a slope of

$$\frac{-E}{4.58} \text{ k cal/mole.}$$

Hence the activation energy can be determined, and Fig. 81 and 82 show the activation energy graphs for P.G.A. and S.P.l. respectively. The values for activation energy were:

P.G.A. $E = 21.0$ k cal/mole $(A=9.34 \times 10^5)$

S.P.l. $E = 19.8$ k cal/mole $(A=3.53 \times 10^5)$

The scatter in experimental data points on the graph is considerable, but it is unlikely that more than a 5% error has occurred in measurement, and extensive statistical treatment upon these points did not yield any additional information. No figure could be deduced for the error in temperature measurement of the specimen, and it is most probable that this was the cause of the majority of the scatter for the kinetic values. The graphs show

that there was no marked change in activation energy over this temperature range, and since the experiments were performed in gas atmospheres that had been purified on different occasions, there has been apparently no significant contamination in the reactant gas.

4. Characteristics of oxidation.

The manner of oxidation was that only exposed edge atoms were removed, thus after a few minutes reaction the bordering atoms lay in $\{10\bar{1}0\}$ planes. This was true for both types of graphite, the only difference being that the length of a particular $(10\bar{1}0)$ plane was much shorter in the case of P.G.A. than for S.P.1. In some cases the length of each particular plane was so short that the borders appeared to have a rounded appearance. Closer examination revealed, however, that within a particular piece of graphite the lengths of each particular plane exposed varied widely and yet there was no observable evidence to suggest why a change in oxidation direction should have taken place. Fig 68b is a typical example of this in that the crystallographic nature of all the exposed planes is consistent but there is wide variation between different points on the same layer as well as between layers. In some cases there is apparent protection by the metal contamination particles, but a similar effect is seen in Fig. 67. It is noticeable that groups of layer planes consisting of approximately 5-20 layers

high behaved as a unit and were oxidised evenly whilst the group of planes above or below would be oxidised in entirely different directions. This produced a serrated edge rather than an even regression. This effect can be seen at the area R in Fig.71 and this difference in oxidation characteristics between groups of layer planes also coincides with the moiré rotation. Moiré fringes arise from one set of layer planes being rotated relative to underlying planes and the diffracted beams produced by these two sets of planes interfere and give rise to the interference pattern. The block of layer planes that is rotated also behaves as a coherent block with regard to oxidation. Extending this data further, the moiré fringes in Fig.67 were all measured and the interplanar rotation calculated.

The calculated angle was plotted against the length of eroded edge that remained in one crystallographic direction (ie. before branching at 120^{o}) for each particular flake of graphite. This graph is shown in Fig.83 and is linear, showing that the cause of changes in oxidation direction was a function of interlayer bonding rather than intra-layer bonding as would be the case if the presence of defects was the reason.

Moiré fringes can be indicative of dislocations though this is not always true as shown previously. However there was no indication that breaks or changes

Fig. 83.

Dependence of length of crystallographic perfection of edge on the relative rotation of the crystal to those above and below it in the layer stack.

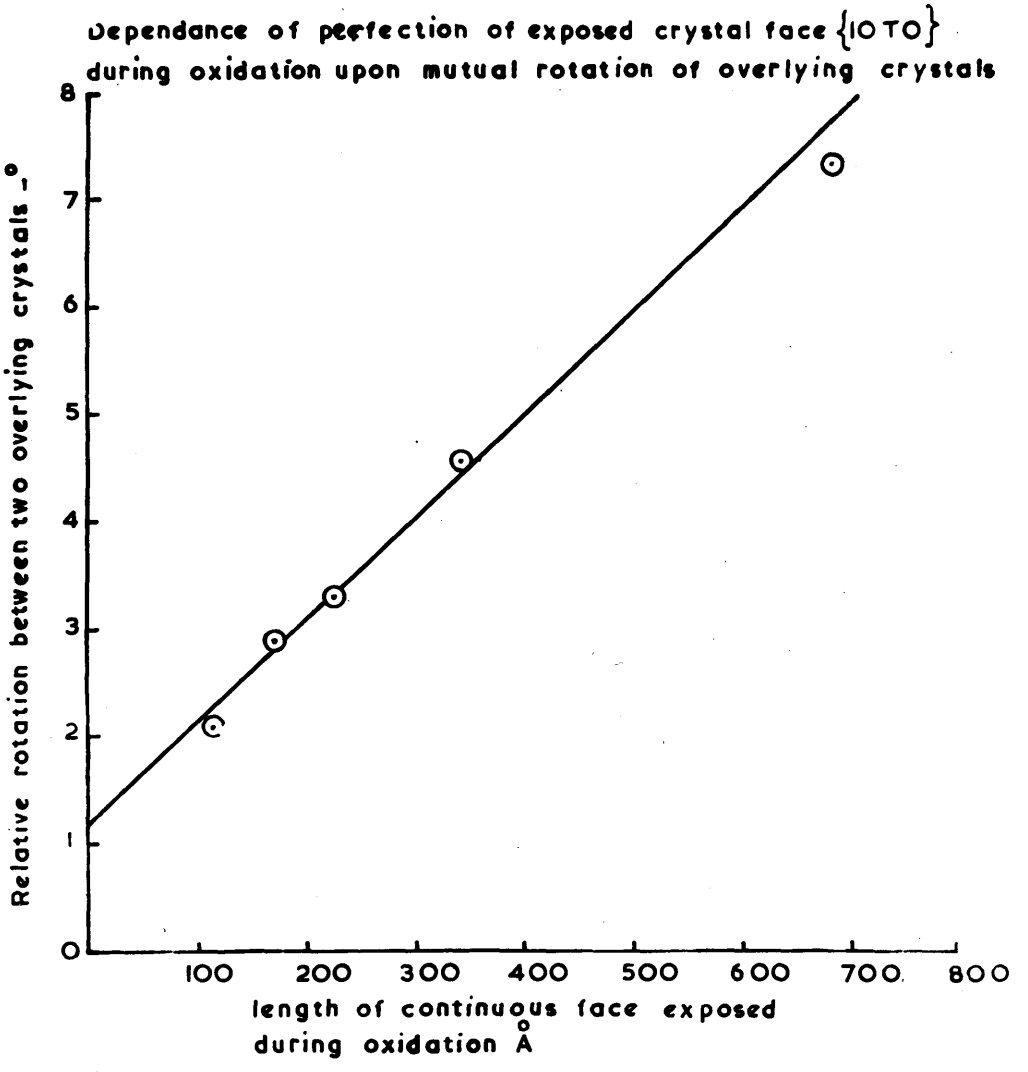
Dependance of perfection of exposed crystal face {10 T0}
during oxidation upon mutual rotation of overlying crystals
Relative rotation between two overlying crystals _°
0
1
2
3
4
5
6
7
8
100
200
300
400
500
600
700
800
length of continuous face exposed
during oxidation Å

in direction of moiré fringes were associated with enhanced oxidation. This would usually have required basal plane pitting to have taken place but no connection between the two phenomena could be established in the few cases when they were both present on a specimen. Other forms of contrast can arise on a specimen as well as moiré interference, and a typical example, Fig.84 shows how S.P.l. graphite has undergone oxidation for 23 minutes at 740°C. There is no evidence that the lines of contrast have any significant effect upon oxidation. These lines arise from buckling and distortion of the lattice which induces strain but not necessarily rupture of C-C bonds.

There were very few cases of basal plane pitting and they were all confined to P.G.A. graphite above 700°C. On only one occasion was extensive pitting observed and this at 745°C so it would appear to be a feature of higher temperature oxidation than was used in this work. This pitting is shown in Fig. 76a and b and there is some evidence that the pits are of a spiral nature. However on another part of the same specimen much less frequent pitting was observed and thus this area may be anomalous. The pits do not appear at all regular though in general the 120° symmetry is observed. Other cases of pitting were confined to badly distorted areas of graphite such as shown in Fig.67 where no accurate interpretation can be made. Beyond the cases cited there was no evidence

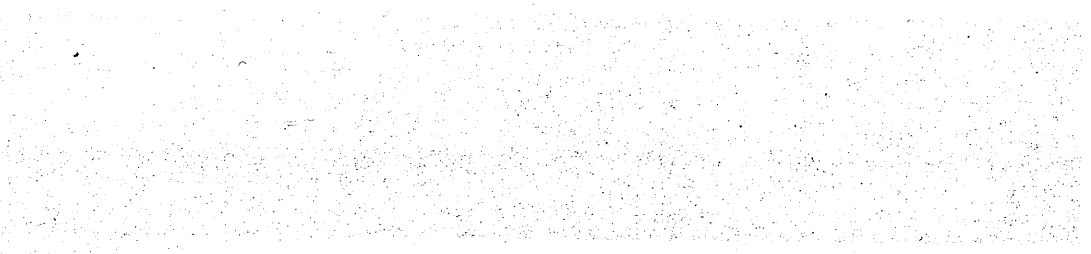

Fig. 84.

S.P.1. graphite after 23 minutes oxidation at 740°C with dry air inside the electron microscope.

Magnification 160,000X.

for basal plane attack, and in many cases where a sheet of graphite was folded over as in Fig. 84 or 77, the basal edge which is visible at the fold shows no erosion. In contrast to this it is seen in many cases that the uppermost layer of a graphite flake regress faster than those below it, but this may be due to other factors.

The rotation effect observable by moire fringes do not necessarily indicate that the rotation itself is responsible for the edge perfection, but may be representative of the energy of the twist boundary.

Effect of Silica Support Films.

These support films were composed of a silicon monoxide/dioxide mixture which was evaporated under vacuo: it could not be regarded as pure silica. It was unexpected that significant diffusion into the graphite occurred in the temperature range employed. P.G.A. graphite was more susceptible to this diffusion than S.P.1. graphite for after 1 hour of reaction at 535°C holes appeared in the support film adjacent to the graphite. It was clear that this diffusion only occurred along the graphite edges as is shown in Fig.70,1. which was representative of several instances, and it was a slow process that was noticeable only after considerable reaction time. When marked silica diffusion had taken place as occurred in the experiments performed at 900°C there was a marked change in the appearance of the graphite. It developed a very rough appearance and the edges became diffuse as oxidation proceeded, but no crystallographic directions were established. Holes also appeared in the graphite but again the edges were ill defined and circular in shape. A series is shown in Fig.85a-d with P.G.A. graphite reacted at 900°C. At one point regular crystallographic edges can be seen developing on the upper surface of the crystal, but in later micrographs these have disappeared into the ill defined mass which the graphite became. Kinetic measurements were not possible on these samples - both S.P.1.

and P.G.A. showed similar effects - but it was clear that at this temperature silica diffusion was more significant than air oxidation. These specimens were degassed at 900°C in vacuo for 1 hour prior to reaction and it was probably during this period that some of the diffusion occurred. However, on admitting air, the graphite very rapidly lost its regular structure with both the edges and basal plane being unevenly eroded. There was no evidence from electron diffraction data of compound formation between the silica and the graphite.

In addition to suppressing the uncatalysed oxidation, the silica appeared to stop any catalysed oxidation by the platinum particles from the mount and the furnace. There was no sign of channelling, but this inhibition may have been due to the formation of a platinum silicate or silicide rather than inhibition of the graphite. Again there was no electron diffraction evidence for this but the contamination masses visible in Fig.85c were unlike those found at lower temperatures as for example in Fig. 71. The destruction of the regular crystallographic mode of oxidation by silica diffusion, shows that at a lower temperature, where crystallographic definition was good, then the effect of silica was not significant unless the area under study was immediately adjacent to the point of diffusion.

Fig.85a.

P.G.A. graphite prior to reaction, and after degassing at 900°C for 1 hour.

Magnification 120,000X.

Fig.85b

P.G.A. graphite after 13 minutes reaction with dry air at 900°C inside the electron microscope.

Magnification 120,000X.

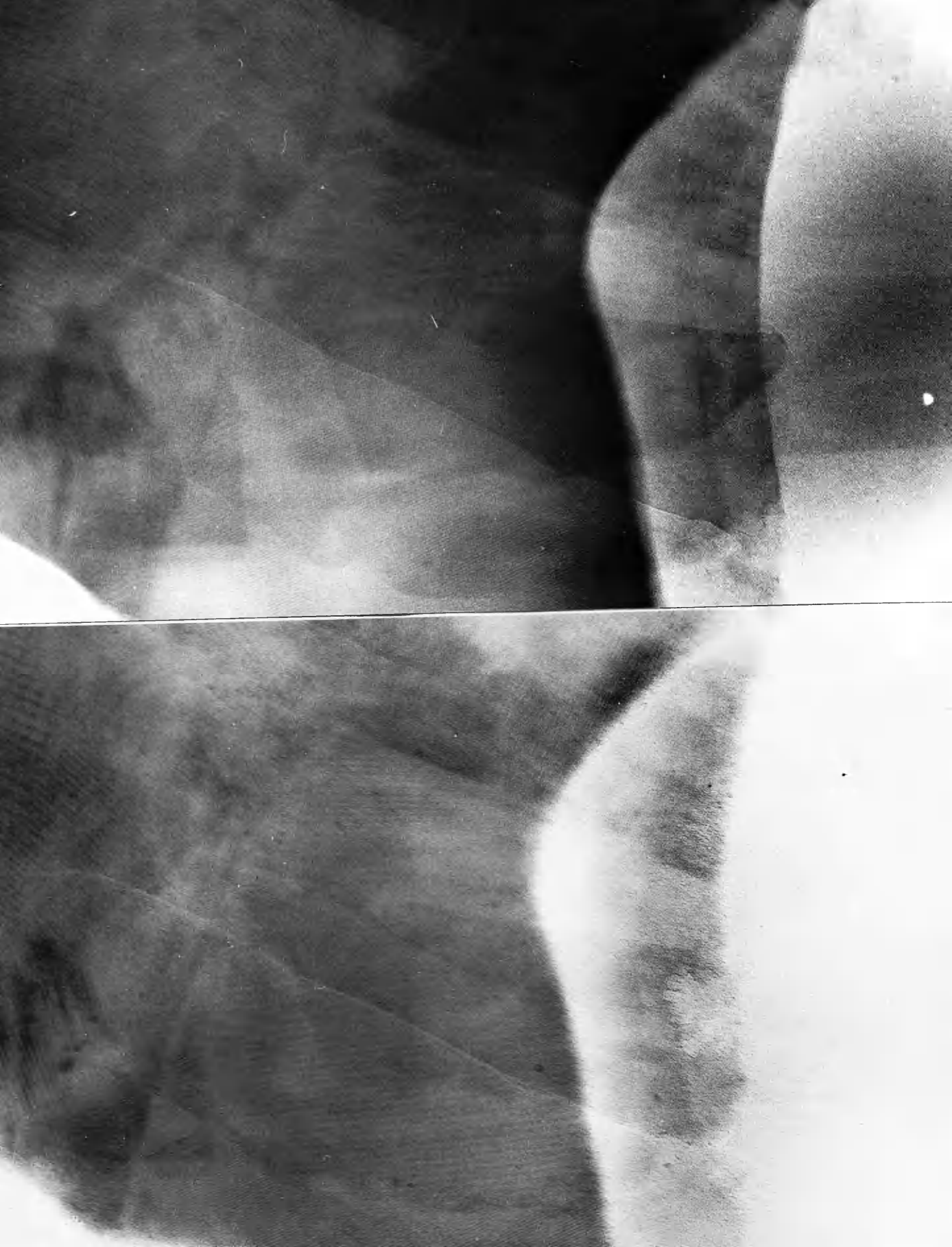

Fig. 85c.

P.G.A. graphite after 20 minutes reaction with dry air at 900°C inside the electron microscope.

Magnification 120,000X.

Fig. 85d.

P.G.A. graphite after 31 minutes reaction with dry air at 900°C inside the electron microscope.

Magnification 120,000X.

D I S C U S S I O N.

Contents

Graphite Morphology

1. High Resolution Studies.

The structure of the supporting film was easily explicable in terms of small, randomly orientated crystallites, but there was no known apparent structural reason why graphite should have appeared to have a granular texture. The granules were approximately 5Å in diameter. The resolution limit of the electron microscope is most simply described in terms of an object that will be imaged as an Airy disk whose diameter can be described as

$$\delta = \lambda \frac{0.61}{\beta_{obj}}$$

where β_{obj} is the half angle of the objective lens aperture. However to reconstruct molecular configuration the objective lens must process the scattered amplitudes and phases out to wide angles without distortion. Lens aberrations and lens current instabilities etc. will all act to distort the phases at the image planes and thus limit the ability to reconstruct an image of molecular detail.

The resolving ability of the electron microscope is meaningless unless the image of size δ can produce sufficient contrast to be visible in the image plane. Therefore the high resolution micrographs cannot be

interpreted unless the contrast of the detail shown by them can be explained.

Contrast is produced by both diffraction contrast and phase contrast. The former has been quantitatively interpreted by Whelan (1958) and is applicable mainly to object detail exceeding 10-15$\mathring{A}$ in size, but phase contrast has not yet been defined to such a rigorous extent. Considering elastically scattered electrons the total elastic scattering cross section Q_{el} can be described by:-

$$Q_{el} = \int_{\alpha=0}^{2\pi}\int_{\beta=0}^{\pi} |\psi_g|^2 \sin\beta \, d\beta \, d\alpha$$

$$= \int_{\alpha=0}^{2\pi}\int_{\beta=0}^{\beta_{obj}} |\psi_g|^2 \sin\beta \, d\beta \, d\alpha + \int_{\alpha=0}^{2\pi}\int_{\beta=\beta_{obj}}^{\pi} |\psi_g|^2 \sin\beta \cdot d\beta \, d\alpha$$

This is derived from the kinematic scattering theory enumerated by Whelan, where ψ_g is the amplitude of the scattered wave (thus $|\psi_g|^2$ is the appropriate intensity distribution) and α the angle variable about the optic axis.

In the second equation the first term relates to the portion of the diffraction pattern falling within the objective aperture and the second term describes that portion of the scattered electrons falling outside the objective aperture. Diffraction contrast is described by this second term since the contrast is produced by

subtraction of the scattered electrons from the transmitted beam; these scattered electrons being cut off by the objective aperture. Phase contrast is described by the first term since it is a recombination of the elastically scattered beam of amplitude D with the transmitted beam of amplitude T. The phase of the scattered beam relative to the transmitted beam is $\left(\frac{\pi}{2} + \chi\right)$, thus the combined wave function at the image plane ψ is:-

$$\psi = T + i\,De^{i\chi}$$

and the intensity $|\psi|^2 = 1 - 2TD\ \mathrm{Sin}\,\chi$

and maximum contrast $G_{max} = 4TD$ if $\mathrm{Sin}\,\chi = 1$

but it is clear that the interpretation of phase contrast is dependent upon the interpretation of the phase difference χ .

Since the focus of the instrument cannot be infinitely varied and specimens - even atom points - have a three dimensional character, this must be taken into account by consideration of the Fresnel transform which is the vertical phase summation in the object. This is analogous to the structure factor in X-ray crystallography. Thus this factor together with χ must be known for a detailed interpretation of phase contrast, and for two image points the contrast G_{12}:

$$G_{12} = \frac{4\pi}{\lambda}\int_0^{\beta_{obj}} (F_1 - F_2)\,\mathrm{Sin}\,\chi\,\beta\,.\,d\beta$$

where $F_1 - F_2$ is the difference between the two real

parts of the Fresnel transforms for the two atoms.

The Fresnel transform, however, cannot be obtained without knowledge of $\sin \chi$ and at present this cannot be quantitatively determined.

From both the dynamical and kinematical derivations for the intensity of the scattered wave

$$\chi = \frac{|K|}{2} \Delta l_o \beta^2 - \frac{|K|}{4} C_o \beta^4 + \chi_{ab} + \chi_t$$

where $|K|$ is wave vector of the scattered beam

Δl_o the defocus value

C_o the spherical aberration coefficient.

χ_{ab} describes the astigmatic phase contribution which can be minimized experimentally.

χ_t describes the effect of lens instabilities and stray magnetic fields.

Determination of the values in this equation has been carried out by Heidenreich (1967) and Thon (1966) and a reasonable agreement between experimental and theoretical results were obtained. The determination of the transform showed that important information could be obtained from the image.

The image point intensity distribution is thus a phase map in which points of equal intensity are points of equivalent phase amplitude and interpretation of the high resolution micrographs is not valid unless this factor is taken into account. The variation of χ with

Δlo explains why a true equivalence cannot be made for micrographs taken under different focus conditions, and whilst there are some points marked on the micrographs, their agreement in subsequent micrographs is purely fortuitous (Figs.23,24,25 and 26).

The algebraic expressions shown, reasonably described the contrast of the images obtained at high resolution and the granular appearance is understandable. The more fundamental problem was what did this appearance represent in structural terms? A random contrast within the specimen could have arisen from defects or parts of the specimen lying in a different plane from the rest, but in this work and in that of Heidenreich the fundamental unit was 5Å: this is not a crystallographic unit expected by consideration of the lattice. It could be suggested that the graphite structure is not composed of completely planar layers of carbon atoms, but that the layers are slightly puckered as shown in Fig.86, the central atom of the approximately 5Å cell being out of plane with the other atoms in the large hexagon. This would divide the lattice plane into units of approximately 5Å rather than 2.46Å units expected from the perfectly planar structure, the central atoms of the 5Å cells being superimposed throughout the layer structure whilst the carbon bonded structure retained its abab....stacking sequence. For this structure to have produced the phase contrast seen in the micrographs

Fig. 86.

Division of graphite lattice into units of 4.92Å inclined at a slight angle to each other.

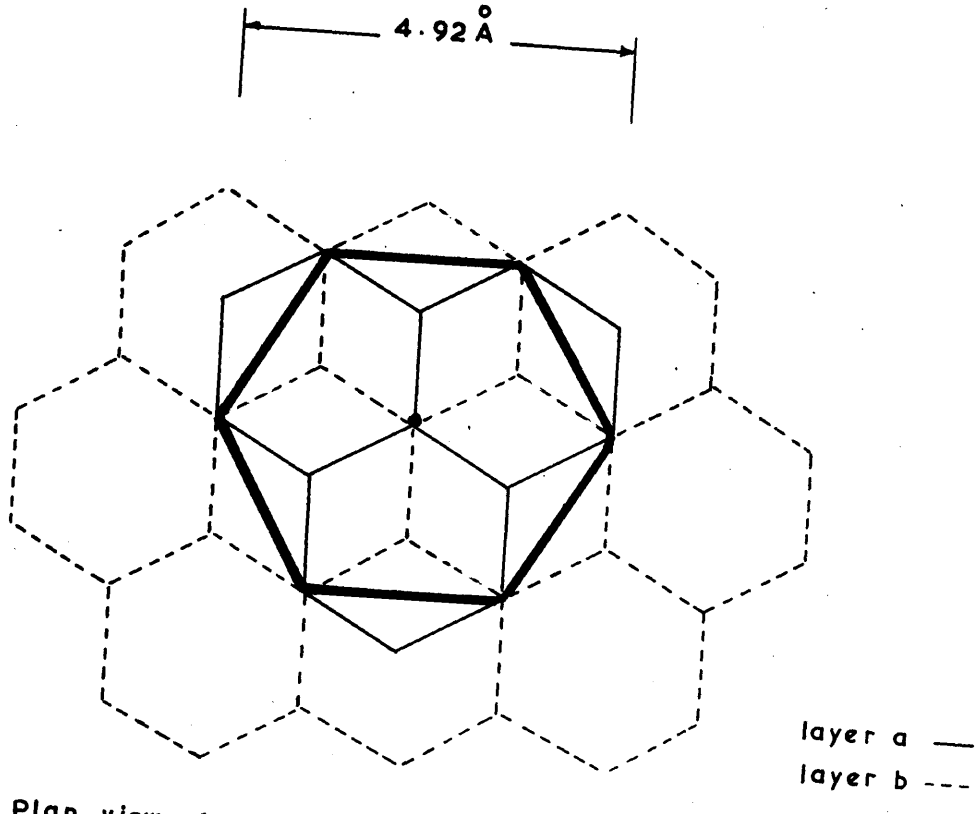

Plan view of graphite lattice showing 4.92 Å cell.

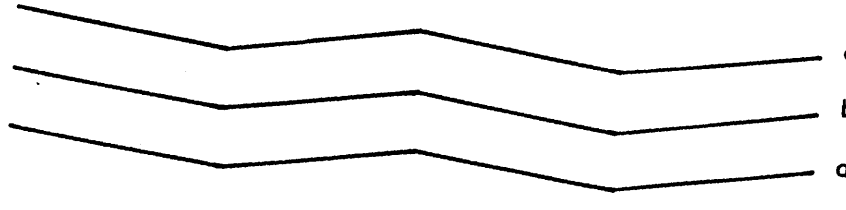

Side view of graphite lattice showing 4.92 Å puckering

the puckering could be as small as 0.02Å. There is also circumstantial evidence for puckering from the X-ray crystallographic studies of Hassel and Mark (1924) and Tsuzuku (1953), whilst Lukesh (1950) observed bond distortion of up to 40' by a similar technique. Conversion of a structure with hexagonal stacking sequence to one of rhombohedral stacking requires a considerable amount of energy, eg. severe mechanical deformation (Bacon 1950), but this change can be achieved chemically by treatment with agents that expand the interlayer spacing and then decompose. Strong acids and $FeCl_3$ are agents of this type (Laidler and Taylor 1940), yet if the graphite networks were perfectly planar it would be unlikely that the layers would have to be expanded to the extent of 5-8Å, as occurs in these treatments, for slip to occur. The expanded lattices of turbostratic carbons represent further evidence for the wide interlayer spacing necessary for free rotation. The puckering would have two effects upon the interlayer bonding: firstly, to prevent rotation and slip by the physical presence of the three dimensional layer character and, secondly, to aid this locking by focussing electrostatic charge at the points of the apexes of the puckers, which would enhance the strength of the interlayer electrostatic attraction.

Electronically slight puckering would not be inadmissable, since the C - C bond length within the layers

is greater than that of benzene, and thus the same degree of planarity would not be expected.

Further considerations of electron scattering theory would tend to discount the puckered lattice hypothesis, because the scattering is dependent upon the wave vector normal to the electron beam. Since this is very small, a much larger amount of puckering, eg. 0.5Å, would be necessary to produce the effect in the micrographs. Such a degree of puckering would be easily observed by X-ray diffraction, and this has not proved to be so.

A further factor to be considered in discussing puckering lies in the fact that the 5Å unit would produce a much larger unit cell size which should be observable by electron diffraction in a form analogous to a super-lattice. No such extra reflections have been observed.

Therefore, it is unlikely that a regular disturbance of the lattice , in the manner suggested, does exist and thus the grain structure remains an enigma. However, these high resolution micrographs do show that graphite is not entirely the simple hexagonal structure that is suggested from X-ray diffraction evidence.

It is probable that this question will not be resolved until higher resolution microscopes are developed. At present the observation of such structures is at the limit of the electron microscope's resolving power.

The other feature of the high resolution studies was that visible pores did not occur through the graphite layers and thus pores about 10-20Å in diameter would only occur at grain boundaries or between the graphite layers. The latter may occur when two layers are rotated relative to each other and the effect of puckering would enhance the open pore volume. The association of rotation and gas accessibility was shown in the uncatalysed oxidation studies where the erosion removed a rotated plane, and the greater the rotation the more the rotated layers behaved as a separate, perfect crystal (Fig. 83).

2. Moiré fringes

These were very common in the specimens investigated and often were continuous over a large area of the graphite flakes. A conservative estimate of non-basal defect concentration in S.P.1 graphite is 10^4 defects/cm^2 (Thomas 1968), so if a random distribution is assumed, a defect should be encountered at 100μ intervals. In the specimens shown in Figs. 27 and 28 there were no discontinuities but Fig.29 was more typical in that there were some discontinuities present, and in a far greater concentration than 1 defect/$10^4\mu^2$. There is no reason to doubt a random defect distribution and this it is probable that

the moiré patterns show more than solely non-basal defects. Basal defects would not be imaged by moiré patterns and thus the layer planes are probably buckled, thereby altering their Bragg reflection angles. This would support the puckered layer theory described previously since a moiré pattern can only arise from slightly rotated crystal (in the case of graphite) and puckering would cause severe out of plane buckling as the layers moved relative to each other. Thus the high defect concentration suggested by the moiré fringes would be largely an artefact.

3. Heavy metal shadowing.

Again the non-regularity of graphite crystals was displayed. The evidence that a large number of graphite flakes were not in the plane of the support film showed that the grain boundary between flakes was of fairly high energy and that interaction occurred across the grain boundary. The interlayer bonding must be sufficiently rigid to have prevented adjustment of the layers to bring all the flakes having basal planes parallel to the support film.

It is of interest that the layer planes appeared to terminate on vertical edges exceeding 20Å in height and that non vertical edges composed of single atom layers were not observed. From the moiré rotation and shadowing experiments it appears feasible to treat a stack of graphite planes approximately 100Å high as three or less

crystal entities rather than to visualise them as being composed of individual atom layers.

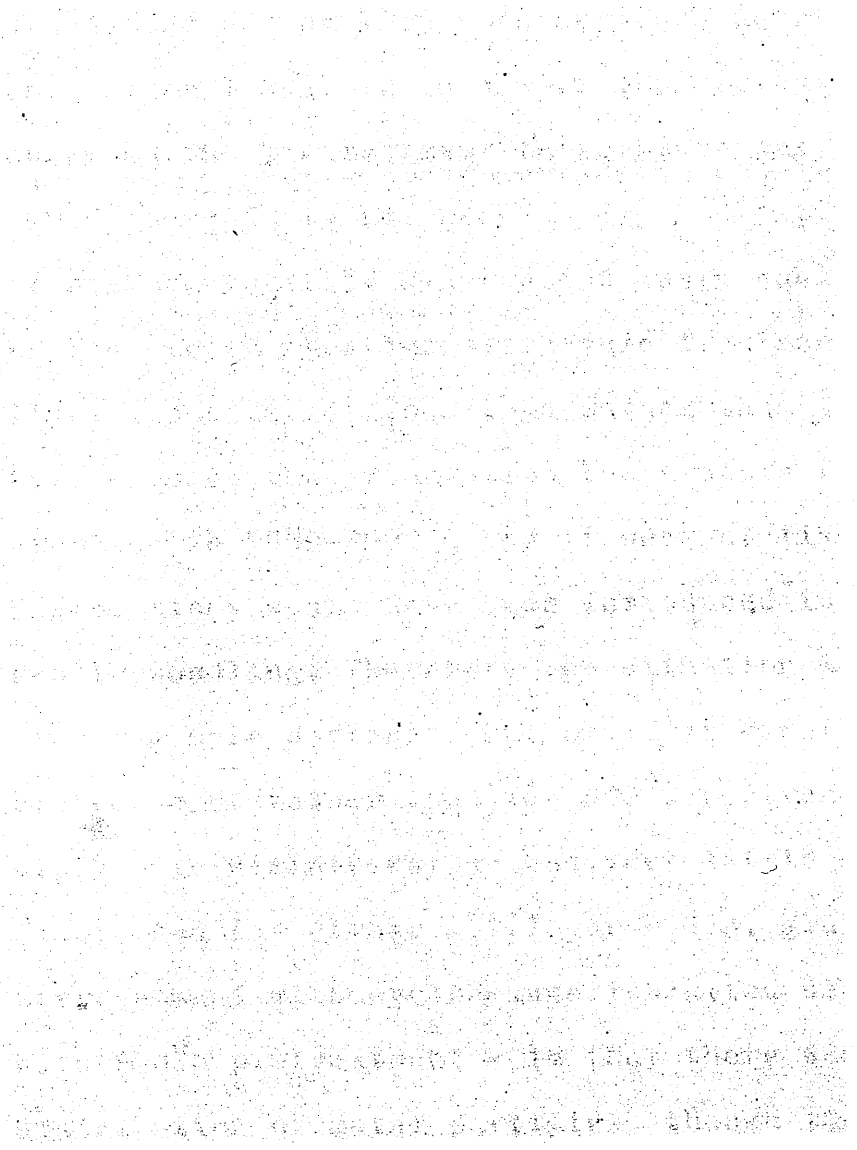

Decoration

This phenomenon has not been completely explained and some of the different theories to account for it have been described already. With respect to mechanism, the most salient point of previous work has been the dependence of mobility upon surrounding atmosphere (Thomas and Walker 1964). In this work the decrease in decoration count as the pretreatment temperature was increased from 600°C to 900°C is not necessarily indicative of annealing of dislocations. If dislocations were easily mobile and of low energy then the ultrasonic treatment would have been likely to cause dislocations rather than the converse. Furthermore, the preparation temperature for synthetic graphite is 2800-3000°C and it was not likely that many dislocations would have been introduced in the subsequent gentle handling. Therefore the situation was that decoration was more distinct, but of lower count, for the 900°C pretreatment rather than the 600°C pretreatment, and ultrasonic disintegration had very little effect upon decoration for either S.P.1. or P.G.A. graphites. Also pretreatment with cyclohexane inhibited decoration - even with 900°C pretreatment - in that there was a random distribution of metal particles, though the total number of metal particles present on the surface was greater. This inhibition was shown by chlorobenzene, acetone, nitrobenzene and tetrachloroethylene, but not by benzene

(Baird, Fryer and Walker 1969). The third piece of relevant information is contained in the work of Brownlee, Fryer and Webb (1969) who showed that the hydrogenation of olefins catalysed by palladium proceeds at a greater rate over a palladium decorated graphite catalyst than over a randomly dispersed palladium/graphite catalyst. From this it can be inferred that there is some electronic interaction between the support and the palladium to favour the formation of the π transition complex that is involved in this reaction. However, the dependence of decoration upon atmosphere, together with the effects of solvents, shows that direct metal/graphite interaction does not take place, and thus electron transfer between palladium and graphite must proceed via chemisorbed species. Therefore the mechanism for decoration postulated is that decoration only takes place on chemisorbed species on graphite, but the concentration of these species will depend upon their nature. Thus surface oxides from air or water only occur in the vicinity of defects or at exposed edge atoms. This is not necessarily true for cyclohexane - with its high peroxide impurities - or the other organic solvents mentioned, Particularly in view of the ordered adsorption observed by Lander and Morrison. In these cases it would be reasonable to obtain different decoration by the silver, both in distribution and density.

The higher temperature of pretreatment would have

desorbed chemisorbed species and therefore a lower decoration count would be expected, also a more distinct decoration would be given, as was the situation. A detail of the studies of Thomas and Walker was their remark upon the effect of oxidising atmospheres. Where the temperature is sufficiently high to cause reaction with the graphite, an entirely different mechanism would predominate, as will be discussed later.

Applying the theory to Thomas's and Hennig's work using etch decoration, they conclusively showed that monomolecular steps were decorated. Thus for decoration on chemisorbed species to have occurred the species were either attached to a single carbon atom (or molybdenum in Thomas's work) or attached to several atoms within the same layer. There could be no interlayer bridging by chemisorbed species. Thus the various planar surface oxides proposed by Hennig are in agreement with this theory. Considerable controversy has arisen about the possibility of a monomolecular film of metal being present, together with an island structure of metal particles. Sumner (1966) showed that for platinum evaporated on to alkali halides at 200^{o}C, there was a definite inter island film formed. This film was not visible in the electron microscope but did not arise from hydrocarbon impurities in the vacuum system since sputter ion pumps were used. The presence of a film of this nature would

explain the mobility of metal particles since the surface energy difference between the particles and the film would probably be sufficient to account for movement at elevated temperatures.

Thus it is believed that decoration occurs on chemisorbed species which may, but not necessarily, occur at a defect. For graphite it is reasonable to assume that decoration on the basal plane is associated with non-basal defects since chemisorption is not thought to take place on a perfect basal plane. However chemisorption on the prismatic planes could occur irrespective of emergent dislocations. Thereis not thought to be any direct correlation between the absolute defect concentration and the decoration count, but for specimens of similar past history their relative decoration counts are probably indicative of their relative defect concentration, particularly for non-basal defects in graphite.

Validity of the decoration method

It is assumed that the decoration count is proportional to the amount of silver deposited on the graphite surface. This assumption has not previously been questioned (Adamson 1966), but it was noticeable that when few defects were present then the silver tended to aggregate in larger droplets than when concentrated on an edge which has a high concentration of sites for nucleation. Therefore the particle count was dependent upon the number of available sites.

The aggregation of the silver would also be very susceptible to the temperature, since activation energy for aggregation would have to be overcome when two large droplets coalesced. Thus there are three variables that must be considered when this decoration technique is applied; the amount of silver, the defect concentration, and the substrate temperature.

The amount of silver can be largely discounted since the background count would tend to normalise the results. This does, however, assume the mechanism for nucleation on the background is similar to that on the graphite. The defect concentration should not - in these experiments - present a serious difficulty because of the very slight changes in defect concentration that were encountered. The temperature is a more difficult parameter to assess, because it was also dependent upon the thermal conductivity

between the graphite and the heating element via the support film and specimen mount. No reliable estimation of temperature variations could be determined.

The final critical parameter concerns the statistical validity of the results. The standard deviation was very large in the results presented but, because of the limitations of specimen size, a large number of particle counts were not possible. However, in spite of the previous assumptions, these results can be concluded as representing a trend, but should not be regarded as precise values.

Catalytic Oxidation.

The rapid onset of platinum catalysed oxidation at approximately 800°C agreed with the studies of Heintz and Parker (1966) who reported an activation energy of 84 kcal/mole for this reaction. Hedley and Presland (1963) also studied this reaction and reported a high mobility of platinum on a single crystal graphite surface which would account for a high pre-exponential factor in the Arrhenius equation, and thus explain the catalytic properties. The channels formed in the present studies were found to be aligned with $\{10\bar{1}0\}$ planes similar to those involved in uncatalysed oxidation, and probably the chemisorbed species taking part in each case was the same.

Palladium, however, showed very much more dramatic characteristics. At 300-400°C nucleation occurred suddenly as did reaction at 500°C. These sudden changes in behaviour were indicative of a high activation energy for each process, the controlling factor being a steric one. From the distortion of the lattice it appeared probable that intercalation occurred and this has recently been proved (Baird, Fryer and Goldie 1969) with a definite compound being formed. It had also been shown that carbon was not significantly soluble in palladium (Raub and Falkenburg 1964), though palladium and other transition metals will 'wet' a graphite surface (Naidich and Kolesnichenko 1961). The following reaction mechanism is believed to have

occurred:-

Initially the temperature was raised so that decoration took place on chemisorbed species (ie. surface oxides) at non-basal defects on the graphite surface. Above this temperature the palladium atoms in the particle were mobile and no rigid bonding could take place with the chemisorbed species. Extensive formation and destruction of bonding then occurred as the palladium removed chemisorbed species from the exposed graphite edge atoms, desorbing CO and CO_2 in the process. As edge atoms were removed in this manner the energy given off in the exothermic reaction was sufficient for palladium carbon intercalation to occur which resulted in distortion of the lattice. Thus the layer planes were further separated, there was easier access for reactant gas and the process continued. However, by this stage the palladium would have gained enough energy for fusion, and with the gaseous products of reaction being emitted in all directions so that the particle was insulated from the surface by a gas layer; the particle thus became mobile. The intercalation reaction acted as a force for movement, and the destruction of surface oxides provided energy for reaction. The reaction only ceased when the intercalation reaction could not occur, because of defect structure or grain boundaries in the graphite. It was observed that when the reacting particle approached the edge of a graphite flake, it

changed direction so that the movement of the particle was always facing unreacted graphite.

Summarizing this:

1. $Pd + C_g\text{-}C(O) \rightarrow Pd(O)C\text{-}C_g$ decoration
2. $Pd(O)C\text{-}C_g \rightarrow Pd + C_g + CO$ destruction of surface oxide
3. $C_g\text{-}2C + O_2 \rightarrow C\text{-}2C(O)$ formation of surface oxide
4. $Pd(O)C\text{-}C_g \rightarrow Pd(C_g) + CO$ mobility and intercalation

This sequence assumes that CO is the reaction product, $C_g\text{-}C(O)$ refers to surface oxide bonded to graphitic carbon. $Pd(O)C\text{-}C_g$ is a palladium-oxygen-carbon bridge compound joined to graphitic carbon. This reaction scheme is obviously much simplified since CO can be produced in various ways depending upon nature of oxygen attack, and also CO_2 may be produced either directly or by the $CO \longleftrightarrow CO_2$ exchange reaction. However, provided the temperature is sufficiently high for reaction 2 to proceed, then reaction 4 will eventually take place which in turn will enhance reaction 3 by separating the carbon layer planes. Reactions 3 and 4 are known to take place, reaction 1 has previously been discussed, and reaction 2 is not unreasonable, but is probably responsible for the high activation energy.

There did not appear to be any loss of palladium from a particle whilst mobile, thus $Pd(C_g)$ was consumed in reaction. A possible reason why this reaction was

confined to only a few particles is that reaction at monomolecular steps would not provide sufficient energy for the sequence to be carried out.

There was also some evidence that the diffusion of silica from the support film was favoured by this reaction. The separation of the atomic planes on intercalation would account for this.

This mechanism is not dissimilar to that proposed by Long and Sykes (1948 and 1950) and Heintz and Parker (1966) except that they favour an electron interchange directly between the metal and the graphite with an intermediate compound π-bonded as in metallocenes. The oxygen they envisage as being present is a $\equiv$C-M-O type structure rearranging on desorbtion to release CO. The π-bonded structure is very likely for palladium since it favours the formation of this type of bond in olefine hydrogenation catalysis, and would correspond to the intercalated compound mentioned above. Heintz and Parker (1966) came to the conclusion that the most important feature in catalysts for graphite oxidation was the volatility of the metal oxide. This would support a C-O-M type structure rather than a C-M-O type. The relationship between the complex mentioned above and the π-bonded intercalation compound is not clear at the present time, but it is suggested that the separation of the layers during intercalation is necessary for sufficient active surface to be presented to the palladium to produce the energy for mobility and fusion.

1. Orientation.

The outstanding preference for exposure of $\{10\bar{1}0\}$ atomic planes was a feature not expected in the light of work performed elsewhere. The most significant study of orientation effect between prismatic planes was that of Hughes and Thomas (1965) who found from the orientation of basal plane pits, that the $\{10\bar{1}0\}$ planes were slightly more reactive than the $\{11\bar{2}0\}$ planes. Their work was performed at a higher temperature than that in the present study, and it was possible that the nature of the defect initiating the basal plane pit had a significant role in the manner of oxidation.

Fig. 87 shows four possible configurations of surface oxides, the first three of which were described by Hennig, who did not consider oxide C in detail since he did not find $\{10\bar{1}0\}$ edges in his reactions. However there is no fundamental difference between oxides A and C with regard to reactivity of individual carbon atoms. Thus if these predominated on the graphite surface then it is difficult to understand a difference in reaction rates for different planes. Considering oxide B in terms of atomic radii the separation of the two bonding carbon atoms is 2.84Å, and assuming C-O single bonds with a bond angle subtended by the oxygen of 111° then the spread of this oxide is 2.4Å.

To accommodate this, considerable strain must be induced into the system, however since it is known that peripheral carbon atoms are in a distorted environment, this argument is not conclusive. The corresponding calculation for oxide D gives a C separation of 2.46Å which is much nearer the span of the oxide species. Therefore if oxide D is sterically favourable then it is expected that the $\{10\bar{1}0\}$ planes are most reactive.

Previously a puckered structure for graphite was described, and it is noticeable from this structure that the 4.92 cell has its edges bounded by $\{10\bar{1}0\}$ planes. Thus adjacent atoms in any one layer comprising the $\{10\bar{1}0\}$ planes will be at the same level parallel to the basal plane, whilst the atoms comprising the $\{11\bar{2}0\}$ planes will not be level with their neighbours. This non planarity could give rise to steric hindrance between oxides of type B in adjacent layers, whereas this would not be the case for type D oxides. Therefore it is believed that the type D oxide predominates on the surface because it is sterically favoured and this is in agreement with the oxidation characteristics found.

Significant erosion along other atomic planes was not observed. In particular basal plane attack was not widespread, in agreement with previous studies in this temperature range.

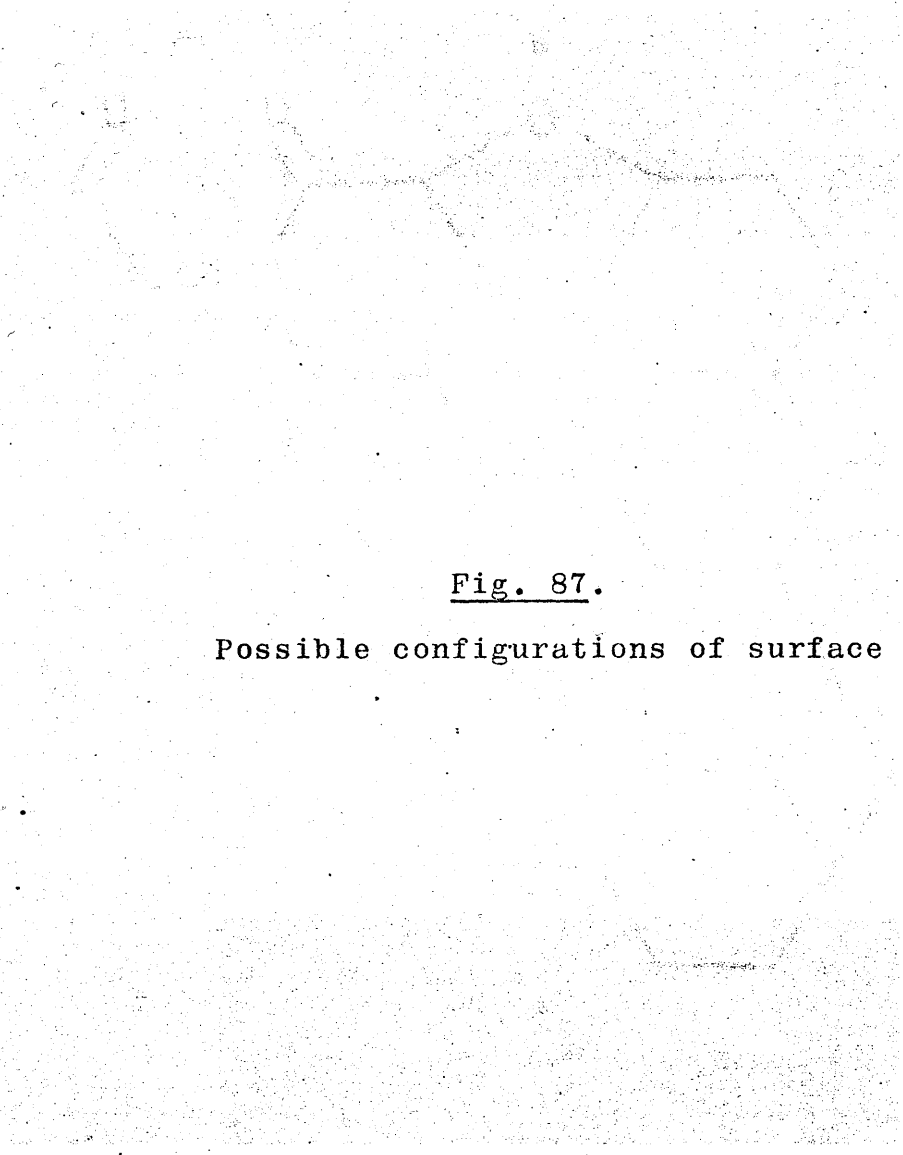

Fig. 87.

Possible configurations of surface oxide.

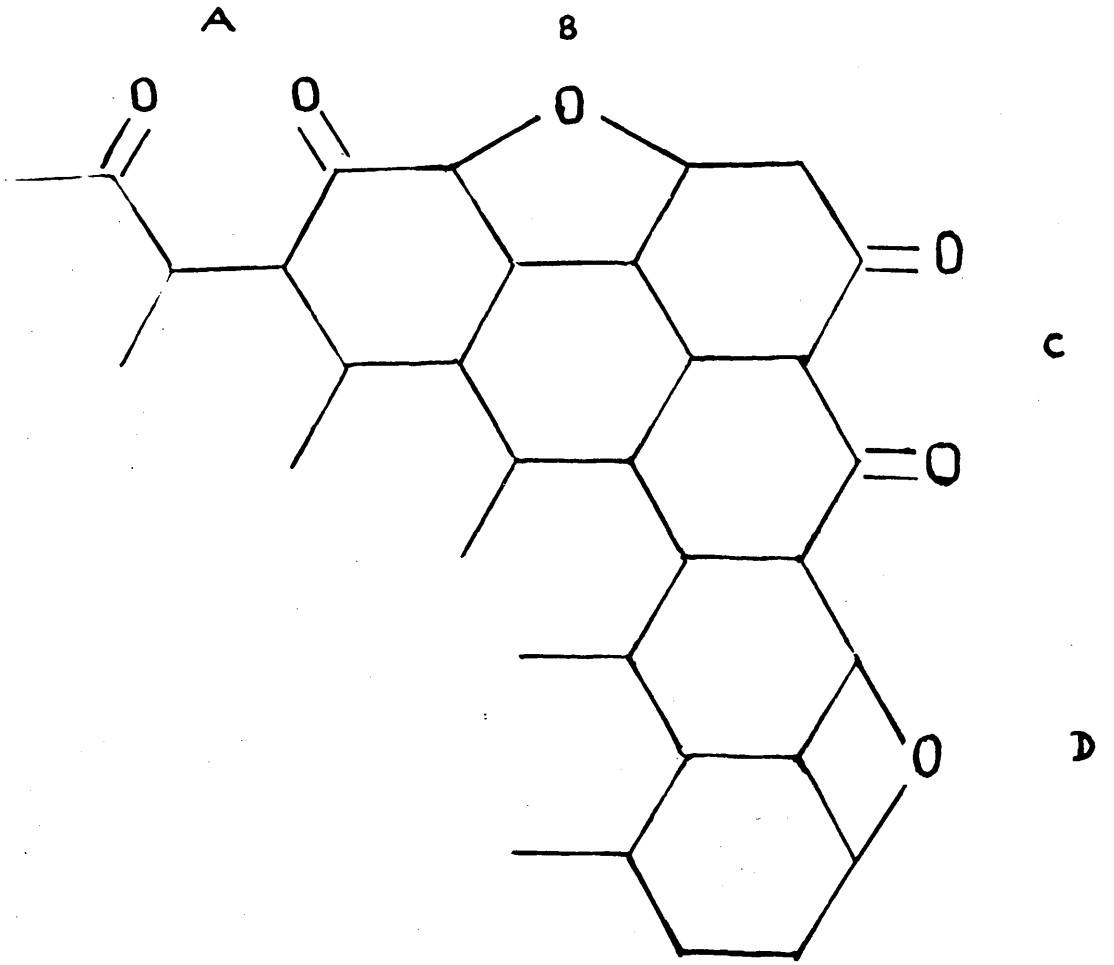
A
B
C
D
O
O
O
O
O
O

2. Kinetic studies.

In the majority of experiments the extrapolation of the linear rate graph passed through the origin showing that there was no significant induction period. Therefore the reactant surface oxides were either formed very rapidly or were not removed during the degassing period. No correlation with temperature could be made for those rate graphs that did not pass through the origin. This result agreed with the findings of other workers (Bonnetain 1959), that below 950°C the surface oxides involved in combustion were not easily desorbed and the effect of a 1 hour degassing below this temperature would be negligible. However, physisorbed oxygen and other impurities would have been removed during this 1 hour treatment.

Since the methods of estimation of the amount of graphite removed in this work were not well established, it was necessary to consider the validity of the methods. The major assumption was that basal plane attack was negligible compared to edge attack. If this was not the case then vertical edges would not have been formed, but all the erosion was manifest in vertical edges. Where pitting had taken place then great care was exercised in measurement. For example if erosion had proceeded along the line of a screw dislocation, then whilst it would have been reasonable to measure pit expansion in terms of the

edges exposed at the top of the pit, edges exposed lower down would have been in a helical configuration rather than circular, thus making precise measurement difficult. The overall accuracy of the method for each individual point on the kinetic graph was probably not more than 5% since there were inaccuracies associated with the magnification calibration in the microscope, distortion of photographic paper during printing, inaccuracies in tracing, and edge measurement. These were experimental errors, but a much more important error was choice of a reaction area as being representative of a particular lattice face of a graphite crystal. This question will be dealt with in greater detail later, but it must be emphasised that the value in this technique lay in its ability to show relative differences in reactivity of different faces of the graphite lattice, rather than to give very accurate absolute values of reaction rates or activation energies.

A further advantage of this method of study was that the internal reaction of the graphite was not measured, and any effects of diffusion within the graphite crystal were unimportant. These various features meant that the results obtained for kinetic data would not necessarily agree with other methods of measurement, as these have estimated carbon removal from a bulk mass of graphite, whereas this method is concerned only with the most reactive crystal planes.

It was believed, however, that the difference between the values of activation energies found in this work and those found by other methods, was not due solely to methods of measurement, but also to the effect of impurities - notably silica.

It was clear that the silica or silicon monoxide from the support film diffused much more readily at higher temperatures, and its inhibitory effect of physically protecting the surface would lower the rates of reaction measured at these higher temperatures. Thus the slope of the activation energy graph would have been diminished and the activation energy correspondingly smaller as was found in practice. Unfortunately the scatter of points on the activation energy graphs was too great to estimate whether these graphs were truly linear or curved. The latter would have been expected if the silica only protected the graphite by means of compound formation with the graphite, since a specific activation energy and temperature would have been required for compound formation. However any curvature that was present was not very great and it would appear likely that this inhibition occurred solely by physical diffusion of the silica or silicon monoxide.

The difference in activation energies between the S.P.1. and P.G.A. graphites was within the experimental error of the method. However since crystallite size of

the S.P.1. was several times greater than that of P.G.A. this difference in size did not play any significant role in their activation energies though it may have accounted for the different values of A in the Arrhenius equation.

A considerable amount of work has been done in elucidating the order of the reaction of graphite with air and oxygen. In this study there was no direct attempt to measure the order of reaction, mainly because the gas pressure over the specimen could not be measured. The linearity of the kinetic data and also the probable pressure range suggests that the reaction order in this work is approaching zero and that the system is probably comparable with that of Blyholder and Eyring (1957)

3. Characteristics of oxidation.

The most noticeable feature of the oxidised graphite was uneven regression of eroded edges. The oxidation obviously commenced at unique points on the graphite edge and these developed into the 120^{0} serrations along the flake. In some cases the particles of metal contaminant around the edge have caused this effect but in others no obvious reason was apparent. It is most probable that these sites of initial attack were slightly more favourable than the surrounding area and might well have been positions of emergent basal dislocations. However, from the fairly even size distribution of eroded areas, the favourability of these sites was very small, and probably

impurity atoms or other minor inhomogeneities would have functioned in a similar manner. The contrast lines produced by normal basal dislocations did not indicate any sites of particular attack and once the erosion had started the advantage of a particular site did not appear to be very significant. There were a few exceptions to this, as shown by the area R in Fig.71c where a particular region has been eroded, and the pits shown in Figs.76a and b; but in these cases there appears to have been a grain boundary and contamination respectively.

Therefore it is not believed that features such as defects or impurity atoms emergent at the crystal edges were important with respect to the kinetics of oxidation, but they do govern the final configuration of the eroded edges. Though the defect concentration of P.G.A. was higher than that of S.P.1., it also contained more impurities so it was not possible to deduce whether reaction was initiated by basal defects or impurities. The work by Thomas (1965) and Hennig (1959) using highly perfect natural graphite crystals showed much less serration of edges, but their experiments were performed in pure oxygen so again a definite deduction cannot be made.

The suggestion has been made (Feates 1968) that the mechanism of oxidation requires a plateau in front of the eroding edge to act as a collection area for reactive species. This theory did not seem likely from the present

work, since if the support film could not have functioned as such a plateau then the lower layers of graphite could never have been eroded, so a 'ghost' of the original graphite flake would always have remained after oxidation, and this was never observed. If the silica film could have acted as a collection plateau then a vertical graphite edge would have been preferentially attacked from the edge nearest the support film, and the shadowing experiments show that if there was any preference then the reverse occurred. In the unlikely event of the collection plateau being above and behind the eroding edge, no vertical edges should ever have been observed, which again was not the case. From the proposed structures of surface oxides, the lack of evidence for collection plateaus, and the catalytic oxidation results, it is believed that the desorption of the surface oxide is the important step in the oxidation reaction, and though other steps can be made to predominate under particular conditions (Bonnetain 1959, Walker 1958) these are not the normal mode of behaviour.

An unexpected result from this work was the coherence of groups of layer planes within a particular graphite crystal. The moiré rotation graph was a vivid example of this but it was clearly shown in many of the micrographs that the oxidised unit corresponded to a rotated crystal that was giving rise to moiré patterns. A possible explanation for this is that between two units

of layer planes there was an expanded C spacing that may have been filled with intercalated gas molecules or other remnants of the past history of each particular graphite sample. Whilst these intercalated molecules did not play any part in reaction, they did separate the individual units that were being eroded. These gaps between units could well have constituted the micropores that have been found in adsorption experiments, and yet would not have been sufficiently numerous to have been distinct in X-ray crystallographic measurements. The larger angles of rotation giving rise to moiré reflections would have been indications of a larger 'C' spacing distortion between the units of layer planes.

Therefore the reactive entities of graphite with air in the temperature range 400-800°C were the $\{10\bar{1}0\}$ edge planes of layer units approximately 20-100Å in thickness, irrespective of lateral dimensions of the crystallites.

The effect of silica in bulk oxidations has been shown to have a positive catalytic effect when added in small quantities to graphite pellets (Rakszawski and Parker 1964) but in larger quantities they believed silica to inhibit oxidation because of formation of a protective coating. This effect at 700°C of increased reaction rate in the presence of silica was quite small and was even less marked at 800°C. A chemical reaction between SiO_2 and graphite has been found not to take place until 1170°C (Minowa, Kato, Mizuta 1961) and thus for the effects reported here only physical diffusion could be considered.

The evidence that the diffusion of silica was more favoured in P.G.A. graphite would agree with the concept of diffusion taking place in a similar manner to intercalation with access only occurring at terminating layer planes. P.G.A. was more disordered than S.P.1. and the smaller crystallite size resulted in more edges being available for access. In this work excess silica was present and so the formation of a protective coating as envisaged by Rakszawski and Parker would have been permissible, but there was no visible evidence of such a layer in the microscope and the inhibitory effect of intercalated layers is believed more likely.

Future Studies.

The results presented in this work showed two distinct features that would benefit from further investigation. The first was the behaviour of metal particles during catalytic oxidation of graphite. More extensive studies utilising a variety of different metals should give information with respect to the effect of the electronic configuration of the metal concerned, and possibly throw more light upon the reactivity of the graphite basal plane. The second feature concerned the anistropy between the prismatic planes involved in uncatalysed oxidation. The characteristics of oxidation in the presence of other gaseous molecules might enable selective poisoning of particular crystal planes to be carried out, and this in turn may furnish further information upon the configuration of surface oxides present on these planes.

I.Abrams, J.W. McBain (1944) J. Appl. Phys. 15 607

I.Y.R. Adamson (1966) Ph.D. thesis. University of Glasgow.

S. Amelinckx, P.Delavignette, M.Heerschap (1965) Chem. and Phys. of Carbon 1 1.

A.F. Armington (1960) Ph.D.Thesis. Pennsylvania State University

J.R. Arthur (1951) Trans. Farad. Soc. 47 164.

R. Audubert, C. Racz (1945) J. Chim. Phys. 42 40.

S.B. Austerman, S.M. Myron, J.W. Wagner (1967) Carbon 5.549

G.E. Bacon (1950) Acta Crystallographica 3. 320.

" (1950) Nature 166 794

" (1958) A.E.R.E. report M/R 2702. 44.

O.P. Bahl, E.L. Evans, J.M. Thomas (1967) Surface Science 8 473

T. Baird, J.R. Fryer, D. Walker (1969) Unpublished work

T. Baird, J.R. Fryer, B. Goldie (1969) Unpublished work.

C.J. Baker (1887) Proc. Roy. Soc.(London) A.12. 424

C. Baker, Y.T.Chou, A.Kelly (1961) Phil.Mag. 6. 1305

N. Bakh, I Levitin (1934) Kolloid. Z. 68. 152.

P. Balk, J.R. Colvin (1961) Kolloid. Z. 176 141

G.A. Bassett (1958) Phil. Mag. 33 1042

" (1960) Proc.Eur.Conf.Electron Micros. Delft 1 270.

D.C. Bassett, D.W. Pashley (1959) J. Inst. Met. 87 449.

J.D.Bernal (1924) Proc.Roy.Soc. (London) A.106 749

H. Bethge (1964) Surface Science 3 33

G. Blyholder, H.Eyring (1957) J.Phys. Chem. 61 682

H.P.Boehm (1966) Advances in Catalysis 16 198

" (1968) Carbon and Graphite Symp. (Newcastle)

" E.Diehl, W.Heck (1964) Rev.Gen.Caout 41. 461

W.Bollmann (1966) J.Appl. Phys. 32 869

L.Bonnetain, X.Duval, M.Letort (1959) Proc. 4th Carbon Conf. 107

D.E.Bradley (1954) Brit. J.Appl.Phys. 5 65

R.O.Brennan (1952) J.Chem.Phys. 20 40

I.Brownlee, J.R.Fryer, G.Webb (1969) J. Catalysis. in Press

J. Butcher, D.M.Grove (1961) Proc. 5th Carbon Conf. 205

K.Carr (1965) Ph.D.Thesis University of Glasgow

E.Charpy (1909) Compt. Rend. 148 920

M. Copisarow (1919) Chem News 118 301

V.E.Cosslett (1951) 'Practical Electron Microscopy' Butterworths, London

A.H.Cotterell (1953) 'Dislocations and Plastic flow in Crystals' Clarendon Press

C.A.Coulson (1960) Proc. 4th Carbon Conf. 215

J.Davy (1831) 'Memoirs of the life of Sir Humphrey Davy' Longman, Rees, Orme, Brown, Green, Longman (London) 1

I.M.Dawson, E.A.C.Follett (1959) Proc.Roy.Soc. (London) A. 253 390

I.M.Dawson, E.A.C. Follett (1960) Proc. Eur.Conf. Electron Micros. (Delft) 337

P.Debye, P.Scherrer (1917) Physik Z. 18 291

V.V. Digonskii, V.N.Krylov (1960) Zhur. Priklad. Khim 33 2638

D.M.Donaldson,J.M.Robertson (1953) Proc.Roy.Soc. A.220.157

J.B.Donnet (1968) Carbon 6 161

" G.Henrich (1960) Bull.Soc.Chim.France 1609

G. Dupouy (1967) J.Electron Micros. (Jap) 16 5.

X.Duval (1947) J.Chim.Phys 44 296

F.K.Earp, M.W.Hull (1957) Ind. Carbon and Graphite Conf. (London) 326

A.E.Ennos (1954) Brit.J.Appl. Phys. 5 27

E.L.Evans, O.P.Bahl, J.M.Thomas (1967) Carbon 5 587

F.S.Feates (1958) A.E.R.E. report R.5754

" (1967) Private Communication

" (1968) Trans.Farad Soc. 64 3093

" (1968) Carbon 6 949

" J.Parry (1964) A.E.R.E. report R. 4819 1964

H.Feilchenfeld (1957) J.Phys.Chem. 61 1133

G.I.Finch,H.Wilman (1936) Proc.Roy.Soc.(London) A.155 345

H.Fernandez-Moran (1966) Proc.6th Int.Conf. Electron Micros. (Kyoto)

E.A.C. Follett (1964) Carbon 1 329

F.E. Fujita, K.Izui (1961) J. Phys. Soc. (Japan) 16 214

J.T. Gallagher, H. Marker (1964) Carbon 2 163.

E.N. Greer, B. Topley (1932) Nature 129 904

C.E. Hall (1948) J. Appl. Phys. 19 271

" (1953) 'Introduction to Electron Microscopy' McGraw-Hill New York

H. Hashimoto, T. Naiki, T. Eto, K. Fujiwara, M.Watanabe, Y.Nagahama (1966) Proc.6th Int.Conf.Electron Micros. (Kyoto)

O. Hassel, H. Mark (1924) Z. Physik 25 317

P. Hawtin, J.A. Gibson (1966) Carbon 4 489

G. Heide (1958) Proc. 4th Int.Conf.Electron Microscopy (Berlin) 1 82

R.D. Heidenreich (1967) J.Electron Micros. (Japan) 16 23

" (1967) Siemens Review 34 1.

" (1968) J. Appl. Cryst. 1 1

" , V.G. Peck (1943) J. Appl. Phys 14 23

K. Hedden, E. Wicke (1957) Proc.3rd Carbon Conf. 249

E.A. Heintz, W.E. Parker (1966) Carbon 4 473

G.R. Hennig (1953)(1955) Proc. 1st and 2nd Carbon Conf. 112.

" (1957) Proc. 3rd Carbon Conf. 265

" (1959) Proc. 4th Carbon Conf. 145

" (1961) Proc. 5th Carbon Conf. 143

" (1962) Z. Electrochem 66 629

" (1962) J. Inorg Nucl.Chem 24 1129

G.R. Hennig (1964) Appl. Phys. lett. 4 52

" (1965a) Carbon 3 107

" (1965b) Science 147 733

" (1966) Chem. and Phys. of Carbon 2. 1.

" , G.J. Dienes, W. Kosiba(1958) Proc. 2nd Int. Conf. on 'Peaceful uses of atomic energy' 7 301

" M. Kanter (1959) Proc. 4th Carbon Conf. 141

P.B. Hirsch, A. Howie, R.B. Nicholson, D.W. Pashley, M.J. Whelan (1965) 'Electron Microscopy of Thin Crystals' Butterworths, London.

U. Hofmann, D. Wilm, E. Csalan (1936) Z. Electrochem 42 506

G. Honjo, N.Kitamura, K.Shimaoka, K.Mihama (1956) J. Phys.Soc.(Japan) 11 527

F.H. Horn (1952) Nature 170 581

W.S. Horton (1961) Proc. 5th Carbon Conf. 2 233

M. Hucher, A. Oberlin (1961) Comptes Rend. 252 3081

E.E.G. Hughes, B.R.Williams, J.M. Thomas (1962a) Nature 193 838

" " J.M. Thomas (1962b) Trans. Farad Soc. 58 2011

A.W. Hull (1922) Phys.Rev. 20 113

D.H.Kay (1965) 'Techniques for Electron Microscopy' Blackwell, Oxford.

A.J. Kennedy (1960) Proc. Phys. Soc. (London) B75 607

T. Komoda (1964) Optik 21 93.

V. Labaton (1965) Private Communication

D. Laidler, A.Taylor (1940) Nature 146 130

N.R. Laine, F.J.Vastola, P.L. Walker Jr. (1963) J.Phys. Chem. 67 2030

J.J. Lander, J. Morrison (1966) Surface Science 4 103.

F.M. Lang, P. Magnier, S. May (1961) Proc. 5th Carbon Conf. 171

" " (1962) Proc. Conf. Corrosion of Reactor Materials (Saltzburg) 2 453

" " (1964) Carbon 2 . 7.

" " P. Gilles, P. Maire (1966) J.Chim Phys. 63 1084

P. Lebeau, M.Picon (1924) Comptes. Rend. 179 264

W.K. Lewis, E.R. Gilliland, R.R. Paxton (1954) Ind. Eng. Chem. 46 1327

H. Levinstein, C.D. Capio (1967) J. Appl. Phys. 38 2761

H. Lipson, A.R. Stokes (1942) Nature 149 328

" " (1942) Proc. Roy.Soc.(London) A 181 101

L.D.Loch, A.E. Austin, R.J. Harrison, W.H. Duckworth U.S. A.E.A. report 1958

F.J. Long, K.W. Sykes (1948) Proc.Roy.Soc.(London) A193.377

" " (1950) J.Chim.Phys. 47 361

" " (1952) Proc.Roy.Soc.(London) A.215.100

H.H.Lowry (1963) 'Chemistry of Coal Utilisation' Wiley New York

V.B.Lukesh (1950) Phys. Rev. 80 226

H. Marsh, T.E. O'Hair, R.Reed (1965) Trans.Farad.Soc.61.255

E. Matuyama (1956) Nature 178 1459

Ch. Mauguin (1926) Bull Soc.Franc min. 49 32

L. Meyer (1932) Z.Physik Chem B.17. 385

" (1938) Trans.Farad.Soc. 34. 1056

S. Minowa, M.Kato, M.Mizuta (1961) Nagoya Kogyo Gijutsu Shikensho Hokoku 10 152

T. Mitsuishi, H.Nagasaki, R.Uyeda (1951) Proc.Imp. Acad. Japan 27 86

G.L. Montet (1961) Proc. 5th Carbon Conf. 1 116

" G.E. Myers (1968) Proc. 8th Carbon Conf.

" " (1968) Carbon 6 225 (abstract of above)

G.E. Myers, M.D. Gordon (1968) Carbon 6 422

Yu V.Naidich, G.A. Kolesnichenko (1961) Poroshkovaya Met. Akad.Nauk Ukr.S.S.R. 1 55

R.E. Nightingale (1962) 'Nuclear Graphite' Academic Press London

P.Nifontoff (1954) Compt. Rend. 23 1870

J.N. Ong Jr. (1964) Carbon 2 281

C. Palache (1941) Am. Mineralogist 26 709

A.R. Patel, O.P. Bahl (1965) Carbon 3 181

D.W.Pashley, A.E.B.Presland (1958) J.Inst.Met. 87 419

" " (1962) Phil.Mag. 7 1407

" M.J.Stowell (1963) Phil.Mag. 8 1605

F. Perrier, G.Dupouy (1966) J.Micros. 5 369

A.E.B.Presland,J.A.Hedley (1963) J.Nucl.Mat. 10 99

J.F. Rakszawski, W.E. Parker (1964) Carbon 2 53

E. Raub, G. Falkenburg (1964) Z.Metallk 55 186

L. Reimer (1959) Z. Naturforsch 14a 759

H.L. Riley (1937) J.Inst.Fuel. 10 149

D.Rivin (1963) Rubber Chem.Technol 36 729

L.E.J.Roberts, E.A.Harper,C.T.Small (1958) A.E.R.E. report C.R. 882.

C. Roscoe, J.M. Thomas (1966) Carbon 4 383

M.L. Rudee (1967) Carbon 5 55

G.W. Sears, J.B.Hudson (1963) J.Chem.Phys. 39 2380.

C.Sella, P.Conjeaud, J.J.Trillat (1959) Compt.Rend.249.1987.

" J.J.Trillat (1963) Colloq.Intern.Centre Nat. Rech.Sci. Paris 122 187

J.W. Shetley (1918) Indian Eng. Feb16.

Siemens Ltd. (1968) Private Communication

V. Sihvonen (1932) Am.Acad.Sci. Fennicae A32 29

" (1934) Z.Electrochem. 40 456

" (1935) Suomen Kemistilehti B 8 21

A. Smith (1863) Proc.Roy.Soc. (London) A12 424

H.S. Spence (1922) Raw Materials 5. 316

J. Stabenow (1968) Siemens Review 35 24

I.G.Stoyanova (1959) Isvest.Akad.Nauk. S.S.S.R. Ser.Fiz. 23 490

" E.M. Belavtseva (1959) Isvest.Akad. Nauk S.S.S.R. Ser. Fiz. 23 754.

B.P. Stoicheff (1954) Canad. J. Phys. 32 329

R.F. Strickland-Constable (1944) Trans.Farad.Soc. 40 333

G. Sumner (1966) Surface Science 4 313

E.W. Thiele (1939) Ind.Eng. Chem. 31 916

J.M. Thomas, E.E.G.Hughes,B.R.Williams (1963) Nature 197.682

" " " (1963) Phil.Mag.8 1513

" " (1964a) Carbon 1 209.

J.M. Thomas, E.E.G. Hughes (1964b) Carbon 1 339

" P.L. Walker Jr. (1964) J.Chem.Phys. 41 587

" (1965) Chem and Phys.of Carbon 1 122

" (1968) Private Communication

" C. Roscoe (1968) Chem and Phys. of Carbon 3. 1.

F. Thon (1966) Proc.6th Int.Conf.Electron Microsc.(Kyoto)

" (1966) Z. Naturforschg. 21 476

F. Trendelenburg, E.Franz,O.Vieland (1933) Z.Tech Physik.14 489

W. Trezbiatowski (1937) Roczniki Chem. 17 173

T. Tsuzuku (1953) Kagaku 23 32

" (1957) Proc.3rd Carbon Conf. 433.

A.R. Ubbelohde (1957) Nature 180 380

" , F.A. Lewis (1960) 'Graphite and its Crystal Compounds'. Oxford.

V.S. Veselovskii, K.V. Vasil'ev (1934) Z.Krist. 89 494

M.Von Ardenne (1948) Kolloid Z. 111 22.

A.C.Van Dorsten, H.F.Premsela (1966) Proc. 6th Int. Conf. Electron Micros. (Kyoto)

P.L.Walker Jr., H.A.McKinstry, C.C. Wright (1953) Ind. Eng.Chem 45 1711

" F.Rusinko Jr., L.G.Austin (1959) 'Advances in Catalysis' Academic Press, New York XI 133

D.Watanabe (1961) J.Phys.Soc.(Japan) 17 Suppl. B.11. 205

M.Watanabe, H.Shinagawa, K.Shirota (1966) Proc. 6th Int. Conf. Electron Micros. (Kyoto)

G.K.Williamson, C.Baker (1960) Proc.Eur.Conf.Electron Micros. (Delft) 1960

" (1960) Proc.Roy.Soc. (London) A.257 457

" C.Baker (1961) Proc. 5th Carbon Conf. 2 521

A. Winkelmann (1956) Z.Metallk 47 627

S. Yamaguchi (1953) Z.Physik 134 618

Yu A.Zarifyanz, V.F. Kiselev, N.N.Lezhnev,O.V.Nikitina (1967) Carbon 5 127

V.K.Zworykin, G.A.Morton,E.Romberg, J.Hillier, A.W. Vance (1945) 'Electron optics and the Electron Microscope' Wiley, New York.

Published work by the author not submitted with this thesis.

J.R.Fryer and D.Mapper.
The rapid separation of Indium using reverse phase partition chromatography.
Analyst. 87 297 1962.

E.A.C.Crouch and J.R.Fryer.
The fast separation of the rare earth elements on the micro-scale.
A.E.R.E. report E.M. 1078. 1962.

J.R.Fryer and D.F.C. Morris
Stability constants of Cobalt (II) bromide complexes.
Electrochim. Acta. 10 473. 1965.

J.R.Fryer and D.F.C.Morris
Stability constants of Manganese (II) bromide complexes.
Talanta 15 1309 1968.

I.C.Brownlee, J.R.Fryer, G.Webb.
The influence of the substrate on the behaviour of graphite-supported palladium catalysts.
Journal of Catalysis. - In Press.